Cheap Metals for Noble Tasks: Low-Valent Molybdenum and Tungsten Nitrosyl Complexes in Homogeneous Hydrogenations and Hydrosilylations

DISSERTATION

zur

Erlangung der naturwissenschaftlichen Doktorwürde

(Dr. sc. nat.)

vorgelegt der

Mathematisch-naturwissenschaftlichen Fakultät

der

Universität Zürich

von

Subrata Chakraborty

aus

Indien

Promotionskomitee

Prof. Dr. Heinz Berke (Vorsitz und Leitung)

Prof. Dr. Greta R. Patzke

Zürich 2013

LIST OF ABBREVIATIONS

AIBN	azobisisobutyronitrile
as	asymmetric
BAr^F_4	tetrakis(3,5-bis(trifluoromethyl)phenyl)borate
COSY	Correlation spectroscopy
Conv	conversion
Cat	catalyst
COD	cyclooctadiene
δ	chemical shift
ν	frequency
d	doublet
DEPT	Distortionless Enhansment by Polarization transfer
DFT	density functional theory
DKIE	deuterium kinetic isotope effect
DBU	1,8 Diazabicycloundec-7-ene
etp^ip	Bis(2-diisopropylphosphinoethyl)phenyl phosphine (iPr$_2$PCH$_2$CH$_2$)$_2$PPh
EPR	electron paramagnetic resonance
equiv.	equivalent
Eq.	equation
Et_2O	Diethylether
GC/MS	Gas chromatography- mass spectrometry
HMBC	Heteronuclear multiple bond correlation
Hz	Hertz
*i*Pr	isopropyl
IR	Infrared

NBD	norbornadiene
NOE	Nuclear Overhauser effect
NMR	Nuclear magnetic resonance
PN^HP	$(i Pr_2PCH_2CH_2)_2NH$
PNP	$(i Pr_2PCH_2CH_2)_2N$
ppm	parts per million
Ph	phenyl
P∩P	2,2′-bis(diphenylphosphino)diphenylether (DPEphos)
q	quartet
r.t.	room temperature
s	singlet
S/C	substrate/catalyst
TOF	turn over frequency
THF	tetrahydrofuran
Temp	temperature
t	triplet

List of Prepared Compounds

Complexes bearing ($^{i}Pr_2PCH_2CH_2)_2PPh$, (etp^{i}p) ligand

- $Mo(NO)Cl_3(etp^{i}p)$
- $W(NO)Cl_3(etp^{i}p)$
- $Mo(NO)Cl_2(etp^{i}p)$
- $W(NO)Cl_2(etp^{i}p)$
- $Mo(NO)Cl(NCMe)(etp^{i}p)$
- $W(NO)Cl(NCMe)(etp^{i}p)$
- $Mo(NO)(CO)Cl(etp^{i}p)$
- $W(NO)(CO)Cl(etp^{i}p)$
- $Mo(NO)Cl(\eta^2\text{-ethylene})(etp^{i}p)$
- $W(NO)Cl(\eta^2\text{-ethylene})(etp^{i}p)$
- $Mo(NO)H(\eta^2\text{-ethylene})(etp^{i}p)$
- $W(NO)H(\eta^2\text{-ethylene})(etp^{i}p)$
- $W(NO)Cl(H)_2(etp^{i}p)$
- $Mo(NO)Cl(\eta^2\text{-}PhSiH_3)(etp^{i}p)$
- $Mo(NO)(CO)H(etp^{i}p)$
- $W(NO)(CO)H(etp^{i}p)$
- $Mo(NO)(CO)(OCHO)(etp^{i}p)$
- $W(NO)(CO)(OCHO)(etp^{i}p)$
- $[Mo(NO)(CO)(etp^{i}p)(THF)]^{+}[B(C_6F_5)_4]^{-}$
- $[W(NO)(CO)(etp^{i}p)(THF)]^{+}[B(C_6F_5)_4]^{-}$

Complexes bearing (iPr$_2$PCH$_2$CH$_2$)$_2$NH, (PN^{H}P) ligand

- $Mo(NO)(CO)(PN^{H}P)Cl$
- $W(NO)(CO)(PN^{H}P)Cl$
- $Mo(NO)(CO)(PN^{H}P)(O\textit{t}Bu)$
- Mo(NO)(CO)(PNP)
- W(NO)(CO)(PNP)
- $Mo(NO)(CO)H(PN^{H}P)$
- $W(NO)(CO)H(PN^{H}P)$

- Mo(NO)(CO)(PNP)(OCO)
- W(NO)(CO)(PNP)(OCO)
- Mo(NO)(CO)(PN^{H}P)(OCHO)
- W(NO)(CO)(PN^{H}P)(OCHO)
- Mo(NO)Cl_3(PN^{H}P)
- W(NO)Cl_3(PN^{H}P)
- Mo(NO)Cl_2(PN^{H}P)
- W(NO)Cl_2(PN^{H}P)

Complexes bearing 2,2′-bis(diphenylphosphino)diphenylether, (DPEphos = P∩P = $(Ph_2PC_6H_4)_2O$):

- [Mo(NO)(P∩P)Cl_2]$_2$[μCl]$_2$
- [Mo(NO)(P∩P)$(NCMe)_3$]$^{+}$[Zn_2Cl_6]$^{2-}{}_{1/2}$
- [Mo(NO)(P∩P)$(NCMe)_3$]$^{+}$[$BAr^{F}{}_4$]$^{-}$
- [Mo(NO)(P∩P)(NCMe)]$_2$[μCl]$_2{}^{2+}$ 2[$BAr^{F}{}_4$]$^{-}$
- Mo(NO)(P∩P)$(CO)_2$Cl
- [Mo(NO)(κ^3-P,P,O-DPEphos)Cl(PMe_3)]
- [Mo(NO)(κ^3-P,P,O-DPEphos)Cl(PPh_3)]

TABLE OF CONTENTS

1 INTRODUCTION

1.1 Homogeneous Catalysis

The catalysis of organic reactions is one of the most important applications of organometallic chemistry. A catalyst is an additive used in substoichiometric amount to bring about a reaction at a temperature below that required for the uncatalyzed thermal reaction.[1] Normally, the catalyst only increases the rate of a process but does not alter its position of equilibrium, which is decided by the relative thermodynamic stabilities of substrate and products.

Catalysis is classified into homogeneous (the catalyst and the substrates are in the same phase) and heterogeneous (catalysis takes place at the surface of a solid catalyst) systems.[2] Heterogeneous catalysts are easily separated from the reaction products but tend to require rather high temperatures and pressures and frequently lead to mixture of products resulting in low selectivity. On the other hand homogeneous catalysts are usually difficult to separate from the product, sometimes requiring special separation techniques. But they operate at low temperature and pressure and gives good selectivity. The bio-chemical catalysis, namely enzymes are natural catalysts which possess both the properties of homogeneous and heterogeneous catalysts and in terms of activity, selectivity and scope enzymes score very high and often seen as a separate group of catalysis. However this is a field not considered in this context at all.

Although the fundamental processes (such as steam reforming, cracking, hydrodesulfurization and reformation) for refining petroleum and its conversion to basic building blocks are based on heterogeneous catalysts, still many important value added fine chemicals, intermediates and pharmaceuticals are manufactured by homogeneous catalytic processes. Some of these products[3] are listed in Table 1.1.

Furthermore, there are ample important homogeneous catalytic reactions applied in chemical industries mediated by various transition metal complexes for example hydrogenation, hydrosilylation, hydroformylation, carbonylation, hydrocyanation and metathesis reactions.

We will discuss in this chapter on homogeneous hydrogenation and hydrosilylation in details.

1.2 Homogeneous Hydrogenation

Homogeneous hydrogenation of unsaturated organic compounds catalyzed by metal complexes is undoubtedly the most studied of the entire class of homogenously catalyzed reactions. This process is usually performed with molecular hydrogen in the presence of metal complexes as catalysts.

Table 1.1. Products of homogeneous catalytic reactions

Structure	Name and use	Process
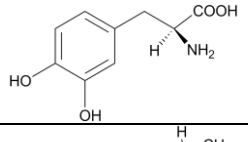	L-Dopa (drug for Parkinson disease)	Asymmetric hydrogenation
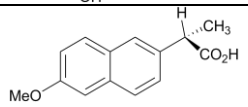	R- Naproxen (Liver toxin) S- anti inflammatory drug	Asymmetric hydroformylation or hydrocyanation
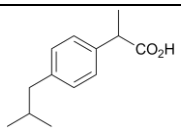	Ibuprofen analgesic	Catalytic carbonylation
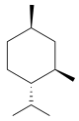	L-Menthol (Flavoring agent)	Asymmetric isomerization
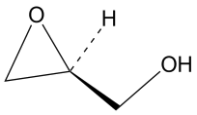	R-Glycidol One of the component of heart drug	Asymmetric epoxidation (Sharpless epoxidation)

The first example of homogeneous hydrogenation using metal compounds was documented by Calvin in 1938 reporting that quinoline solutions of copper acetate were capable of hydrogenating unsaturated substrates such as *p*-benzoquinone.[4] Since then several outstanding discoveries have been made in this field. For example, the discovery of Wilkinson catalyst (Wilkinson awarded Noble prize in 1973 for pioneering work on the chemistry of organometallic so called sandwich complexes),[5] discovery of η^2-H_2 binding complexes by Kubas,[6] Shvo's bifunctional catalyst,[7] the development of efficient enantioselective catalytic hydrogenations and transfer hydrogenations by Knowles and Noyori (both awarded the Nobel prize in 2001),[8] and the "metal-free" bifunctional dinuclear heterolysis of dihydrogen and hydrogenation catalysis discovered by Stephan and co-workers in 2006.[9]

Indeed, advances in hydrogenation systems have contributed significantly to progress rapidly in homogeneous catalysis, because of the ability of the H_2 molecule to interact with transition metal complexes forming intermediate metal hydrides (M-H) or metal dihydrogen (M-H_2) complexes in

a wider range of catalytic processes. Therefore to obtain proper perspective, we need to be aware of how activation (the bond cleavage process) of H_2 occurs on metal complexes.

1.2.1 Hydrogen Activation

Hydrogen is the simplest molecule and this is available as a clean resource in abundance at a very low cost.

The hydrogen molecule (H_2) is held together by a very strong two electron H-H covalent bond with a dissociation energy of 428 kJ mol^{-1}(104 kcal $mole^{-1}$). The H atoms in this molecule display strongly overlapping s orbitals causing a large HOMO/LUMO gap. Therefore this molecule is only meagerly polarizable and together with its high bond strength it is not well prepared for reactivity. Reaction of the dihydrogen molecule with a transition-metal center bearing suitable ligand sphere provides an effective way to activate it.

Homolytic and heterolytic splitting of dihydrogen

The H_2 molecule can bind side-on (η^2) to a metal center primarily *via* donation of its two σ electrons to a vacant d orbital to form a stable dihydrogen complex. The stabilization of H_2 complexes is owing to the capability of transition metal complexes for back donation of electrons from a filled metal d orbital to the σ* anti bonding orbital of H_2. The back donation is analogous to that of Dewar-Chatt-Duncanson model for olefin coordination (Figure 1.1).[10]

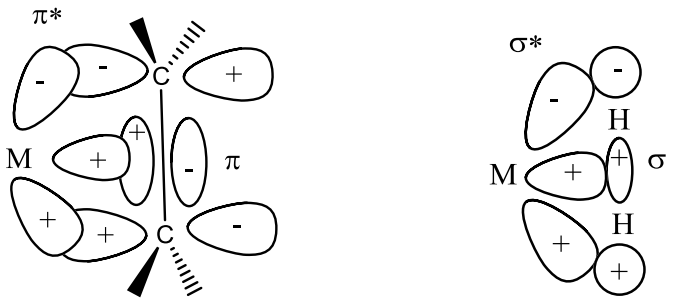

M-π bond M-σ bond

Figure 1.1. Dewar-Chatt-Duncanson model for olefin coordination (left) and bonding model for H_2 coordination (right).

The dihydrogen molecule thus becomes strongly polarized by orbital interactions. This polarization can be enhanced by strengthening the back-bonding leading to the overpopulation of the σ*H_2 orbital. This resulted in concomitant elongation of the H-H bond passing through the

states of "stretched dihydrogen" complexes and "compressed dihydride" complexes with eventual oxidative addition of the H_2 molecule forming dihydride complexes.

This route of dihydrogen cleavage on mononuclear metal centre is seen as "homolytic splitting".

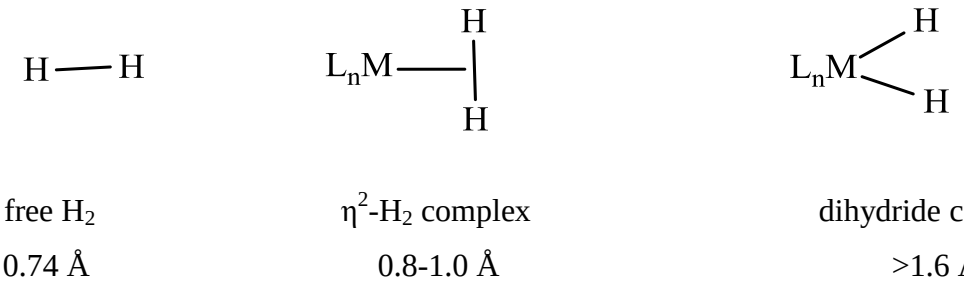

free H_2	η^2-H_2 complex	dihydride complex
0.74 Å	0.8-1.0 Å	>1.6 Å

Figure 1.2. Binding mode of H_2 with transition metals and H-H distances.

The first structurally characterised dihydrogen metal complex $W(CO)_3(P\textit{i}Pr_3)_2(H_2)$[11] was discovered by Kubas and coworkers in 1983 although several transition metal hydride complexes have been well characterized long before and were known to be part of homogeneous catalytic reaction courses. The first hydride complex $H_2Fe(CO)_4$ was discovered by Hieber[12] in 1931.

Dihydrogen complexes generally have higher thermodynamic and kinetic acidity compared to most metal hydride complexes.[6a,13] Free H_2 is an extremely weak acid (pKa = 35 in THF), but binding it to an electrophilic cationic metal increases the acidity up to 40 orders of magnitude The pKa of H_2 can become as low as -6 and thus the acidity of η^2-H_2 becomes as strong as that in sulfuric or triflic acid.[14] Therefore the presence of a base can lead to the deprotonation of the metal dihydrogen complex leading to "heterolytic" splitting of dihydrogen.

Heterolytic splitting of H_2 ligands in mononuclear complexes could be commenced by a hinging distortion of the H_2 ligand[15] where the base deprotonates the acidic hydrogen atom and the other hydrogen atom remain attached to the metal as a hydride (Scheme 1.1).

The splitted proton from the H_2 ligand can migrate to either an external Lewis base (intermolecular) or a ligand/anion (intramolecular).[16]

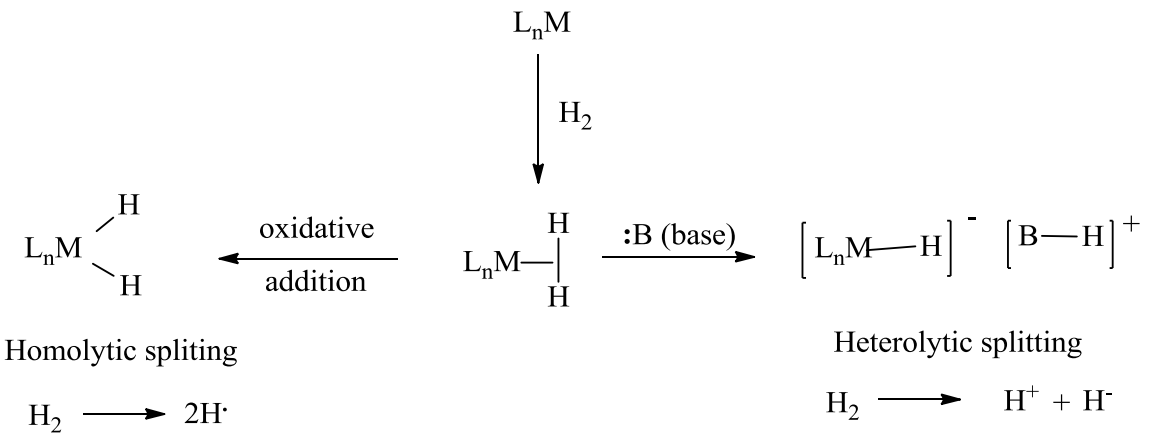

Scheme 1.1. Splitting mode of H_2 on mononuclear metal centre.

Heterolytic cleavage of H_2 by Ru complexes dates back to the mid 1960s. Wilkinson and co-workers clearly demonstrated it by the reaction of $RuCl_2(PPh_3)_3$ with H_2 in the presence of ethanol, giving $RuHCl(PPh_3)_3$ and HCl, where ethanol served as a base.[17] Nowadays deprotonation of metal dihydrogen complexes using simple bases (such as Et_3N) has become a common phenomenon.[18]

Metal-Ligand Cooperation in Heterolytic Hydrogen Activation

Activation of H_2 molecule *via* "metal-ligand cooperation" have attracted much attention in recent years. The transition metal complexes bearing suitable basic ligands split H_2 molecule heterolytically where the proton goes to the attached ligand and hydride stays at the metal centre therefore no need to use external base as deprotonating agent.

Variations of heterolytic H_2 splitting have been reported between various metal centers and adjacent nucleophilic heteroatoms (such as N, O, and S), facilitated by the close proximity between the metal center and the heteroatom.[19] For example, amido ligands are recognised as suitable cooperative ligands in activating dihydrogen and also in homogeneous catalysis.[20] These ligands can stabilize the unsaturated metal centres *via* a p_π-d_π bonding interactions and is viewed as Frustrated lewis Pair type systems.[21]

Fryzuk and coworkers demonstrated the heterolytic splitting of H_2 on organometallic amido complexes of rhodium and iridium[22] in mid 1980's and on ruthenium complex in 1991.[23] The heterolytic splitting of H_2 on Fryzuk's Ru-amide system is shown in Scheme 1.2.

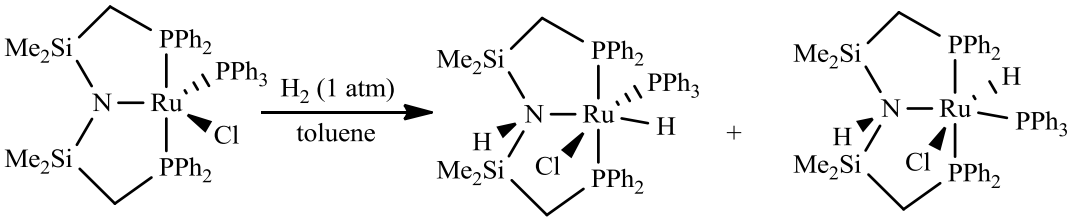

Scheme 1.2. Heterolytic H_2 cleavage by a Ru amido complex.

Heterolysis of H_2 is a crucial step in Noyori's elegant catalytic system[24] where H_2 is cleaved in the form of a hydride and a proton between the Ru(II) center and a highly basic amido ligand. Furthermore, The Milstein group has reported reversible H_2 splitting between the metal center and a non-adjacent carbon atom in pyridine based pincer (PNN)Ru and (PNP)Ru compounds.[25] These complexes can undergo deprotonation at the pyridinylmethylenic carbon, resulting in dearomatization of the pyridine moiety. The dearomatized complex can then activate H-H bond by cooperation between the metal and the ligand, thereby regaining aromatization (Scheme 1.3). Such processes occur with no formal change in the metal oxidation state.

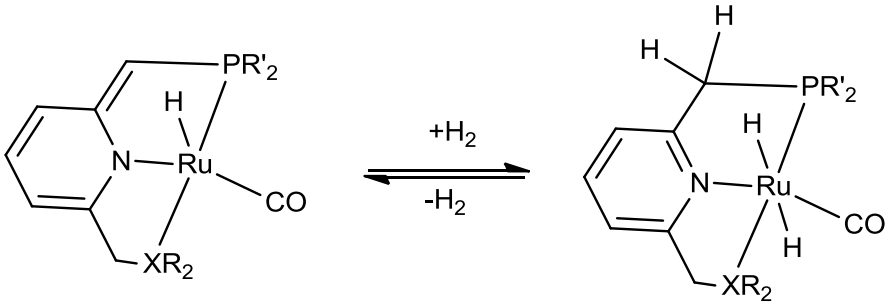

X = N, P; R = *i*Pr$_2$, *t*Bu

Scheme 1.3. Activation of H-H bond by Milstein's PNN and PNP based Ru system.

An acridine based pincer (PNP)Ru(H)Cl(CO) complex was also recently reported by Milstein which displays unique "long-range" metal-ligand cooperation in the activation of H_2.[26] The

acridine-PNP ligand affords a flexible ligand framework, as it forms six-membered rings. Reaction of (PNP)Ru(H)Cl(CO) with H_2/KOH resulted in dearomatization of the central acridine ring as a result of heterolytic splitting of H_2 (Scheme 1.4). DFT calculations show that this process involves the formation of a Ru dihydride intermediate bearing a bent acridine ligand in which C9 is in close proximity to a hydride ligand followed by through-space hydride transfer.

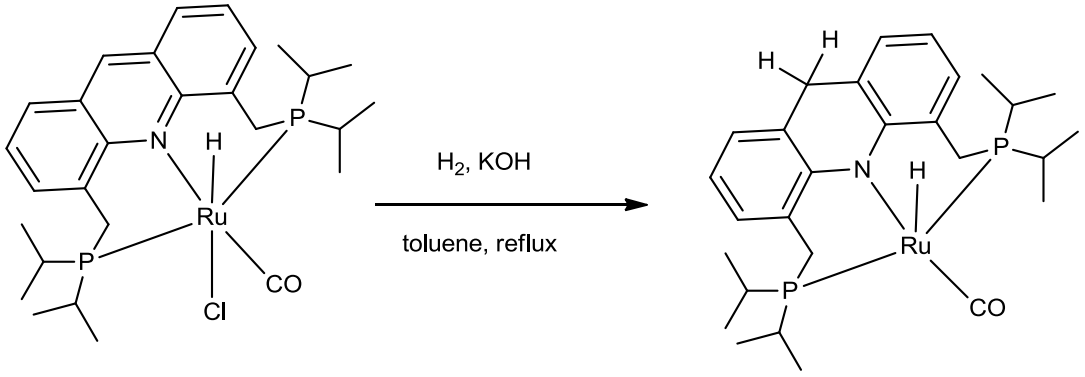

Scheme 1.4. Long range metal ligand cooperation in hydrogen activation.

To summarize the hydrogen activation section, homolytic hydrogen splitting increases the oxidation state of the metal centre by two and the formal oxidation state of the metal centre does not change in the heterolytic splitting mode which make this process more facile compared to oxidative addition.

"Homolytic splitting" of dihydrogen in transition metals is the basis for Wilkinson-type hydrogenation catalysis. On the other hand "Heterolytic splitting" of dihydrogen is the basis for hydrogenation processes denoted as "ionic hydrogenations",[27] "bifunctional catalysis"[24] or "hydridic protonic reaction".[28] We will discuss here both type of hydrogenations in details.

1.2.2 Willkinson and Osborn type Hydrogenation

The much studied Wilkinson's catalyst, $[RhCl(PPh_3)_3]$ complex, was discovered in 1965 by Wilkinson and other groups.[5, 29, 30] The complex is an efficient hydrogenation catalyst for unsaturated substrates working under very mild conditions. This compound catalyzes the chemospecific hydrogenation of alkenes in the presence of other easily reduced groups such as -NO_2 or -CHO, and terminal alkenes in the presence of internal alkenes.[5,31] The most accepted

mechanism for alkene hydrogenation is mainly due to Halpern and is supported by careful kinetic and spectroscopic studies of cyclohexene hydrogenation.[32]

The key step of Wilkinson hydrogenation involves homolytic cleavage of H_2. This splitting leads to homopolar or nearly homopolar dihydride H-M-H. The generated highly covalent H-M-H bonds in subsequent reaction steps undergo H transfer by insertion of the unsaturated XY substrate. The second H transfer is accomplished by reductive elimination (Scheme 1.5).[15] Therefore the metal complex need not necessarily contain metal hydride bonds, but gives rise to intermediate MH_2 (alkene) species during the catalytic course.

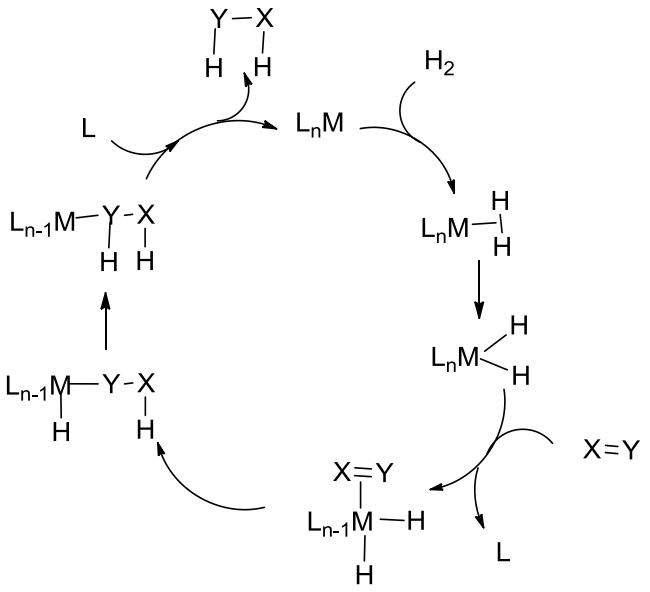

Scheme 1.5. General scheme for Wilkinson-type hydrogenation catalyses {$L_nM = RhCl(PPh_3)_3$}.

The catalytic potential of $[Rh(diene)L_n]^+$ (n = 2 or 3; L=phosphine, phosphite or arsine; diene = NBD, COD) systems as hydrogenation catalysts was discovered by Osborn and coworkers. Under a hydrogen atmosphere the diene is hydrogenated, generating the reactive $[RhH_2S_xL_n]^+$ species which, in some cases such as in $[RhH_2(solvent)_2L_2]^+$ intermediates, can be isolated relatively easily from coordinating solvents such as acetone or ethanol. In contrast to Wilkinson's catalyst, a large number of donor ligands can be used and several easy preparative routes are available. These rhodium(III) complexes function as homogeneous hydrogenation catalysts under mild conditions for the reduction of alkenes, dienes, alkynes, and ketones.[33]

In 1963 Bath and Vaska prepared a monohydride complex [$RhH(CO)(PPh_3)_3$], which was studied in detail by Wilkinson and coworkers as an active catalyst for hydrogenation, isomerization, and hydroformylation reactions.[34-37] The general mechanism for this type of complex containing metal hydride bonds are shown in Scheme 1.6 which follows "Osborn type" catalytic cycles. The first step is the ligand dissociation followed by coordination of the substrate to the catalyst. This is followed by the migratory insertion of the hydride to the coordinated substrate and then hydrogenolysis of the metal alkyl species to yield the saturated alkane. This hydrogenolysis proceeds through oxidative addition of H_2 followed by reductive elimination to regenerate the mono hydride catalyst.

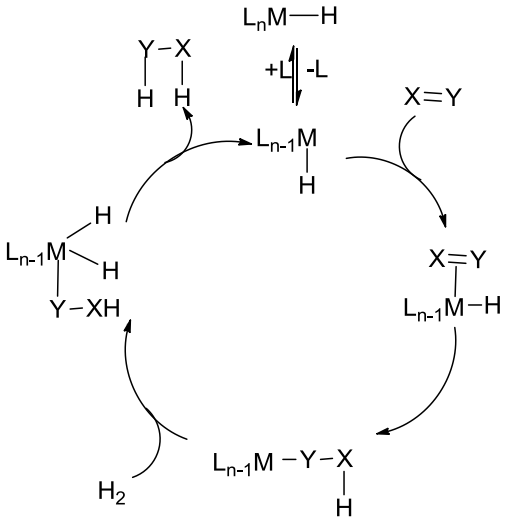

Scheme 1.6. [$RhH(CO)(PPh_3)_3$] catalysed Osborn type hydrogenation mechanism starting from a monohydride species

Nevertheless, irrespective of the monohydride or dihydride route, a key prerequisite of catalysis for such kind of systems is coordinative unsaturation, that is open site at the metal centre or atleast labile ligands. Wilkinson and Osborn type hydrogenations are also denoted as "classical" hydrogenaton mechanism.

Later on, Crabtree and coworkers discovered the cationic iridium complex $Ir(cod)(PCy_3)(py)]PF_6$ sometimes referred to as Crabtree's catalyst which was found to be highly active for olefin hydrogenations (TOF for 1-hexene, 6400 h^{-1}) in particular sterically hindered tetra substituted olefins like $Me_2C=CMe_2$, (TOF = 4000 h^{-1}).[38]

Recently our group has also demonstrated several rhenium nitrosyl based olefin hydrogenation catalysts, which follow Osborn type catalytic cycles and were found to be even more efficient compared to these known noble metal systems.[39] For example The "Re(I) diiodide/hydrosilane/$B(C_6F_5)_3$" co-catalytic systems were shown to furnish the most efficient rhenium catalyst so far known for the hydrogenation of alkenes. Both the activity and longevity were superior to previously reported catalytic systems. The coordination of super electrophile silylium cation to NO causes facilitation of "NO bending" which was demonstrated to be vital to accomplish excellent catalytic performance.

A comparative study of the activity of various well-known catalysts towards 1-hexene hydrogenation is shown in Table 1.2.

Table 1.2. Comparision of catalytic activity of several well-known Wilkinson and Osborn type catalysts in 1-hexene hydrogenation.[5,35-39]

Catalyst	Solvent	Temp (°C)	H_2 (bar)	TOF (h^{-1})
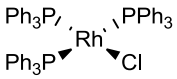 Wilkinson catalyst	C_6H_6/EtOH	25	1	650
$RuHCl(PPh_3)_3$	C_6H_6	25	1	9000
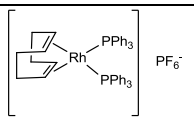 Schrock Osborn catalyst	CH_2Cl_2	25	1	4000
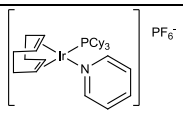 Crabtree catalyst	CH_2Cl_2	0	1	6400
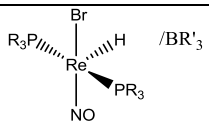 Berke/Jiang catalyst	Solvent free	23	1	1725
	Solvent free	23	10	17000
	CH_2Cl_2	90	10	56000

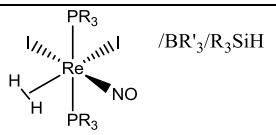 /BR'$_3$/R$_3$SiH Berke/Jiang catalyst	Solvent free	23	10	6.0×10^5

1.2.3 Ionic Hydrogenation

Ionic hydrogenation is principally a new approach towards catalytic homogeneous hydrogenations requiring heterolysis of dihydrogen as shown in Scheme 1.7.

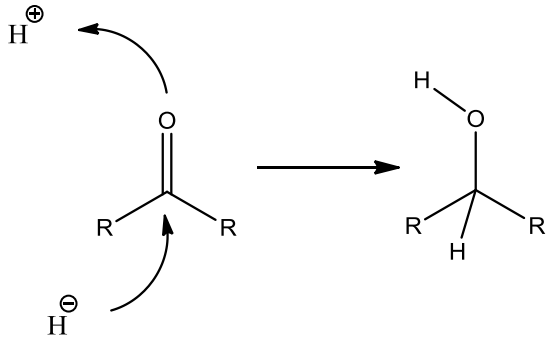

Scheme 1.7. Ionic hydrogenation of ketone

Ionic hydrogenations can be distinguished in their H-transfer steps with respect to the sequence of the H^- and H^+ transfers. The following types of H transfers are observed in stoichiometric or catalytic ionic hydrogenation processes: (a) proton before hydride transfer (b) hydride before proton transfer and (c) simultaneous hydride and proton transfers.[15]

In the case when a proton is expected to be transferred before the hydride, then naturally the tendency of the proton donor to release a proton should be higher than the tendency of the hydride source to release hydride (and vice versa for case b). On the other hand for simultaneous hydride and proton transfer, both the hydride and proton should have medium hydridicity and acidity. This is often seen in "bifunctional catalysis". Herein we will discuss "proton before hydride" and "simultaneous proton and hydride transfer" mechanism in details.

Ionic hydrogenation via "proton before hydride transfer"

Ionic hydrogenation was originally coined for hydrogenations of organic compounds using hydride and proton sources. The first stoichiometric ionic hydrogenation was developed by Kursanov and co-workers in 1974 using stoichiometric quantities of CF_3CO_2H acid and Et_3SiH as

the hydride-transfer reagent.[40] Later on this concept was also applied to appropriate related types of stoichiometric and catalytic reactions in organometallic chemistry.

In 1985 the Darensbourg[41] and Gibson[42] groups reported the reduction of aldehydes by group 6 carbonyl hydrides and CH_3CO_2H. Bullock and coworkers systematically investigated stoichiometric hydrogenation of alkenes, alkynes and carbonyl groups since 1989 using molybdenum and tungsten hydride complexes. [43, 44, 45] They also reported an isopropyl alcohol complex which was formed during stoichiometric reduction of aldehydes and ketones (Equation 1.1) using $HW(CO)_3Cp$ (H^- donor) and triflic acid (H^+ donor).[46]

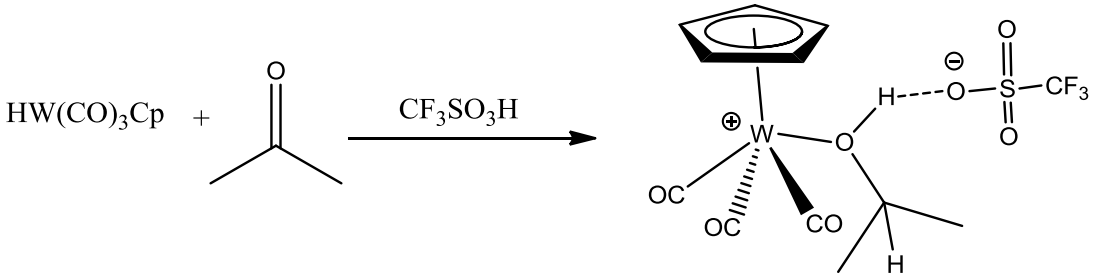

Equation 1.1

Detailed kinetic on stoichiometric hydrogenation of aldehyde revealed that such reactions involve the rapid, reversible protonation of the substrate olefin or ketone, followed by hydride transfer from the metal (or the Si of the silane) as shown in (Equation 1.2).

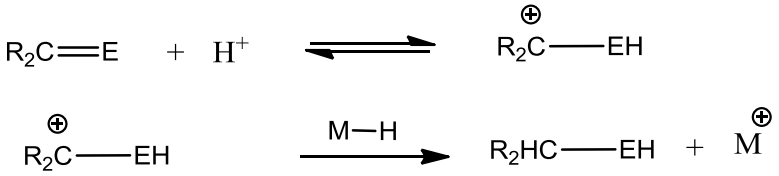

E = CHR, O

Equation 1.2

The advantages of using transition metal hydride complexes in ionic hydrogenations are the potential of developing catalytic cycles in which H_2 can be used as the source of both the H^+ and H^-. In contrast to hydrosilanes such as $HSiEt_3$, which may in many cases immediately evolve hydrogen upon protonation, many transition-metal hydrides can be protonated to give stable

dihydrogen complex in which an H_2 ligand is bound to the metal, while protonation at the metal gives a dihydride complex (Scheme 1.8).

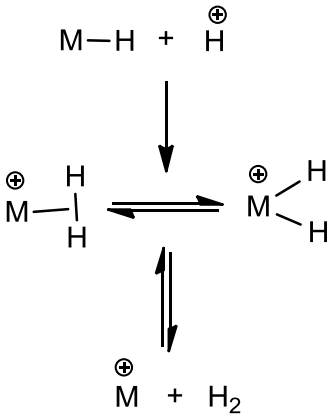

Scheme 1.8. Protonation of a metal hydride and subsequent formation of H_2

As we already discussed earlier (Section 1.2.1), dihydrogen complexes generally have a higher kinetic acidity compared to the corresponding dihydrides,[6a, 13] so this might be expected to favor dihydrogen complexes as proton donors in ionic hydrogenations. However, it will not necessarily make a big difference whether a dihydride or a dihydrogen complex (or an equilibrium mixture of the two) is the proton donor, as long as this species is sufficiently acidic.

Indeed, Bullock and coworkers demonstrated that when aldehydes or ketones were added to the cationic tungsten dihydride complex $[W(Cp)(CO)_2(PMe_3)(H)_2]^+$, stoichiometric hydrogenation occurs within a few minutes at room temperature where the source of the proton and hydride is the same metal centre.[47]

The catalytic ionic hydrogenation of 3-pentanone with $[CpM(CO)_2(PR_3)(\eta^1\text{-}O{=}CEt_2)]^+A^-$, where M = Mo or W, R = CH_3, Ph, or Cy, and A^- = PF_6^-, BF_4^-, or $BAr^F{}_4$ - [$Ar^F{}_4$ = 3,5-bis-(trifluoromethyl)phenyl] (Equation 1.3)[48, 49] was also reported by Bullock. The hydrogenation work under the mild conditions of 23 °C and 4 atm H_2. However the reaction progress slowly with a maximum TOF of 2 h^{-1} for M=Mo and PR_3 = PCy_3.

A mechanism with "proton before hydride transfer" was also proposed as shown in Scheme 1.9.

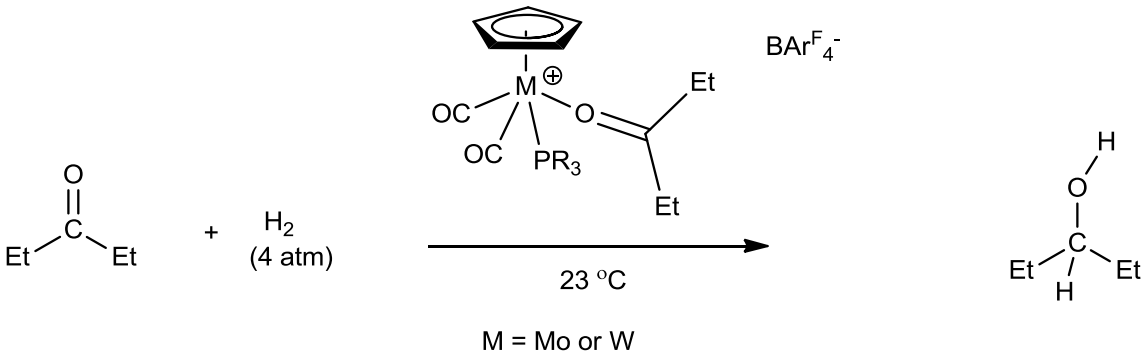

Equation 1.3

A series of Mo and W complexes and also platinum group metals as catalysts were reported subsequently for the ionic hydrogenation of ketones.[50, 51-54]

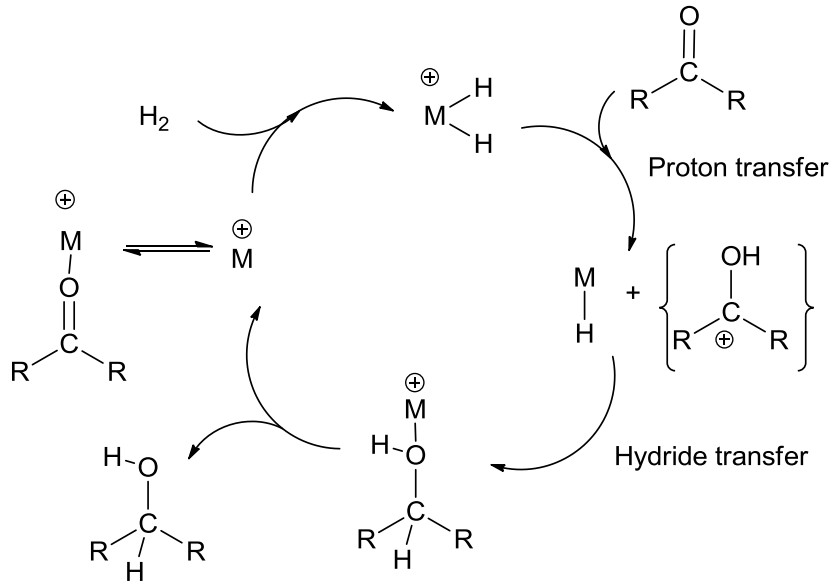

Scheme 1.9. Mechanism proposed by Bullock for catalytic ionic hydrogenations of ketones.

The concept of "ionic hydrogenation" was not only limited to olefins and ketones. It could be extended for ionic hydrogenation of C=N double bonds by Ito and coworkers.[55]

In 2001 Norton and coworkers[56] demonstrated that platinum group metal based Ru hydride complexes bearing chiral diphosphanes can catalyze enantioselective hydrogenations of C=N double bonds of iminium cations. An ionic mechanism with was also proposed based on

mechanistic investigation where hydride transfer to the iminium cation was found to be enantio-discriminating and rate deetermining step (Equation 1.4).

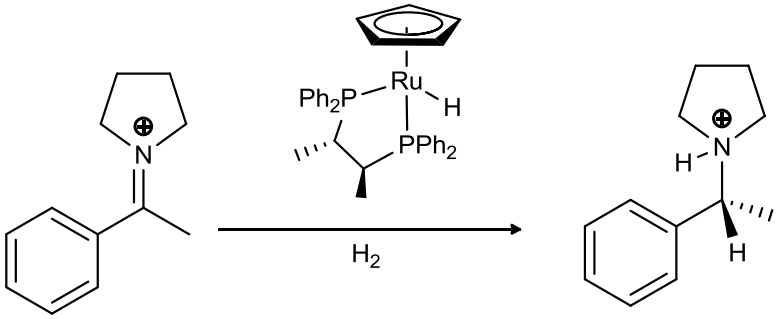

Equation 1.4

Ionic hydrogenation via "simultaneous Proton and hydride transfer" (Metal Ligand Bifunctional Catalysis)

In the past few decades several catalysts have been discovered that appear to proceed through ionic mechanisms in which the source of the proton is a NH or a OH bond, and the hydride is delivered from a metal hydride species. The mechanism of this type of ionic hydrogenation involves ligand assisted heterolytic splitting of hydrogen and simultaneous proton and hydride transfer to the substrate *via* a six membered cyclic transition state (Scheme1.10).

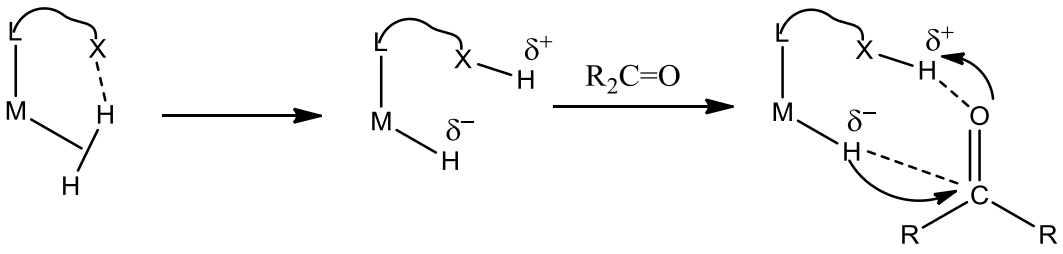

Scheme 1.10. General scheme for metal ligand bifunctional catalysis with the crucial H transfers occuring in the secondary coordination sphere.

The substrate binding to the catalyst is not necessaryly needed and the H transfers occurs in most of the cases in the "secondary coordination sphere".[28] Noyori has denoted the term of concerted transfer of proton and hydride as "metal-ligand bifunctional catalysis". Often they are denoted as protonic-hydridic reactions.

Plenty of typical bifunctional catalysis have recently been reported by several groups such as Shvo-Casey type "ionic hydrogenations", and also those established by the groups of Noyori, Morris, and Ikariya.[57-60]

Shvo's bifunctional catalytic system

In the mid 1980s a robust bimetallic ruthenium complex $[2,3,4,5\text{-}Ph_4(\eta^5\text{-}C_4CO)]_2H\}Ru_2(CO)_4(\mu\text{-}H)$ was reported by Shvo and co-workers which found enormous utility as a versatile catalyst for hydrogen transfer reactions in organic synthesis such as the hydrogenation of aldehydes, alkenes, and alkynes.[7, 61] The catalyst precursor is joined by a bridging hydride and an O-H-O hydrogen bond connecting the two cyclopentadienone ligands (Scheme 1.11). The dimeric precatalyst is in equilibrium with a monomeric reducing hydroxycyclopentadienyl hydride as hydrogen donor and an unsaturated oxdizing dienone dicarbonyl species as hydrogen acceptor, both being involved in the catalytic cycle.

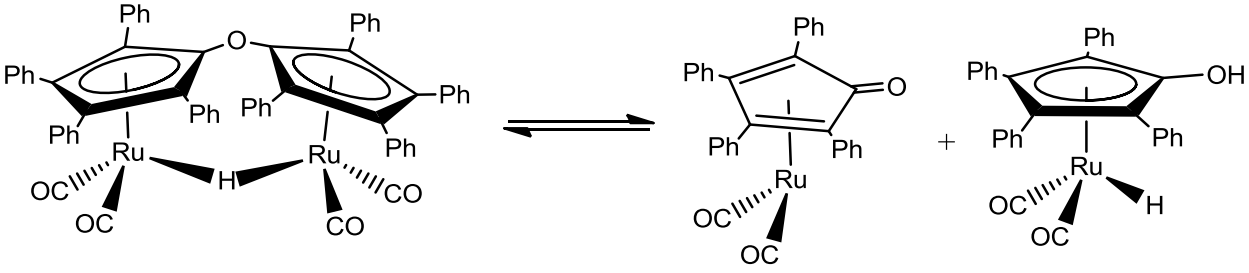

Scheme 1.11. Activation equilibrium of Shvo s bifunctional Ruthenium precatalyst.

Detailed mechanistic studies based on low temperature kinetics and kinetic isotope effects indicated a concerted second coordination-sphere mechanism involving simultaneous transfer of hydride from ruthenium and proton from the CpOH group (Scheme 1.12).[62]

However the mechanistic study still remain controversial since a primary coordination sphere mechanism would also cope with the experimental observations.[63, 64]

Recently our group has developed an active rhenium catalyst based on the principles of Shvo's catalysis. The new type of hydroxycyclopentadiene Re(I) nitrosyl complexes $[Re(H)(NO)(L)(C_5H_4OH)]$ (L = PCy_3, $P\mathit{i}Pr_3$) are active catalysts in the transfer hydrogenation of

ketones and imines using 2-propanol as solvent and as H_2 donor. DFT calculations suggested a secondary-coordination-sphere concerted H transfer mechanism.[65]

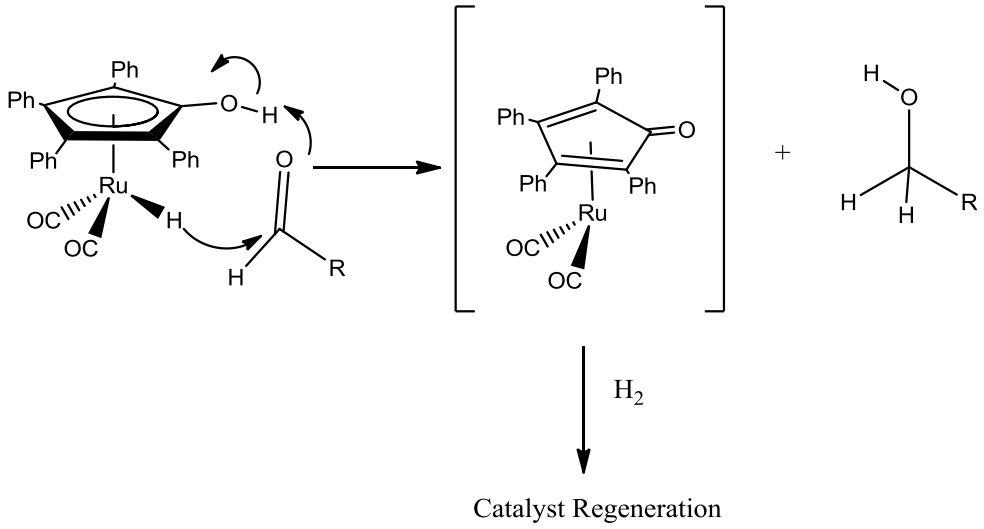

Scheme 1.12. Proposal of Casey for the concerted delivery of H^+ and H^- for ketone and imine hydrogenation

Noyori bifunctional catalytic system

In 1995 Noyori's group found out that the activity of ketone hydrogenation using $RuCl_2(PPh_3)_3$ system as catalyst could be remarkably improved with the addition of ethylenediamine and a solution of KOH in 2-propanol (Equation 1.5).[66] The screening of various amines revealed that at least one primary or secondary amine end was necessary along with the inorganic base to improve activities. The notion of a "N-H effect" in catalytic activity led to tremendous explosion in the field of metal ligand bifunctional catalysis.

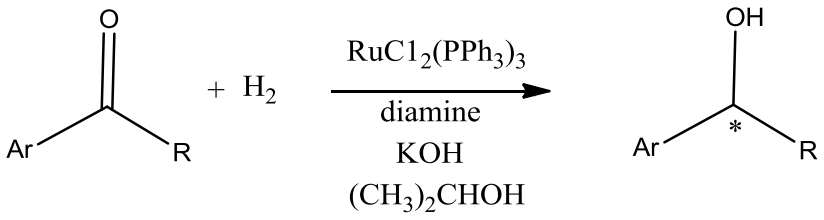

Equation 1.5

Subsequently Noyori and coworkers isolated the stable precatalysts amino phosphine complexes *trans*-[$RuCl_2$(phosphane)$_2$(1,2-diamine)] which showed more rapid hydrogenation of ketones than the in situ composed systems (Figure 1.3).[67, 68]

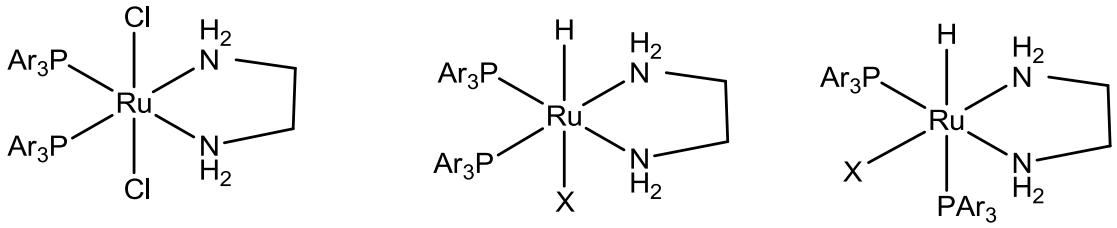

Figure 1.3. Noyori bifunctional catalyst precursor (left) and active catalysts (middle and right); (X = OR, H).

In these hydrogenation, the metal and the ligand participate cooperatively in the bond-forming and breaking processes. A more detailed mechanistic model is given in Scheme 1.13. The 18-electron-RuH species reduces the ketone substrate by the pericyclic mechanism and the formal 16-electron Ru-amide complex reacts directly with H_2 in a [2+2] manner, or by a stepwise mechanism assisted by an alcohol and a base, to give back the reducing RuH form. The reduction process of the Ru-H species is established by the hydrogen-bonded NH_2 end of the diamine ligand, which forms a fac relationship with the hydride ligand in the octahedral geometry. Neither ketone substrate nor alcoholic product interacts with the metallic center throughout the hydrogenation.

Similarly $RuCl_2$(diphosphine)(diamine) systems combining chiral diphosphines such as (*R*)-BINAP, and chiral primary diamines are also extremely active hydrogenation catalysts. In addition they are effective enantioselective catalysts for the hydrogenation of a wide variety of prochiral ketones and imines.[24] Morris and co-workers have also developed highly reactive Ru catalysts that appear to function by a similar Noyori type mechanism.[68, 69]

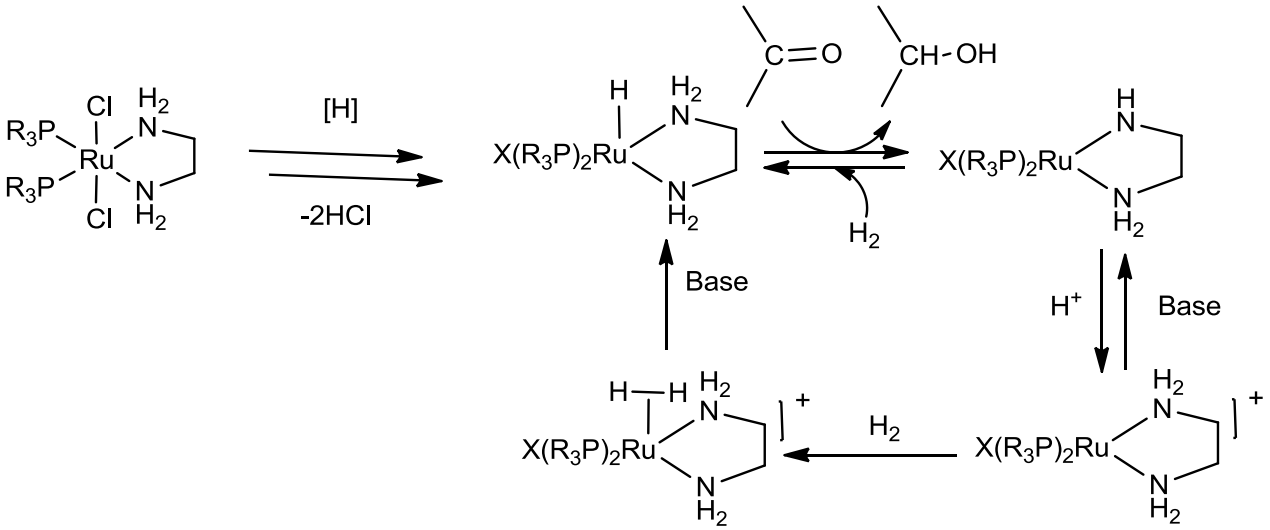

Scheme 1.13. Noyori's metal ligand bifunctional catalysis for hydrogenation of ketones applying a $RuCl_2(PR_3)_2$(diamine)/base system in 2-propanol. (X = H, OR)

Furthermore, Noyori and Ikariya and co-workers also found that "N-H effect" is also in operation in the catalyses with new chiral Ru catalysed highly efficient asymmetric transfer hydrogenation of ketones and imines[70] bearing N-sulfonylated 1,2-diamines and amino alcohols as chiral ligands. Exemplary Noyori's effective transfer hydrogenation precatalyst, true catalyst and active species are shown in Figure 1.4.

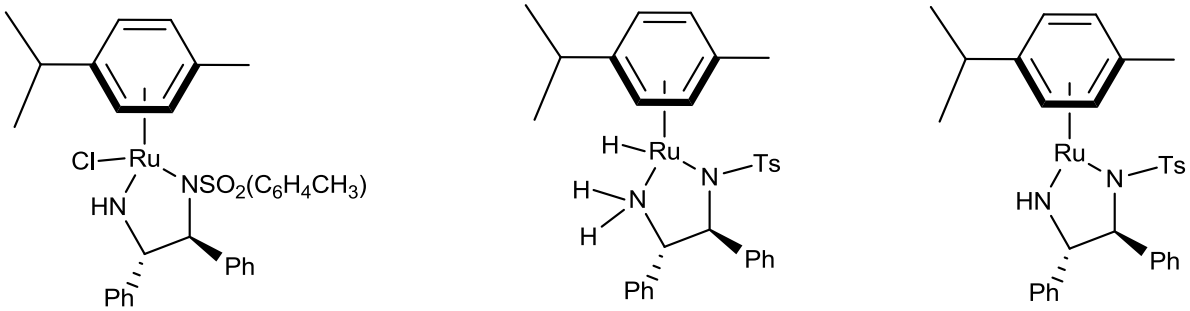

Figure 1.4. Noyori s transfer hydrogenation precatalyst, true catalyst and active species.

A range of experimental findings, kinetic isotope effect measurement by Casey et al, theoretical study performed by Noyori, Andersson and vanLeeuwen showed that this transfer hydrogenation takes place by metal-ligand bifunctional mechanism.[71]

The catalysts also show a secondary coordination sphere hydride transfer mechanism (Scheme 1.14). The hydride transfer from ruthenium and proton transfer from the amino group to the C=O bond of a ketone or C=N bond of an imine leads to the formation of the alcohol or amine products, respectively. The amido complex that is produced is unreactive to H_2 (except at high pressures), but readily reacts with *i*PrOH or formate to regenerate the hydride catalyst.

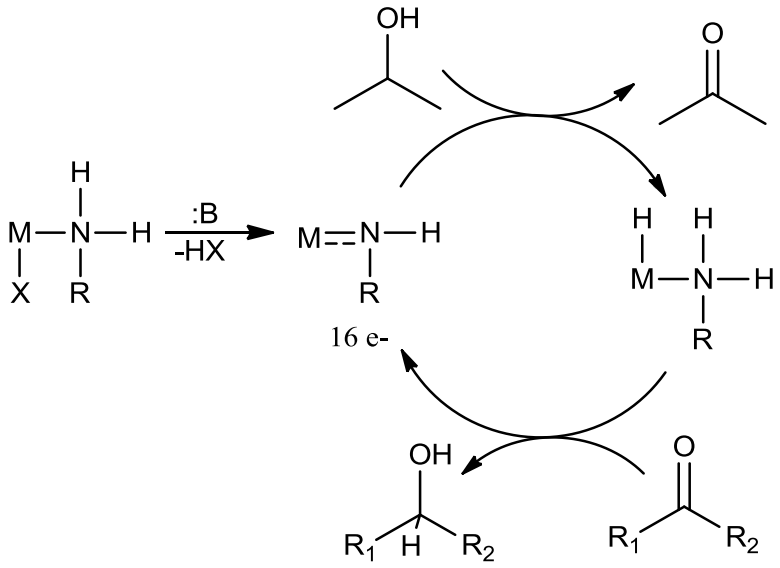

Scheme 1.14. Noyori's metal ligand bifunctional catalysis in transfer hydrogenations

However similar to the controversy of Shvo type catalysts for imine hydrogenations, Backvall and coworkers[72] started to argue in 2006 based on experimental evidence that in transfer hydrogenations of imines the concerted mechanism proposed for the hydride/proton addition of species Ru(H)(TsDPEN)(p-cymene) to ketones (aldehydes) and is not operating for imines (Equation 1.6). The hydride species Ru(H)(TsDPEN)(p-cymene), which reacts fast with ketones (aldehydes), does not react with imines and for the case of imine acidic activation is needed indicating stepwise but not concerted H transfers, which could occur by protonation of the imine with acid leading to activation of the C= N bond prior to hydride transfer (Equation 1.6).

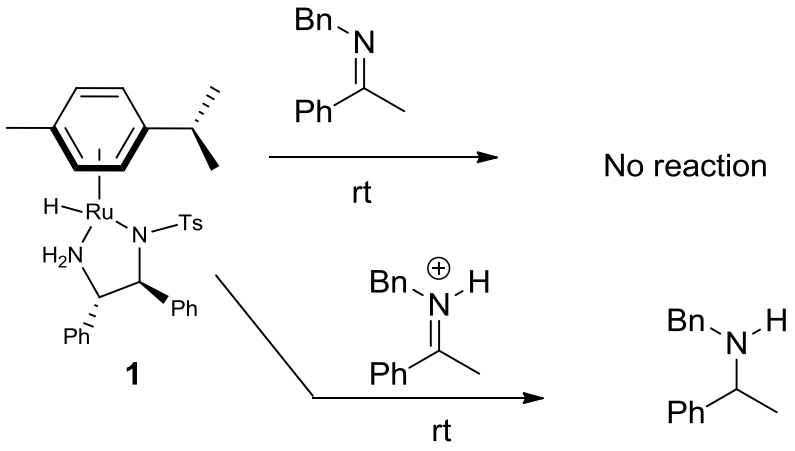

Equation 1.6

Furthermore, Milstein's pincer-type bifunctional catalysts are so active since they get support by the aromatization-dearomatization of the pyridyl ligand facilitating hydrogenations and transfer hydrogenations.[25a, 73] Similarly Grützmacher's diolefinic amido Rh catalysts are based on the Rh/NH bifunctionality. They promote hydrogenation and transfer hydrogenation of olefinic compounds.[74] Based on the understanding from a number of profound quantitative studies, such processes often show low activation barriers and are therefore valuable alternatives to Wilkinson-type hydrogenations.

1.3 Hydrosilylation

Related to homogeneous hydrogenations are hydrosilylations apllying the Si-H bond for reductions. Hydrosiliylations are meanwhile applications of homogeneous catalysis of general importance.

Hydrosilylation is the 1,2- addition of Si-H bonds to unsaturated functions like C=C, C=O or C=N bonds. This reaction is widely used for both large and small scale synthesis. The addition of a Si-H bond to alkenes gives alkylsilanes and for aldehydes and ketones yields silyl ethers and in the case of imines the silylamines are generated.

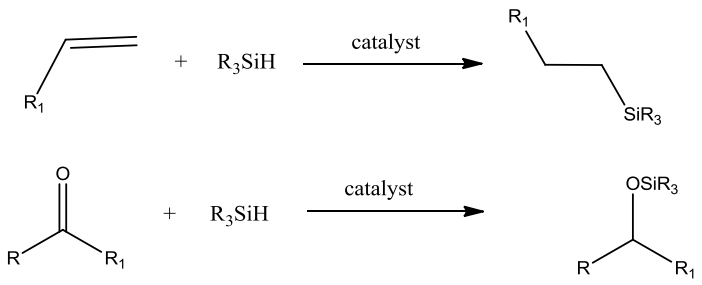

Scheme 1.15. Hydrosilylation products of alkenes and ketones

In the context of homogeneous catalysis the most important application of hydrosilylation reaction is in the "curing" of silicone rubber. Such curing leads to cross-linking of the polymer chains and turns a syrupy polymer to a gum rubber. Furthermore, hydrosilylations are often used as convenient alternatives to homogeneous hydrogenations. For example the hydrosilylation of aldehyde and ketones leads to the reduction of carbonyl compounds forming silyl ethers, which are the protected form of alcohols.

Since the discovery of Speier's catalyst[75] H_2PtCl_6 in 1957, numerous papers have appeared relating to the scope of this transformation and the possible mechanism involved.

Today a large variety of catalyst is available for hydrosilylation and most of these catalysts operate according to the well established Chalk-Harrod mechanism.[76]

In the classical Chalk-Harrod mechanism of olefin hydrosilylation a Si-H bond adds oxidatively to the metal atom of an olefin complex (Scheme 1.16). Migration of the hydride ligand onto the coordinated olefin generates the silyl alkyl intermediate, which undergoes reductive elimination to form the Si-C bond of the product. Later this mechanism was adopted by Ojima for hydrosilylation of carbonyl compounds.[77]

Recently high-valent transition metal oxo complexes of Re and Mo have been utilized in catalytic hydrosilylation reactions[78] and their mechanisms were investigated in details. In one example, namely *cis*-$Re(O)_2I(PPh_3)_2$, Toste et al. proposed an unconventional mechanism in which the silane (Si-H) adds across one of the Re=O multiple bonds.[79] In a recent publication Tilley et al. describe a catalytically active silylene complex, the Si-H bond of which adds to olefins. The catalyst for this special type of hydrosilylation is the base-stabilized silylene complex $[Cp^*(P\textit{i}Pr_3)(H)_2Ru{=}Si(H)Ph{\cdot}Et_2O][B(C_6F_5)_4]$ ($Cp^*=\eta^5$-C_5Me_5), in which the ether is

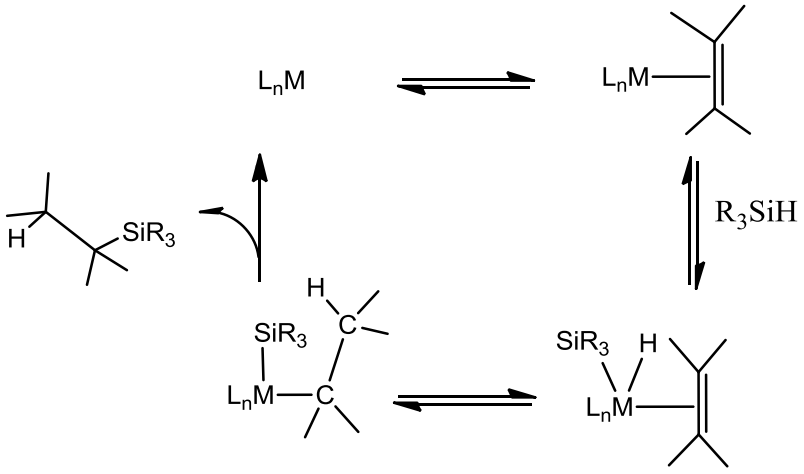

Scheme 1.16. Classical Chalk-Harrod mechanism for the hydrosilylation of olefins.

only loosely bound.[80] Bullock and coworkers[81] demonstrated a tungsten carbene complexes catalyze the hydrosilylation of ketones and exhibit an unusual property in the hydrosilylation of aliphatic substrates, that the catalyst precipitates at the end of the reaction. The hydrosilylations are carried out under solvent-free conditions, using the ketone and $HSiEt_3$ as solvent. the catalyst precipitates and can be readily recovered and used again. The complex $[W(Cp)(CO)_2(IMes)(SiEt_3)H]^+[B(C_6F_5)_4]^-$ (IMes = the carbene ligand 1,3-bis(2,4,6-trimethylphenyl)-imidazol-2- ylidene) is a resting state of the reaction.

Furthermore, asymmetric hydrosilylation with high enantioselectivities,[82] ionic hydrosilylations[83] with heterolysis of the Si-H bond, Lewis acid[84] catalysed hydrosilylation reactions and also early transition metal[85] catalysed hydrosilylation which proceed *via* sigma bond metathesis is well documented by several authors.

1.4 Goal of the Work

Platinum group metals dominate a very significant part of contemporary catalysis research. Their ability to maintain reversible redox cycles, the excellent tunability of their steric and electronic characteristics by a host of ligand sets, the pronounced affinity to a π systems, and an outstanding compatibility with many functional groups are just the most elementary of the many factors that contribute to this privileged roles. Yet these noble metals in general are very expensive, whereas other commonly used late transition metals are either toxic and/or require special treatment of the

waste stream due to serious environmental concerns (cobalt, nickel, copper). Therefore, it is a worthwhile endeavor to search for possible alternatives in a quest for more affordable and sustainable methodology.

There is an increasing interest to substitute such catalysts by more easily available biorelevant metals. In this respect homogeneous catalysis using iron and with middle transition elements molybdenum and tungsten complexes offers highly attractive alternatives. Indeed this area has become one of the 'hot topics' in catalysis and several research groups have been inspired to join on this particular issue of "Cheap Metals for Noble Tasks".[86]

Table 1.3 Approximate Cost (US $) per Mole of Transition Metals.

Sc	Ti	V	Cr	Mn	Fe	Co	Ni	Cu	Zn
13,000	13	180	8	5	3	28	8	2	
Y	Zr	Nb	Mo	Tc	Ru	Rh	Pd	Ag	Cd
660	51	72	23	---	5,700	67,000	6,600	240	23
La	Hf	Ta	W	Re	Os	Ir	Pt	Au	Hg
600	820	500	37	5,400	15,000	14,000	30,000	17,000	49

Costs calculated in US dollars from Strem '08-'10 catalog using lowest cost metal powder with purity ≥99%. Mercury cost calculated from lowest cost pure elemental form.

In this context, significant attentation have already been paid on iron catalysis[87] and indeed progress has been achieved but exploration on molybdenum and tungsten based homogeneous catalysis still remain insufficiently explored.

Therefore the goal of this Thesis is to develop earth abundant and less toxic molybdenum and tungsten metal based highly efficient catalysts for homogeneous hydrogenations and hydrosilylations.

Some initial work has already been carried out by Bullock for ionic hydrogenation of ketones using Mo and W and also of hydrosilylation by several other groups as they were discussed in Section 1.2.3 and Section 1.3. However the catalytic activities of these systems were generally quite low and incomparable with the activities achieved with platinum group metals.

Since in the past few decades our group has investigated the ligand sphere tuning properties and reactivity of transition metal hydride complexes.[88, 89] The crucial influence was proved to be the nitrosyl ligand location *trans* to the hydride and was found to be effecting the hydridicity of the complexes to promote hydride transfer to unsaturated substrates. Furthermore, a recent report from our group has revealed that nitrosyl ligand is even capable of contributing significantly in homogeneous hydrogenation through binding with a super electrophile leaving a coordinative unsaturation site on the metal centre.[49]

In this dissertation synthesis of several molybdenum and tungsten nitrosyl complexes in various oxidation states (+II, +I, 0) will be reported bearing the chelating tridentate $(i\text{Pr}_2\text{PCH}_2\text{CH}_2)_2\text{PPh}$, ($\text{etp}^i\text{p}$) ligand, the cooperating $(i\text{Pr}_2\text{PCH}_2\text{CH}_2)_2\text{NH}$, ($\text{PN}^H\text{P}$) ligand and the large bite angle $(\text{Ph}_2\text{PC}_6\text{H}_4)_2\text{O}$, (DPEphos) ligand.

Several inspirations for this work came from our group by Balz Dudle where rhenium (+I) diphosphine complexes bearing in addition an ethylene ligand and a hydride functionality allowed to accomplish Osborn type hydrogenations of olefins.[90] We expected that the design of similar type of complexes with molybdenum and tungsten bearing chelate polydentate ligand might lead us to achieve efficient catalysts for olefin hydrogenations. Subsequently we also extended the work of our group by Alexander Dybov for ionic hydrogenation where molybdenum and tungsten nitrosyl complexes bearing bidentate phosphine ligands showed catalytic activity towards imine hydrogenation at room temperature with "proton before hydride" mechanism.[91] We set out to replace bidentate phosphine ligands with a tridentate chelate phosphines which helped to stabilize the catalyst at higher temperatures to improve the catalytic performance.

Following two types of target systems (Figure 1.5) of molybdenum and tungsten nitrosyl complexes bearing the tridentate $(i\text{Pr}_2\text{PCH}_2\text{CH}_2)_2\text{PPh}$ ligand will be reported here and developed for olefin and imine hydrogenation catalyses.

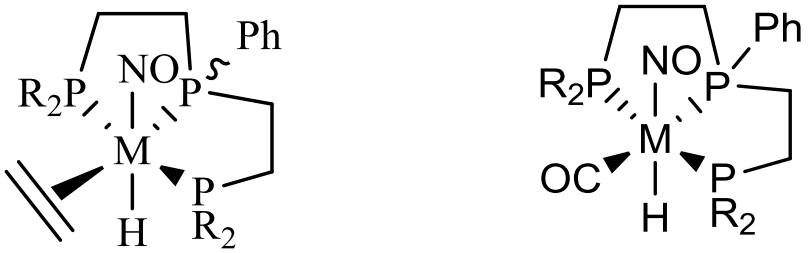

Figure 1.5. Target molecules for olefin hydrogenations (left) and ionic hydrogenation of imines (right), M = Mo, W; R = $i\text{Pr}_2$.

Furthermore, metal ligand bifunctional catalysis has attracted much attention in recent years. In bifunctional catalysis simultaneous transfer of the proton and the hydride is perceived to happen in the secondary coordination sphere. In principal, one can expect in such cases of catalysis less influence from the metal center. Therefore we realised that by the design of a Noyori type catalyst the goal to find an efficient hydrogenation catalyst could also be reached. Therefore molybdenum and tungsten amido catalysts suited for the bifunctional hydrogenation of imines bearing the protic $(i\text{Pr}_2\text{PCH}_2\text{CH}_2)_2\text{NH}$ ligand will also be pursued. (Figure 1.6).

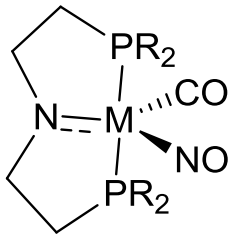

M = Mo, W; R = *i*Pr$_2$

Figure 1.6. Target catalyst for the Noyori type bifunctional hydrogenation of imines

Finally, the catalytic efficiency of a novel molybdenum nitrosyl complex bearing $(\text{Ph}_2\text{PC}_6\text{H}_4)_2\text{O}$, (DPEphos) ligand (Figure 1.7) will be probed in the hydrosilylations of aldehyde and ketones.

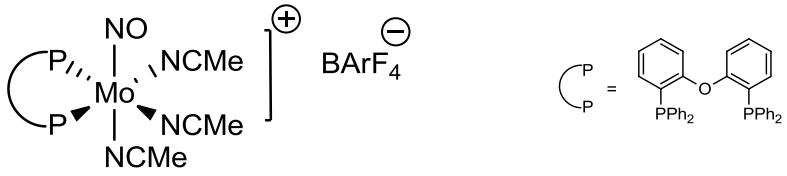

Figure 1.7. Target molecule for hydrosilylation of aldehydes and ketones

1.5 REFERENCES

(1) Crabtree, R. H. *The Organometallic Chemistry of the Transition Metals*, Wiley VCH, Weinheim, **2005**.

(2) Bowker, M. *Basis and Applications of Heterogeneous Catalysis*, OUP, New York, **1998**.

(3) Bhaduri, S.; Mukesh, D. *Homogeneous Catalysis: Mechanisms and Industrial Applications* Wiley VCH, Weinheim, **2000.**

(4) (a) Calvin, M. *Trans. Faraday Society*, **1938**, *34*, 118. (b) Calvin, M. *J. Am. Chem. Soc*., **1939**, *61*, 2230.

(5) Osborn, J. A.; Jardine, F. H.; Young, J. F.; Wilkinson, G. *J. Chem. Soc.* A **1966**, *12*, 1711- 1732.

(6) (a) Kubas, G. J. Metal Dihydrogen and σ-Bond Complexes: Structure, Theory, and Reactivity, Kluwer, New York, **2001**. (b) Kubas, G. J. *Chem. Rev*. **2007**, *107*, 4152.

(7) Shvo, Y.; Czarkie, D.; Rahamim, Y.; Chodosh, D. F.; *J. Am. Chem. Soc*. **1986**, *108*, 7400.

(8) Knowles, W. S.; Noyori, R.; *Acc. Chem. Res*. **2007**, *40*, 1238.

(9) (a) Welch, G. C.; Juan, R. R. S.; Masuda, J. D.; Stephan, D. W., *Science* **2006**, *314*, 1124. (b) Chase, P. A.; Welch, G. C.; Jurca, T.; Stephan, D. W. *Angew. Chem*. **2007**, *119*, 8196; *Angew. Chem. Int. Ed*. **2007**, *46*, 8050.

(10) (a) Dewar, M. J. S. *Bull. Soc. Chim. Fr*. **1951**, 18, C79. (b) J. Chatt, J.; Duncanson, L. A. J. Chem. Soc. **1953**, 2929. (c) Kubas, G. J. *J. Organometal. Chem.* **2001**, *635*, 37.

(11) Kubas, G. J.; Ryan, R. R.; Swanson, B. I.; Vergamini, P. J.; Wasserman, H. J., *J. Am. Chem. Soc.* **1984,** *106*, 451.

(12) (a) Hieber, W.; Leutert, F., *Naturwissenschaften* **1931,** *19*, 360. (b) Hieber, W.; Schulten, H., *Z. Anorg. Allg. Chem.* **1937,** *232*, 29.

(13) (a) Jessop, P. G.; Morris, R. H. *Coord. Chem. Rev.* **1992**, *121*, 155-284. (b) Heinekey, D. M.; Oldham, W. J. Jr., *Chem. Rev.* **1993**, *93*, 913-926.

(14) (a) Morris, R. H. *Can. J. Chem.* **1996**, *74*, 1907. (b) Jia G.; Lau, C. P. *Coord. Chem. Rev.*, **1999**, *83*, 190-192.

(15) Berke, H. *ChemPhysChem* **2010**, *11*, 1837-1849.

(16) Kubas, G. J., *Catal. Lett.* **2005**, *104*, 79.

(17) (a) Evans, D.; Osborn, J. A.; Jardin F. H.; Wilkinson, G., *Nature*, **1965**, *208*, 1203. (b) Hallman, P. S.; McGarvey, B. R.; Wilkinson, G., *J. Chem. Soc*. *A*, **1968**, 3143.

(18) (a) Clot, E.; Eisenstein, O.; Lee, D. H.; Macchioni, A.; Crabtree, R. H., *New J. Chem.* **27**, 80, 2003. (b) Heinekey, D. M., *J. Am. Chem. Soc.* **2005**, *127*, 850. (c) Crabtree, R. H. *Angew. Chem.Int.Ed.* **1993**, *32*, 789.

(19) (a) Peruzzini, M.; Poli, R., *Recent Advances in Hydride Chemistry*, Elsevier, Amsterdam, **2001**. (b) Linck, R. C.; Pafford, R. J.; Rauchfuss, T. B., *J. Am. Chem. Soc.*, **2001**, *123*, 8856. (c) Ienco, A.; Calhorda, M. J.; Reinhold, J.; Reineri, F; Bianchini, C; Peruzzini, M; Vizza F.; Mealli, C., *J. Am. Chem. Soc.*, **2004**, *126*, 11954. (d) Ohki, Y.; Takikawa, Y.; Sadohara, H.; Kesenheimer, C.; Engendahl, B.; Kapatina, E.; Tatsumi, K.; *Chem.-Asian J*., **2008**, *3*, 1625; (e) Maire, P.; Büttner, T.; Breher, F.; Le Floch, P.; Grützmacher, H., *Angew. Chem., Int. Ed*., **2005**, *44*, 6318; (f) Shvo, Y.; Czarkie, D.; Rahamim, Y.; Chodosh, D. F., *J. Am. Chem. Soc*., **1986**, *108*, 7400. (g) Casey, C. P.; Johnson, J. B.; S. W. Singer, S. W.; Cui, Q., *J. Am. Chem. Soc*., **2005**, *127*, 3100.

(20) (a) Schneider, S.; Meiners, J.; Askevold, B.; *Eur. J. Inorg. Chem.* **2012**, 412-429. (b) Grützmacher, H., *Angew. Chem. Int. Ed*. **2008**, *47*, 1814-1818.

(21) Berke, H.; Jiang, Y.; Xianghua, Y.; Chungfang, J.; Chakraborty, S.; Landwehr, A.; *Topics Curr. Chem*. **2013**.

(22) (a) Fryzuk, M. D.; MacNeil, P. A., *Organometallics* **1983**, *2*, 355. (b) Fryzuk, M. D.; MacNeil, P. A. *Organometallics* **1983**, *2*, 682. (c) Fryzuk, M. D.; MacNeil, P. A., Rettig, S. J. *J. Am. Chem. Soc.* **1987**, *109*, 2803.

(23) Fryzuk, M. D.; Montgomery, C. D.; Rettig, S. J.; *Organometallics* **1991**, *10*, 467.

(24) Noyori, R.; Okhuma, T. *Angew. Chem*. **2001**, *113*, 40; *Angew. Chem. Int. Ed*. **2001**, *40*, 40.

(25) (a) Zhang, J.; Leitus, G.; Ben-David, Y.; Milstein, D. *J. Am. Chem. Soc*., **2005**, *127*, 10840. (b) Zhang, J.; Leitus, G.; Ben-David Y.; Milstein, D. *Angew. Chem., Int. Ed*., **2006**, *45*, 1113. (c) Ben-Ari, E.; Leitus, G.; Shimon, L. J.W.;Milstein, D. *J. Am. Chem. Soc.* **2006**, *128*, 15390-15391.

(26) Gunanathan, C.; Gnanaprakasam, B.; Iron, M. A.; Shimon, L. J. W.; Milstein, D. *J. Am. Chem. Soc*. **2010**, *132*, 14763-14765.

(27) Bullock, R. M. *Chem. Eur. J*. **2004**, *10*, 2366-2374.

(28) Clapham, S. E.; Hadzovic, A.; Morris, R. H., *Coord. Chem. Rev*., **2004**, *248*, 2201.

(29) (a) Osborn, J. A.; Wilkinson, G.; Young, J. F. *Chem. Commun*. **1965**, 17. (b) Bennett, M. A. Longstaff, P. A. *Chem. Ind. (London)* **1965**, 846.

(30) (a) Coffey, R. S. British Patent 1121642, **1965**. (b) Vaska, L.; Rhodes, R. E. *J. Am. Chem. Soc*. **1965**, *87*, 4970.

(31) Jardine, F. H. *Progress Inorg. Chem*. **1981**, *28*, 63.

(32) (a) Halpern, J. *Inorg. Chim. Acta* **1981**, *50*, 11, (b) Landis, C. R.; Halpern, J. *J. Am. Chem. Soc.* **1987**, *109*, 1746-1754.

(33) (a) Shapley, J. R.; Schrock, R. R.; Osborn, J. A. *J. Am. Chem. Soc*. **1969**, *91*, 2816. (b) Schrock, R. R.; Osborn, J. A. *J. Am. Chem. Soc*. **1976**, 98, 2134-2143. (c) Schrock, R. R.; Osborn, J. A. *J. Am. Chem. Soc.* **1976**, *98*, 2143. (d) Schrock, R. R.; Osborn, J. A. *J. Am. Chem. Soc.* **1976**, *98*, 4450. (e) Schrock, R. R.; Osborn, J. A. *Chem. Commun*. **1970**, 567.

(34) (a) Bath, S. S.; Vaska, L. *J. Amer. Chem. Soc.* **1965**, *85*, 3500. (b) Vaska, L. *Inorg. Nucl. Chem. Lett*. **1965**, *1*, 89.

(35) (a) Evans, D.; Yagupsky, G.; Wilkinson, G. *J. Chem. Soc. (A)* **1968**, 2660. (b) Yagupsky, M.; Brown, C. K.; Yagupsky, G.; Wilkinson, G. *J. Chem. Soc. (A)* **1970**, 937.

(36) (a) O'Connor, C.; Yagupsky, G.; Evans, D.; Wilkinson, G. *Chem. Commun*. **1968**, 420; (b) O'Connor, C.; Wilkinson, G. *J. Chem. Soc. (A)* **1968**, 2665. **(**c) Yagupsky, G.; Wilkinson, G. *J. Chem. Soc. (A)* **1970**, 941.

(37) (a) Evans, D.; Osborn, J. A.; Wilkinson, G.; *J. Chem. Soc. (A)* **1968**, 3133. (b) Yagupsky, G.; Brown, C. K.; Wilkinson, G.; *Chem. Commun*. **1969**, 1244. (c) Yagupsky, G.; Brown, C. K.; Wilkinson, G. *J. Chem. Soc. (A)* **1970**, 1392. (d) Brown, C. K.; Wilkinson, G.; *J. Chem. Soc. (A)* **1970**, 2753.

(38) (a) Crabtree, R. H.; Felkin, H. Morris, G. E. *J. Organomet. Chem.* **1977**, *141*, 205. (b) Crabtree, R. H.; Felkin, H.; Fillebeen- Khan, T.; Morris, G. E. *J. Organomet. Chem.* **1979**, *168*, 183.(c) Crabtree, R. H. *Acc. Chem. Res.* **1979**, *12*, 331. (d) Crabtree, R. H.; Demou, P. C.; Eden, D.; Mihelcic, J. M.; Parnell, C. A.; Quirk, J. M.; Morris, G. E. *J. Am. Chem. Soc.* **1982**, *104*, 6994.

(39) (a) Jiang, Y., Hess, J., Fox, T., Berke H. *J. Am. Chem. Soc*. **2010**, *132*, 18233-18247. (b) Jiang, Y.; Birgitta Schirmer, B.; Blacque, O.; Fox, T.; Grimme, S.; Berke H. *J. Am. Chem. Soc*. **2013**, *135*, 4088-4102.

(40) Kursanov, D. N.; Parnes, Z. N.; Loim, N. M. *Synthesis*, **1974**, 633-651.

(41) Gaus, P. L.; Kao, S. C.; Youngdahl, K.; Darensbourg, M. Y. *J. Am. Chem. Soc.* **1985**, *107*, 2428-2434.

(42) Gibson, D. H.; El-Omrani, Y. S. *Organometallics* **1985**, *4*, 1473-1475.

(43) (a) Bullock, R. M.; Rappoli, B. J. *J. Chem. Soc., Chem. Commun.* **1989**, 1447-1448.

(44) Bullock. R. M.; Song, J.-S. *J. Am. Chem. Soc.* **1994**, *116*, 8602-8612.

(45) Luan, L.; Song, J.-S.; Bullock, R. M. *J. Org. Chem.* **1995**, *60*, 7170-7176.

(46) Song, J.-S.; Szalda, D. J.; Bullock, R. M.; Lawrie, C. J. C.; Rodkin, M. A.; Norton, J. R. *Angew. Chem., Int. Ed.* **1992**, *31*, 1233-1235.

(47) Song, J. S, Szalda, D. J., Bullock, R. M., *Organometallics* **2001**, *20*, 3337-3346.

(48) Bullock, R. M.; Voges, M. H. *J. Am. Chem. Soc.* **2000**, *122*, 12594-12595.

(49) Voges, M. H.; Bullock, R. M. *J. Chem. Soc. Dalton Trans*. **2002**, 759-770.

(50) Wu, F.; Dioumaev, V. K.; Szalda, D. J.; Hanson, J.; Bullock, R. M. *Organometallics* **2007,** *26*, 5079-5090.

(51) Fagan, P. J.; Voges, M. H.; Bullock, R. M. *Organometallics* **2010**, *29*, 1045-1048.

(52) Guan, H.; Iimura, M.; Magee, M. P.; Norton, J. R.; Zhu G. *J. Am. Chem. Soc.* **2005**, *127*, 7805-7814.

(53) Namorado, S.; Antunes, M. A.; Veiros, L. F.; Ascenso, J. R.; Duarte, M. T.; Martins, A. M. *Organometallics* **2008,** *27*, 4589-4599.

(54) (a) Esteruelas, M. A.; García-Yebra, C.; E. Ońate *Organometallics* **2008,** *27*, 3029-3036. (b) Kimmich, B. F. M.; Fagan, P. J.; Hauptman, E.; Marshall, W. J.; Bullock, R. M. *Organometallics* **2005,** *24*, 6220-6229. (c) Kimmich, B. F. M.; Fagan, P. J.; Hauptman, E.; Bullock, R. M. *Chem. Commun*. **2004**, 1014-1015. (d) Dioumaev, V. K.; Szalda, D. J. Hanson, J.; Franz, J. A.; Bullock, R. M. *Chem. Commun*. **2003**, 1670-1671.

(55) (a) Minato, M.; Fujiwara, Y.; Ito, T. *Chem. Lett.* **1995**, 647-648. (b) Minato, M.; Fujiwara, Y.; Koga, M.; Matsumoto, N.; Kurishima, S.; Natori, M.; Sekizuka, .; Yoshioka, K.-i.; Ito, T. *J. Organomet. Chem.* **1998**, *569*, 139-145.

(56) Magee, M. P.; Norton J. R.; *J. Am. Chem. Soc.* **2001,** *123*, 1778-1779.

(57) (a) Casey, C. P.; Strotman, N. A.; Beetner, S. E.; Johnson, J. B.; Priebe, D. C.; Vos, T. E.; Khodavandi, B.; Guzei, I. A. *Organometallics* **2006**, *25*, 1230.

(58) (b) Casey, C. P.; Guan, H. R. *J. Am. Chem. Soc*. **2007**, 129, 5816. (c) Comas-Vives, A.; Ujaque, G.;Lledos, A. *Organometallics* **2007**, 26, 4135.

(59) (a) Noyori, R.; Hashiguchi, S. *Acc. Chem. Res*. **1997**, *30*, 97. (b) Muniz, K. *Angew. Chem*. **2005**, *117*, 6780; *Angew. Chem. Int. Ed*. **2005**, *44*, 6622. (c) Samec, J. S. M.; Bäckvall, J. E.; Anderson, P. G.; P. Brandt, P. *Chem. Soc. Rev*. **2006**, *35*, 237.

(60) (a) Ito, M.; Ikariya, T. *Chem. Commun*. **2007**, 5134. (b) T. Ikariya, A. J. Blacker, *Acc. Chem. Res.* **2007**, *40*, 1300.

(61) (a) Blum, Y.; Czarkie, D.; Rahamim, Y.; Shvo, Y.; *Organometallics* **1985**, *4*, 1459-1461. (b) Menashe, N.; Salant, E.; Shvo, Y.; *J. Organomet. Chem*. **1996**, *514*, 97-102. (c) Shvo,Y.; Goldberg, I.; Czerkie, D.; Reshef, D.; Stein, Z., *Organometallics* **1997**, *16*, 133-138.

(62) Casey, C. P.; Singer, S. W.; Powell, D. R.; Hayashi, R. K.; Kavana, M., *J. Am. Chem. Soc.* **2001**, *123*, 1090-1100.

(63) (a) Samec, J. S. M.; Ell, A. H.; Bäckvall, J. E. *Chem. Commun*., **2004**, 2748. (b) Ell, A. H.; Johnson J. B.; Bäckvall, J. E. *Chem. Commun*., **2003**, 1652.

(64) Casey C. P.; Johnson, J. B. *J. Am. Chem. Soc*., **2005**, *127*, 1883.

(65) Landwehr, A.; Dudle, B.; Fox, T.; Blacque, O.; Berke, H., *Chem. Eur. J*. **2012**, *18*, 5701-5714.

(66) (a) Ohkuma, T.; Ooka, H.; Hashiguchi, S.; Ikariya, T.; Noyori, R. *J. Am. Chem. Soc*. **1995**, *117*, 2675.

(67) (a) H. Doucet, T. Ohkuma, K. Murata, T. Yokozawa, M. Kozawa, E. Katayama, A. F. England, T. Ikariya, R. Noyori, *Angew. Chem*. **1998**, *110*, 1792-1796; *Angew. Chem. Int. Ed*. **1998**, 37, 1703-1707.

(68) (a) K. Abdur-Rashid, M. Faatz, A. J. Lough, R. H. Morris, *J. Am. Chem. Soc*. **2001**, *123*, 7473-7474;

(69) K. Abdur-Rashid, S. E. Clapham, A. Hadzovic, J. N. Harvey, A. J. Lough, R. H. Morris, *J. Am. Chem. Soc*. **2002**, *124*, 15104-15118.

(70) (a) Haack, K. J., Hashiguchi, S., Fujii, A., Ikariya, T., Noyori, R., *Angew. Chem. Int. Ed. Engl*. **1997**, *36*, 285. (b) Hashiguchi, S.; Fujii, A.; Takehara, J.; Ikariya, T.; Noyori, R. *J. Am. Chem. Soc.* **1995**, *117*, 7562-7563. (b) Takehara, J.; Hashiguchi, S.; Fujii, A.; Inoue, S.; Ikariya, T.; Noyori, R. *J. Chem. Soc., Chem. Commun.* **1996**, 233-234.

(71) (a) Casey, C. P.; Johnson, J. B. *J. Org. Chem*., **2003**, *68*, 1998. (b) Yamakawa, M.; Ito, H.; Noyori, R. *J. Am. Chem. Soc*., **2000**, *122*, 1466. (c) Alonso, D. A.; Brandt, P.; Nordin, S. J. M.; Andersson, P. G. *J. Am. Chem. Soc*., **1999**, *121*, 9580. (d) Petra, D. G. I.; Reek, J. H.; Handgraaf, J. -W; Meijer, E. J.; Dierkes, P.; Kamer, P. C. J.; Brussee, J.; Choemaker, H. E. S.; vanLeeuwen, P. W. N. M. *Chem.-Eur. J*. **2000**, *6*, 2818.

(72) Åberg, J. B.; Samec, J. S. M.; Bäckvall, J. -E. *Chem. Commun*. **2006**, 2771-2773.

(73) Kohl, S.; Weiner, L.; Schwartsburd, L.; Konstantinovski, L.; Shimon, L. J. W. , Ben-David, Y.; Iron, M.; Milstein, D. *Science*, **2009**, *74*, 324.

(74) a) Läng, F.; Breher, F.; Stein, D.; Grützmacher, H. *Organometallics*, **2005,** *24*, 2997. (b) Maire P, Breher F, Schönberg H, Grützmacher H. *Organometallics*, **2005**, *24*, 3207

(75) Speier, J. L.; Webster, J. A.; Barnes, G. H. *J. Am. Chem. Soc.*,**1957**, *79*, 974.

(76) Chalk, A. J.; Harrod, J. F. *J. Am. Chem. Soc.* **1965**, *87*, 16.

(77) (a) Ojima, I.; Nihonyanagi, M.; Nagai, Y. *J. Chem. Soc., Chem. Commun*. **1972**, *938*. (b) Ojima, I.; Nihonyanagi, M.; Kogure, T.; Kumagai, M.; Horiushi, S.; Nakatsugawa, K. *J. Organomet. Chem*. **1975**, *94*, 449. (c) Ojima, I.; Kogure, T. *Organometallics* **1982**, *1*, 1390.

(78) Fernandes, A. C.; Fernandes, R.; Romão, C. C.; Royo, B.; *Chem. Commun.*, **2005**, 213 - 214.

(79) (a) Kennedy-Smith, J. J.; Nolin, K. A.; Gunterman, H. P.; Toste, F. D. *J. Am. Chem. Soc*., **2003**, *125*, 4056. (b) Nolin, K. A.; Krumper, J. R.; Pluth, M. D.;. Bergman, R. G; Toste, F. D. *J. Am. Chem. Soc.* **2007**, *129*, 14684.

(80) (a) Glaser, P. B.; Tilley, T. D. *J. Am. Chem. Soc*. 2003, 125, 13640-13641. (b) Elisa Calimano, E.; Tilley, T. D. Organometallics 2010, 29, 1680 - 1692.

(81) Dioumaev, V. K.; Bullock, R. M.; *Nature*, **2000**, *424* 530 - 532.

(82) (a) Corma, A.; Gonzalez-Arellano, C.; Iglesias, M.; Sanchez, F. *Angew. Chem. Int. Ed*. **2007**, *46*, 7820-7822. (b) Shaikh, N. S.; Enthaler, S.; Junge, K.; Beller, M. *Angew. Chem. Int. Ed*. **2008**, *47*, 2497-2501. (c) Han, J. W.; Tokunaga, N.; Hayashi, T. *J. Am. Chem. Soc*. **2001**, *123*, 12915-12916. (d) Jensen, J. F.; Svendsen, B. Y.; Cour, T. V.; Pedersen, H. L.; Johannsen, M. *J. Am. Chem. Soc*. **2002**, *124*, 4558. (e) Flückiger, M. ; Antonio Togni, A. *Eur. J. Org. Chem.* **2011**, 4353. (f) Junge, K.; Wendt, B.; Addis, D.; Zhou, S.; Das, S.; Beller, M. *Chem. Eur. J*. **2010**, *16*, 68 - 73.

(83) (a) Ison, E. A.; Trivedi, E. R.; Corbin, R. A.; Abu-Omar, M. M. *J. Am. Chem. Soc*. **2005**, 127, 15374. (b) Du, G.; Fanwick, P. E.; Abu-Omar, M. M. *J. Am. Chem. Soc*. **2007**, *129*, 5180.

(84) (a) Roesler, R.; Har, B. J. N.; Piers, W. E. *Organometallics*, **2002**, *21*, 4300. (b) Song, Young-S.; Yoo, B. R.; Lee, Gyu-H.; Jung, N. *Organometallics* **1999**, *18*, 3109-3115. (c) Parks, D. J.; Blackwell, J. M.; Piers, W. E. *J. Org. Chem.* **2000**, *65*, 3090-3098. (d) Rubin,

M.; Schwier, T.; Gevorgyan, V.; *J. Org. Chem.* **2002**, *67*, 1936-1940. (e) Asao, N.; Sudo, T.; Yamamoto, Y.; *J. Org. Chem.* **1996**, *61*, 7654 - 7655.

(85) Berc, S. C.; Kreutzer, K. A.; Buchwald, S. L. *J. Am. Chem. Soc*. **1991**, *113*, 5093.

(86) (a) Bullock, R. M. *Handbook of Homogeneous Hydrogenation*, Wiley-VCH, Weinheim, **2007**. (b) Bullock, R. M. Catalysis without precious metals, Wiley-VCH, Weinheim, **2010**.

(87) (a) Casey, C. P.; Guan, H. R., *J. Am. Chem. Soc.* **2007,** *129*, 5816. (b) Bullock, R. M., *Angew. Chem. Int. Ed.* **2007,** *46*, 7360.

(88) (a) Jacobsen, H., Berke, H., *Dalton Trans.*, **2002**, 3117-3122. (b) Vanderzeijden, A. A. H.; Bosch, H. W.; Berke, H., *Organometallics* **1992,** *11*, 2051.

(89) (a) Chen, Z.; Schmalle, H. W.; Fox, T.; Berke, H. *Dalton Trans.* **2005**, 580. (b) Fupei, L.; Schmalle, H. W.; Fox, T.; Berke, H. *Organometallics* **2003,** *22*, 3382. (c) Fupei, L.; Heiko, J.; Schmalle, H. W.; Fox, T.; Berke, H., *Organometallics* **2000**, *19*, 1950.

(90) Dudle, B.; Rajesh, K.; Blacque, O.; Berke, H. *J. Am. Chem. Soc*. **2011**, *133*, 8168-8178.

(91) Dybov, A.; Blacque, O.; Berke, H. *Eur. J. Inorg. Chem.* **2011**, 652-659.

2. Trisphosphine Substituted Molybdenum and Tungsten Nitrosyl Hydride Complexes: Syntheses and Hydrogenation Catalyses

2.1 INTRODUCTION

The development of organometallic catalysts for homogeneous hydrogenations and their application as industrial processes has undoubtedly been a feat in the past few decades. Nevertheless, the majority of the work in this field applied precious metal catalysts based on rhodium, ruthenium and iridium complexes. The reaction courses were found to follow mainly Wilkinson or Osborn type mechanisms.[1] Economic constraints, limited availability and often high toxicity issues of precious metal catalysts, initiated in recent years global research efforts to replace platinum group metals with non-precious, low toxicity metals ("Cheap Metals for Noble Tasks").[2] In this respect compounds with the middle transition elements molybdenum and tungsten would be attractive catalyst replacements. Our group has a long-standing interest in the exploration of middle transition element based catalyses using rhenium, molybdenum and tungsten. Excellent performance could be well demonstrated for rhenium based catalysts in hydrogenations and related hydrosilylations.[3]

The more recent discoveries of polar hydrogenations[4], [5] eventually led to a preference of the inexpensive metals, molybdenum, tungsten, ruthenium and iron to be apt for such catalyses. Key steps in such reaction pathways[6] are heterolytic cleavage of H_2 and H transfer steps, the latter occur either stepwise as proton and hydride or hydride and proton transfers or in a concerted or nearly concerted fashion to an unsaturated substrate. Noyori has denoted the concerted hydride and proton transfer as ʻmetal-ligand bifunctionality.ʼ[7]

In 1974 Kursanov[8] et al., first observed stoichiometric ionic hydrogenation using CF_3COOH as proton donor and Et_3SiH as a hydride source. In the mean time several research groups[9] utilized this concept for stoichiometric and catalytic hydrogenations of various ketones, alkenes and alkynes. In 1995 Ito and coworkers[10] extended this field towards hydrogenations of C=N bonds. Hydrogenations of imines are generally considered a difficult process and it remains relatively challenging when compared to those of C=C and C=O functionalities. The most serious drawback among such reactions is the poisoning of the catalyst by the starting material, the hydrogenated products or by-products of hydrolysis (amines). Besides this, the reluctance of

certain imines to coordinate to a metal center in an η^2-(C=N) fashion may restrict their susceptibility towards homogeneous hydrogenation.

A simple strategy to tune the catalyst for efficient polar hydrogenations proceeding with proton and hydride transfers can be as follows: Hydride ligands attached to a metal centre could be obtained from H_2 complexes by deprotonation with a base. Dihydrogen complexes are generally more acidic than metal dihydrides so that the earlier are the species to be deprotonated in the presence of, for instance, imines as bases to form iminium salts and the metal hydrides. Hence the subsequent transfer of the hydride to the highly electrophilic carbon of the iminium salt is facilitated. This strategy using protolysis equilibria in hydrogenations is fairly independent of the type of transition metal and is well suited for hydrogenation of C=N bonds often denoted also as ionic hydrogenations.[11]

In particular molybdenum and tungsten complexes were envisaged to be superior for ionic hydrogenations of the polar C=O or C=N bonds over the homopolar C=C bonds due to their ability to transfer the proton and the hydride from the same metal dihydrogen or dihydride complex, which was well studied applying various thermodynamic and kinetic aspects of non platinum group metal catalysts.[12] Nevertheless, there are reports of ionic hydrogenations of less polar alkenes[13] and alkynes[14] based on Ru, Rh, Ir and Os[15] compounds, but also Mo and W catalysed stoichiometric ionic hydrogenations. In 2000 Bullock and coworkers[16] reported that [$MCp(CO)_2(PPh_3)H$, M = Mo, W] complexes can in the presence of the trityl cation $[Ph_3C]^+[BAr^F{}_4]^-$ hydrogenate 3-pentanone in the presence of hydrogen under mild conditions albeit with a low TOF value of 2 h^{-1}. A ketone complex $Cp(CO)_2(PPh_3)W(\eta^1\text{-}O{=}CEt_2)$ could be isolated. Subsequently, Baricelli[17] and coworkers reported the $Mo(CO)_3(PPh_3)(NCMe)$ complex to be active for the hydrogenation of aromatic and aliphatic alkenes with a maximum TOF of 48 h^{-1} in the hydrogenation of styrene.

In recent years our group has also investigated[18] the chemistry of mononitrosyl hydrido complexes of molybdenum and tungsten with a series of bidentate phosphine ligands. Complexes of the type $Mo(NO)(P\text{^}P)(CO)_2H$ (P^P = bidentate ligand) showed hydrogenation activities at room temperature, exclusively in the presence of the $[H(Et_2O)_2][B(C_6F_5)_4]$ acid towards imines resulting in TOFs of up to 123 h^{-1}. An ionic mechanism *via* proton before hydride transfer was anticipated. These types of complexes did not perform as hydrogenation catalysts at higher

temperatures. They also required longer reaction times for full conversion of various *para* substituted imines.

So our approach to homogeneous molybdenum and tungsten catalysis was developed in further using tridentate phosphines, which could stabilise the catalyst at elevated temperature to get improved catalytic performance. In this chapter, the development of novel molybdenum and tungsten catalysts and their application in effective olefin and imine hydrogenations will be described.

2.2 Results and Discussion

2.2.1 Preparation of the Bis(2-diisopropylphosphinoethyl)phenyl phosphine (etp^{i}p) ligand

Initially the diisopropylvinylphosphine (**1**) was prepared according to an analogous procedure described by Dyer[19] with slight modifications (Scheme 2.1). The reaction of diisopropylchlorophosphine with vinylmagnesiumbromide proceeded at -30 °C and led to the formation of diisopropylvinylphosphine in 72% yield. The $^{31}P\{^1H\}$ NMR spectra showed a singlet resonance at δ = 6.5 ppm. The ^1H NMR spectra exhibited multiplets in the range between 6.4-5.7 ppm for the vinylic protons. The methyne protons appeared in the region δ = 1.8-1.6 ppm. Multiplets at δ = 1.1-0.96 ppm were assigned to the methyl protons.

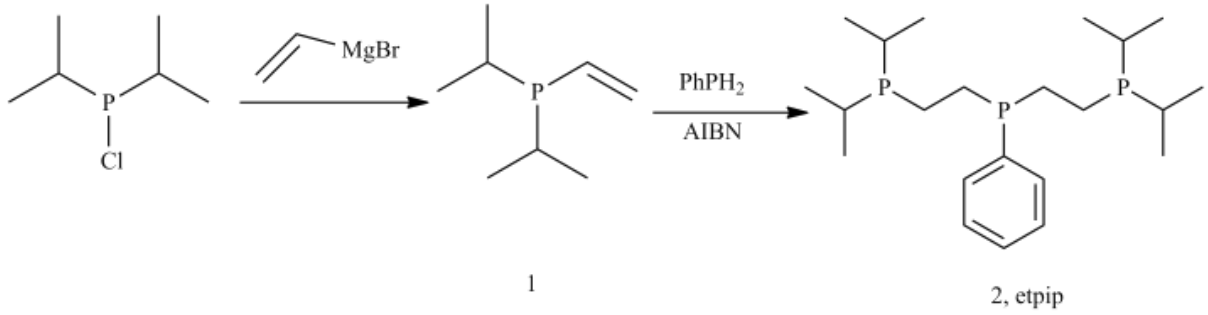

Scheme 2.1. Preparation of the etp^{i}p (**2**) ligand.

Then the bis(2-diisopropylphosphinoethyl)phenyl phosphine **{**(iPr$_2$PCH$_2$CH$_2$)$_2$PPh, **2**, etp^{i}p} ligand was obtained according to an analogous procedure depicted by Bleeke[20] with high yield (75%) *via* radical coupling of two equivalents of diisopropylvinylphosphine with phenyl

phosphine in the presence of AIBN (Scheme 2.1). The etp^{i}p ligand was fully characterized by ^{1}H, ^{31}P{^{1}H} and ^{13}C{^{1}H} NMR spectroscopies. The ^{31}P{^{1}H} NMR spectrum of **2** showed a doublet at δ = 11.5 ppm ($^3J_{pp}$ = 26.9 Hz) for the terminal phosphorus atoms and a triplet at δ = -14.4 ppm ($^3J_{pp}$= 26.9 Hz) for the central phosphorus atom. Thus, the obtained etp^{i}p ligand was employed in the preparation of various molybdenum and tungsten nitrosyl complexes.

2.2.2 Preparation of various molybdenum and tungsten nitrosyl complexes bearing etp^{i}p ligand

Preparation of [M(NO)Cl$_3$(etp^{i}p)] complexes (M = Mo, 3a; W, 3b)

Treatment of one equivalent of the etp^{i}p ligand in THF solutions of M(NO)Cl$_3$(NCMe)$_2$, (M= Mo, W) at room temperature led to precipitation of the isomeric mixtures of the pentagonal bipyramidal Mo(NO)Cl$_3$(etp^{i}p) {**3a(up)** and **3a(down)**} and W(NO)Cl$_3$(etp^{i}p) {**3b(up)** and **3b(down)**} complexes in 55% and 52% yields, respectively (Scheme 2.2). The isomers **3a(up)** and **3a(down)** and **3b(up)** and **3b(down)** correspond to the relative position of the phenyl ring of the internal phosphorus atom: Ph adjacent to the Cl atom: *transoid*, down and NO ligand: *cisoid*, up.

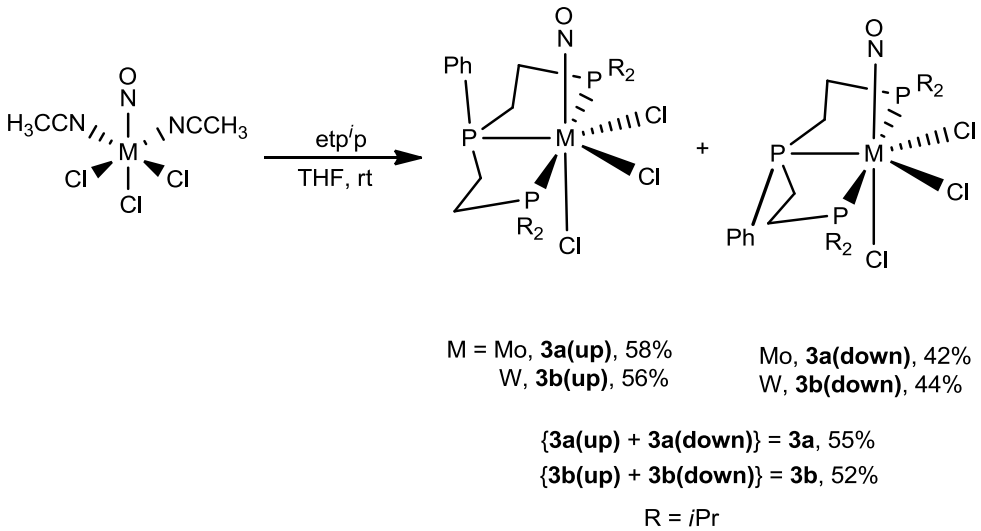

Scheme 2.2. Preparation of the isomeric mixtures of M(NO)Cl$_3$(etp^{i}p)

3a and **3b** are soluble only in CH_2Cl_2 except for the latter, which was also found to be sparingly soluble in THF. **3b(up)** and **3b(down)** could be partly separated by repeated extractions with

THF. After several extractions (3x10 mL) **3b(up)** prevailed in the combined THF solutions in a ratio of 9:1{**3b(up)** : **3b(down)**} as indicated by ^{31}P NMR spectra. The presence of two different sets of doublets and triplets in the ^{31}P NMR spectra of the reaction mixture of **3a** and **3b** spoke for the existence of isomers {58% and 42% for **3a(up)** and **3a(down)**; 56% and 44% for **3b(up)** and **3b(down),** respectively}. The ^{31}P{^{1}H} NMR spectra of the isomeric mixtures of **3a** revealed two sets of doublets at δ = 76 ($^{3}J_{PP}$ = 72 Hz, **3a(up)**), 77 ($^{3}J_{PP}$ = 76 Hz, **3a(down)**) ppm for the terminal phosphorus atoms and two sets of triplets at δ = 89 ($^{3}J_{PP}$ = 76 Hz, **3a(down)**), 98 ($^{3}J_{PP}$ = 72 Hz, **3a(up)**) ppm for the central phosphorus atoms (Figure 2.1). The doublet sets in the ^{31}P NMR of the isomeric mixtures of **3b** appeared at δ = 55 ($^{3}J_{PP}$ = 46 Hz, **3b(up)**), 56 ($^{3}J_{PP}$ = 49 Hz, **3b(down)**) ppm and the triplet sets at δ = 80 ($^{3}J_{PP}$ = 46 Hz, **3b(up)**), 72 ($^{3}J_{PP}$ = 49 Hz, **3b(down)**) ppm.

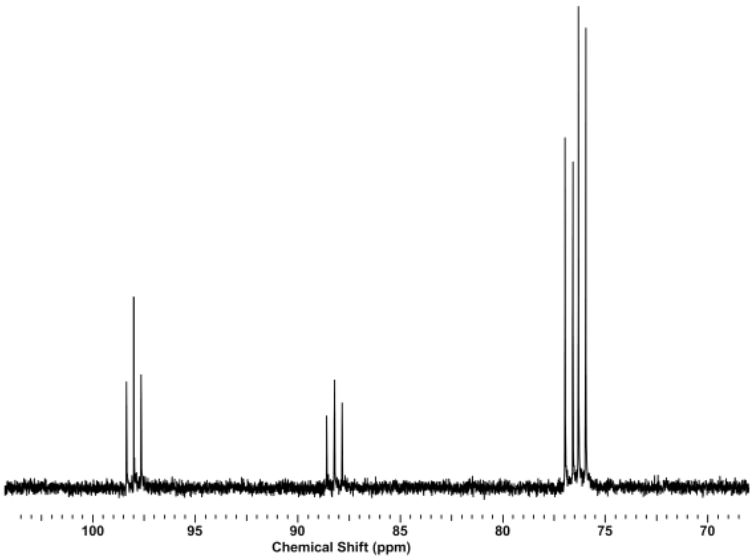

Figure 2.1. ^{31}P{^{1}H} NMR spectra of the isomeric mixture of **3a** {**3a(up)** and **3a(down)**} at room temperature in CD_2Cl_2.

The ^{1}H NMR spectra of the mixture of **3a** and **3b** in CD_2Cl_2 showed in either case of metal complexes doubled sets of multiplets for the methyl, methylene, methyne and phenyl protons again indicating the presence of isomers. However, in the IR spectra the isomers of **3a** and **3b** were not distinguished. The isomeric mixtures of **3a** and **3b** displayed only one strong ν(NO) band at 1647 and 1618 cm^{-1} respectively, indicating strong back-bonding to the NO ligand. Unfortunately the **up**/**down** isomers could not be fully separated, neither by crystallization nor chromatography. Nevertheless, owing to some solubility difference of the isomers of **3a** in

CH_2Cl_2, we were able to co-crystallize **3a(up)** and **3a(down)** in the form of yellow colored single crystals suitable for X-ray diffraction analysis upon layering pentane onto a concentrated CH_2Cl_2 solution of the **3a** mixtures.

Perspective views of the single crystal X-ray structures of **3a(up)** and **3a(down)** are depicted in Figure 2.2. The crystal structure analysis of **3a(up)** and **3a(down)** revealed pentagonal bipyramidal molybdenum centres with three phosphorus atoms of the etp^{i}p ligand and two chloride ligands attached to the metal center occupying the pentagonal plane in either case. The *trans* NO/Cl axis of **3a(down)** is disordered in a ratio of 0.935(2):0.065(2), which is due to the presence of the two isomeric products, while **3a(up)** has no *trans* NO/Cl disorder. The O(1A)-N(1A)-Mo bond angle of **3a(down)** is 176.16 (16)° and for **3a(up)** Mo(1)-N(1)-O(1) angle is 173.73(13)° which are close to linearity.

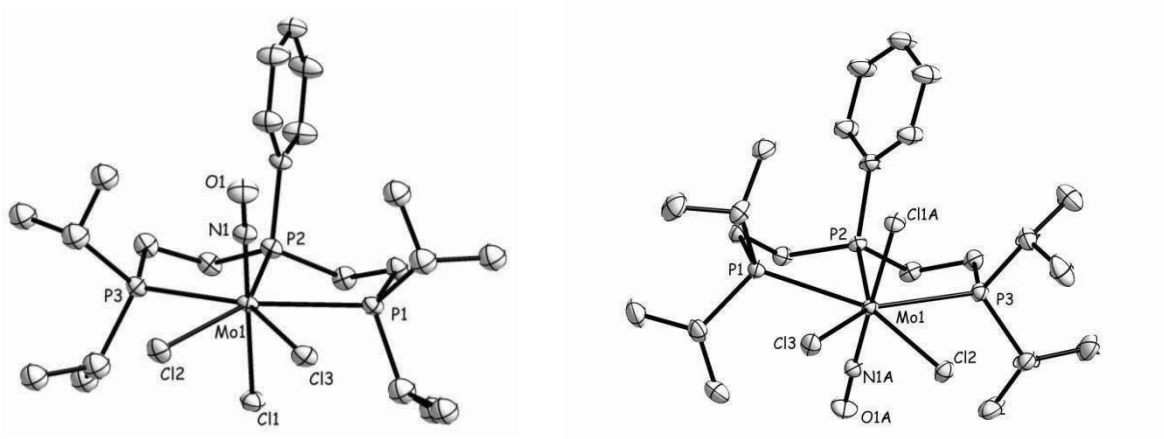

Figure 2.2. Molecular structures of Mo(NO)Cl_3(etp^{i}p), **3a(up)**, (left) and **3a(down)**, (right) with thermal ellipsoids drawn at the 50% probability level.

Selected bond distances(Å) and bond angles(°) for **3a(up)**: Mo(1)-N(1) 1.7749(15), Mo(1)-P(1) 2.6342(5), Mo(1)-P(2) 2.5357(4), Mo(1)-P(3) 2.6307(5), N(1)- O(1) 1.1769(19), Mo(1)-Cl(1) 2.5031(5), Mo(1)-Cl(2) 2.4930(4), Mo(1)-Cl(3) 2.5060(4), N(1)-Mo(1)-Cl(1) 179.37(5), P(1)-Mo(1)-P(3) 145.003(15), N(1)-Mo(1)-P(2) 97.71(4), Mo(1)-N(1)-O(1) 173.73(13).

Selected bond distances(Å) and bond angles(°) for **3a(down)**: Mo(1)-N(1A) 1.788(2), Mo(1) - P(1) 2.6415(4), Mo(1)-P(2) 2.5202(5), N(1A)-O(1A) 1.202(3), Mo(1)-Cl(1A) 2.4569(5), N(1A)-

Mo(1)-Cl(1A) 178.05(5), P(2)-Mo(1)-P(3) 71.878(14), N(1A)-Mo(1)-P(2) 82.44(6), Mo(1)-N(1A)-O(1A) 176.16(16).

It became also apparent from the structure analyses that the isomers of the **3a** mixture do not differ much in their bond lengths and bond angles except in the stereochemical orientation of the phenyl ring.

A X-ray diffraction study on a single crystal of **3b(up)** was also carried out, which is shown in Figure 2.3. The crystal was obtained by layering pentane onto a concentrated CH_2Cl_2 solution of the **3b** mixture. Similar to the **3a** isomers, the crystal structure revealed a pentagonal bipyramidal geometry with *trans* NO/Cl ligands which did not display disorder.

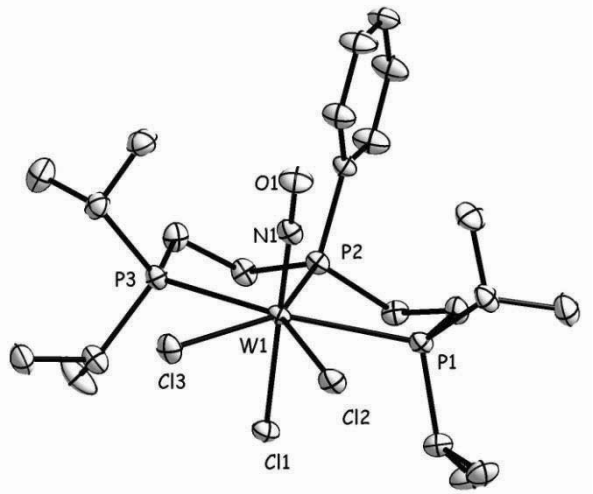

Figure 2.3. Molecular structure of $W(NO)Cl_3(etp^ip)$, **3b(up)** with thermal ellipsoids drawn at the 50% probability level. All hydrogen atoms and solvated dichloromethane molecules are omitted for clarity Selected bond distances(Å) and bond angles(^{o}): W(1)-N(1) 1.781(2), W(1)-P(1) 2.6298(6), W(1)-P(2) 2.5331(5), W(1)-P(3) 2.6276(5), N(1)- O(1) 1.189(3), W(1)-Cl(1) 2.4928(6), W(1)-Cl(2) 2.4954(5), W(1)-Cl(3) 2.4822(5), N(1)-W(1)-Cl(1) 179.52(6), P(1)-W(1)-P(3) 145.082(18), N(1)-W(1)-P(2) 97.33(6).

Since the metal centres of the isomers of **3a** and **3b** compounds possess the +II oxidation state, reduction was thought to be attempted to prepare various low oxidation state complexes, eventually suitable as catalyst precursors for homogeneous hydrogenations.

Preparation of [M(NO)Cl_2(etp^{i}p)] complexes 4a and 4b.

Reduction of the isomers of **3a** and **3b** with one equivalent of 1% Na/Hg in THF at room temperature led to formation of the green 17 e^- species Mo(NO)Cl_2(etp^{i}p) (**4a**) and W(NO)Cl_2(etp^{i}p) (**4b**) in 59% and 54% yields, respectively (Scheme 2.3). They were found to be quite soluble in THF and CH_2Cl_2, but sparingly soluble in toluene and benzene. Due to the paramagnetic character of **4a** and **4b**, no signals were observable in the $^{31}P\{^1H\}$ and ^1H NMR

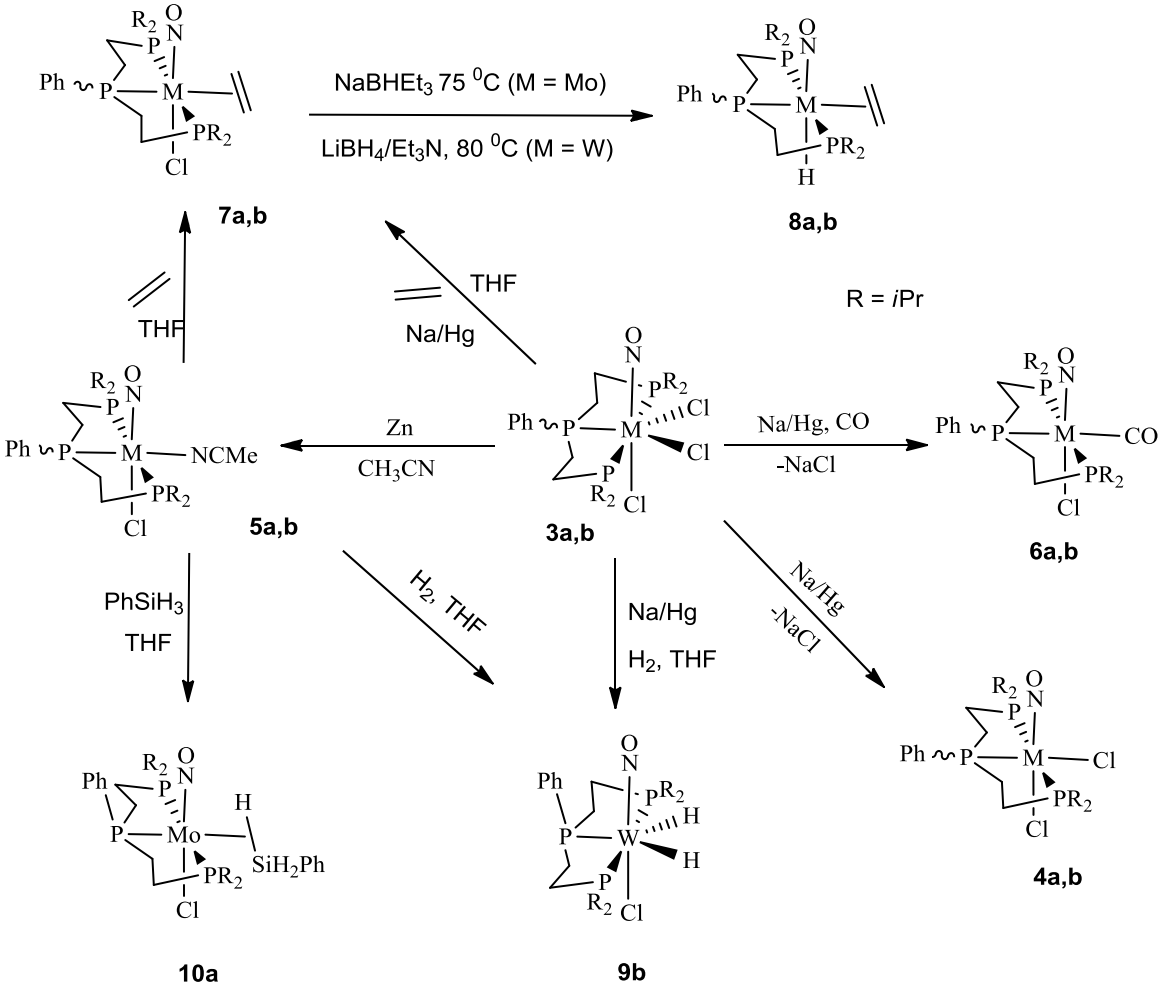

Scheme 2.3. Preparation of various molybdenum and tungsten nitrosyl complexes *via* reduction of the isomeric mixtures of **3a** and **3b**

spectra. These compounds were characterized by IR spectroscopy, elemental analysis and X-ray diffraction studies. The IR spectra displayed two sharp bands at 1589 and 1564 cm^{-1} for **4a** and

4b, respectively, assigned to nitrosyl stretching vibrations. The nitrosyl stretching frequencies of **4a** and **4b** at lower wavenumbers than any of the **3a** and any of the **3b** mixtures indicating a higher degree of back-donation from the metal centre to the nitrosyl ligand. The molecular structures of **4a** and of **4b** revealed neutral pseudo octahedral complexes. Selected bond angles and bond distances for **4a** and **4b** are given in Figure 2.4. The three phosphorus atoms of the etp^{i}p ligand and the two chloride ligands attached to the metal centre occupy "equatorial" positions. The nitrosyl and the other chloride ligand are *trans* disposed. No NO/Cl disorder was found in the structures of **4a** or **4b** but despite this the presence of isomeric mixtures in solution with one prevailing component could not be fully ruled out.

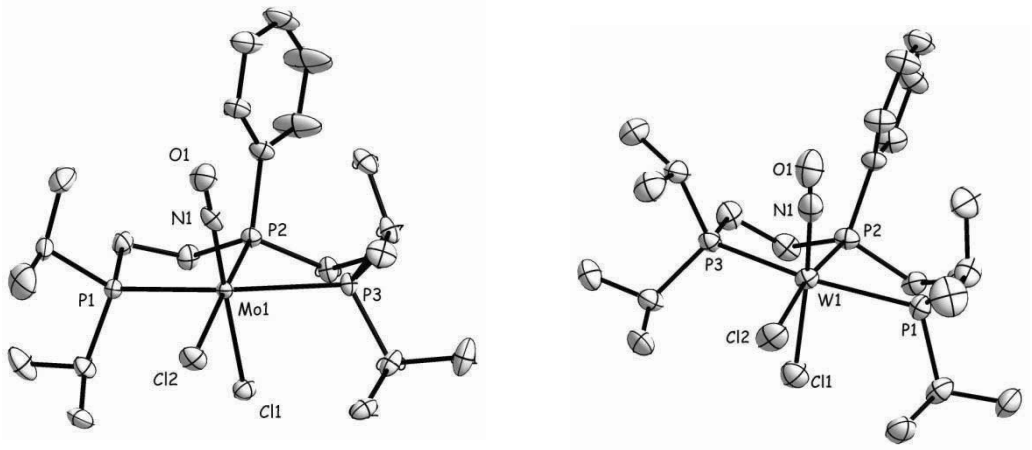

Figure 2.4. Molecular structures of Mo(NO)Cl$_2$(etp^{i}p), **4a** (left) and [W(NO)Cl$_2$(etp^{i}p), **4b**, (right) with thermal ellipsoids drawn at the 30% and 50% probability levels respectively.

Selected bond distances(Å) and bond angles(^{o}) for **4a**: Mo(1)-N(1) 1.818(3), Mo(1)-P(1) 2.5716(7), Mo(1)-P(2) 2.4888(7) Mo(1)-P(3) 2.5625(7), Mo(1)-Cl(1) 2.5230(7), Mo(1)-Cl(2) 2.4375(7) N(1)-Mo(1)-Cl(1) 179.01(8), P(1)-Mo(1)-P(3) 154.01(2), N(1)-Mo(1)-P(2) 99.09(8).
Selected bond distances(Å) and bond angles(^{o}) for **4b**: W(1)-N(1) 1.858(5), W(1)-P(1) 2.5488(11), W(1)-Cl(1) 2.5162(13), N(1)-W(1)-Cl(1) 176.37(13), P(1)-W(1)-P(3) 155.71(4), N(1)-W(1)-P(2) 99.57(13), O(1)-N(1)-W(1) 175.6(5)

4a and **4b** are rare paramagnetic complexes with the metal centres in +I oxidation state and of low-spin d^5 configurations. To examine the paramagnetic behavior, solution EPR measurements were carried out on **4a** and **4b** in toluene at 293 K. The spectra are displayed in Figure 2.5, which

showed two signals with hyperfine splitting for **4a**. The coupling patterns of the two signals are due to coupling of one unpaired electron of each compound with the internal phosphorus

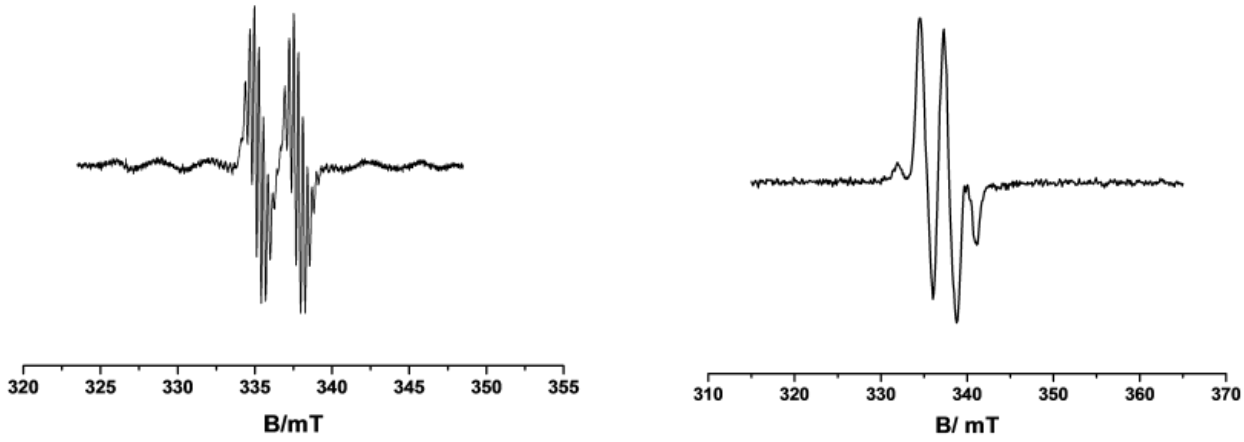

Figure 2.5. EPR spectra of **4a** (left**)** and **4b** (right) in toluene at 298 K.

atom (^{31}P, I =1/2). Hyperfine splitting arises from the coupling with the hydrogen atoms of the phenyl ring (^{1}H, *I* = 1/2). Another six weak signals are observed owing to the very weak coupling of the unpaired electron with the molybdenum centre (^{95,97}Mo I = 5/2, combined 26%). There is no coupling with the terminal phosphorus atoms, which was interpreted in terms of the unpaired electron residing in a d orbital in the (Cl_2, NO, P_{int}) plane.

The EPR spectrum of **4b** (Figure 2.5) in toluene at room temperature showed two sharp signals along with two weak signals. This could be explained in terms of the coupling of the unpaired electron with the central phosphorus atom (^{31}P, I = 1/2) along with the coupling with the tungsten nucleus (I=1/2). However, unlike in the case of molybdenum no hyperfine splitting was observed at room temperature for **4b**.

The magnetic susceptibility data of **4a** were obtained in the temperature range of 5-300 K and are exemplarily displayed in Figure 2.6. At low temperature an effective magnetic moment of 1.73 μ_B was determined which is in accord with the low-spin d^5 electronic configuration of **4a** bearing one unpaired electron.

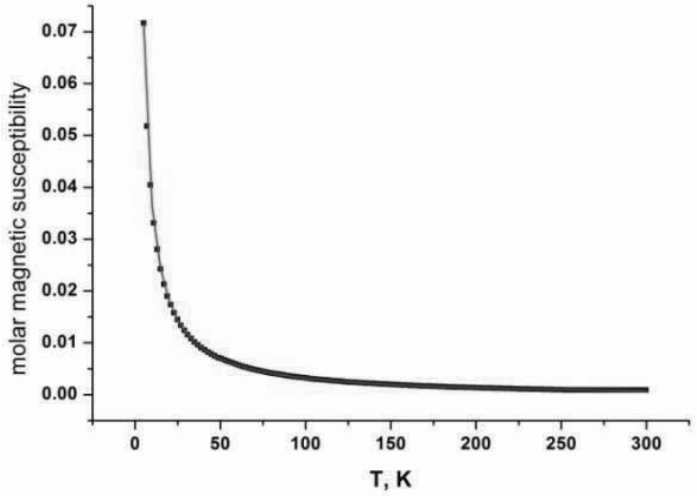

Figure 2.6. Temperature dependent magnetic susceptibility data of **4a** recorded in the range of 5-300K.

Preparation of M(NO)Cl(NCMe)(etp^{i}p) complexes M = Mo, 5a; W, 5b.

Reduction of the isomeric mixture of **3a** could also be accomplished stirring an acetonitrile solution of **3a** for 3 days at room temperature with excess of zinc to form the diamagnetic isomeric species Mo(NO)Cl(NCMe)(etp^{i}p), (52%, **5a(up)** and 48%, **5a(down)**) respectively in 75% total yield (Scheme 2.3). The ^{31}P {^{1}H} NMR spectra of the isomeric mixture of **5a** revealed two singlets at δ = 102.5 and 67.7 ppm (1:2 ratio) assigned to the major isomer **5a(up)** and two other singlets at δ 95 and 62.8 ppm corresponding to minor isomer **5a(down)**. It was surprising to see that no coupling was observed in the ^{31}P{^{1}H} NMR spectra although quite different phosphorus environments exist in both the isomers. The IR spectra in the range of 1500-2000 cm^{-1} showed only one sharp band at 1598 cm^{-1} assigned to the ν(NO) stretching vibrations of both isomers. It is worth mentioning that **4a** could also be used to prepare isomeric mixtures of **5a**.

Single crystals of the isomeric mixture of **5a** suitable for a X-ray diffraction study could be obtained after several days by layering pentane onto a concentrated toluene solutions at -30 °C. The coordination geometry of the **5a** was found to be pseudo octahedral (Figure 2.7). The three phosphorus atoms and the coordinated acetonitrile ligand were lying in a plane. The NO and Cl ligands were found to be disordered over two sets of positions with a site-occupancy factor of

0.5. supporting the presence of both **5a(up)** and 5a**(down)** isomers. The structure of the isomers of **5a** was further confirmed by ^{1}H NMR, $^{13}C\{^{1}H\}$ NMR, C-H correlation, ^{13}C DEPT experiments and its composition was established by elemental analysis.

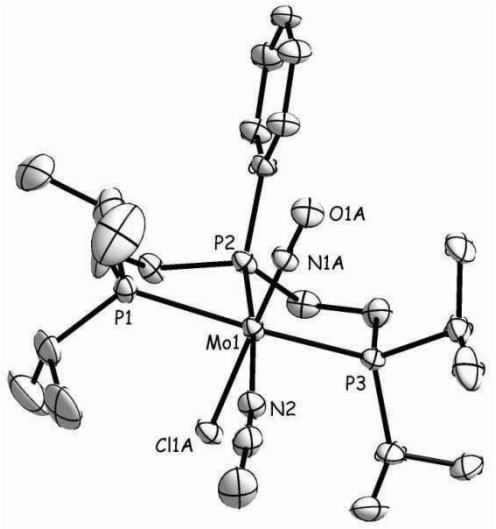

Figure 2.7. Molecular structures Mo(NO)Cl(NCMe)(etp^{i}p), **5a**. Thermal ellipsoids are drawn at the 30% probability level. Selected bond distances(Å) and bond angles(^{o}) for **5a**: Mo(1)-N(1A) 1.773(7), Mo(1)-P(1) 2.4899(13), Mo(1)-N(2) 2.195(4), N(1A)-O(1A) 1.232(8), N(1A)-Mo(1)-Cl(1A) 177.40(2), P(1)-Mo(1)-P(3) 158.57(4), N(1A)-Mo(1)-P(2) 99.3(2).

When **3b** was reacted with excess of zinc in CH_3CN at room temperature, the ^{31}P NMR spectra in CD_3CN revealed the appearance of two intense new signals at δ 52.9 and 86.8 ppm (with tungsten satellites) in a 2:1 ratio assigned to the major isomer **5b(up)** along with two weak signals at δ 48 and 76 ppm (2:1 ratio) assignable to the minor isomer **5b(down).** However, the purity of the desired isomeric mixture of **5b** was 90% according to the ^{31}P NMR spectra in acetonitrile solution. Another weak unidentified signal at δ 61 ppm accounted for the residual 10% of the mixture, which however could not be attributed to a specific compound and remained unidentified. The IR spectra revealed in the range of 1500-2000 cm^{-1} only a singlet assignable to the nitrosyl stretching frequencies at 1566 cm^{-1}. Further the formation of the **5b(up)** and **5b(down)** was confirmed by ^{13}C and C-H correlations. However when acetonitrile solutions of **5b(up)** and **5b(down)** were evaporated and dissolved again in THF, several other signals

appeared in the ^{31}P NMR spectra. This was interpreted in terms of a labile ligand which could at least partly be replaced by THF or N_2 and even the existence of a dinuclear chloro bridged species could not be ruled out. The presence of several species is also anticipated for the solid state mixture of **5b(up)** and **5b(down)** mixture**,** which prevented the satisfactory elemental analyses.

Therefore being aware of this situation we also attempted reduction of the isomeric mixtures of **3b** with excess of Na/Hg under nitrogen atmosphere in THF at room temperature to obtain a N_2 coordinated tungsten complex. However after 16 h of reaction time the reaction mixture also showed according to ^{31}P NMR spectroscopy presence of as yet several unidentified species leaving the existence of a dinitrogen complex uncertain.

Preparation of [M(NO)(CO)Cl(etp^{i}p)] complexes M = Mo, **6a**; W, **6b**

3a and **3b** could also be reduced with excess of Na/Hg in the presence of carbon monoxide (1 bar) at room temperature to form the diamagnetic yellow isomeric complexes Mo(NO)(CO)Cl(etp^{i}p) {**6a(up)**, 70%; **6a(down)**, 30%} and W(NO)(CO)Cl(etp^{i}p) **{6b(up)**, **(**73%); **6b(down)**, 27%} in 65% and 60% yields, respectively (Scheme 2.3). The ^{31}P NMR spectra of **6a** revealed two doublets at δ = 68.9 ($^3J_{PP}$ = 6.3 Hz, **6a(up)**) and 59.9 ($^3J_{PP}$ = 9.7 Hz, **6a(down)**) ppm and two triplets at δ = 80.5 ($^3J_{PP}$ = 7.5 Hz, **6a(up)**) and at 63.3 ($^3J_{PP}$ = 9.0 Hz, **6a(down)**) ppm, whereas for **6b** doublets appeared in the ^{31}P{^{1}H} NMR spectra at δ = 55.2 [$^3J_{PP}$ = 5.2 Hz, $^1J_{PW}$ = (d, satellites), 288.7 Hz, **6b(up)**], 49 ppm [$^3J_{PP}$ = 2.2 Hz, $^1J_{PW}$ =(d, satellites), 281 Hz, **6b(down)**]. and two triplets at δ = 72.6 [$^3J_{PP}$ = 4.5 Hz,$^1J_{PW}$ = (d, satellites), 215.4 Hz, **6b(up)**], 48.7 [$^3J_{PP}$ = 2.2 Hz, $^1J_{PW}$ = (d, satellites), 210 Hz, **6b(down)**] ppm. The IR spectra, showed strong bands at 1918 and 1569 cm^{-1} of the isomeric mixture of **6a** and 1902 and 1559 cm^{-1} for the isomeric mixture of **6b,** which were assigned to the vibration of the carbonyl and nitrosyl ligands, respectively. The crystal structure analysis of **6a** and **6b** revealed that the metal centres possess pseudo-octahedral geometries with three phosphorus atoms and the carbonyl ligands in the P_3 plane (Figure 2.8).

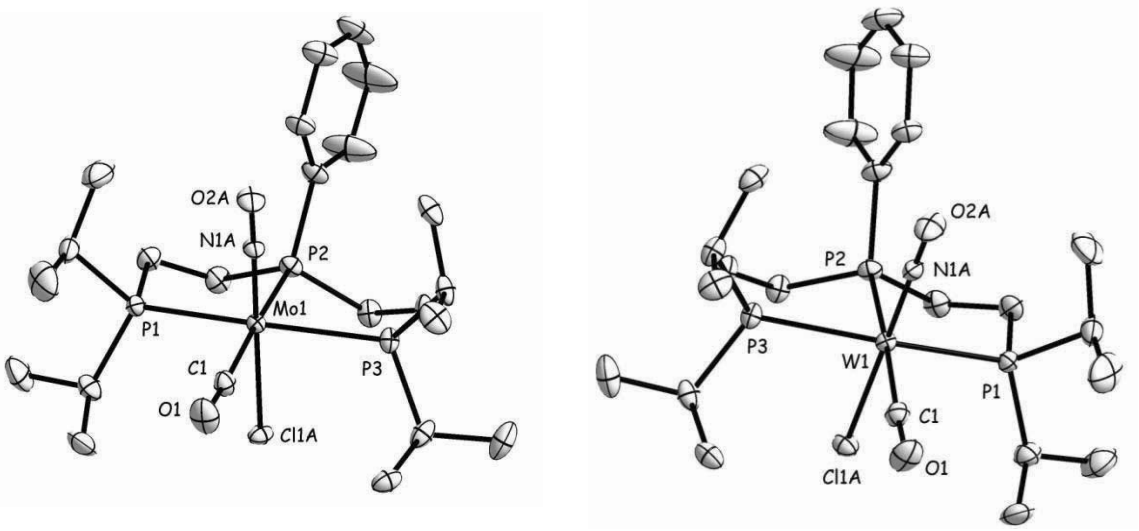

Figure 2.8. Molecular structures of [Mo(NO)(CO)Cl(etp^{i}p)**], 6a**, (left) and W(NO)(CO)Cl(etp^{i}p), **6b**. (right). Thermal ellipsoids are drawn at the 30% probability level. All H atoms and the toluene solvate were removed for clarity.

Selected bond distances(Å) and bond angles(^{o}) for **6a**: Mo(1)-N(1A) 1.788(3), Mo(1)-P(1) 2.5145(5), Mo(1)-Cl(1) 2.5178(10), N(1A)-O(2A) 1.221(5), Mo(1)-C(1) 2.020(2), C(1)-O(1) 1.139(2) N(1A)-Mo(1)-Cl(1A) 176.40(8), P(1)-Mo(1)-P(3) 156.272(16), N(1A)-Mo(1)-P(2) 101.27(8).

Selected bond distances(Å) and bond angles(^{o}) for **6b**: W(1)-N(1A) 1.836(4), W(1)-P(1) 2.5002(7), W(1)-Cl(1A) 2.5136(10), N(1A)-O(2A) 1.172(6), W(1)-C(1) 1.997(3), C(1)-O(1) 1.156(3) N(1A)-W(1)-Cl(1A) 176.39(10), P(1)-W(1)-P(3) 156.26(2), N(1A)-W(1)-P(2) 101.34(10).

The *trans* NO/Cl axes were found positionally disordered in the ratios of 0.76:0.24 for **6a** and 0.83:0.17 for **6b**. This NO/Cl disorder spoke for the existence of isomers in the crystal of **6a** and **6b**. These solid solutions showed grossly the ratio of the isomers as they exist in solution so that it looks as if the crystal lattice does not differentiate the isomers of type **6a,b(up)** and **6a,b(down)** different from what the solution environment does.

Preparation of the complexes M(NO)Cl(η^2-ethylene)(etp^{i}p) M = Mo, 7a; W, 7b

Treatment of the isomeric mixtures of **3a,b** with 5 equiv. of Na/Hg at room temperature in the presence of 1 bar ethylene in THF resulted in the formation of the isomeric mixtures of the ethylene complexes **7a** and **7b** in 87% and 92% yields, respectively. The IR spectra of **7a** and **7b** showed sharp signals at 1547 and 1531 cm^{-1}, respectively, attributed to the nitrosyl stretching frequency. The ^{31}P NMR spectra of **7a** revealed only one doublet at δ 58.4 (d, $^3J_{PP}$ = 17.2 Hz, ^{i}Pr$_2$P) ppm for the terminal phosphorus atoms of the etp^{i}p ligand for both the isomers **7a(up)** and **7a(down)**. However for the internal phosphorus atom two triplets at δ 81.3 (t, $^3J_{PP}$ = 18 Hz, PPh, **7a(up)**) and 66 (t, $^3J_{PP}$ = 18.7 Hz, PPh, **7a(down)**) ppm could be observed appearing in a 2:1 ratio. The doublet signal of the terminal phosphorus atoms of the minor isomer **7a(down**) overlaps with the signal of major isomer **7a(up)**. This was supported by the ratio of 6:2:1 of the three signals (doublet : triplet : triplet) in the ^{31}P NMR spectra appearing with 70% of the major isomer **7a(up)** and 30% of the minor isomer **7a(down)**. The ^{1}H NMR spectra of **7a** revealed several signals in the region of methyl, methylene and methine protons due to the presence isomeric mixture. Nevertheless, the coordinated ethylene protons of the isomeric mixtures could be assigned as multiplets at δ = 1.31 ppm as confirmed from C/H correlations and 1D NOE experiments. In the ^{13}C NMR spectra, the singlet resonance at δ = 32.7 ppm was attributed to the ethylene carbon atoms so that either free rotation of the ethylene ligand around the metal-ethylene bond prevails or that the olefin is fixed in the P_3-M plane.

The ^{31}P NMR spectra of the isomeric mixture of **7b** showed two distinct sets of doublets at δ 39.8 (d, $^3J_{PP}$ = 7.5 Hz, (P^{i}Pr) $^1J_{PW}$ = (d, satellites), 231Hz, **7b(up**)), 41 (d, $^3J_{PP}$ = 8.2 Hz, (P^{i}Pr) $^1J_{PW}$ = (d, satellites), 227.4 Hz, **7b(down)**) ppm for the terminal phosphorus atoms and two sets of triplet at δ 74.3 (t, $^3J_{PP}$ = 7.5 Hz, (PPh) $^1J_{PW}$ = (d, satellites), 207.2 Hz, **7b(up)**) and 57 (t, $^3J_{PP}$ = 8.2 Hz, (PPh) $^1J_{PW}$ = (d, satellites), 195 Hz, **7b(down)**) for the central phosphorus atoms owing to the presence of isomeric mixtures **7b(up)** and **7b(down)** in 75% and 25%, respectively. In the ^{1}H NMR spectra, the multiplet resonance at δ 1.45 ppm was assigned to the ethylene carbon atoms. **7a** and **7b** are quite soluble in THF, toluene and benzene. These complexes could also be prepared by the reaction of 1 bar of ethylene to THF solutions of the isomeric complexes **5a** and **5b** at room temperature in quantitative yields.

Single crystals suitable for X-ray diffraction studies of the isomeric mixtures of **7a** and **7b** could be obtained from a concentrated toluene solution at room temperature after several days.The crystal structures analysis of **7a** and **7b** revealed pseudo octahedral geometries showing η^2-ethylene binding mode (Figure 2.9).

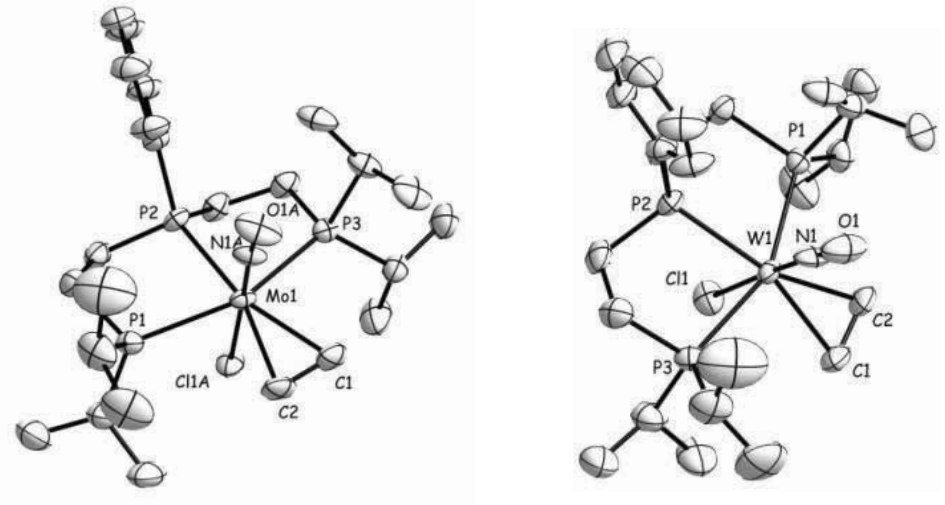

Figure 2.9. Molecular structures of [Mo(NO)Cl(η^2-ethylene)(etp^{i}p)] **7a** (left) and [W(NO)Cl(η^2-ethylene)(etp^{i}p)] **7b** (right) with thermal ellipsoids drawn at the 50% probability level.

Selected bond distances(Å) and bond angles(^{o}) for **7a**: Mo(1)-N(1A) 1.810(4), Mo(1)-P(1) 2.5597(7), Mo(1)-C(1) 2.256(2), Mo(1)-C(2) 2.275(2), C(1)-C(2) 1.401(4), N(1A)-O(1A) 1.220(4) N(1A)-Mo(1)-Cl(1A) 177.81(13), P(1)-Mo(1)-P(3) 154.99(2), C(1)-Mo(1)-C(2) 72.74(15).

Selected bond distances(Å) and bond angles(^{o}) for **7b**: W(1)-N(1) 1.825(6), W(1)-P(1) 2.5273(10), W(1)-C(1) 2.245(4), W(1)-C(2) 2.229(4), C(1)-C(2) 1.419(6), N(1)-O(1) 1.185(8) N(1)-W(1)-Cl(1) 177.75(15), P(1)-W(1)-P(3) 154.45(3), C(1)-W(1)-C(2) 36.99(16).

The axially coordinated *trans* NO and Cl of **7a** and **7b** were found to be disordered in a ratio of 0.65:0.35 and 0.78:0.22, respectively supporting the presence of isomeric mixtures **7a,b(up)** and **7a,b(down)**. The C1-C2 bond distance of the ethylene molecule is 1.401(4) Å for **7a** and for **7b** it was found to be 1.419(6) Å indicating π donation of electrons to the metal centre.

Preparation of the M(NO)H(η^2-ethylene)(etp^{i}p), (M = Mo, 8a; W, 8b) complexes

Reaction of the ethylene complex **7a** with $NaBHEt_3$ at 75 °C for 30 min led to the formation of the light yellow ethylene hydride complex **8a** in 85% yield. In the IR spectra the ν_{NO} stretching vibration was observed at 1571 cm^{-1}. However a metal hydride stretching vibration could not be assigned presumably because of a too low intensity. The ^{31}P NMR spectra of **8a** revealed two sets of doublet at δ 89.8 (d, $^3J_{PP}$ = 17.6 Hz, $^i Pr_2P$) and 79.5 (d, $^3J_{PP}$ = 21.8 Hz, $^i Pr_2P$) ppm for the terminal phosphorus atoms and two sets of triplet at δ 96.1 (t, $^3J_{PP}$ = 17.6 Hz, PPh) and 92.5 ppm (t, $^3J_{PP}$ = 21.6 Hz, PPh) for the central phosphorus atom speaking for the inequivalence of the phosphorus atoms and the presence of isomeric mixtures **8a(up)** and **8a(down)** (Figure 2.10). The isolated major isomer **8a(up)** and minor isomer **8a(down)** ratio was found to be only 9:1.

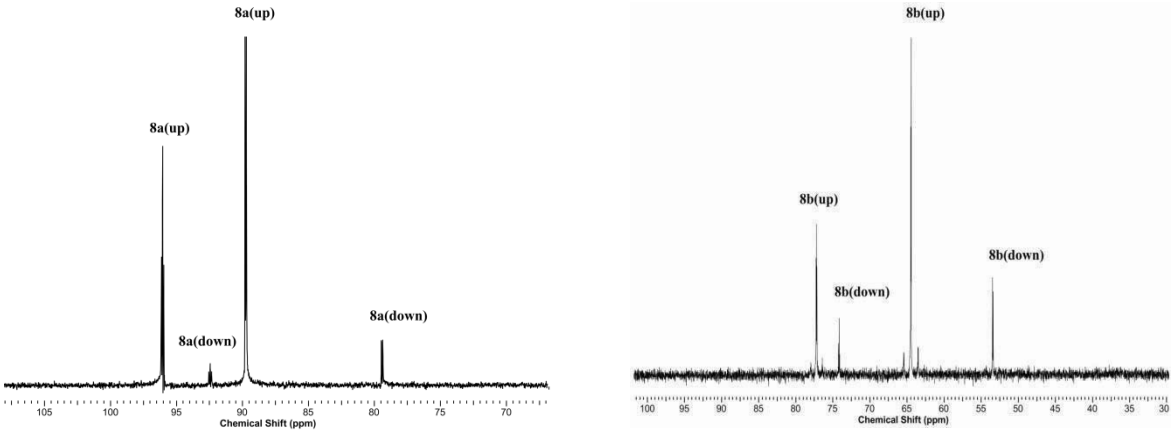

Figure 2.10. $^{31}P\{^1H\}$ NMR spectra of the **up** and **down** isomeric mixtures of **8a** (left) and **8b**(right) at room temperature in THF.

The isomeric **8a** mixture could also be prepared at room temperature, however it required longer reaction times (at least 24 h). In the ^1H NMR spectra two quartet signals at δ = -3.9 (q, $^2J_{PH}$ = 46.4 Hz,) and -6.0 (q, $^2J_{PH}$ = 65.2 Hz) ppm with distinctly different P,H coupling constants could be assigned to the metal attached hydride ligands of the **8a(down)** and **8a(up)** isomers, respectively. We therefore anticipated that the Mo-H bond of **8a(down)** with the smaller P,H coupling constant may have been loosened catching some contact.

The ethylene protons of both isomers could be found as superimposed multiplets at δ 2.19-2.12 ppm in the ^1H NMR spectra as revealed by the C/H correlation spectra. A sharp singlet resonance

at δ 32.7 in the ^{13}C NMR spectra was attributed to the carbon atoms of the attached ethylene moiety. Further the complex was characterized by P-H, C/H correlations and 1D-NOE experiments and the purity of the complex was confirmed by satisfactory elemental analysis. The mixture of **8a** was found to be quite stable until a temperature of 120 °C and the NMR spectra did not significantly change to this temperature. The compounds were quite soluble in THF, toluene and benzene and sparingly soluble in pentane.

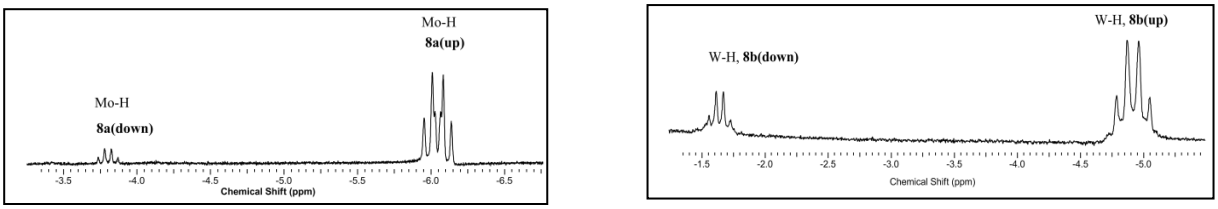

Figure 2.11. Hydride signal regions in the ^{1}H NMR spectra of the **up** and **down** isomeric mixtures of **8a** (left) and **8b**(right) at room temperature in THF.

In a similar way as for **7a**, when the isomeric mixture of **7b** was treated with $NaBHEt_3$ and heated at 90 °C the ^{31}P NMR spectra exhibited several unidentified signals along with the signals of the isomeric hydride complexes of **8b**. The mixture of isomers of **8b** could not be isolated in pure form due to the presence of as yet unidentified products. However the **8b** isomeric mixture could be prepared from **7b** using a $LiBH_4/Et_3N$ reagent at 80 °C furnishing an excellent yield (74%). Two sets of doublets and triplets were found in the ^{31}P NMR spectra (Figure 2.10) and attributed to the internal and terminal phosphorus atoms of the isomeric mixture of **8b** with following assignments: 77.2 {t, $^{3}J_{PP}$ = 6.1 Hz, (PPh) $^{1}J_{PW}$ = (d, satellites), 187 Hz, **8b(up)**), 74 {t, $^{3}J_{PP}$ = 10.1 Hz, (PPh) $^{1}J_{PW}$ = (d, satellites), 231.8 Hz, **8b(down)**}, 64.4 {d, $^{3}J_{PP}$ = 6.3 Hz, (P^{i}Pr) $^{1}J_{PW}$ = (d, satellites), 187 Hz, **8b(up)**}, 52.4 (d, $^{3}J_{PP}$ = 10.6 Hz, (P^{i}Pr) $^{1}J_{PW}$ = (d, satellites), 231.8 Hz, **8b(down)**}. From the intensities of the ^{31}P NMR spectra we concluded that the isomeric mixtures of **8b** were present in solution in a 4 : 1 ratio. The ethylene protons were observed as overlayed in the region at δ 2.29-2.09 ppm in the ^{1}H NMR spectra, in addition to several overlayed multiplets for the methyl, methelene and methine protons. Nevertheless, two distinct quartets appeared in the expected upfield region for the H_W nuclei at δ = -1.6 {q, $^{2}J_{PH}$ = 34.3 Hz, **8b(down)**} and -4.95 (q, $^{2}J_{PH}$ = 51.9 Hz, **8b(up)**} ppm (Figure 2.11). In the ^{13}C NMR spectrum a multiplet resonances

at δ 30.5 ppm was assigned to the ethylene carbon atoms of **8b(up)** and **8b(down)** which apparently appear at the same chemical shift and due to the two carbon atoms are both symmetry related by structure or because there is fast rotation about the W-(ethylene) bond. The IR spectra exhibited just one resonance at 1622 cm^{-1} assigned to the ν_{NO} stretching vibration of both isomers **8b(up)** and **8b(down)**. Similar to the isomeric mixture of **8a**, that of **8b** was also found to be soluble in THF, toluene and benzene, but it is not soluble in pentane at all. Furthermore, the composition of the isomers of **8b** was established by elemental analysis.

Preparation of the $W(NO)Cl(H)_2(etp^ip)$ complex 9b

Reaction of the isomeric mixture of **3b** with excess of Na/Hg at room temperature afforded in the presence of 2 bar of H_2 in THF the dihydride complex **9b** (Scheme 2.3) in 87% yield. The ^{31}P NMR spectra of **9b** revealed only one triplet at δ 80.5 (t, $^3J_{PP}$ = 22 Hz, PPh, $^1J_{PW}$ = (d, satellites), 166 Hz) ppm and one doublet at δ 66.5 (d, $^3J_{PP}$ = 22 Hz, $^iPr_2P$, $^1J_{PW}$ = (d, satellites), 179 Hz) ppm indicating formation of only one isomer or interconversion of both expected isomers fast on the NMR time scale. The ^1H NMR spectra of **9b** revealed a characteristic doublet of triplet signal at δ 4.41(dt, $^2J_{PH}$ = 17 Hz, $^2J_{PH}$ = 6 Hz, W-H) ppm attributed to the metal attached two hydride ligands (Figure 2.12). The doublet of triplet splitting pattern arises due to the coupling with the inequivalent terminal and internal phosphorus atoms of the attached etp^ip ligand. The size of the P-H coupling constants and the relative sharpness excludes the formation of a η^2 dihydrogen ligand. For a H_2 ligand we would expect in a room temperature spectrum a broad singlet. The IR spectra of **9b** showed a sharp band at 1532 cm^{-1} attributed to the nitrosyl stretching vibration. **9b** was found to be stable for several days under hydrogen atmosphere. However in the absence of hydrogen and in solid state slow formation of several species was observed as indicated by ^{31}P NMR spectroscopy. This could be due to slow release of hydrogen from the tungsten center and subsequent coordination of nitrogen forming a N_2 complex. In case N_2 can not coordinate formation of a dinuclear species has to be assumed. A satisfactory elemental analysis could not be obtained. Nevertheless "pure" **9b** could be regenerated from this impure solid material in solution putting it under hydrogen atmosphere.

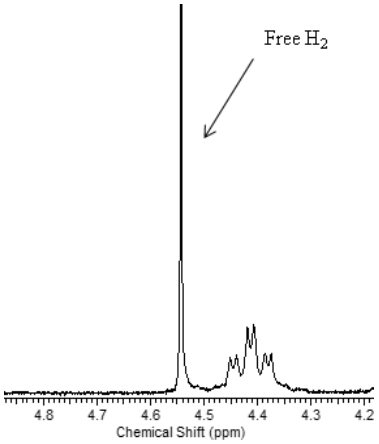

Figure 2.12. ^{1}H NMR spectra of the hydride signal region of **9b** at room temperature (THF-d_8).

The labile acetonitrile ligand of the isomeric mixture of **5b** could also be reacted with H_2 to give **9b** (Scheme 2.3). This reaction could be carried out with "impure" **5b** which may contain also a THF ligand or were a dinuclear species. However it was surprising to see that we could not observe in the NMR spectra isomeric mixtures of the dihydride **9b** when placed under H_2 atmosphere.

Preparation of the Mo(NO)Cl(η^2-PhSiH$_3$)(etp^{i}p), 10a

We attempted the preparation of the hydride species from the acetonitrile complex **5a** using ionic hydrides $LiBH_4$ or $NaBHEt_3$. However these experiments led to decomposition of the reaction mixtures. Therefore we opted to choose the mild hydride transfer reagent phenylsilane. In this case, addition of 2 equiv. of phenylsilane to a THF solution of **5a** at room temperature resulted in the formation of yellow color sigma silane Mo(NO)Cl(η^2-PhSiH$_3$)(etp^{i}p), **10a** complex in 90% yield (Scheme 2.3). The ^{31}P NMR spectra revealed one triplet at δ = 84 (t, $^3J_{PP}$ = 19 Hz, PPh) and one doublet at δ 66 ppm (d, $^3J_{PP}$ = 19 Hz, ^{i}Pr$_2$P) confirming the presence of only one isomer. In the ^{1}H NMR spectra a broad singlet at δ 5.5 ppm was assigned to the η^2 bonded Si-H moiety of the PhSiH$_3$ ligand. The remaining H_{Si} atoms of the PhSiH$_3$ ligand could be observed as broad singlets at δ 4.1 and δ 0.7 ppm. The assignment of these H_{Si} atoms were confirmed by 1D NOE experiment which upon irradiation showed exchange of these three H atoms of the attached PhSiH$_3$ ligand. Furthermore, the observed H_{Si} signals were in the similar range with a cationic sigma silane complex [CpRu(PiPr$_3$)(CH$_3$CN)(η^2-H$_3$SiPh)][B(C$_6$H$_5$)$_4$] reported by Nikonov and

coworkers.[21] The possibility of oxidative addition of $PhSiH_3$ to form a silyl hydride complex can be excluded on the basis that a clean quartet signal is expected of the oxidatively added Mo-H ligand which we could not observe. In addition the P-H correlation experiment did not reveal any metal hydride bonds. The solid state IR spectra of the obtained yellow species showed a sharp signal at 1576 cm^{-1} attributed to the nitrosyl stretching frequency. The ^{29}Si NMR spectra exhibited a resonance at δ -25 ppm which is significantly downfield shifted compared to free $PhSiH_3$ (^{29}Si = -60 ppm) supporting the presence of a silicon moiety attached with the metal centre and this resonance showed correlation with *ortho*-Ph (multiplet, 7.8 ppm) of $PhSiH_3$ in the ^{1}H-^{29}Si HMBC experiment. Finally the composition of **10a** was confirmed by obtaining satisfactory elemental analysis.

Preparation of the M(NO)(CO)H(etp^{i}p) complexes (M = Mo, 11a;W, 11b)

Reaction of the chloride derivatives **6a** and **6b** with excess of $LiBH_4$ in Et_3N at 90 °C temperature resulted in the formation of the hydride complexes Mo(NO)(CO)H(etp^{i}p) **11a** and W(NO)(CO)H(etp^{i}p) **11b** (Scheme 2.4) in 67% and 58% yields, respectively. The $^{31}P\{^{1}H\}$ NMR

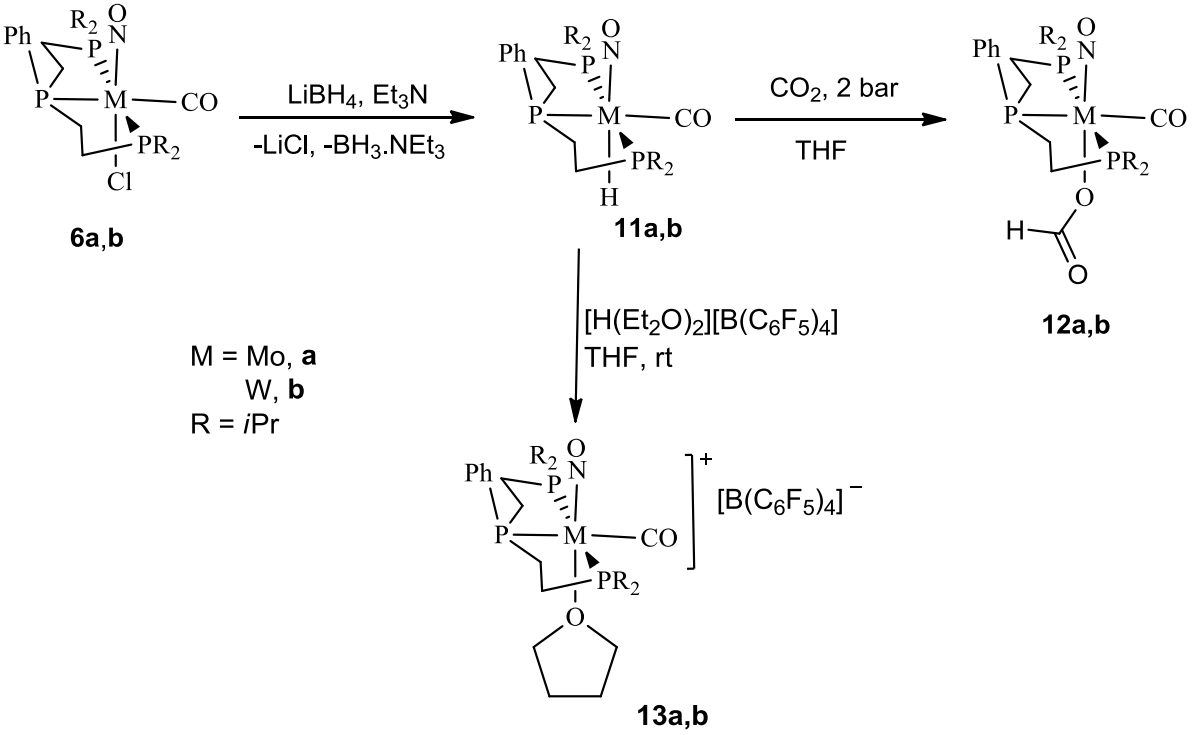

Scheme 2.4. Synthetic access to the carbonyl hydrides **11a**,**b** and derivatives.

spectra of **11a** exhibited a doublet at δ = 92.9 ppm ($^3J_{PP}$ = 5.9 Hz) and a triplet at δ = 97.2 ppm ($^3J_{PP}$ = 5.9 Hz). and the ^{31}P NMR spectra of **11b** exhibited the doublets and triplets at δ = 72.3 ($^3J_{PP}$ = 5.2 Hz, $^1J_{PW}$ = (dd, satellites), 295 Hz) and 79.5 ppm ($^3J_{PP}$ = 5.2 Hz, $^1J_{PW}$ = (dt, satellites), 220.7 Hz), respectively, which indicated the presence of only the "**up**" isomer of type **11a,b(up)**.

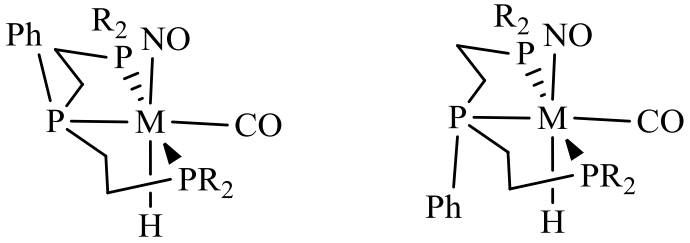

Figure 2.13. Expected **up** and **down** isomers of **11a,b** (M = Mo, W; R = *i*Pr$_2$). The "**down**" isomers are not formed.

However the "**down**" isomer **11a,b(down)** were also expected to be formed (Figure 2.13), since the precursor chloride complexes **6a,b** contain the isomeric mixture **6a,b(up)** and **6a,b(down)** in an approximately 7:3 ratio. Monitoring the isomeric reaction mixture of **6a,b** with $LiBH_4/Et_3N$ at 90 °C by $^{31}P\{^1H\}$ NMR spectra or ^{1}H NMR spectra did not reveal the presence of **11a(down)** or **11b(down)** so that the **down** isomers do not appear as reaction intermediates as well. Related low temperature (-60 °C) ^{31}P NMR experiments on **11a** and **11b** in the ^{31}P NMR indicated the absence of signals for **11a,b(down)**. Thus we concluded that kinetic distinction occured in that the **6a,b(down)** isomers did not react according to Scheme 2.4 with the $LiBH_4/Et_3N$ reagent presumably for steric reasons.

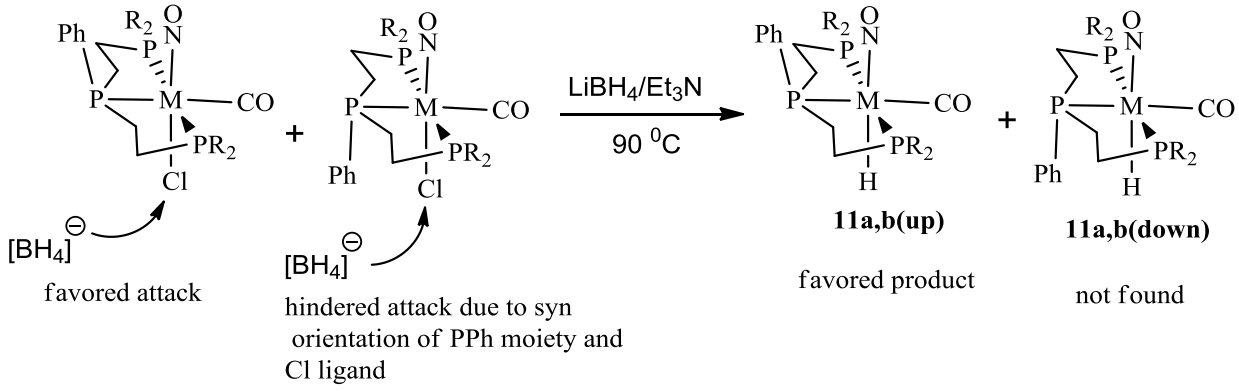

Scheme 2.5. Rationalisation for the exclusive formation of **11a,b(up)** isomers.

In the **down** isomers the phenyl groups "protect" the chloride ligand from attack of $[BH_4]^-$ (Scheme 2.5). This notion is strongly supported by the yields of **11a(up)** and **11b(up)** in an amount the **up** isomers were present in the **6a,b** mixture.

The ^{1}H NMR spectra of **11a(up)** and **11b(up)** at room temperature revealed characteristic quartet signals for the attached hydride ligands at δ = -5.5 ($^2J_{PH}$ = 74 Hz) of **11a(up)** and -5.35 ppm ($^2J_{PH}$ = 66.9 Hz) of **11b(up)** (Figure 2.14), in addition to the multiplets of the methyl, methylene and methyne protons of the etp^{i}p ligand. Strong bands in the IR spectra at 1888 cm^{-1} for **11a(up)** and 1859 cm^{-1} for **11b(up)** were attributed to the metal attached carbonyl ligands. Broad bands in the IR spectra for **11a(up)** and **11b(up)** at 1619 and 1637 cm^{-1}, respectively, were assigned to the M-H stretching vibrations. These complexes are quite soluble in THF, CH_2Cl_2, and benzene but sparingly soluble in pentane. The composition of **11a** and **11b** could be confirmed by correct elemental analyses.

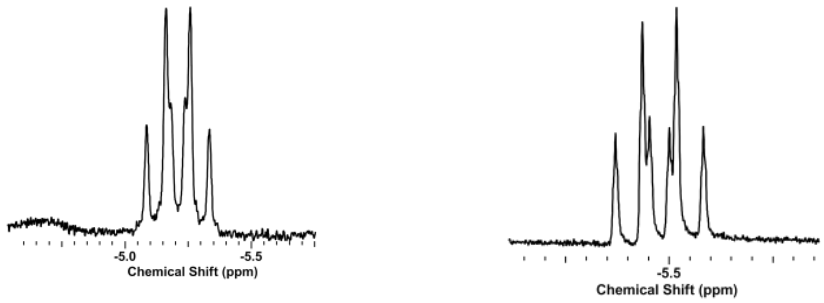

Figure 2.14. ^{1}H NMR spectra of the hydride signals regions of **11a(up)** (left) and **11b(up)** (right) at room temperature (C_6D_6).

Suitable single crystals for X-ray diffraction studies were obtained for **11a(up)** and **11b(up)** from concentrated pentane solutions at -30 °C after several days. The molecular structures of **11a(up)** and **11b(up)** are depicted in Figure 2.15. Similar to the chloride complexes **6a** and **6b**, the hydride complexes **11a** and **11b** revealed distorted octahedral geometries with the three phosphorus atoms in plane with the carbonyl ligand. The nitrosyl and hydride ligands were found to be disposed *trans* to each other in both cases of compounds. The phenyl rings of the etp^{i}p ligands were found syn to the nitrosyl ligand confirming the presence of the **up** isomers **11a,b(up)**.

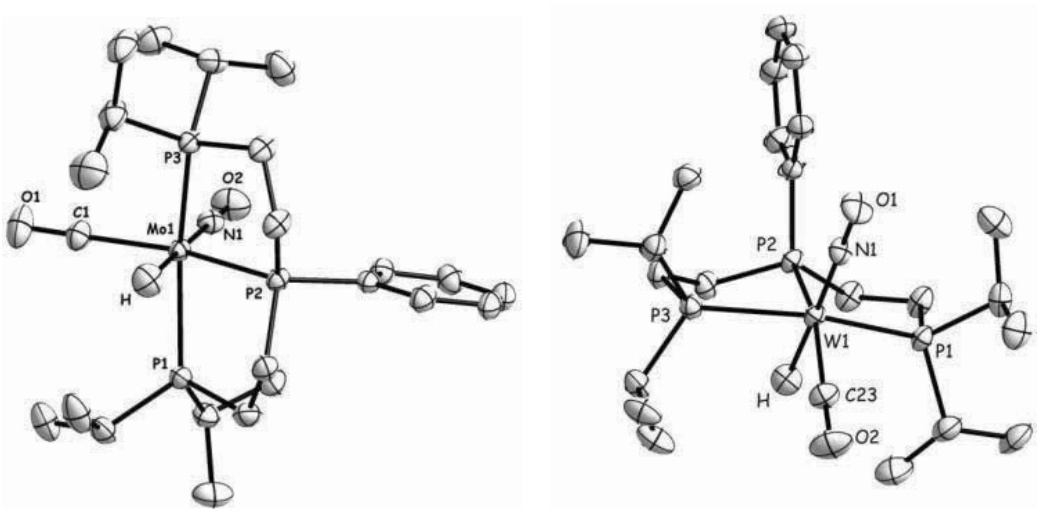

Figure 2.15. Molecular structures of [Mo(NO)(CO)H(etp^{i}p)] **11a(up)**, (left) and [W(NO)(CO)H(etp^{i}p)] **11b(up)**, (right) with thermal ellipsoids drawn at the 50% probability level.

Selected bond distances(Å) and bond angles(^{o}) for 11**a(up)**: Mo(1)-N(1) 1.8271(15), Mo(1)-P(1) 2.4727(5), Mo(1)-C(1) 1.9944(17), Mo(1)-H 1.795(19), C(1)-O(1) 1.1530(19), N(1)-O(2) 1.2096(18) N(1)-Mo(1)-H 177.9(6), P(1)-Mo(1)-P(3) 152.62(2), N(1)-Mo(1)-C(1) 97.10(7)

Selected bond distances(Å) and bond angles(^{o}) for **11b(up)**: W(1)-N(1) 1.830(2), W(1)-P(1) 2.4635(6), W(1)-C(23) 1.986(2), W(1)-H 1.79(3), C(23)- O(2) 1.163(3), N(1)-O(1) 1.219(3), N(1)-W(1)-H 177.0(9), P(1)-W(1)-P(3) 152.88(2), N(1)-Mo(1)-C(23) 97.01(9).

Preparation of the M(NO)(CO)(OCHO)(etp^{i}p) complexes, **12a and 12b**

The hydridic reactivity of complexes **11a** and **11b** was tested via the reaction with CO_2[22], [23].
At room temperature the reaction of **11a** with CO_2 in THF resulted in rapid formation of the formate complex Mo(NO)(CO)(OCHO)(etp^{i}p) (**12a**) with insertion of CO_2 into the Mo-H bond of **11a**. **11b** required for the same reaction 60 °C to form **12b**, apparently due to a less hydridic character of the H_W atom (Scheme 2.4). The ^{1}H NMR spectra of **12a** and **12b** revealed singlets at δ = 7.9 (**12a**) and 7.75 ppm (**12b**) attributed to the formate protons. In the ^{13}C NMR spectra, the formate carbon atoms appeared at δ = 164 (**12a**) and 166 ppm (**12b**) in addition to the carbonyl carbon atoms at δ = 232 and 233 ppm. The ^{31}P NMR spectra of **12a** and **12b** exhibited doublets at

68.4 ($^3J_{PP}$ = 7.5 Hz), 57 ($^3J_{CP}$ = 4.5 Hz) ppm and triplets at 78.9 ($^3J_{PP}$ = 7.5 Hz), 73 ($^3J_{PP}$ = 4.5 Hz) ppm, respectively. Due to the presence of only the "**up**" isomer in the synthetic precursors **11a,b**, **12a** and **12b** were also formed as only one isomer provided that the CO2 insertion takes place with retention at the metal centres, and apparently this is the case. Strong bands in the IR spectra at 1917 and 1638 cm^{-1} for **12a** and at 1897 and 1644 cm^{-1} for **12b** were assigned to the metal attached carbonyl ligands and to the $\nu_{(CO2)}$ vibrations of the formate groups. Finally the composition of the formate complexes **12a** and **12b** were confirmed by elemental analyses.

Reaction of 11a and 11b with $[H(Et_2O)_2][B(C_6F_5)_4]$

The $[B(C_6F_5)_4]^-$ anion is classified as non-coordinating and bulky[24, 25] which allows in many cases observation of dihydrogen or dihydride complexes upon protonation of transition metal hydrides.[26] A weakly coordinating H_2 ligand cannot be replaced by the $[B(C_6F_5)_4]^-$ anion, which is a weaker electron donor. In case the H_2 ligand generated via protonation of a transition metal hydrides is not stabilised enough by interaction with by the metal centre, weakly coordinating solvent, such as THF, can stabilise the $16e^-$ cationic complexes which are promising precursor complexes for ionic hydrogenations of ketones and imines.

We observed that the reaction of the hydride **11a** with the acid $[H(Et_2O)_2][BC_6F_5)_4]$ led at room temperature to the evolution of hydrogen gas with the solution turning green instantaneously, to form the cationic THF complex $[Mo(NO)(CO)(etp^ip)(THF)]^+[B(C_6F_5)_4]^-$, **13a**. The ^{1}H NMR spectrum revealed disappearance of the characteristic hydride signal of **11a** at -5.5 ppm and the ^{31}P NMR spectrum of the obtained new complex showed upfield shifts of the phosphorus signals with two major singlets at δ 69.1 ppm and at 75.7 ppm appearing in a 2:1 ratio. However, other as yet unidentified weak signals were also observed at δ 67.8 and 69.8 ppm. The purity of the complex was estimated to be 90% as revealed from the ^{31}P NMR spectrum. The solid state IR spectrum of the obtained green solid revealed a signal at 1943 cm^{-1} assignable to the ν_{CO} stretching vibrations. The shift of the carbonyl stretching vibrations to higher wavenumbers in comparison to **11a** supported the formation of the cationic complex $[Mo(NO)(CO)(etp^ip)(THF)]^+[B(C_6F_5)_4]^-$, **13a**. The signals of the coordinated THF were found in the ^{1}H NMR spectra at δ 3.1 ppm and 1.1 ppm.

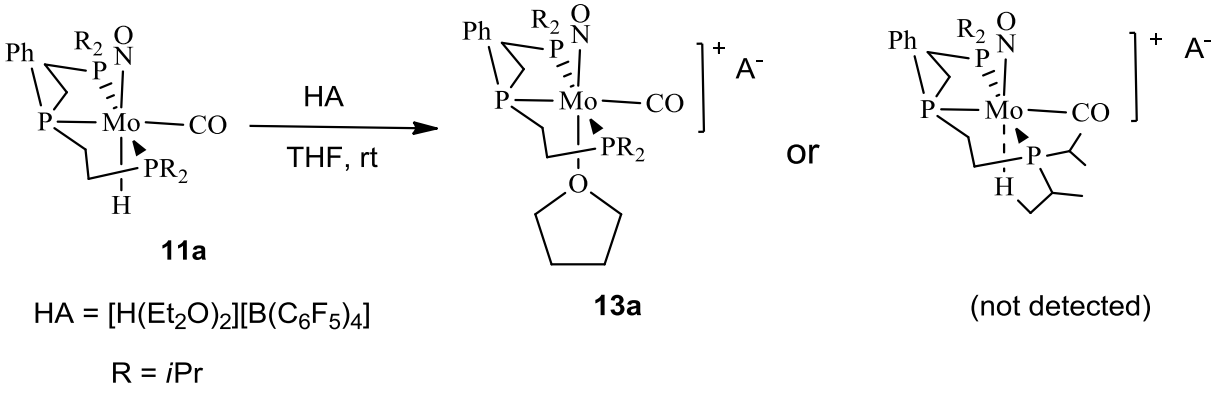

Scheme 2.6. Possible products of the reaction of **11a** with $[H(Et_2O)_2][B(C_6F_5)_4]$

The THF coordination to the metal centre was also confirmed by 1D NOE experiments, which established exchange of the coordinated THF signals with free THF.

Our group has previously reported[27] that the protonation of a $Mo(dippe)_2(NO)H$ complex with $[H(Et_2O)_2][BAr^F{}_4]$ produced the 16 e^- cationic complex $[Mo(dippe)_2(NO)][BAr^F{}_4]$ stabilised by an agostic interaction of one of the H_{Me} atoms of the dippe ligand with the metal centre. However, for **13a** evidence for the stabilization of the 16e- cationic species through loss of THF and agostic interaction of the methyl protons of the etp^{i}p ligand could not be provided, since the proton coupled ^{13}C DEPT experiment showed comparable C,H coupling constants of the C_{Me} atoms. Furthermore the elemental analyses confirmed the composition of $[Mo(NO)(CO)(etp^ip)(THF)]^+[B(C_6F_5)_4]^-$ salt, **13a** (Scheme 2.6).

In a similar way, when a THF-d_8 solution of **11b** was mixed with equimolar amounts of $[H(Et_2O)_2][B(C_6F_5)_4]$, the solution also turned green and the ^1H NMR spectra revealed the disappearance of the typical hydride signal at δ -5.4 ppm of **11b** and the formation of $[W(NO)(CO)(etp^ip)(THF)]^+[B(C_6F_5)_4]^-$, **13b** complex. ^{31}P NMR spectra showed appearance of new doublet and triplet signals at δ 56.9 ($^3J_{PP}$ = 4.3 Hz, $^1J_{PW}$ = (dd, satellites), 284 Hz), and 69.5 ($^3J_{PP}$ = 4.3 Hz, $^1J_{PW}$ = (dd, satellites), 284 Hz) ppm respectively, for the terminal and central phosphorus atom. The solid state IR spectra of **13b** showed sharp bands at 1926 and 1613 cm^{-1} which were assigned to the $\nu_{(CO)}$ and $\nu_{(NO)}$ vibrations of the coordinated carbonyl and nitrosyl ligands. The ^1H NMR showed several signals in the expected methyl, methylene and methyne regions for the etp^{i}p ligand along with two broad signals at δ 3.4 and 1.4 ppm for THF which is

apparently showing exchange between the free and the bound state fast on the NMR time scale. However the 1D NOE experiment did not manifest any other exchanges of nuclei. The free THF solvent which is in great stoichiometric excess and the averaged signal with the coordinated THF is that of the free THF. Furthermore, satisfactory elemental analyses supported the composition of the complex $[W(NO)(CO)(etp^{i}p)(THF)]^{+}[B(C_6F_5)_4]^{-}$. As an alternative reaction mode one could envisage formation of a cationic dihydride complex $[W(NO)(CO)(H)_2(etp^{i}p)][B(C_6F_5)_4]$ via protonation of **11b** at the hydride position and subsequent oxidative addition of the formed H_2 ligand in a way similar to the previously reported work by our group[27]. However this possibility was excluded, since evidence for metal dihydride signals was not provided by the ^{1}H NMR spectra or in the ^{31}P-^{1}H correlation spectra (Scheme 2.7).

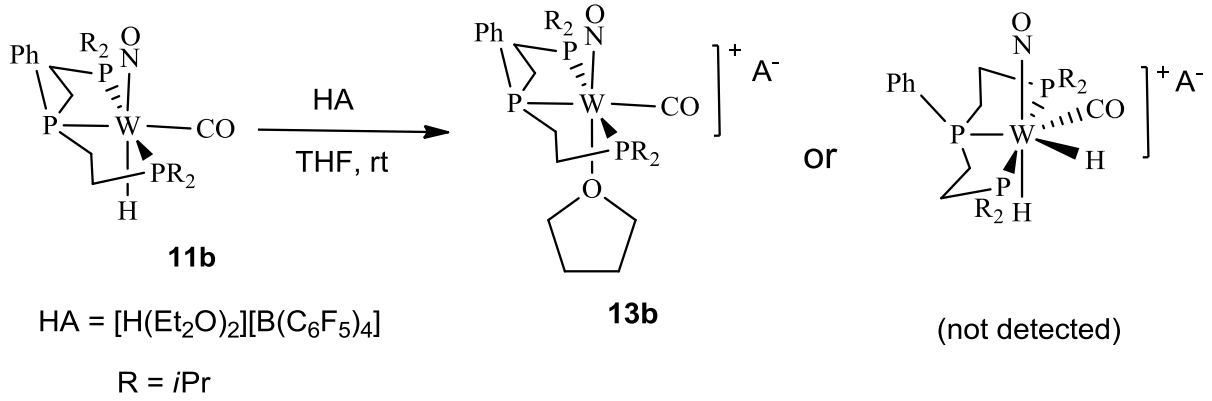

Scheme 2.7. Alternative reaction modes of **11b** with $[H(Et_2O)_2][B(C_6F_5)_4]$

2.2.3 Hydrogenations of Olefins Using M(NO)H(η²-ethylene)(etp^{i}p), (M = Mo, 8a; W, 8b) Catalysts

In previous work of our group applying rhenium nitrosyl DPEphos complexes[3b] we realised that *cis* dispositon of the ethylene and the hydride ligand would be a suitable prerequisite for a catalyst or catalyst precursors in homogeneous hydrogenations of olefins bearing a functionality and a vacant site similar to Wilkinson or Osborn type catalysts. Therefore having prepared the complexes **8a** and **8b,** good catalytic performance of these complexes seemed feasible in olefin hydrogenations following Osborn type pathway. Indeed this idea turned out to be accomplishable.

Table 2.1. Catalytic hydrogenation of olefins using catalyst **8a** and **8b** in absence and presence of $B(C_6F_5)_3$ (BCF) and R_3SiH mixture.

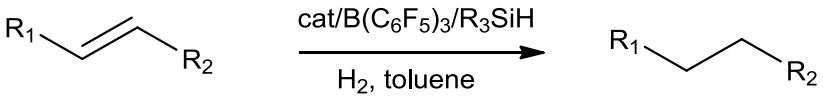

Entry[a]	Cat/ (mol%)	Substrates (mL)	Cocatalyst	Temp (°C)	H_2 (bar)	Time (h)	TOF (h^{-1})[b]	Conv (%)[c]
1	**8a**/0.23	1-hexene (0.2)	-	r.t.	60	22	-	-
2	**8a**/0.23	1-hexene (0.2)	-	100	60	14	12	39
3	**8a**/0.045	1-hexene (1)	-	140	60	0.5	912	21
4	**8a**/0.023	1-hexene (2)	Et_3SiH/BCF	140	60	2	5253	75
5	**8b**/0.020	1-hexene (2)	Et_3SiH/BCF	140	60	0.5	8200	80
6	**8a**/0.023	1-hexene (2)	Et_3SiH/BCF	140	20	0.5	2100	24
7	**8a**/0.023	1-hexene (2)	BCF	140	60	0.5	1990	23
8	**8a**/0.045	1-hexene (1)	Et_3SiH	140	60	0.5	2223	50
9	**8a**/0.045	1-hexene (1)	Et_3SiH/BCF	120	20	0.5	914	21
10	**8a**/0.045	1-hexene (1)	Et_3SiH/BCF	r.t.	60	20	15	14
11	**8a**/0.023	1-hexene (2)	Me_2PhSiH/BCF	140	60	0.5	3200	36
12	**8a**/0.023	1-hexene (2)	$MePhSiH_2$/BCF	140	60	0.5	2267	25
13	**8a**/0.023	1-hexene (2)	$^{i}Pr_3SiH$/BCF	140	60	0.5	4589	51
14	**8a**/0.023	1-hexene (2)	$PhSiH_3$/BCF	140	60	0.5	1382	15.6
15	**8a**/0.023	1-hexene (2)	Ph_2MeSiH/BCF	140	60	0.5	3373	38
16	**8a**/0.023	1-hexene (2)	Ph_2SiH_2/BCF	140	60	0.5	2322	26
17[d]	**8a**/0.023	1-hexene (2)	Et_3SiH/BCF	140	60	0.5	3732	43
18	**8a**/0.028	1-octene (2)	Et_3SiH/BCF	140	60	<2	3500	75
19	**8b**/0.049	1-octene (2)	Et_3SiH/BCF	140	60	0.5	3615	88
20	**8a**/0.041	Styrene (1)	Et_3SiH/BCF	140	60	2	2079	84
21	**8b**/0.037	Styrene (1)	Et_3SiH/BCF	140	60	0.5	2064	39
22	**8a**/0.053	1,7-octadiene (1)	Et_3SiH/BCF	140	60	2	1056	65
23[e]	**8a**/0.037	Cyclohexene (1)	Et_3SiH/BCF	140	60	<10	200	100
24	**8a**/0.047	Cyclooctene (1)	Et_3SiH/BCF	140	60	3	1355	55

25[e]	**8a**/0.047	α-amethyl styrene (1)	Et_3SiH/BCF	140	60	16	205	60
26	**8a**/0.089	1,5 cyclooctadiene (0.5)	Et_3SiH/BCF	140	60	14	200	74

[a]Unless and otherwise stated 2 mg of catalyst **8a** or **8b**, 5 equiv. of $B(C_6F_5)_3$ and 5 equiv. of silane, certain volume (mL) of olefins according to Table 1, 0.8 mL toluene were used. [b]TOFs were determined after initial 30 min of reaction by ^1H NMR using THF as internal standard. [c]Conversions were determined by ^1H NMR using THF internal standard. [d]the reaction was carried out without solvents. [e]TOFs were determined after 1 h.

Initially the hydrogenation of 1-hexene was carried at room temperature under 60 bar of H_2 and with a loading of 0.23 mol% of **8a**. However the hydrogenation failed under these circumstances (Table 2.1, entry 1)**.** This was envisaged be due to the robust nature of **8a** showing no sign of intra or intermolecular reactivity. As we already mentioned in the discussion of the preparation of **8a**, it is quite stable and remains intact even higher temperature. Also intramolecular transfer of the hydride onto the ethylene moiety or decomposition by ligand loss did not occur below 120 °C. Hydrogenation could nevertheless be initiated raising the temperature to 100 °C under 60 bar H_2 when presumably the hydride transfer became turned on. After 14 h, a conversion of 39% producing hexane could be achieved with a TOF of 12 h^{-1}. The catalytic performance of **8a** was boosted when the temperature was increased to 140 °C under 60 bar of H_2, which furnished a TOF of 912 h^{-1} and a conversion of 21% after initial 30 min of reaction time and a loading of 0.045 mol% **8a** (Table 2.1, entry 3).

Thus we planned to employ the hydrosilane/$B(C_6F_5)_3$ reagent as a co-catalyst to in-situ generate silylium ions expected to attach to the O_{NO} atoms.[28],[29]The resulting silylium derivatized NO species were thought to show facile bending at the N atom with reversible opening of a coordination site, very important for a catalytic reaction course. Indeed our group has already seen a drastic boost of the catalytic performance of rhenium nitrosyl iodo systems using the silane/ $B(C_6F_5)_3$ reagent as cocatalyst.[30]

When 0.023 mol% of the catalyst **8a** was mixed with 5 equiv. of the Et_3SiH/ $B(C_6F_5)_3$ reagent for the hydrogenation of 1-hexene under 60 bar of H_2 and 140 °C in toluene, the ^1H NMR pursuit exhibited after 30 min 59% of conversion corresponding to a TOF of 5253 h^{-1} (Table 2.1, entry 4), which is the highest TOF achieved till date by a molybdenum system in olefin hydrogenations and quite unexpectedly the tungsten derived **8b**/$B(C_6F_5)_3$/Et_3SiH system was found to be

catalytically even more active than the **8a**/$B(C_6F_5)_3$/Et_3SiH molybdenum system. When 0.020 mol% of **8b** and $B(C_6F_5)_3$/Et_3SiH mixture were loaded with 2 ml of 1-hexene in toluene at 140 °C under 60 bar H_2, the catalytic reaction mixture revealed by ^1H NMR after initial 30 min a conversion of 80% (using THF internal standard) corresponding to a TOF of 8200 h^{-1} (Table 2.1, entry 5). In addition the obtained hydrogenation product hexane could be identified by ^{13}C NMR spectroscopy.

It should be mentioned at this point that the two-component systems **8a**/Et_3SiH and **8a**/$B(C_6F_5)_3$ proved to be catalytically less active under the same conditions leading to TOFs of 1990 and 2223 h^{-1} respectively (Table 2.1, entries 7 and 8). The **8a**/Et_3SiH/$B(C_6F_5)_3$ combination was also found to be active in hydrogenations at room temperature. A loading of 0.045 mol% of the catalyst **8a** in presence of 5 equiv. of the Et_3SiH/$B(C_6F_5)_3$ mixture, led to a conversion of 14% after 20 h of reaction time with a TOF of 15 h^{-1} under 60 bar H_2 in toluene at 25 °C (Table 2.1, entry 10).

The hydrogenation rate was found to be pressure dependent. When 0.023 mol% of catalyst **8a** was loaded with 1-hexene (2 mL) in presence of $B(C_6F_5)_3$/Et_3SiH and under 20 bar H_2 at 140 °C a TOF of 2100 h^{-1} could be achieved after 30 min corresponding to a conversion of 21%. In addition various other silanes, such as Me_2PhSiH, $PhMeSiH_2$, iPr_3SiH, $PhSiH_3$, Ph_2MeSiH and Ph_2SiH_2 were also screened in combination with **8a**/$B(C_6F_5)_3$ leading to higher the catalytic performance. The results are listed in Table 2.1. However, those combinations were found to be catalytically less active than the **8a**/$B(C_6F_5)_3$/Et_3SiH system.

Hence, several other alkenes were tested in the hydrogenation at 140°C and 60 bar H_2 using the **8a**/$B(C_6F_5)_3$/Et_3SiH system showing the optimum conditions. With terminal alkenes, such as 1-octene, a conversion of 75% was achieved by addition of only 0.028 mol% of **8a** in the presence of the Et_3SiH/ $B(C_6F_5)_3$ reagent at 140 °C and with 60 bar of H_2 pressure furnished in less than 2 h with an initial TOF of 3500 h^{-1} (Table 2.1, entry 18). On the other hand, a loading 0.049 mol% of **8b** with Et_3SiH/ $B(C_6F_5)_3$ reagent showed an initial TOF of 3615 h^{-1} corresponding to 88% conversion of 1-octene to octane under otherwise similar conditions (Table 2.1, entry 19). The hydrogenation of styrene afforded under the same conditions 84% conversion after 2 h of reaction time with a TOF of 2079 h^{-1} (Table 2.1, entry 20) for the **8a**/Et_3SiH/$B(C_6F_5)_3$ system. For the **8b**/Et_3SiH/$B(C_6F_5)_3$ combination, an initial TOF of 2064 h^{-1} could be achieved with a 39% conversion of styrene to the corresponding ethyl benzene (Table 2.1, entry 21). In the cases the

disubstituted olefins cyclohexene and also for α-methylstyrene, the hydrogenation rates were found to be sluggish (Table2.1, entries 23 and 25). For instance, in the hydrogenation of cyclohexene catalyzed by 0.037 mol% of **8a** in presence of the $B(C_6F_5)_3/Et_3SiH$ mixture brought about a TOF of 200 h^{-1} could be achieved, and the reaction took quite long for completion (~10 h). For α-methylstyrene, only 60% conversion could be obtained after 16 h corresponding to an initial TOF of 205 h^{-1}. A loading of 0.053 mol% catalyst **8a** with $B(C_6F_5)_3/Et_3SiH$ mixture led to 65% conversion after 2 h for the hydrogenation of 1,7 octadiene though the hydrogenation proceeded well in the initial half an hour with a TOF of 1355 h^{-1} (Table 2.1, entry 22). For cyclooctene an initial TOF of 1355 h^{-1} could be achieved with a loading of 0.047 mol% of the catalyst **8a** and the $B(C_6F_5)_3/Et_3SiH$ mixture (Table 2.1, entry 21).

A reaction without solvent was also carried out. Under these "neat" conditions an initial TOF of 3732 h^{-1} could be achieved using a loading of 0.023 mol% **8a** in the presence of the $B(C_6F_5)_3/Et_3SiH$ mixture at 140 °C under 60 bar H_2 in absence of any solvent (Table 2.1, entry 16).

Nevertheless, we realized that within the initial half an hour of the reaction the hydrogenations proceeded quite well but the reactions started to slow down as it then progress for longer period of time. For instance, in the hydrogenation of 1-hexene (2 mL), a 59% conversion was achieved after 30 min of reaction with a loading of 0.023 mol% catalyst **8a** and in the presence of $Et_3SiH/B(C_6F_5)_3$ under 60 bar H_2 at 140 °C, but the reaction went to only 75% conversion after 2 h. This could be due to the fact that the catalyst started to decompose at an early stage under these relatively harsh conditions. Furthermore, the competitive reaction paths of isomerization converting the terminal olefins to form the more stable sterically hindered internal olefins could also be another reason for the decrease of the reaction rates. Indeed, the ^1H NMR spectra of the above mentioned reaction did not show after 2 h the presence of 1-hexene, instead multiplets in the ^1H NMR at δ 5 ppm, could be attributed to the olefinic protons of the sterically hindered 3-hexene indicating isomerisation of 1-hexene. However, in the hydrogenations of other olefins, the competitive isomerisation so fast forming stable internal olefins which hampered even full conversion with the given reaction times (Table 2.1, entries 4, 18, 22, 24 and 26).

Deuterium Kinetic Isotope Effect Studies

Exemplary deuterium isotope kinetics were studied using 20 bar of H_2 or D_2 in the hydrogenation of styrene catalyzed by the **8a**/$B(C_6F_5)_3$/Et_3SiH system at 140 °C. A loading of 0.041 mol% of the catalyst **8a** in presence of the $B(C_6F_5)_3$/Et_3SiH mixture (1:5 molar ratio) to a solution of styrene in toluene revealed a TOF of 821 h^{-1} under 20 bar H_2 in toluene. On the other hand under the same conditions when the reaction was carried out under 20 bar D_2, a TOF of 1498 h^{-1} resulting in an inverse DKIE of k_H/k_D = 0.55. This implies that H-H bond splitting is not rate limiting, because rate-determining H_2 splitting generally is expected to cause relatively high positive values. We therefore have to assume a late transition state with the X-H,D/Y-H,D bond forming process to be rate determining for instance in the reductive elimination step.

Taking all the facts together an Osborn type cycle with "olefin before H_2 coordination" as shown in Scheme 2.8 could be established for the olefin hydrogenations catalysed by **8a** or **8b** in

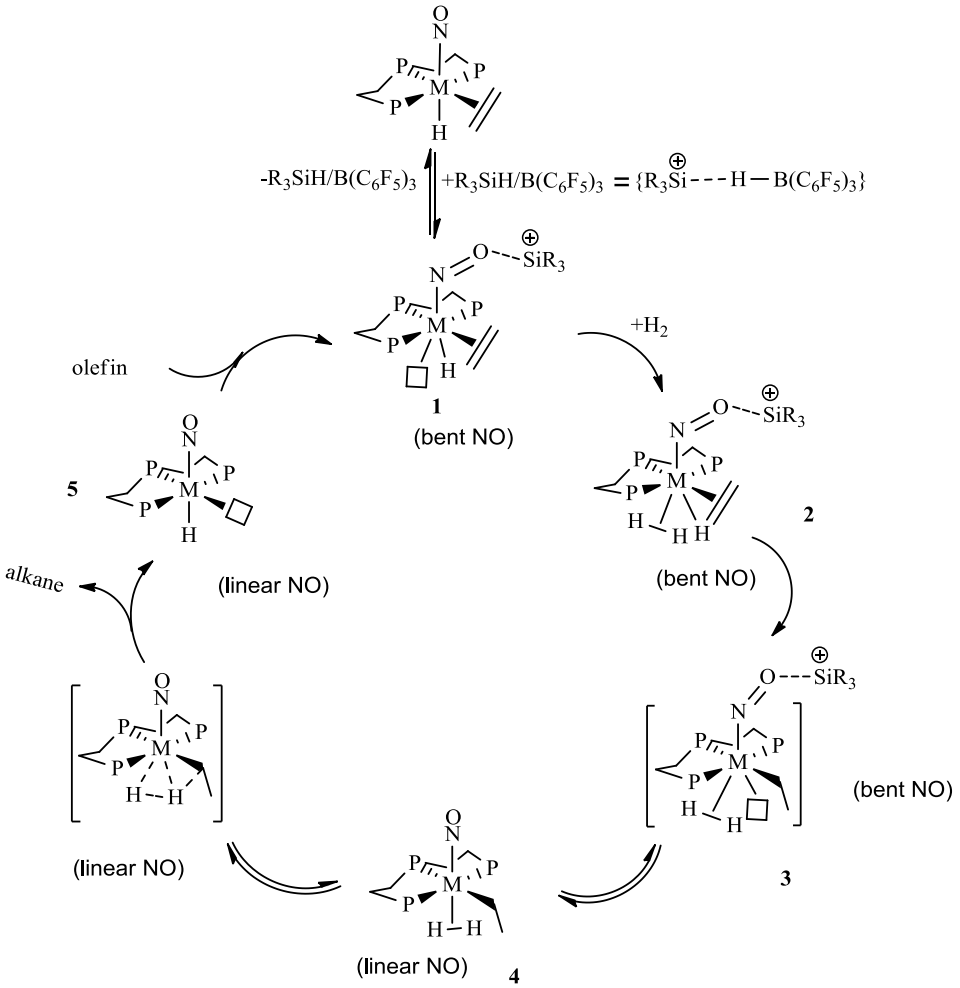

Scheme 2.8. Proposed "Osborn type" catalytic cycle for the Olefin hydrogenations

presence of the Et_3SiH/BCF cocatalytic system. An in situ generated silylium cation can initially attach to the O_{NO} atom of the nitrosyl ligand reversibly and enforce bending of the linear nitrosyl ligand leading to unsaturated 16 e^- species **1** (a linear nitrosyl is 3 electron donor, whereas a bent nitrosyl is one electron donor). Then H_2 uptake takes place to the unsaturated species **1** forming a "trihydride" species **2**. The early uptake of H_2 by bending is supported by strong H_2 pressure dependence (Table 2.1. entry 6). Then hydride transfer to the coordinated ethylene moiety occurs forming the unsaturated species **3.** This bent species **3** is presumably in equilibrium with the non bent form **4** and also is supposed to be in equilibrium with the oxidatively added H_2 species as shown in Scheme 2.8. Subsequent hydrogenolysis of the metal-alkyl bond produces the alkane product and the coordinatively unsaturated intermediate species **5**. Then coordination of the olefin and reversible bending of NO ligand by super electrophile Et_3Si^+ closes the catalytic cycle regenerating **1**.

2.2.4 Hydrogenation of Imines Catalysed by Mo(NO)(CO)H(etp^{i}p), 11a and W(NO)(CO)H(etp^{i}p), 11b Complexes.

Complexes **11a** and **11b** were initially tested for the hydrogenation of *N*-benzylideneaniline using $[H(Et_2O)_2][B(C_6F_5)_4]$ as a cocatalyst. A preliminary hydrogenation test with *N*-benzylideneaniline was carried out under 60 bar of H_2 at room temperature using THF as a solvent and with a loading of 1 mol% of the catalyst **11a**. However, a gas chromatographic analysis of the reaction mixture did not reveal any conversion of the *N*-benzylideneaniline to the corresponding amine. An increase of the temperature to 140 °C did also not reveal improvement of the catalysis with formation of an amine product. But when stoichiometric amounts of $[H(Et_2O)_2][B(C_6F_5)_4]$ and **11a** were applied as a cocatalytic system with otherwise the same reaction conditions, hydrogenation of *N*-benzylideneaniline occurred at room temperature showing a TOF of 13.3 h^{-1}. The GC/MS analysis, as well as a ^1H NMR spectrum confirmed formation of 40% of the *N*-benzylamine product after 3 h of reaction time (Table 2.2, entry 1). When the temperature was increased to 140 °C and 0.2 mol%

Table 2.2. Hydrogenation of various imines using **11a** and **11b** as catalysts in presence of stoichiometric amounts of $[H(Et_2O)_2][B(C_6F_5)_4]$.

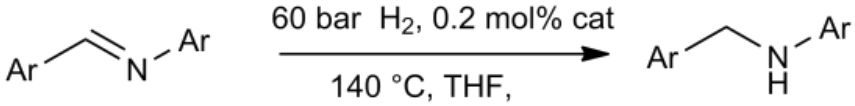

Entry[a]	Substrates	Cat	TOF[b] [h^{-1}]	Time [h]	Conv[c] [%]
1	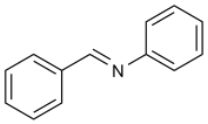	**11a**	384	0.5	38[d]
			590	2	89
			290	0.5	12[e]
			155	0.5	16[f]
			130	0.5	13[g]
			13	3	40[h]
		11b	160	<8	100
2	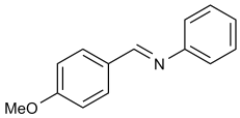	**11a**	1960[i]	0.25	>98
		11b	740	<3	>99
3	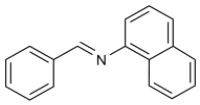	**11a**	10	25	73
		11b	6	12	29
4	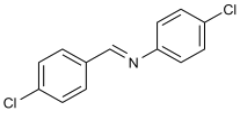	**11a**	82	15	56
		11b	60	12	>97
5	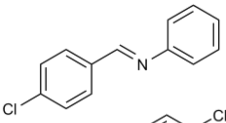	**11a**	10	13	11
6	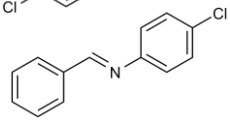	**11a**	90	25	64
		11b	110	14	32
7	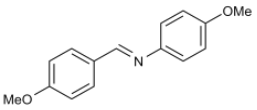	**11a**	810	0.5	81
		11b	268	3	85

8	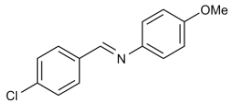	**11a**	-	11	5
9	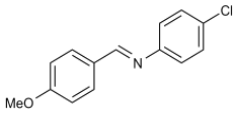	**11a** **11b**	110 230	25 <14	77 100
10	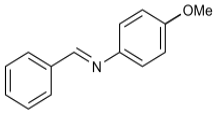	**11a**	398	2	56
11	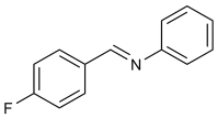	**11a**	86	14	18
12	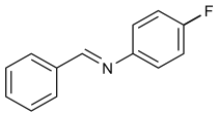	**11a**	485	3	74

[a] Unless and otherwise stated 140 °C temperature, 60 bar H_2 and 1 equiv. of the $[H(Et_2O)_2][(B(C_6F_5)_4]$ acid (with respect to the catalyst), 1 mL of THF were used as reaction conditions. [b] TOFs were determined after initial 30 min. by GC/MS. [c] Conversions determined by GC/MS on the basis of the consumption of the substrates. [d] at 80°C. [e] 25 bar H_2 [f] C_6H_5Cl was used as solvent. [g] Toluene was used as solvent. [h] The reaction was carried out at room temperature using 1 mol% catalyst and average TOF was determined after 3 h of reaction time. [i] TOF was determined after 15 min. by GC/MS.

of the catalyst **11a** was loaded under 60 bar H_2 using THF as a solvent, the initial TOF value raised to 590 h^{-1} (Table 2.2, entry 1). Then various solvents were screened to improve the catalysts activities. Changing the solvent to chlorobenzene and toluene with a loading of 0.2 mol% of the catalyst **11a** and a stoichiometric amount of $[H(Et_2O)_2][B(C_6F_5)_4]$ under 60 bar H_2 and 140 °C temperature, TOF values of 155 h^{-1} and 130 h^{-1} were reached (Table 2.2, entry 1) in the hydrogenation of *N*-benzylideneaniline. Lower solubility or in most cases insolubility of the iminium salt (an intermediate generated in the catalytic cycle) in non polar solvents might be one reason for the drastic decrease in the rate of the hydrogenation reactions. From the reduced activity in non-polar solvents we concluded that that weakly coordinating solvent molecules are required to stabilize the unsaturated intermediate appearing in the catalytic reaction course, perhaps also species similar in structure to **13a**. Therefore THF seemed to be an ideal solvent for the given hydrogenation course.

H_2 pressure dependency was also observed in THF (Figure 2.16). We carried out five hydrogenation reactions of *N*-benzylideneaniline in THF at 140 °C using 0.2 mol% of the catalyst

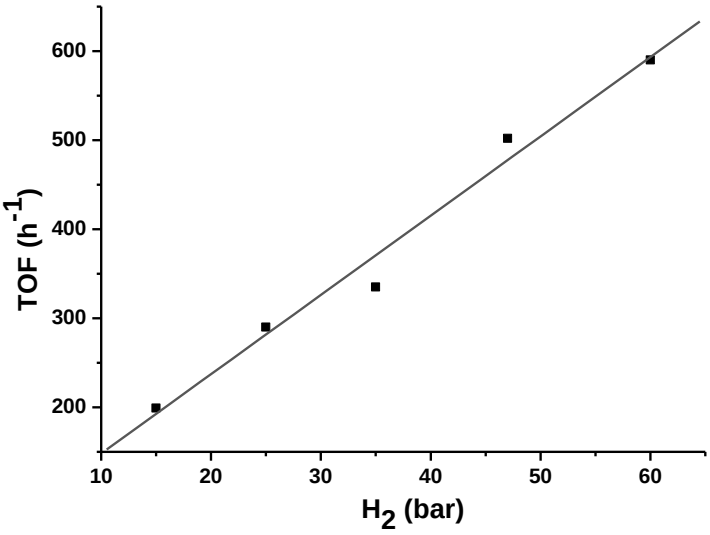

Figure 2.16. Plot of initial TOF (h^{-1}) vs hydrogen pressure (bar). 1.81 mmol of *N*-benzylideneaniline, 2 mg of the catalyst **7a** (0.2 mol%), 5 mg of $[H(Et_2O)B(C_6F_5)_4]$ in 1 mL THF and 140 °C temperature were used as reaction conditions and TOFs were determined after initial 30 min by GC/MS.

11a in presence of 5 mg of $[H(Et_2O)B(C_6F_5)_4]$ under various hydrogen pressures. A plot of the initial TOFs (h^{-1}) versus hydrogen pressures showed linear dependency of the rate.

However, when the hydrogenation of *N*-benzylideneaniline was carried out using **11b** as a catalyst (0.2 mol%) in the presence of $[H(Et_2O)_2][B(C_6F_5)_4]$, a TOF of 160 h^{-1} was reached under 60 bar H_2 and 140 °C in THF and the reaction was found to be completed within less than 8 h as revealed by GC/MS. Via various optimization experiments a temperature of 140 °C and a 60 bar H_2 pressure was found to be the optimum condition to achieve a maximum TOF of 1960 h^{-1} (Table 2.2, entry 2) for the hydrogenation of *N*-(4-methoxybenzylidene)aniline in THF substituted with an electron donating group at the carbon side of the imine. Under these conditions **11b** also showed higher catalytic activity in the presence of $[H(Et_2O)_2][B(C_6F_5)_4]$ revealing a TOF of 740 h^{-1} (Table 2.2, entry 2).

Various *para* substituted imines were then additionally tested for the hydrogenations with **11a** and **11b** as catalysts. Among the derivatives tested, we realized that chloride substituted imines were not so effective in the hydrogenations catalysed by **11a** or **11b** and even longer reaction

times did not reveal complete conversions of the imines to corresponding amines (Table 2.2, entries 4, 5, 6 and 8). Poisioning of the catalyst with chloride release and blocking of crucial intermediates by it was assumed to be reason for the low activities observed. However due to the limited scope of the hydrogenation reactions of various *para* substituted imines, we could not correlate a full series of derivatives for a Hammett plot which was to provide a rationalisation of the mechanism of the catalyses. Nevertheless, as mentioned already electron donating group on the benzylidene side were found to be more active than electron withdrawing groups (Table 2.2, entries 5, 6, 8, 9, 11 and 12) and electron withdrawing groups on the nitrogen side seemed to be not having much influence on the rate of the reaction as we can see it from the obtained initial TOF values in entries 1, 10, and 12 from Table 2.2.

The hydrogenation of acetophenone was also attempted. A loading of 1 mol% of the catalyst **11a** in the presence of stoichiometric amounts of $[H(Et_2O)_2][B(C_6F_5)_4]$ under 60 bar H_2 and 140 °C revealed only 7% conversion of acetophenone to corresponding 1-phenyl ethanol after 2 h with an average TOF of 3.5 h^{-1}. Blocking of the vacant site of the catalytically active species by the alkoxide or the alcohol product could be a reason for the poor activities in these cases.

MECHANISTIC INVESTIGATIONS

To investigate the mechanism of the reaction course of the imine hydrogenation reactions, a stoichiometric reaction was carried out between *N*-benzylideneaniline and **11a**. But no insertion was observed even after heating the reaction mixture to 140 °C for a long time (at least 3 h). To check the ionic mechanism with proton before hydride transfer and iminium salts as intermediates, an iminium salt was prepared from the reaction of *N*-benzylideneaniline with $[H(Et_2O)_2][B(C_6F_5)_4]$ at room temperature.[31] The formation of the iminium salt $[PhCH=NHPh]^+[B(C_6F_5)_4]^-$ was confirmed by ^1H NMR observing a typical downfield shift of the iminium CH proton from δ 8.6 (imine) to 9.6 (iminium salt) in THF-d_8. The salt was then mixed with **11a** in THF. The hydride transfer from the metal hydride to the electrophilic carbon atom of the iminium salt was observed at room temperature instantaneously as indicated by the ^1H NMR spectrum with disappearance of the signal of the iminium salt from 9.6 ppm and appearance of a doublet at 4.3 ppm (amine CH_2 proton).

An exemplary DKIE experiment was also carried out. With a loading of 0.2 mol% **11a** and stoichiometric amount of $[H(Et_2O)_2][B(C_6F_5)_4]$ in THF at 140 °C under 25 bar D_2 a TOF of 210

h^{-1} was revealed. The DKIE k_H/k_D was found to be 1.38. Due to this low DKIE value, heterolytic cleavage of H_2 is excluded as the rate limiting step and based on these observations a mechanistic scheme as depicted[18] in Scheme 2.9 could be set up.

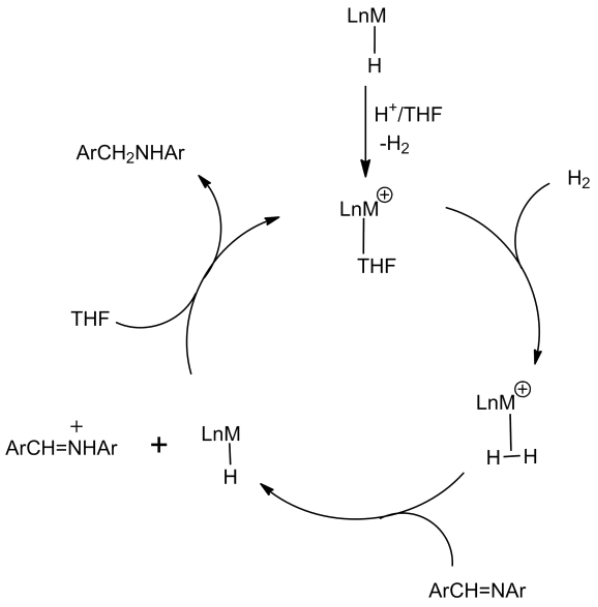

Scheme 2.9. Proposed ionic mechanism for the imine hydrogenations

The initial protonation of the hydride complex resulted in H_2 evolution and creation of a vacant site, which became stabilised by a weakly coordinating THF molecule. The THF could be replaced by H_2 to form a H_2 complex, particularly more stable under H_2 pressure, which is the key species in the catalytic cycle. An iminium salt is formed subsequently *via* proton transfer from the highly acidic metal dihydrogen complex to the imine. The deprotonation of the metal dihydrogen complex corresponds to the heterolytic splitting step of H_2, which, however, seemed less plausible as the rate limiting step due to the low DKIE effect. The iminium cation is the other key intermediate during the course of the hydrogenation reactions. Its presence was actually validated by the mentioned separate stoichiometric experiments. The next step consists of rapid hydride transfer to the highly electrophilic carbon centre of the iminium cation regenerating the cationic complex and generating the amine product. However, unlike in the reported work by Norton[11b] and Bullock[16] where hydride transfer is the rate limiting step, we could not observe

the L_nM-H intermediate during the course of the hydrogenation reactions. In fact, in a separate experiment hydride transfer from the corresponding metal hydride to the iminium salt was found at room temperature to be very fast on the NMR time scale. Therefore in the case of use of M(NO)(CO)H(etp^{i}p)) (M = Mo, W) as a catalyst, the hydride transfer could be excluded as the rate limiting step. Hence it seemed more plausible to assume in these imine hydrogenations that H_2 addition to the cationic metal complex is rate limiting step which gets support from the linear pressure dependency of the hydrogenation rate (Figure 2.16).

We also performed the hydrogenation reaction of *N*-benzylideneaniline at 140 °C and 60 bar H_2 with a loading of 0.25 mol% catalyst **11a** (5 mg) and stoichiometric amounts of $[H(Et_2O)_2][B(C_6F_5)_4]$ in THF to check the fate of the catalyst during catalysis and what species remaining at the end of these reactions under these relatively harsh conditions. The reaction was stopped after 20 min before it went to full conversion. The GC/MS analysis revealed 67% conversion of the imine to the corresponding amine. The ^{31}P NMR spectra of the reaction mixture showed several signals along with identifiable 30% of the cationic THF complex and after completion of the reaction, the ^{31}P NMR spectra showed two major signals at δ 59 and 57 ppm in a 2:1 ratio after full conversion which are expected to correspond to as yet unidentified species. These unidentified products were found to be catalytically inactive. Therefore it can be concluded that within the initial half an hour of the course of the hydrogenation, the reaction proceeds at a faster rate and after a while the catalyst started to decompose with a considerable effect on the total catalytic activity making the rate of the reaction sluggish.

2.3 Conclusion

Several molybdenum and tungsten nitrosyl complexes with varying oxidation states ranging from +II to 0 were prepared bearing the new chelating triphosphine (iPr$_2$PCH$_2$CH$_2$)$_2$PPh (etp^{i}p) ligand. Most of the complexes appeared as isomeric mixtures differing in the *syn* or *anti* nitrosyl ligand orientation of the phenyl ring attached to the internal phosphorus atom. The [M(NO)Cl$_3$(etp^{i}p)] (M = Mo, **3a**; W, **3b**) complexes could be reduced to the diamagnetic species M(NO)Cl(NCMe)(etp^{i}p) (M = Mo, **5a**; W, **5b**) and M(NO)(CO)Cl(etp^{i}p) (M = Mo, **6a**; M = W, **6b**) and the paramagnetic complexes M(NO)Cl$_2$(etp^{i}p) (M = Mo, **4a** and M = W, **4b**). According to the EPR spectra and magnetic susceptibility measurements **4a** and **4b** exhibited characteristic

paramagnetic behaviour. Two ethylene complexes Mo(NO)Cl(η^2-ethylene)(etp^{i}p) **7a** and W(NO)Cl(η^2-ethylene)(etp^{i}p) **7b** were obtained upon reduction of **3a,b** under ethylene atmosphere at room temperature. The ethylene hydride complexes M(NO)H(η^2-ethylene)(etp^{i}p) (M = Mo, **8a**; W, **8b**) could also be prepared and tested for their performance in olefin hydrogenations. A maximum TOF of 5253 h^{-1} was achieved in the hydrogenation of 1-hexene using the **8a**/$B(C_6F_5)_3$/Et_3SiH cocatalytic system. On the other hand **8b**/$B(C_6F_5)_3$/Et_3SiH combination showed even better performance in olefin hydrogenation yielding a maximum TOF of upto 8200 h^{-1} in the hydrognation of 1-hexene under at 140 °C under 60 bar H_2. Two carbonyl hydride complexes M(NO)(CO)H(etp^{i}p) (M = Mo, **11a**; W = **11b**) were also isolated and were found to react with CO_2 by insertion of CO_2 into the M-H bond forming formate complexes. **11a** and **11b** were catalytically active in hydrogenations of imines in the presence of the cocatalyst $[H(Et_2O)_2][B(C_6F_5)_4]$. A maximum TOF of 1960 h^{-1} was achieved for the hydrogenation of *N*-(4-methoxybenzylidene)aniline catalysed by **11a** whereas **11b** turned out to be less active than **11a**. Preliminary mechanistic studies were carried out and based on these "a proton before hydride transfer" mechanism was proposed.

2.4 Experimental section

General: All manipulations were carried out under an atmosphere of nitrogen using either dry glove box or Schlenk techniques. Reagent grade solvents benzene, tetrahydofuran, pentane, toluene, diethyl ether were dried with sodium benzophenone ketyl and distilled prior to use under N_2 atmosphere. Dichloromethane and cyclohexane were dried over calcium hydride and distilled. Deuterated solvents were dried with sodium benzophenone (THF-d_8, C_6D_6) and calcium hydride (CD_2Cl_2) and distilled via *freeze thaw pump* cycle before use. The $M(NO)Cl_3(NCMe)_2$ (M = Mo and W)[32] complexes and $[H(Et_2O)_2][B(C_6F_5)_4]$[33] were prepared according to literature procedures. Other reagents were purchased and used without further purification. NMR spectra were measured with a Varian Mercury 200 spectrometer (at 200.1 MHz for ^{1}H, at 81.0 MHz for ^{31}P), with Varian Gemini-300 instrument (^{1}H at 300.1 MHz, ^{13}C at 75.4 MHz), with Bruker-DRX 500 spectrometer (500.2 MHz for ^{1}H, 202.5 MHz for ^{31}P, 125.8 MHz for ^{13}C) and Bruker-DRX 400 spectrometer (400.1 MHz for ^{1}H, 162.0 MHz for ^{31}P, 100.6 MHz for ^{13}C). All chemical shifts for ^{1}H and $^{13}C\{^1H\}$ NMR are expressed in ppm relative to tetramethylsilane (TMS) and for $^{31}P\{^1H\}$ relative to 85% H_3PO_4 as an external standard reference. Signal patterns are as followed:

s, singlet; d, doublet; t, triplet; q, quartet; m, multiplet. IR spectra were obtained either ATR or KBr methods using Bio-rad FTS-45 instrument. Elemental analyses were carried out at Anorganisch-Chemisches Institute of the University of Zurich. The GC-MS spectra were recorded on a Varian Saturn 2000 spectrometer equipped with a Varian 450-GC chromatograph.

Preparation of Diisopropylvinylphosphine (1)

A solution of chlorodiisopropylphosphine (4.78 g, 0.031 mol) in 50 mL ether was allowed to cool to -30 ºC and a solution of vinylmagnesiumbromide in THF (31.40 mL, 1M solution in THF) was added dropwise with constant stirring over a course of 0.5 h. The resulting mixture was allowed to stir at -30 °C for further 0.5 h before allowing it to warm to room temperature. The liquid was separated from a white precipitate *via* a cannula under nitrogen atmosphere and concentrated at atmospheric pressure. The product was obtained as a colorless liquid by distillation. Yield: 3.26 g, 72%. ^{1}H NMR (300 MHz, CD_2Cl_2): δ = 6.4-5.7 (m, 3H, CH_2 =CHP), 1.8-1.6 (m, 2H, CH), 1.1-0.96 (m, 12H, CH_3). ^{31}P{^{1}H}NMR (121 MHz, CD_2Cl_2): δ = 6.5 (s), ^{13}C{^{1}H}NMR (75.5 MHz, CD_2Cl_2): δ = 135.9 (d, $^{2}J_{CP}$ = 20 Hz, CH_2=CH). 131.6 (d, $^{1}J_{CP}$ = 30.7 Hz, CH_2=CH), 23.4 (d, $^{2}J_{CP}$ = 9.7 Hz, CH), 19.9 (d, $^{1}J_{CP}$ = 17.59 Hz, CH_3), 18.7 (d, $^{2}J_{CP}$ = 8.5 Hz, CH_3).

Preparation of [(^{i}Pr$_2$PCH$_2$CH$_2$)$_2$PPh], (2, etp^{i}p)

Diisopropylvinylphosphine (3.80 g, 0.0264 mol), phenylphosphine (1.45 g, 0.013 mol) and AIBN (0.20 g, 1.21 mmol) were mixed together in 50 mL of cyclohexane under nitrogen atmosphere and refluxed for 48 h. The reaction was monitored by ^{31}P NMR. After completion of the reaction the resulting solution was filtered. The trisphosphine product was obtained as a colorless air sensitive liquid after removal of the cyclohexane solvent by distillation (3.95 g, 75%) ^{1}H NMR (500 MHz, $CDCl_3$): δ = 7.51-7.27 (m, 5H, Ph), 1.83-1.80 (m, 4H, -PCH_2), 1.68-1.63 (m, 4H, CH), 1.39-1.30 (m, 4H, PCH_2), 1.05-0.93 (m, 24H, CH_3). ^{31}P{^{1}H} NMR (202 MHz, $CDCl_3$) 11.5 (d, $^{3}J_{PP}$ = 26.93 Hz, $^{i}Pr_2P$), -14.5 (t, $^{3}J_{PP}$ = 26.9 Hz, PPh) ^{13}C{^{1}H}NMR (125.8 MHz, $CDCl_3$): δ = 137.6 (d, $^{1}J_{CP}$ = 16.1 Hz, C-*ipso*), 132.4 (d, $^{2}J_{CP}$ = 18.2 Hz, C-*ortho)*, 128.8 (s, C-*para*), 128.3 (d, $^{3}J_{CP}$ = 6.8 Hz, C-*meta*), 26.2 (d, $^{1}J_{CP}$ = 14.4 Hz, PCH_2), 26.1 (d, $^{1}J_{CP}$ = 13.9 Hz, PCH_2), 23.2 (d, $^{1}J_{CP}$ = 3 Hz, CH), 23.1 (d, $^{1}J_{CP}$ = 3.4 Hz, CH), 20 (d, $^{2}J_{CP}$ = 9.8 Hz, CH_3) 19.8 (d, $^{2}J_{CP}$ = 9.8 Hz, CH_3) 18.8 (d, $^{2}J_{CP}$ = 3.4 Hz, CH_3), 18.7 (d, $^{2}J_{CP}$ = 3.4 Hz, CH_3), 17.3 (d, $^{1}J_{CP}$ = 13.1 Hz, PCH_2), 17.2 (d, $^{1}J_{CP}$ = 13.1, PCH_2).

General procedure for the preparation of [M(NO)Cl_3(etp^{i}p)] (M = Mo, 3a; W, 3b)

M(NO)Cl_3(NCMe)$_2$ (1.6 mmol) was dissolved in 15 mL of THF. Then a solution of etp^{i}p ligand (1.6 mmol) in 5 ml THF was added into that solution. The resulting mixture turns deep red immediately and it was kept for stirring for 2 h. Precipitation of a solid was observed, which was separated from the solution and dried in *vacuo*. Washing with THF and pentane followed. Finally the solid was extracted with CH_2Cl_2 and dried in *vacuo.* Recrystallisation of the solid from a cold dichloromethane/pentane mixture afforded the desired product in crystalline form.

3a {mixture of **3a(up)** and **3a(down)}**: Yield: 55%. ^{1}H NMR (500 MHz, CD_2Cl_2): δ = 8.3-7.5 (m, Ph), 3.79-3.7 (m, PCH_2), 2.9-2.6 (m, PCH), 2.5-2.3 (m, PCH_2), 1.52-1.17 (m, CH_3). ^{31}P{^{1}H} NMR (202.5 MHz, CD_2Cl_2): δ = 76 (d, $^3J_{PP}$ = 72 Hz, **3a(up)**), 98 (t, $^3J_{PP}$ = 72 Hz, **3a(up)**), 77 (d, $^3J_{PP}$ = 76 Hz, **3a(down)**), 89 (t, $^3J_{PP}$ = 76 Hz, **3a(down)**) ^{13}C{^{1}H} NMR (125.8 MHz, CD_2Cl_2): δ = 133.6 (m, Ph), 132 (m, Ph), 130 (m, Ph), 129.7 (m, Ph), 30 (m, PCH_2), 29 (m, PCH), 28 (m, PCH), 22 (s, CH_3), 20 (m, CH_3), 17 (m, CH_2), 16 (m, CH_2). IR (cm^{-1}, ATR): 1648 (ν_{NO}). Anal.Calcd for $C_{22}H_{41}Cl_3MoNOP_3$: C, 41.89; H, 6.55; N, 2.22. Found: C, 41.75; H, 6.30; N, 2.01.

3b {mixture of **3b(up)** and **3b(down)}**: Yield: 52%. ^{1}H NMR (500 MHz, CD_2Cl_2): δ 7.9-7.5 (m, Ph), 3.79-3.76 (m, PCH_2), 3.0-2.9 (m, PCH_2), 2.68-2.60 (m, PCH), 2.54-2.39 (m, PCH_2), 1.48-1.15 (m, CH_3). ^{13}C{^{1}H}NMR (125.8 MHz, CD_2Cl_2): δ 133.6 (m, Ph), 132 (s, Ph), 129 (m, Ph), 29.4 (m, PCH_2), 29 (m, CH), 28 (m, CH), 20.6 (s, CH_3), 20.1 (s, CH_3), 19.6 (s, CH_3), 17.5 (m, PCH_2). ^{31}P{^{1}H} NMR (202.5 MHz, CD_2Cl_2): δ = 55 {d, $^3J_{PP}$ = 46 Hz, **3b(up)**}, 80 (t, $^3J_{PP}$ = 46 Hz, **3b(up)**), 56 {d, $^3J_{PP}$ = 49 Hz, **3b(down)**}, 72 {t, $^3J_{PP}$ = 49 Hz, **3b(down)**}. IR (cm^{-1}, ATR): 1618 (ν_{NO}). Anal.Calcd for $C_{22}H_{41}Cl_3NOP_3W$: C, 36.77; H, 5.75; N, 1.95. Found: C, 36.65; H, 5.71; N, 1.99.

General procedure for the preparation of M(NO)Cl_2(etp^{i}p), (M = Mo, 4a; W, 4b):

M(NO)Cl_3etp^{i}p (0.16 mmol) was added to a stirred suspension of 1% sodium amalgam (0.16 mmol) in 10 mL THF. The reaction mixture was kept stirring for 2 h at room temperature. The color of the solution turned green. The final supernatant green solution was filtered off from the mercury containing residue and evaporated to dryness. The residue was washed with pentane and dried. Finally the product was extracted with toluene and concentrated. Recrystallisation from cold toluene/pentane solution at -30 °C afforded green crystals.

4a: Yield: 59%. IR (cm^{-1}, ATR): 1589 (ν_{NO}). Anal.Calcd for $C_{22}H_{41}Cl_2MoNOP_3$: C, 44.38; H, 6.94; N, 2.35. Found: C, 44.42; H, 6.95; N, 2.39.

4b: Yield: 54%. IR (cm^{-1}, ATR): 1564 (ν_{NO}). Anal.Calcd for $C_{22}H_{41}Cl_2NOP_3W$: C, 38.67; H, 6.05; N, 2.05. Found: C, 38.75; H, 6.06; N, 2.03.

Preparation of Mo(NO)(NCMe)Cl(etp^{i}p), 5a:

To a solution of $Mo(NO)Cl_3(etp^ip)$ (50 mg, 0.08 mmol) in 10 mL CH_3CN, 5 equiv. of zinc granules were added. The resulting mixture was kept stirring for three days at room temperature. After completion of the reaction, the red colored solution was filtered off from excess zinc and evaporated to dryness. The obtained solid was washed with pentane twice and dried in *vacuo* and then extracted with THF to obtain a red powder in 75% (38 mg) yield. ^{1}H NMR (500 MHz, CD_3CN): δ = 7.8-7.4 (m, -Ph), 2.59-2.49 (m, PCH_2), 2.42-2.24 (m, CH_2), 1.83-1.80 (m, CH), 1.65-1.54 (m, CH), 1.36-1.06 (m, CH_3). $^{31}P\{^1H\}$ NMR (162 MHz, CD_3CN): 102.5 {s, PPh, 5a(up)}, 67.7 {s, $^iPr_2P$, **5a(up)}**, 94.9 {s, PPh, **5a(down)**}, 62.8 {s, $^iPr_2P$, **5a(down)}**. $^{13}C\{^1H\}$NMR (100.6 MHz, CD_3CN): δ = 133.8 (d, $^1J_{CP}$ = 11.5 Hz, C-*ipso*), 133 (d, $^2J_{CP}$ = 10.4 Hz C-*ortho)*, 131.5 (s, C-*para*), 129. (d, $^3J_{CP}$ = 8.8 Hz, C-*meta*), 27.9 (m, CH), 27.5 (m, CH_2)27 (m, CH), 26.8 (m, CH_2), 26.7 (m, CH), 20.7 (s, CH_3), 20.5 (CH_3), 19.9 (CH) 20 (s, CH_3), 19.9 (s, CH_3), 18.8 (s, CH_3), 18.7 (s, CH_3) IR (cm^{-1}, ATR): 1598 (ν_{NO}). Anal.Calcd for $C_{24}H_{44}ClMoNO_2P_3$: C, 47.97; H, 7.38; N, 4.66. Found: C, 48.15; H, 7.41; N, 4.57.

Preparation of W(NO)(NCMe)Cl(etp^{i}p), 5b

A solution of $W(NO)Cl_3(etp^ip)$ (200 mg, 0.28 mmol) in 15 mL of CH_3CN was added to excess of zinc granules (10 equiv.) and kept stirring atleast for 3 days at room temperature. After completion of the reaction, solution was filtered off from excess zinc and evaporated to dryness. The obtained solid was washed with pentane twice and dried in *vacuo* and then washed with toluene to remove paramagnetic impurities and finally dried to obtain a red powder. 90% purity on the basis of ^{31}P NMR. ^{1}H NMR (400 MHz, THF-d_8): δ = 7.86 (m, -Ph), 7.3 (m, Ph), 2.66 (m, PCH_2), 2.27(m, CH), 1.35-1.10 (m, CH_3). $^{31}P\{^1H\}$ NMR (162 MHz, CD_3CN): 52.9 {s, PPh, **5b(up)**}, 86.8 {s, $^iPr_2P$, **5b(up)**}, {48 (s, PPh, **5b(down)**}. 76 {s, $^iPr_2P$, **5b(down)**}. IR (cm^{-1}, ATR): 1566 (ν_{NO}). Anal.Calcd for $C_{24}H_{44}ClN_2OP_3W$: C, 41.85; H, 6.44; N, 4.07. Found: C, 39.80; H, 5.77; N, 4.83.

General procedure for the preparation of M(NO)(CO)Cl(etp^{i}p), (M = Mo, 6a; W = 6b)

$M(NO)Cl_3(etp^ip)$ (0.48 mmol) was added to a suspension of 1% sodium amalgam (5 eq. 2.4 mmol) in 15 mL THF in a young Schlenk tube . Then the nitrogen atmosphere was removed via a *freeze thaw pump* cycle and the tube was filled with CO (1 bar) and sealed. Stirring was continued overnight at room temperature to ensure the completion of the reaction. The final supernatant solution was filtered off from the mercury containing residue and evaporated to dryness. The residue was washed with pentane and extracted with toluene. Recrystallisation from cold toluene/pentane solution afforded pure crystals in moderate yields.

6a {mixture of 6a(up) and 6a(down)}: Yield: 65%. ^{1}H NMR (400 MHz, CD_2Cl_2): δ = 7.7-7.3 (m, -Ph), 2.45-2.31 (m, PCH_2), 2.25-2.19 (m, CH_2), 1.59-1.54 (m, CH), 1.41-1.38 (m, CH_3), 1.34-1.25 (m, CH_3), ^{31}P{^{1}H} NMR (162 MHz, CD_2Cl_2): 80.5 {t, $^3J_{PP}$ = 7.5 Hz, PPh, **6a(up)**}. 68.9 (d, $^3J_{PP}$ = 6.4 Hz, $^iPr_2P$, **6a(up)**}. 63.3 (t, $^3J_{PP}$ = 9 Hz, PPh, **6a(down)**}. 59.9 (d, $^3J_{PP}$ = 9.7 Hz, $^iPr_2P$, **6a(down)**}. ^{13}C{^{1}H}NMR (125.8 MHz, CD_2Cl_2): δ = 133.6 (d, $^1J_{CP}$ = 11.9 Hz, C-*ipso*), 132.7 (s, C-*ortho)*, 130.7 (s, C-*para*), 128.6 (d, $^3J_{CP}$ = 8.3 Hz, C-*meta*), 26.5 (m, PCH_2), 24.2 (m, PCH_2), 20.7 (CH), 19.9 (CH) 19.8 (CH_3), 19.5 (CH_3), 17.7 (CH_3), 17.4 (CH_3) IR (cm^{-1}, ATR): 1918(ν_{CO}), 1569 (ν_{NO}). Anal.Calcd for $C_{23}H_{41}ClMoNO_2P_3$: C, 46.99; H, 7.03; N, 2.38. Found: C, 47.14; H, 7.15; N, 2.29.

6b {mixture of **6b(up)** and **6b(down)}**: Yield 60%. ^{1}H NMR (400 MHz, CD_2Cl_2): δ = 7.9-7.3 (m, Ph), 2.72-2.61 (m, -PCH_2), 2.51-1.25 (m, PCH_2), 1.84-1.54 (m, CH), 1.42-1.08 (m, CH_3). ^{31}P{^{1}H} NMR (162 MHz, CD_2Cl_2): 72.6 {t, $^3J_{PP}$ = 4.5 Hz, PPh, $^1J_{PW}$ = (d, satellites), 215.4 Hz, **6b(up)}**, 55.2 {d, $^3J_{PP}$ = 5.2 Hz, (P^iPr) $^1J_{PW}$ = (d, satellites), 288 7 Hz, **6b(up)**}. 49 (d, $^3J_{PP}$ = 2.2 Hz, (PPh) $^1J_{PW}$ = (d, satellites), 281 Hz, **6b(down)**}, 48.7 {t, $^3J_{PP}$ = 2.24 Hz, (P^iPr) $^1J_{PW}$ = (d, satellites), 210 Hz, **6b(down)**}. ^{13}C{^{1}H}NMR (125.8 MHz, CD_2Cl_2): δ = 133.7 (s, Ph), 132.4 (s, Ph*)*, 130.9 (s, Ph), 128.6 (d, $^3J_{CP}$ = 9.54 Hz, C-*meta*), 27.8 (m, PCH_2), 27.1 (m, PCH_2), 20.8 (CH), 20.1 (CH) 19.7 (CH_3), 19.5 (CH_3), 17.6 (CH_3), 17.4 (CH_3) IR (cm^{-1}, ATR): 1906 (ν_{CO}), 1561 (ν_{NO}). Anal.Calcd for $C_{23}H_{41}ClNO_2P_3W$: C, 40.88; H, 6.12; N, 2.07. Found: C, 41.04; H, 6.20; N, 2.08.

General procedure for the preparation of M(NO)Cl(η^2-ethylene)(etp^{i}p) M = Mo, 7a; W, 7b

To a suspension of 1% sodium amalgam (5 equiv., 0.93 mmol) in 10 mL THF $M(NO)Cl_3(etp^ip)$ (0.185 mmol) was added in a young Schlenk tube. The schlenk was taken out from the glove box and the nitrogen atmosphere was removed via a *freeze thaw pump* cycle. Then the tube was filled with ethylene (1 bar) and sealed. Stirring was continued overnight at room temperature to ensure the completion of the reaction. The final supernatant solution was filtered off from the mercury containing residue and evaporated to dryness. The residue was washed with pentane and extracted with toluene. Recrystallisation from cold toluene/pentane solution afforded pure crystals of **7a** and **7b** in excellent yields.

7a {mixture of **7a(up)** and **7a(down)}**: Yield: 87%. ^{1}H NMR (500 MHz, THF-d_8): δ = 8.25-8.22 (m, -Ph), 8.02-7.99 (m, -Ph), 8.25-8.22 (m, -Ph), 7.46-7.38 (m, -Ph), 2.91-2.82 (m, PCH_2), 2.61-2.51 (m, CH), 2.45-2.36 (m, CH_2), 2.32-2.27 (m, CH), 2.02-1.99 (m, CH_2), 1.59-1.52 (m, CH_2), 1.37-1.10 (m, CH_3), 1.31 (ethylene CH_2 overlapped with CH_3 protons). ^{31}P{^{1}H} NMR (162 MHz, THF-*d*$_8$): 81.3 {t, $^3J_{PP}$ = 18 Hz, PPh, **7a(up)**}, 66 {t, $^3J_{PP}$ = 18.7 Hz, PPh, **7a(down)**}, 58.4 (d, $^3J_{PP}$ = 17.2 Hz, ^{i}Pr$_2$P, **7a(up)** and **7a(down)** overlapped**}**. ^{13}C{^{1}H}NMR (125.8 MHz,THF-*d*$_8$): δ = 134.9 (Ph), 131.6 (Ph), 129 (Ph), 30.7 (s, ethylene carbons), 30.3 (CH), 27 (CH_2), 28 (CH), 26.5 (m, CH), 26 (m, CH_2), 23 (CH_2), 20.5 (CH_3), 20.2 (CH_3), 19.5 (CH_3), 19.3 (CH_3), 18.3 (CH_3). IR (cm^{-1}, ATR): 1547 (ν_{NO}). Anal.Calcd for $C_{24}H_{45}ClMoNOP_3$: C, 49.03; H, 7.71; N, 2.38. Found: C, 49.34; H, 7.72; N, 2.19.

7b {mixture of **7b(up)** and **7b(down)}**: Yield 92%.^{1}H NMR (500 MHz, THF-d_8): δ = 8.20-8.17 (m, -Ph), 8.05-8.01 (m, -Ph), 7.46-7.44 (m, -Ph), 3.02-2.89 (m, PCH_2), 2.65-2.57 (m, CH_2), 2.42-2.32 (m, CH), 2.24-2.13 (m, CH), 1.58-1.51 (m, CH_2), 1.58-1.51 (m, ethylene CH_2), 1.38-1.27 (m, CH_3), 1.24-1.12 (m, CH_3). ^{31}P{^{1}H} NMR (162 MHz, THF-d_8): 74.3 {t, $^3J_{PP}$ = 7.5 Hz, (PPh) $^1J_{PW}$ = (d, satellites), 207.2 Hz, **7b(up)**}, 39.8 {d, $^3J_{PP}$ = 7.5 Hz, (P^{i}Pr) $^1J_{PW}$ = (d, satellites), 231Hz, **7b(up)**}, 57 {t, $^3J_{PP}$ = 8.2 Hz, (PPh) $^1J_{PW}$ = (d, satellites), 195 Hz, **7b(down)**}, 41 (d, $^3J_{PP}$ = 8.2 Hz, (P^{i}Pr) $^1J_{PW}$ = (d, satellites), 227.4 Hz, **7b(down)**}. ^{13}C{^{1}H} NMR (125.8 MHz, THF-*d*$_8$): 33.2 (ethylene carbons). IR (cm^{-1}, ATR): 1531 (ν_{NO}). Anal.Calcd for $C_{24}H_{45}ClNOP_3W$: C, 42.65; H, 6.71; N, 2.07. Found: C, 42.88; H, 6.56; N, 2.04.

Preparation of Mo(NO)H(η^2-ethylene)(etp^{i}p), 8a {mixture of 8a(up) and 8a(down)}

To a solution of Mo(NO)Cl(η^2-ethylene)(etp^{i}p) (70 mg, 0.12 mmol) in 10 mL THF in a Young Schlenk $NaHBEt_3$ (143 μL, 1M in THF) was added. The resulting solution was taken out from the glove box and kept for heating at 75 °C with constant stirring for 1 h. The reaction was monitored by ^{31}P NMR spectroscopy. After completion of the reaction the Schlenk tube was cooled and taken into the glove box. The reaction mixture was filtered and the solvent was removed in *vacuo*. A sticky red oily product was obtained which was washed with minimum amount of pentane to obtain solid product. The product was then extracted with benzene and then with toluene and dried in *vacuo*. Finally again it was extracted with benzene and dried. The light yellow powder of **8a** was obtained in 85% yield (55 mg).

^{1}H NMR (500 MHz, THF-d_8): δ = 7.99-7.75 (m, -Ph), 7.38-7.37 (m, -Ph), 2.71-2.61 (m, PCH_2), 2.61-2.55 (m, PCH), 2.33-2.30 (m, CH), 2.28-2.24 (m, PCH_2), 2.19-2.12 (m, ethylene CH_2), 1.32-1.23 (m, CH_3), 1.06-0.93 (m, CH_3), -3.9 (q, $^2J_{PH}$ = 46.4 Hz, Mo-H). -6.0 (q, $^2J_{PH}$ = 65.2 Hz, Mo-H). ^{31}P{^{1}H} NMR (202 MHz, THF-d_8): 96.1 {t, $^3J_{PP}$ = 17.6 Hz, PPh, **8a(up)**}. 89.8 {d, $^3J_{PP}$ = 17.6 Hz, ^{i}Pr$_2$P, **8a(up)**}. 92.5 {t, $^3J_{PP}$ = 21.6 Hz, PPh, **8a(down)**}. 79.5 {d, $^3J_{PP}$ = 21.8 Hz, ^{i}Pr$_2$P, **8a(down)}**. ^{13}C{^{1}H}NMR (125.8 MHz, THF-d_8): δ = 135 (Ph), 131 (Ph), 130.7 (s, C-*para*), 128.6 (Ph), 33.5 (m, PCH_2), 32.7 (s, ethylene CH_2), 30 (m, CH), 24 (m, CH) 20.6 (CH_2), 19.5 (CH_3), 19.1 (CH_3), 18.9 (CH_3), 16.5 (CH_3). IR (cm^{-1}, ATR): 1571 (ν_{NO}). Anal.Calcd for $C_{24}H_{46}MoNOP_3$: C, 52.08; H, 8.38; N, 2.53. Found: C, 52.42; H, 8.55; N, 2.29.

Preparation of W(NO)H(η^2-ethylene)(etp^{i}p), 8b {mixture of 8b(up) and 8b(down)}

A solution of W(NO)Cl(η^2-ethylene)(etp^{i}p) (150 mg, 0.22 mmol) in 20 mL Et_3N was mixed with $LiBH_4$ (24 mg, 1.11 mmol) in a Young Schlenk. The mixture and kept at 80 °C with constant stirring for 4 h. The reaction was monitored by ^{31}P NMR spectroscopy. After completion of the reaction the Schlenk tube was cooled and taken into the glove box. Without filtering the reaction mixture was dried in *vacuo* to remove Et_3N solvent. The obtained sticky oily product extracted with benzene at least twice to remove excess $LiBH_4$ and then twice with toluene. After drying the toluene solution and washing with pentane, complex **8b** was obtained as yellow powder in 74% yield (105 mg).

^{1}H NMR (300 MHz, THF-d_8): δ = 8.02 (m, -Ph), 7.41-7.32 (m, -Ph), 2.98-2.67 (m, PCH_2), 2.47-2.38 (m, CH), 2.29-2.09 {m, ethylene CH_2 for **8b(up)** and **8b(down)**, 1.87 (m, PCH_2), 1.32 (m, CH_3), 1.14-0.95 (m, CH_3), -1.55 {q, $^{2}J_{PH}$ = 34.3 Hz, W-H, **8b(down)**},-4.95 (q, $^{2}J_{PH}$ = 51.9 Hz, W-H, **8b(up)**}. ^{31}P{^{1}H} NMR (121 MHz, THF-d_8): 77.2 {t, $^{3}J_{PP}$ = 6.1 Hz, (PPh) $^{1}J_{PW}$ = (d, satellites), 187 Hz, **8b(up)**), 74 {t, $^{3}J_{PP}$ = 10.1 Hz, (PPh) $^{1}J_{PW}$ = (d, satellites), 231.8 Hz, **8b(down)**}, 64.4 {d, $^{3}J_{PP}$ = 6.3 Hz, (P^{i}Pr) $^{1}J_{PW}$ = (d, satellites), 187 Hz, **8b(up)**}, 52.4 (d, $^{3}J_{PP}$ = 10.6 Hz, (P^{i}Pr) $^{1}J_{PW}$ = (d, satellites), 231.8 Hz, **8b(down)**}.Selected ^{13}C{^{1}H}NMR (75 MHz, THF-d_8): δ = 30.5 {m, ethylene carbon of **8b(up)** and **8b(down)**}, IR (cm^{-1}, ATR): 1622 (ν_{NO}). Anal. Calcd for $C_{24}H_{46}NOP_3W$: C, 44.94; H, 7.23; N, 2.18. Found: C, 45.71; H, 8.14; N, 2.72.

Preparation of W(NO)Cl(H)$_2$(etp^{i}p), 9b

In an Young Schlenk tube a suspension of 1% sodium amalgam (0.58 mmol and $W(NO)Cl_3$(etp^{i}p) (82 mg, 0.114 mmol) were mixed to in 10 mL THF. The schlenk tube was taken out of the glove box. The nitrogen atmosphere was removed via a *freeze thaw pump* cycle and the tube was filled with 2 bar of H_2 and sealed. The resulting reaction mixture was kept for stirring overnight at room temperature. The final supernatant solution was filtered off from the mercury containing residue and evaporated to dryness. The residue was washed with pentane twice and then extracted THF. The product was obtained as red solid in 85% yield. Since in the solid state **9b** was found not to be stable for long time therefore satisfactory elemental analysis could not be obtained.

^{1}H NMR (500 MHz, THF-d_8): δ = 8.1 (m, -Ph), 7.5 (m, Ph), 4.41(dt, $^{2}J_{PH}$ = 17 Hz, $^{2}J_{PH}$ = 6 Hz, W-H), 2.70-2.6 (m, PCH_2), 2.42-2.32 (m, CH), 1.51'1.46(m, CH_2), 1.38-1.22 m, CH_3), ^{31}P{^{1}H} NMR (162 MHz, THF-d_8): 80.5 (t, $^{3}J_{PP}$ = 22 Hz, PPh, $^{1}J_{PW}$ = (d, satellites), 166 Hz). 66.5 (d, $^{3}J_{PP}$ = 22 Hz, $^{i}Pr_2P$, $^{1}J_{PW}$ = (d, satellites), 179 Hz). IR (cm^{-1}, ATR): 1532 (ν_{NO})

Preparation of Mo(NO)Cl(η^{2}-H$_3$SiPh)(etp^{i}p) 10a

To a solution of Mo(NO)(NCMe)Cl(etp^{i}p) (15 mg, 0.025 mmole) in 5 mL THF $PhSiH_3$ (6 μL) was added. The resulting mixture was kept for stirring for 15 min. Formation of the sigma silane complex **9a** could be observed by ^{31}P NMR spectroscopy. The final solution evaporated to dryness to remove THF and excess $PhSiH_3$. Finally the yellow product was obtained in pure form by washing with pentane (90% yield).

^{1}H NMR (500 MHz, THF-d_8): δ = 7.97(m, -Ph), 7.82 (m, Si-Ph), 5.6 (broad singlet, Si-H), 4.1 (bs, Si-H), 2.76 (m, PCH_2), 2.55 (m, CH_2), 2.39 (m, CH), 1.33-1.15 (m, CH_3), 0.7 (bs, Si-H).^{31}P{^{1}H} NMR (162 MHz, THF-d_8): 84 (t, $^{3}J_{PP}$ = 19 Hz, PPh). 66 (d, $^{3}J_{PP}$ = 19 Hz, $^{i}Pr_2P$. IR (cm^{-1}, ATR): 1576 (ν_{NO}). Anal.Calcd for $C_{28}H_{49}ClMoNOP_3Si$: C, 50.34; H, 7.39; N, 2.10. Found: C, 50.09; H, 6.99; N, 2.01. ^{1}H-^{29}Si HMBC = -25 ppm. Further structure established by 1D NOE and ^{1}H-^{29}HMBC and P-H correlation experiments.

General procedure for the preparation of M(NO)(CO)H(etp^{i}p), (M = Mo, 11a; W, 11b)

M(NO)Cl(CO)(etp^{i}p) (0.51 mmol) and $LiBH_4$ (2.5 mmol) were mixed in 20 mL of triethylamine in a Young Schlenk tube. The resulting mixture was heated in triethylamine to 90 °C with constant stirring for two days. After completion of the reaction monitored by ^{31}P NMR spectroscopy the solution was filtered off and the solvent was removed in *vacuo*. A sticky red oily product was obtained, which was extracted with benzene twice and dried in *vacuo*. Finally the product was obtained as a yellow **11a(up)** or red powder **11b(up)** after washing with minimum amount of pentane and dried in *vacuo*.

11a(up): Yield: 67%. ^{1}H NMR (500 MHz, 293K, C_6D_6): δ = 7.7-7.04 (m, 5H, -Ph), 2.2-2.1 (m, 4H, PCH_2), 1.94-1.86 (m, 4H, CH), 1.7-1.5 (m, 4H, PCH_2), 1.35-0.93 (m, 24H, CH_3), -5.5 (q, $^{2}J_{PH}$ = 74 Hz, Mo-H). ^{31}P{^{1}H} NMR (202.5 MHz, C_6D_6): 97.2 (t, $^{3}J_{PP}$ = 5.9 Hz, PPh). 92.9 (d, $^{3}J_{PP}$ = 5.9 Hz, $^{i}Pr_2P$). ^{13}C{^{1}H} NMR (125.8 MHz, C_6D_6): δ = 240 (m, CO), 136.4 (d, $^{1}J_{CP}$ = 17.6 Hz, C-*ipso*), 133.4 (d, $^{2}J_{CP}$ = 14.2 Hz, C-*ortho)*, 130.4 (s, C-*para*), 128.5 (d, $^{3}J_{CP}$ = 8.9 Hz, C-*meta*), 31.8 (t, $^{1}J_{CP}$ = 8.4 Hz, PCH_2), 33.6 (t, $^{1}J_{CP}$ = 8.4 Hz, PCH_2), 28.2 (m, CH), 24.6 (m, CH), 19.2 (d, $^{1}J_{CP}$ = 12.5 Hz, CH_3) 18.8.5 (s, CH_3), 18.5 (s, CH_3). IR (cm^{-1}, KBr): 1888(ν_{CO}). 1619 (ν_{Mo-H}), 1537 (ν_{NO}). Anal.Calcd for $C_{23}H_{42}MoNO_2P_3$: C, 49.91; H, 7.65; N, 2.53. Found: C, 50.03; H, 7.57; N, 2.56.

11b(up): Yield: 58%. ^{1}H NMR (400 MHz, C_6D_6): δ = 7.7-7.1 (m, 5H, Ph), 2.31-2.29 (m, 4H, -PCH_2), 2.0-1.9 (m, 4H, CH), 1.74-1.63 (m, 4H, CH_2), 1.23-0.9 (m, 24H, CH_3), -5.35 (q, $^{1}J_{PH}$ = 66.85 Hz, W-H). ^{31}P{^{1}H} NMR (162 MHz, C_6D_6): 79.5 (t, $^{3}J_{PP}$ = 5.2 Hz, (PPh) $^{1}J_{PW}$ = (d, satellites), 220.65 Hz), 72.3 (d, $^{3}J_{PP}$ = 5.24 Hz, (P^{i}Pr) $^{1}J_{PW}$ = (d, satellites), 295 Hz). ^{13}C{^{1}H} NMR (125.8 MHz, C_6D_6): δ = 236 (m, CO), 135.6 (d, $^{1}J_{CP}$ = 22.65 Hz, C-*ipso*), 133.9 (d, $^{2}J_{CP}$ = 14.3 Hz, C-*ortho*), 131 (s, C-*para*), 128.9 (d, $^{3}J_{CP}$ = 9.5 Hz, C-*meta*), 34.09 (t, $^{1}J_{CP}$ = 8.3 Hz,

PCH_2), 33.8 (t, $^1J_{CP}$ = 8.3 Hz, PCH_2), 29.2 (m, CH), 26.9 (m, CH), 19.8 (d, $^1J_{CP}$ = 15.5 Hz, CH_3) 19.5 (s, CH_3), 19 (s, CH_3). IR (cm^{-1}, KBr): 1859 (ν_{CO}), 1638 (ν_{W-H}), 1526 (ν_{NO}). Anal.Calcd for $C_{23}H_{42}NO_2P_3W$: C, 43.07; H, 6.60; N, 2.18. Found: C, 43.27; H, 6.56; N, 2.20.

General procedure for the preparation of M(NO)(CO)(OCHO)(etp^{i}p), (M = Mo, 12a; W, 12b)

A solution of M(NO)(CO)H(etp^{i}p), (**11a** or **11b**) (0.027 mmol) was frozen in a Young NMR tube. The nitrogen atmosphere was removed *via* a freeze thaw pump cycle. Then the tube was filled with 2 bar of carbon dioxide and sealed. Formation of **12a** took place upon shaking the NMR tube within 10 min. in quantitative yield. **12b** was obtained in quantitative yield by heating **11b** at 60 °C for 10 min.

12a: ^{1}H NMR (400 MHz, 293K, THF-d_8): δ = 7.91(m, 2H, Ph), 7.9 (s, OCHO), 7.5 (m, 3H, Ph), 2.45-2.34 (m, 4H, -PCH_2), 2.23-2.16 (m, 4H, CH), 1.97-1.60 (m, 4H, PCH_2), 1.32-1.10 (m, 24H, CH_3). ^{31}P{^{1}H} NMR (162 MHz, THF-d_8): 78.9 (t, $^3J_{PP}$ = 7.5 Hz, PPh), 68.4 (d, $^3J_{PP}$ = 7.5 Hz, P^{i}Pr). ^{13}C{^{1}H} NMR (125.8 MHz, THF-d_8): δ = 232 (m, CO), 164 (d, $^1J_{CP}$ = 4.8 Hz, OCHO), 132.7 (d, $^2J_{CP}$ = 11.9 Hz, C-*ortho*), 129 (s, C-*para*), 127 (d, $^3J_{CP}$ = 9.5 Hz, C-*meta*), 25 (m, PCH_2), 24 (m, PCH), 22.3 (m, CH_2), 22.1 (m, PCH_2), 18.5 (m, CH_3), 18 (m, CH_3), 17.7 (m, CH_3), 15.9 (s, CH_3). IR (cm^{-1}, KBr): 1917 (ν_{CO}), 1638 (ν_{OCHO}), 1576 (ν_{NO}). Anal.Calcd for $C_{24}H_{42}MoNO_4P_3$: C, 48.25; H, 7.09; N, 2.34. Found: C, 47.98; H, 7.02; N, 2.21.

12b: ^{1}H NMR (400 MHz, THF-d_8): δ = 7.93-7.89 (m, 2H, Ph), 7.75 (s, OCHO), 7.46-7.44 (m, 3H, Ph), 2.65-2.42 (m, 4H, -PCH_2), 2.31-2.29 (m, 2H, CH), 2.13 (m, 2H, PCH_2), 1.99-1.96 (m, 2H, CH), 1.58 (m, 2H, PCH_2), 1.34-1.12 (m, 24H, CH_3). ^{31}P{^{1}H} NMR (162 MHz, THF-d_8): 73 (t, $^3J_{PP}$ = 4.5 Hz, (PPh) $^1J_{PW}$ = (dt, satellites), 225.9 Hz), 57 (d, $^3J_{PP}$ = 4.49 Hz, (P^{i}Pr) $^1J_{PW}$ = (dd, satellites), 298 Hz). ^{13}C{^{1}H} NMR (125.8 MHz, THF-d_8): δ = 233 (m, CO), 166.9 (d, $^1J_{CP}$ = 6 Hz, OCHO), 134.7 (d, $^2J_{CP}$ = 11.9 Hz, C-*ortho*), 132 (s, C-*para*), 129.4 (d, $^3J_{CP}$ = 9.5 Hz, C-*meta*), 28.4 (m, PCH_2), 28 (t, $^1J_{CP}$ = 10.73 Hz, PCH), 25.4 (m, CH_2), 25.5 (m, PCH_2), 25 (m, CH), 20.8 (s, CH_3), 20.3 (s, CH_3) 20.1 (s, CH_3), 18 (s, CH_3). IR (cm^{-1}, KBr): 1897 (ν_{CO}), 1644(ν_{OCHO}), 1559 (ν_{NO}). Anal.Calcd for $C_{24}H_{42}NO_4P_3W$: C, 42.06; H, 6.18; N, 2.04. Found: C, 41.89; H, 6.19; N, 1.93.

Preparation of $[Mo(NO)(CO)(etp^{i}p)(THF)]^{+}[B(C_6F_5)_4]^{-}$, 13a

A solution of $[H(Et_2O)_2][B(C_6F_5)_4]$ (12 mg, 0.014 mmol) in 0.5 ml THF was added dropwise to a yellow solution of **11a** (8 mg, 0.014mmol) in 1 ml THF. The resulting solution turned green immediately with evolution of hydrogen. The solution was kept stirring for 10 min. Finally it was evaporated to dryness in *vacuo* and the solid was washed with pentane to obtain a green solid. Yield 90% based on the ^{31}P NMR spectrum. ^{1}H NMR (500 MHz, 223K, THF-d_8): δ = 7.8 (m, 2H, Ph), 7.6 (m, 3H, Ph), 3.1 (broad singlet, THF), 2.42 (m, 4H, -PCH_2), 1.9-1.8 (m, 4H, CH), 1.7-1.5 (m, 4H, PCH_2), 1.23-1.09 (m, CH_3), 1.1 (broad singlet, THF). $^{31}P\{^{1}H\}$ NMR (202 MHz, Toluene-d_8, 223K): 69.1 (singlet, $P^{i}Pr$), 75.7 (singlet, PPh) IR (cm^{-1}, KBr): 1943 (ν_{CO}), 1643 (ν_{NO}). Anal.Calcd for $C_{51}H_{50}BF_{20}MoNO_3P_3$: C, 46.95; H, 3.86; N, 1.07. Found: C, 46.87; H, 4.06; N, 1.04.

Reaction of $W(NO)(CO)H(etp^{i}p)$ with $[H(Et_2O)_2][B(C_6F_5)_4]$ to obtain 13b

To a solution of **11b** (8 mg, 0.0125 mmol) in 0.5 mL THF-d_8, $[H(Et_2O)_2][B(C_6F_5)_4]$ (11 mg, 0.013 mmol) was added. Similar to Mo the reaction, the resulting solution turned green immediately with the evolution of hydrogen. The solvent was evaporated to dryness and washed with pentane.^{1}H NMR (300 MHz, 293K, THF-d_8): δ = 7.9 (m, 2H, Ph), 7.6 (m, 3H, Ph), 3.03-2.9 (m, 4H, -PCH_2), 2.7-2.5 (m, 4H, CH), 2.2-2.0 (m, 4H, PCH_2), 1.47-1.12 (m, 24H, CH_3). $^{31}P\{^{1}H\}$ NMR (202 MHz, tol-d_8): 56.9 (d, $^{3}J_{PP}$ = 4.3 Hz, $^{1}J_{PW}$ = (dd, satellites), 284 Hz), 69.5 (t, $^{3}J_{PP}$ = 4.3 Hz, $^{1}J_{PW}$ = (dd, satellites), 284 Hz). IR (cm^{-1}, ATR): 1926 (ν_{CO}), 1613 (ν_{NO}). Anal.Calcd for $C_{47}H_{42}BF_{20}NO_2P_3W.C_4H_8O$: C, 43.99; H, 3.62; N, 1.01. Found: C, 44.25; H, 3.80; N, 1.06.

X-ray diffraction analyses

Single-crystal X-ray diffraction data were collected at 183(2) K on an Agilent Technologies Xcalibur Ruby area-detector diffractometer using a single wavelength Enhance X-ray source with MoKα radiation (λ= 0.71073 Å).[34] The selected suitable single crystals were mounted using polybutene oil on a flexible loop fixed on a goniometer head and immediately transferred to the diffractometer. Pre-experiment, data collection, data reduction and analytical absorption correction[35] were performed with the program suite *CrysAlisPro*.[36] The structures were solved by direct methods using *SHELXS97*.[37] The structure refinements were performed by full-matrix least- squares on F^2 with *SHELXL97*.[37] *PLATON*[38] was used to check the result of the X-ray

analysis. All programs used during the crystal structure determination process are included in the *WINGX* software.[39]

General Procedure for the catalytic alkene hydrogenations

A stock solution of freshly made catalysts **8a** or **8b** (10 mg in 1 mL of toluene) was prepared. An aliquot (0.2 mL) of that stock solution was added to a mixture of $B(C_6F_5)_3/R_3SiH$ (5 equiv. with respect to catalyst). Then a certain volueme (mL) of alkenes according to Table 1 was added into that mixture. The entire mixture was transferred to a steel autoclave. The autoclave was charged with required hydrogen pressure and kept in preheated (140°C) oil bath. After appropriate reaction time the autoclave was immediately taken out and cooled to room temperature. Then 200 μL of THF was added into that solution. The mixture was finally analysed by ^{1}H NMR immediately to identify the products and to determine the yields.. The TOFs and conversions were determined on the basis of ^{1}H NMR integration using THF as internal standard.

General procedure for the catalytic imine hydrogenation experiments:

A stock solution of freshly made catalyst **11a** or **11b** (10 mg in 5 mL of THF) was prepared. An aliquot (1 mL) of that stock solution was added to stoichiometric amounts of $[H(Et_2O)_2][B(C_6F_5)_4]$ (solution turned light green). Then imine (500 equivalents with respect to the catalyst) was added into that green solutions. The entire mixture was transferred to a steel autoclave. The autoclave was charged with the required hydrogen pressure and kept in a preheated oil bath (140°C). After appropriate reaction time the autoclave was immediately taken out and cooled to room temperature. The reaction mixture was taken out of the autoclave and filtered through silica gel. Without further purification a GC/MS spectrum was taken to determine the conversions of the hydrogenation products (on the basis of substrate concentration) and to identify the products. byproducts were observed according to GC/MS spectra except for the imines and amines.

GC/MS data for various imines and amines formed during hydrogenation reaction catalyses by 11a, 11b:

PhCH=NPh: rt = 9.083 min, m/z = 181; $PhCH_2NHPh$: rt = 9.339 min, m/z = 183; *p*-ClC_6H_4CH=N-*p*-C_6H_4Cl: rt = 11.790 min, m/z = 248; *p*-$ClC_6H_4CH_2NH$-*p*-C_6H_4Cl: rt = 12.612 min, m/z = 251;PhCH=N(α-naphtyl): rt = 13.255 min, m/z = 231; $PhCH_2NH$(α-naphtyl): rt =

13.662 min, m/z = 233; *p*-$MeOC_6H_4CH$=NPh: rt = 10.912 min, m/z = 211; *p*-$MeOC_6H_4CH_2$NHPh: rt = 10.989 min, m/z = 213; *p*-ClC_6H_4CH=NPh: rt = 10.298 min, m/z = 215; *p*-$ClC_6H_4CH_2$NHPh: rt = 10.722 min, m/z = 217 ; PhCH=N-*p*-C_6H_4Cl: rt = 10.379 min, m/z = 215; *p*-$ClC_6H_4CH_2$NHPh: rt =10.861 min, m/z = 217; *p*-$MeOC_6H_4CH$=N-*p*-C_6H_4OMe: rt = 13.219 min, m/z = 241; *p*-$MeOC_6H_4CH_2$NH-*p*-C_6H_4OMe: rt = 12.916 min, m/z = 243; *p*-ClC_6H_4CH=N-*p*-C_6H_4OMe: rt = 12.355 min, m/z = 245; *p*-$ClC_6H_4CH_2$NH-*p*-C_6H_4OMe: rt = 12.499 min, m/z = 247; *p*-$MeOC_6H_4CH$=N-*p*-C_6H_4Cl: rt = 12.567 min, m/z = 245; *p*-$MeOC_6H_4CH_2$NH-*p*-C_6H_4Cl: rt = 12.980 min, m/z = 247; *p*-FC_6H_4CH=NPh: rt = 8.925 min, m/z = 199; *p*-$FC_6H_4CH_2$NHPh: rt = 9.314 min, m/z = 201 ; PhCH=N-*p*-C_6H_4F: rt = 9.004 min, m/z = 199; $PhCH_2$NH-*p*-C_6H_4F: rt = 9.334 min, m/z = 201; Ph(CO)CH_3: rt = 4.438 min, m/z = 120; PhCH(OH)CH_3: rt = 4.356 min, m/z = 122.

2.5 APPENDIX

Table 2.3. Crystallographic data for **3a1**, **3b1**, and **3a2**.

	3a1	**3b1**	**3a2**
empirical formula	$C_{22}H_{41}Cl_3MoNOP_3$ $\cdot CH_2Cl_2$	$C_{22}H_{41}Cl_3NOP_3W$ $\cdot CH_2Cl_2$	$C_{22}H_{41}Cl_3MoNOP_3$
formula weight ($g\cdot mol^{-1}$)	715.68	803.58	630.76
temperature (K)	183(2)	183(2)	183(2)
wavelength (Å)	0.71073	0.71073	0.71073
crystal system, space group	monoclinic, $P2_1/c$	monoclinic, $P2_1/c$	triclinic, $P\bar{1}$
a (Å)	9.9523(1)	9.9398(1)	8.6718(2)
b (Å)	16.8232(2)	16.8284(2)	8.9624(2)
c (Å)	18.8977(2)	18.8808(2)	18.3710(4)
α (deg)	90	90	76.996(2)
β (deg)	96.170(1)	96.182(1)	80.720(2)
γ (deg)	90	90	80.415(2)
volume ($Å^3$)	3145.71(6)	3139.84(6)	1360.32(5)
Z, density (calcd) ($Mg\cdot m^{-3}$)	4, 1.511	4, 1.700	2, 1.540
abs coefficient (mm^{-1})	1.013	4.276	0.970
F(000)	1472	1600	652

crystal size (mm^3)	0.46 x 0.19 x 0.16	0.45 x 0.36 x 0.27	0.27 x 0.14 x 0.13
θ range (deg)	2.39 to 30.51	2.39 to 32.58	2.79 to 30.51
reflections collected	38044	48694	22171
reflections unique	9581 / R_{int} = 0.0384	11431 / R_{int} = 0.0397	8310 / R_{int} = 0.0294
completeness to θ (%)	100.0	100.0	99.9
absorption correction	analytical	analytical	analytical
max/min transmission	0.89 and 0.77	0.38 and 0.19	0.897 and 0.834
data / restraints / parameters	7558 / 0 / 315	9323 / 0 / 315	7032 / 3 / 298
goodness-of-fit on F^2	1.085	1.053	1.039
final R_1 and wR_2 indices [$I > 2\sigma(I)$]	0.0294, 0.0725	0.0252, 0.0597	0.0277, 0.0685
R_1 and wR_2 indices (all data)	0.0429, 0.0755	0.0365, 0.0616	0.0357, 0.0702
largest diff. peak and hole ($e \cdot Å^{-3}$)	1.476 and -0.953	1.470 and -1.458	0.723 and -0.435

Table 2.4. Crystallographic data for **4a**, **4b**, and **5a**.

	4a	**4b**	**5a**
empirical formula	$C_{22}H_{41}Cl_2MoNOP_3$	$2(C_{22}H_{41}Cl_2NOP_3W) \cdot C_7H_8$	$2(C_{24}H_{44}ClMoN_2OP_3) \cdot C_7H_8$
formula weight ($g \cdot mol^{-1}$)	595.31	1458.55	1293.96
temperature (K)	183(2)	183(2)	183(2)
wavelength (Å)	0.71073	0.71073	0.71073
crystal system, space group	monoclinic, $P\,2_1/c$	monoclinic, $P\,2_1/n$	monoclinic, $P\,2_1/c$
a (Å)	12.8371(2)	11.8724(1)	15.0638(5)
b (Å)	12.1528(1)	18.5755(2)	10.5782(4)
c (Å)	17.5884(2)	13.9509(2)	20.9919(7)
α (deg)	90	90	90
β (deg)	97.1310(1)	100.416(1)	106.624(4)
γ (deg)	90	90	90
volume ($Å^3$)	2722.68(6)	3025.97(6)	3205.20(19)
Z, density (calcd) ($Mg \cdot m^{-3}$)	4, 1.452	2, 1.601	2, 1.341
abs coefficient (mm^{-1})	0.869	4.172	0.665
F(000)	1236	1464	1356
crystal size (mm^3)	0.36 x 0.23 x 0.23	0.14 x 0.13 x 0.08	0.32 x 0.21 x 0.06
θ range (deg)	2.32 to 30.51	2.65 to 28.28	2.75 to 28.28
reflections collected	24969	41397	35940

reflections unique	8307 / R_{int} = 0.0377	7494 / R_{int} = 0.0385	7949 / R_{int} = 0.0828
completeness to θ (%)	100.0	99.8	99.9
absorption correction	analytical	analytical	analytical
max/min transmission	0.854 and 0.791	0.754 and 0.627	0.967 and 0.863
data / restraints / parameters	6383 / 0 / 279	5901 / 70 / 347	5719 / 85 / 376
goodness-of-fit on F^2	1.062	1.026	1.039
final R_1 and wR_2 indices [$I > 2\sigma(I)$]	0.0424, 0.1141	0.0351, 0.0833	0.0625, 0.1558
R_1 and wR_2 indices (all data)	0.0588, 0.1195	0.0542, 0.0873	0.0913, 0.1776
largest diff. peak and hole (e·Å^{-3})	1.352 and -0.839	3.711 and -1.247	1.378 and -0.722

Table 2.5. Crystallographic data for **6a**, **6b**, and **7a**.

	6a	**6b**	**7a**
empirical formula	$C_{23}H_{41}ClMoNO_2P_3$	$C_{23}H_{41}ClNO_2P_3W$	$C_{24}H_{45}ClMoNOP_3$
formula weight (g·mol^{-1})	587.87	675.77	587.91
temperature (K)	183(2)	183(2)	183(2)
wavelength (Å)	0.71073	0.71073	0.71073
crystal system, space group	monoclinic, $P\,2_1/c$	monoclinic, $P\,2_1/c$	monoclinic, $P\,2_1/c$
a (Å)	12.8561(1)	12.8278(1)	12.8015(4)
b (Å)	12.3654(1)	12.3530(1)	12.0380(3)
c (Å)	17.5941(1)	17.5831(2)	18.4127(5)
α (deg)	90	90	90
β (deg)	96.729(1)	96.4620(1)	97.646(3)
γ (deg)	90	90	90
volume (Å^3)	2777.68(4)	2768.55(4)	2812.25(14)
Z, density (calcd) (Mg·m^{-3})	4, 1.406	4, 1.621	4, 1.389
abs coefficient (mm^{-1})	0.761	4.462	0.749
F(000)	1224	1352	1232
crystal size (mm^3)	0.33 x 0.26 x 0.20	0.22 x 0.19 x 0.09	0.35 x 0.19 x 0.13
θ range (deg)	2.29 to 30.51	2.66 to 30.51	2.80 to 30.49

reflections collected	46604	57925	41056
reflections unique	8490 / R_{int} = 0.0570	8458 / R_{int} = 0.0732	7788 / R_{int} = 0.0478
completeness to θ (%)	100.0	99.9	99.9
absorption correction	analytical	analytical	analytical
max/min transmission	0.892 and 0.833	0.753 and 0.473	0.941 and 0.823
data / restraints / parameters	7085 / 2 / 316	6585 / 0 / 298	6436 / 3 / 316
goodness-of-fit on F^2	1.073	0.948	1.061
final R_1 and wR_2 indices [$I > 2\sigma(I)$]	0.0304, 0.0850	0.0261, 0.0568	0.0367, 0.0791
R_1 and wR_2 indices (all data)	0.0388, 0.0876	0.0394, 0.0585	0.0498, 0.0855
largest diff. peak and hole (e·Å^{-3})	0.735 and -0.619	1.415 and -0.799	1.035 and -0.521

Table 2.6. Crystallographic data for **7b**, **11a**, and **11b**.

	7b	**11a**	**11b**
empirical formula	$C_{24}H_{45}ClNOP_3W$	$C_{23}H_{42}MoNO_2P3$	$C_{23}H_{42}NO_2P_3W$
formula weight (g·mol^{-1})	675.82	553.43	641.33
temperature (K)	183(2)	183(2)	183(2)
wavelength (Å)	0.71073	0.71073	0.71073
crystal system, space group	monoclinic, $P\,2_1/c$	monoclinic, $P\,2_1/c$	monoclinic, $P\,2_1/c$
a (Å)	12.7859(4)	16.5384(3)	16.5197(3)
b (Å)	12.0397(3)	10.4479(1)	10.4466(1)
c (Å)	18.3677(8)	15.9771(3)	15.9539(2)
α (deg)	90	90	90
β (deg)	97.436(4)	101.325(2)	101.052(2)
γ (deg)	90	90	90
volume (Å^3)	2803.71(17)	2706.95(8)	2702.18(6)
Z, density (calcd) (Mg·m^{-3})	4, 1.601	4, 1.358	4, 1.576
abs coefficient (mm^{-1})	4.403	0.681	4.471
F(000)	1360	1160	1288
crystal size (mm^3)	0.31 x 0.27 x 0.14	0.29 x 0.21 x 0.18	0.29 x 0.25 x 0.15
θ range (deg)	2.80 to 27.48	2.51 to 30.51	2.51 to 30.51

reflections collected	20224	28378	48781
reflections unique	6435 / R_{int} = 0.0381	8249 / R_{int} = 0.0356	8240 / R_{int} = 0.0338
completeness to θ (%)	99.9	100.0	100.0
absorption correction	analytical	analytical	analytical
max/min transmission	0.657 and 0.432	0.907 and 0.858	0.603 and 0.389
data / restraints / parameters	5436 / 1 / 298	6357 / 0 / 283	6985 / 0 / 283
goodness-of-fit on F^2	1.025	0.947	1.077
final R_1 and wR_2 indices [$I > 2\sigma(I)$]	0.0315, 0.0666	0.0293, 0.0631	0.0221, 0.0585
R_1 and wR_2 indices (all data)	0.0414, 0.0714	0.0438, 0.0657	0.0284, 0.0595
largest diff. peak and hole (e·Å^{-3})	1.135 and -0.708	0.589 and -0.472	1.940 and -0.671

2.6 REFERENCES

[1] a) J. A. Osborn, F. H. Jardine, J. F. Young, G. Wilkinson, *J. Chem. Soc*. A **1966**, *12*, 1711-1732; (b) R. R. Schrock, J. A. Osborn, *J. Am. Chem. Soc*. **1976**, *98* (8), 2134-2143; c) R. R. Schrock, J. A. Osborn, *J. Chem. Soc., Chem. Commun.* **1970**, 567-568; d) C. R. Landis, J. Halpern, *J. Am. Chem.Soc*. **1987**, *109*, 1746-1754.

[2] a) R. M. Bullock, *Handbook of Homogeneous Hydrogenation*, Wiley-VCH, Weinheim, **2007**; b) M.R. Bullock, Catalysis without precious metals, Wiley-VCH, Weinheim, **2010**; c) R. M. Bullock, M. H. Voges. *J. Am. Chem. Soc.*, **2000**, *122*, 50; d) M. H. Voges, R. M. Bullock, *Dalton Trans*. **2002**, 759-770; (f) K. Junge, K. Schröder, M. Beller, *Chem. Commun.* **2011**, *47*, 4849-4859; g) C. P. Casey, H. Guan, *J. Am. Chem. Soc.* **2009**, *131*, 2499-2507; h) R. Langer, G. Leitus, Y. Ben-David, D. Milstein, *Angew. Chem. Int. Ed.* **2011**, *50*, 2120 - 2124; i) C. Sui-Seng, F. Freutel, A. J. Lough, R. H. Morris, *Angew. Chem. Int. Ed.* **2008**, *47*, 940-943; j) C. P. Casey, H. Guan. *J. Am. Chem. Soc*. **2007**, *129*, 5816-5817.

[3] a) Y. Jiang, J. Hess, T. Fox, H. Berke, *J. Am. Chem. Soc*. **2010**, *132*, 18233-18247; b) B. Dudle, K. Rajesh, O. Blacque, H. Berke, *J. Am. Chem. Soc*. **2011**, *133*, 8168-8178; c) A. Choualeb, E. Maccaroni, O. Blacque, H. W. Schmalle, H. Berke, *Organometallics* **2008**, 27, 3474-3481; d) H. Dong, H. Berke, *Adv. Synth. Catal*. **2009**, *351*, 1783-1788; e) Y. Jiang, Y, O. Blacque, T. Fox, C. M. Frech, H. Berke, *Chem. Eur. J.* **2009**, 15, 2121-2128;

f) Y. Jiang, O. Blacque, T. Fox, C. M. Frech, H. Berke, *Organometallics* **2009**, 28, 5493-5504.

[4] a) J. S. Song, D. J. Szalda, R. M. Bullock, C. J. C. Lawrie, M. A. Rodkin, J. R. Norton, *Angew. Chem., Int. Ed.* **1992**, *31*, 1233-1235; b) R. M. Bullock, *Chem. Eur. J.* **2004**, *10*, 2366-2374. c) R. M. Bullock, *Angew. Chem. Int. Ed.* **2007**, *46*, 7360 - 7363.

[5] a) S. E. Clapham, A. Hadzovic, R. H. Morris, *Coord. Chem. Rev*. **2004**, *248*, 2201; b) H. Berke, *ChemPhysChem* **2010**, *11*, 1837-1849; c) S. Namorado, M. A. Antunes, L. Veiros, J. R. Ascenso, M. T. Duarte, A. M. Martins, *Organometallics* **2008**, *27*, 4589–4599; d) J. S. M. Samec, J. E. Bäckvall, P. G. Andersson, P. Brandt, *Chem. Soc. Rev*. **2006**, *35*, 237.

[6] a) Y. Shvo, D. Czarkie, Y. Rahamim, D. F. Chodosh, *J. Am. Chem. Soc.* **1986**, *108*, 7400; b) M. Ito, T. Ikariya, *Chem. Commun*. **2007**, *5134-5142*; c) C. P. Casey, H. R. Guan, *J. Am. Chem. Soc*. **2007**, *129*, 5816;

[7] a) R. Noyori, M. Yamakawa, S. Hashiguchi, *J. Org. Chem*. **2001**, *66*, 7931-7944; b) K. J. Haack, S. Hashiguchi, A. Fujii, T. Ikariya, R. Noyori, *Angew. Chem. Int. Ed.* **1997**, *36*, 285-288; c) K. Muniz, *Angew. Chem. Int. Ed*. **2005**, *44*, 6622; d) R. Noyori, S. Hashiguchi, *Acc. Chem. Res*. **1997**, *30*, 97-102; e) R. Noyori, T. Okhuma, *Angew. Chem. Int. Ed*. **2001**, *40*, 40; f) R. Noyori, *Angew. Chem. Int. Ed.* **2002**, *41*, 2008-2022; g) M. Yamakawa, H. Ito, R. Noyori, *J. Am. Chem. Soc*. **2000**, *122*, 1466-1478.

[8] D. N. Kursanov, Z. N. Parnes, N. M. Loim, *Synthesis* **1974**, 633.

[9] a) P. L. Gaus, S. C. Kao, K. Youngdahl, M. Y. Darensbourg, *J. Am. Chem. Soc.* **1985**, *107*, 2428-2434; b) D. H. Gibson, Y. S. El-Omrani, *Organometallics* **1985**, *4*, 1473-1475; c) S. M. Geraty, P. Harkin, J. G. Vos, *Inorg. Chim. Acta* **1987**, *131*, 217-220; d) R. M. Bullock, B. J. Rappoli, *J. Chem. Soc., Chem. Commun.* **1989**, 1447-1448.

[10] a) M. Minato, Y. Fujiwara, T. Ito, *Chem. Lett.* **1995**, 647-648; b) M. Minato, Y. Fujiwara, M. Koga, N. Matsumoto, S. Kurishima, M. Natori, N. Sekizuka, K. Yoshioka, T. Ito, *J. Organomet. Chem.* **1998**, *569*, 139-145.

[11] a) M. P. Magee, J. R. Norton, *J. Am. Chem. Soc.* **2001**, *123*, 1778–1779; b) H. Guan, M. Iimura, M. P. Magee, J. R. Norton, G. Zhu. *J. Am. Chem. Soc.* **2005**, 127, 7805-7814;

[12] a) T.-Y. Cheng, B. S. Brunschwig, M. R. Bullock, *J. Am. Chem. Soc.* **1998**, *120*, 13121-13137; b) T. Y. Cheng, R. M. Bullock, *J. Am. Chem. Soc.* **1999**, *121*, 3150-3155; c) F. Wu, V. K. Dioumaev, D. J. Szalda, J. Hanson, R. M. Bullock, *Organometallics* **2007**, *26*,

5079-5090; d) M. H. Voges, R. M. Bullock, *Dalton Trans.* **2002**, 759-770; e) N. Sarker, J. W. Bruno, *J. Am. Chem. Soc*. **1999,** *121*, 2174-2180; f) B. F. M. Kimmich, P. J. Fagan, E. Hauptman, W. J. Marshall, R. M. Bullock, *Organometallics* **2005**, *24*, 6220–6229.

[15] a) T. Y. Cheng, R. M. Bullock, *Organometallics* **2002**, *21*, 2325-2331; b) P. J. Fagan, M. H. Voges, R. M. Bullock, *Organometallics* **2010**, *29*, 1045-1048; c) R. M. Bullock, J. -S. Song, D. J. Szalda, *Organometallics* **1996,** *15*, 2504-2516; d) M. A. Esteruelas, C. G. Yebra, E. On˜ate *Organometallics* **2008,** *27*, 3029-3036

[13] R. M. Bullock, J. S. Song, *J. Am. Chem. Soc.* **1994**, *116*, 8602-8612.

[14] L. Luan, J. S. Song, R. M. Bullock, *J. Org. Chem.* **1995**, *60*, 7170-7176.

[16] Bullock, R. M.; Voges, M. H. *J. Am. Chem. Soc.* **2000**, *122*, 12594-12595.

[17] P. J. Baricelli, L. G. Melean, S. Ricardes, V. Guanipa, M. Rodriguez, C. Romero, A. J. Pardey, S. Moya, M. Rosales, *J. Organomet. Chem* **2009**, *694*, 3381-3385.

[18] A. Dybov, O. Blacque, H. Berke, *Eur. J. Inorg. Chem.* **2011**, 652-659.

[19] C. E. Anderson, D. C. Apperley, A. S. Batsanov, P. W. Dyer, J. A. K. Howard *Dalton Trans*, **2006**, 4134–4145.

[20] J. R. Bleeke, G. G. Stanley, J. J. Kotyk, *Organometallics* **1986**, *5*, 1642-1647.

[21] D. V. Gutsulyak, S. F. Vyboishchikov, G. I. Nikonov, *J. Am. Chem. Soc.* **2010**, *132*, 5950–5951.

[22] a) Z. Chen, H. W. Schmalle, T. Fox, H. Berke, *Dalton Trans.* **2005**, 580-587. b) J. Höck, H. Jacobsen, H. W. Schmalle, G. R. J. Artus, T. Fox, J. I. Amor, F. Bäth, H. Berke, *Organometallics* **2001**, *20*, 1533-1544.

[23] a) F. Furno, T. Fox, H. W. Schmalle, H. Berke, *Organometallics* **2000**, *19*, 3620-3630; b) F. Liang, H. Jacobsen, H. W. Schmalle, T. Fox, H. Berke, *Organometallics* **2000**, *19*, 1950-1962; c) Y. Zhao, H. W. Schmalle, T. Fox, O. Blacque, H. Berke, *Dalton Trans.* **2006**, 73-85.

[24] M. Brookhart, B. Grant, A. F. Volpe, *Organometallics* **1992**, *11*, 3920–3922.

[25] P. J. Alaimo, B. A. Arndtsen, R. G. Bergman, *J. Am. Chem. Soc.* **1997**, *119*, 5269–5270.

[26] G. J. Kubas, *Metal Dihydrogen and Bond Complexes: Structure,Theory and Reactivity*, Kluwer Academic/Plenum Publishers, New York, **2001**.

[27] A. Dybov, O. Blacque, H. Berke, *Eur. J. Inorg. Chem.* **2010**, 3328–3337

[28] (a) S. Rendler, M. Oestreich, *Angew. Chem., Int. Ed*. **2008**, *47*, 5997. (b) D. T. Hog, M. Oestreich, *Eur. J. Org. Chem*. **2009**, 5047. (c) H. F. T. Klare, M. Oestreich, J.-i Ito, H. Nishiyama, Y. Ohki, K. Tatsumi, *J. Am. Chem. Soc*. **2011**, *133*, 3312. (d) M. Mewald, R. Froehlich, M. Oestreich, *Chem. Eur. J*. **2011**, *17*, 9406. (e) K. Muether, R. Froehlich, C. Mueck-Lichtenfeld, S. Grimme, M. Oestreich, *J. Am. Chem. Soc*. **2011**, *133*, 12442.

[29] (a) J. M. Blackwell, E. R. Sonmor, T. Scoccitti, W. E. Piers, *Org. Lett*. **2000**, *2*, 3921. (b) D. J. Parks, J. M. Blackwell, W. E. Piers, *J. Org. Chem*. **2000**, *65*, 3090. (c) A. Berkefeld, W. E. Piers, M. Parvez, *J. Am. Chem. Soc*. **2010**, *132*, 10660.

[30] Y. Jiang, B. Birgitta Schirmer, O. Blacque, Fox, T. F Grimme, S.; Berke H. *J. Am. Chem. Soc*. **2013**, *135*, 4088-4102.

[31] Stoichiometric amount of *N*-benzylidene aniline and $[H(Et_2O)_2][B(C_6F_5)_4]$ acid were mixed in Et_2O and kept for stirring overnight. The product was dried in *vacuo* and ^1H NMR spectra measure in THF d_8. The disappearance of the ^1H NMR signals for the acid at δ 14 ppm (Et_2OH^+) and the imine at δ 8.6 ppm (CH) and appearance of a signal at 9.6 ppm for the iminium salt (CH) in THF d_8 confirmed the formation of the$[PhCH=NHPh]^+[B(C_6F_5)_4]^-$ salt.

[32] L. Bencze, J. Kohan, Inorg. *Chim. Acta*, **1982,** *65*, L17-L19.

[33] P. Jutzi, C. Muller, A. Stammler, H. G. Stammler, *Organometallics* **2000,** *19*, 1442.

[34] Agilent Technologies (formerly Oxford Diffraction), Yarnton, Oxfordshire, England, **2012**.

[35] R. C. Clark, J. S. Reid, Acta Crystallographica Section A **1995**, **51**, 887.

[36] *CrysAlisPro*, Version 1.171.36.20, Agilent Technologies, Yarnton, Oxfordshire, England, **2012**.

[37] G. Sheldrick, Acta Crystallographica Section A **2008**, *64*, 112.

[38] A. L. Spek, J Appl Crystallogr **2003**, *36*, 7.

[39] L. Farrugia, J Appl Crystallogr **1999**, *32*, 837.

3 Low-Valent Molybdenum and Tungsten Amides for Bifunctional Splitting of Hydrogen and Efficient Imine Hydrogenations

3.1 INTRODUCTION

Catalytic hydrogenations of polar unsaturated functional groups are widely applied in industry and academia. Their reaction courses proceed mainly along Wilkinson and Osborn hydrogenation mechanisms[1] involving the following key steps (a) coordination of the unsaturated substrate on the vacant metal center (b) *cis*-insertion of the substrate into a metal-hydride bond (c) homolytic splitting of H_2 *via* oxidative addition to a metal center, and (d) reductive elimination of a C-H bond forming the saturated product. Alternatively, hydrogenations may occur with metal-ligand "bifunctional"[2,3] more or less simultaneous polar H atom transfers to unsaturated substrates. Preceeding heterolytic splitting of H_2 creates a protic and a hydridic function, which is followed by stepwise or concerted H^+ and H^- atom transfers to the unsaturated organic substrates. These reactions are also denoted as protonic-hydridic catalyses or ionic hydrogenations[4,5] depending somewhat on the character of the H atom transfers. Lately bifunctional homogeneous catalyses attracted increasing attention triggered through the elegant initial work of Noyori[6] and Ikariya,[7] Milstein,[8] and Shvo [9a, 9c, 9d] and Casey.[9b] In these catalyses heterolytic cleavage of H_2 occurs across a double-bonded metal to O- or N-ligand function. In recent years transition metal hydrides bearing protic $(^{i}Pr_2PCH_2CH_2)_2NH$ ligands[10] were found suitable for various types of bifunctional H_2 transformations, like hydrogenations,[11a] transfer hydrogenations,[11b,12] and also dehydrogenations.[13] However traditionally, catalysts used in these reactions were mostly based on the platinum group metals Ru, Rh and Ir,[14] which in larger scale transformations have to be recycled. Therefore efforts to replace these metals with non-precious, and moreover less toxic metals ("Cheap Metals for Noble Tasks")[15] is therefore an appealing challenge. This is the reason why in recent years iron catalysis[16] has been paid significant attention. In this context, molybdenum and tungsten catalysis would also satisfy to a high degree the given requirements and offer valuable alternatives to platinum group metals mainly due to their low costs and environmental benign nature. However, the organometallic chemistry of molybdenum and tungsten to utilize them in effective homogeneous hydrogenations is still insufficiently explored. The initial work of Bullock and coworkers[17] on

ionic hydrogenations of ketones and the work of our group[18] on hydrogenations of imines catalyzed by molybdenum and tungsten systems seem to be promising cases for the catalyst tuning efforts despite the low activities describing the state of the art.

The efforts of replacing expensive and toxic platinum group metals by applying complexes of the non-precious middle transition elements rhenium, molybdenum and tungsten, is a long-standing quest of our research group. In fact, rhenium nitrosyl based catalysts could be developed to an excellent state of performance for hydrogenations of olefins (activities comparable to precious metals)[19] and various hydrogen related reactions, like hydrosilylations,[20] dehydrogenative silylations[21] and dehydrogenative aminoborane coupling reactions.[22]

Since in bifunctional catalysis simultaneous transfer of the proton and the hydride is perceived to happen in the secondary coordination sphere, one might in principal anticipate less influence of the metal center which consequently would make many transition metals suited for the given task. In this chapter we therefore demonstrated the ability of appropriately substituted molybdenum and tungsten centers in low oxidation states to interact with H_2 and then further hydrogenation catalyses with imines were tested.

3.2 RESULTS AND DISCUSSION

3.2.1 Preparation of amino and amido complexes of molybdenum and tungsten bearing (^{i}Pr$_2$PCH$_2$CH$_2$)$_2$NH ligand.

The reaction of the precursor complexes Mo(NO)(CO)$_4$(ClAlCl$_3$) and W(NO)(CO)$_4$(ClAlCl$_3$) with (^{i}Pr$_2$PCH$_2$CH$_2$)$_2$NH (PN^{H}P) in THF at 90 °C resulted in the formation of the Mo(NO)(CO)(PN^{H}P)Cl **1a** and W(NO)(CO)(PN^{H}P)Cl **1b** (Scheme 3.1), which were isolated in 74% and 78% yields, respectively. The IR spectra of **1a** and **1b** exhibited strong ν_{CO} absorptions at 1912 and 1894 cm^{-1} and ν_{NO} absorptions were observed at 1573 and 1556 cm^{-1} respectively. The ^{31}P{1H} NMR spectra of **1a** revealed two sharp singets at δ = 60.2 and 59.1 ppm and for **1b** the singlets were observed at δ = 52 [s, $^{1}J_{P\text{-}W}$ (d, satellite)= 305.9 Hz] and 51.0 [s, $^{1}J_{P\text{-}W}$ (d, satellite) = 302.9 Hz] ppm. The observation of two signals in the ^{31}P{^{1}H} NMR spectra for each **1a** and **1b** supported the existence of *cisoid* and *transoid* isomers of the nitrosyl groups with respect to the position of the amine proton (N-H) in **1a** or **1b**. The ^{1}H NMR spectra of **1a** and **1b** exhibited several multiplets in the δ = 3.5-1.2 region for CH$_2$, CH and CH$_3$ protons due to the presence of isomeric mixtures. In the ^{13}C NMR spectra, the C

atoms adjacent to N-H moiety of PN^{H}P ligand of **1a** and **1b** could be observed at δ = 50.95 (t, $^{v}J_{C\text{-}P}$ = 4.8 Hz, NCH_2) and 52.59 (t, $^{v}J_{C\text{-}P}$ = 4.8 Hz, NCH_2) ppm, respectively.

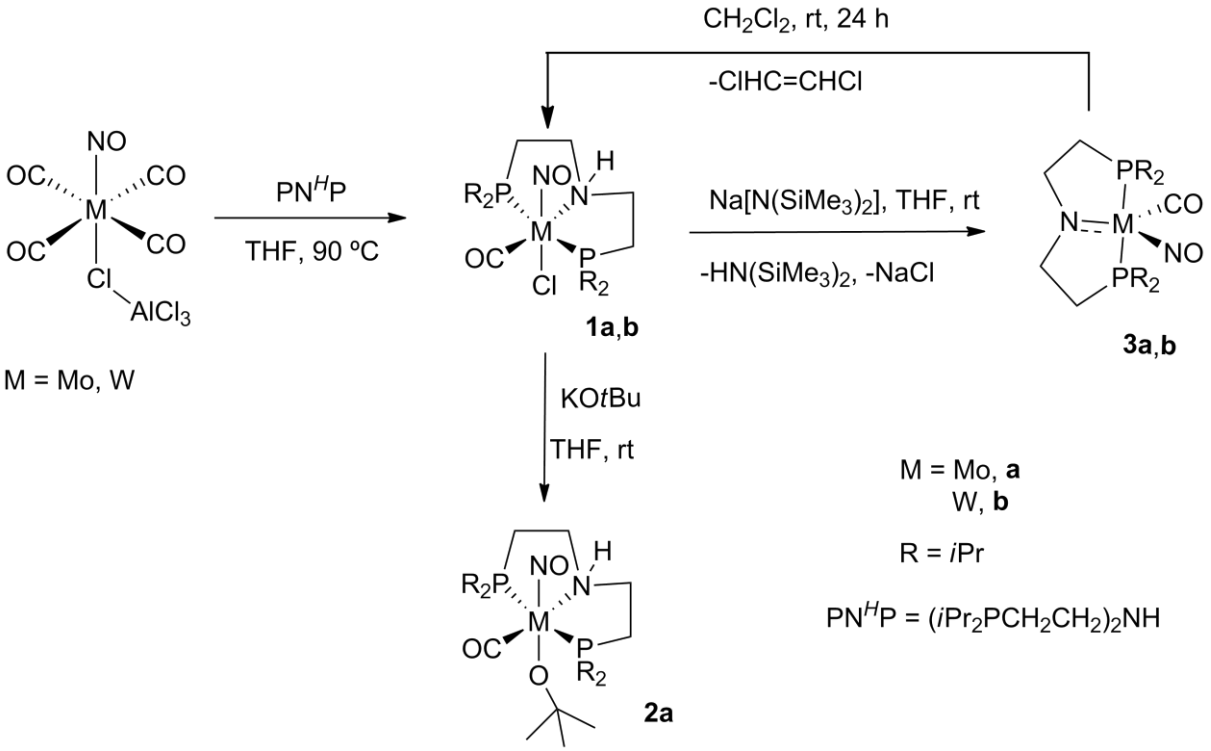

Scheme 3.1. Preparation of the amino and amido complexes of molybdenum and tungsten.

Single crystal X-ray diffraction studies of **1a** and **1b** showed that the metal centres possess distorted octahedral geometries. The nitrosyl groups were found *trans* to the chloride ligand in both the cases. The molecular structures of **1a** and **1b** are shown in Figure 3.1.

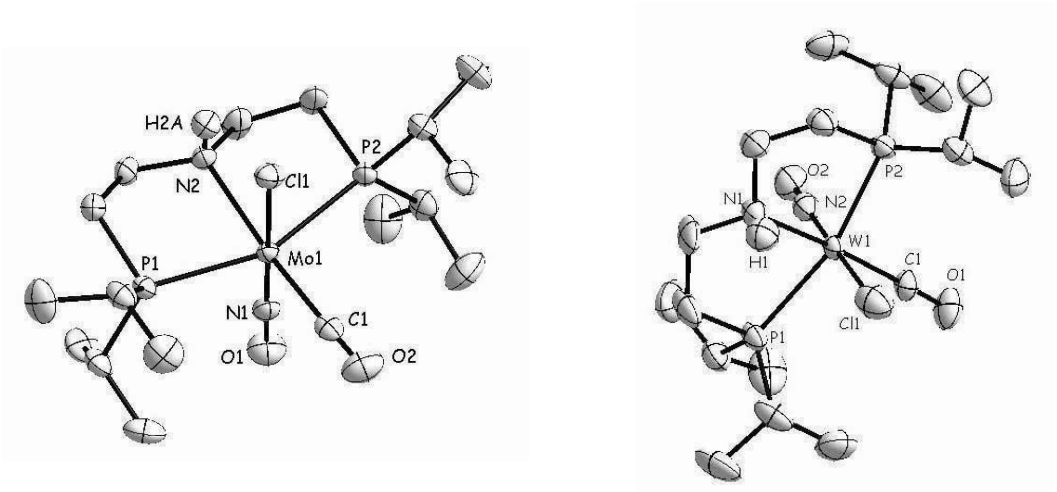

Figure 3.1. Molecular structures of Mo(NO)(CO)(PN^{H}P)Cl **1a** and W(NO)(CO)(PN^{H}P)Cl **1b** Thermal ellipsoids are drawn at the 50% probability level. All hydrogen atoms except N-H atom are omitted for clarity.

Selected bond distances(Å) and bond angles(°) for **1a**: Mo1-N2 2.2776(11), Mo1-N1 1.8110(13), Mo1C1 2.0375(15), C1-O2 1.0649(18), N1-Mo1-C1 88.84(5), P2-Mo1-P1 157.710(12), C1-Mo1-N2 171.65(5).

Selected bond distances (Å) and bond angles (°) for **1b**: N1-W1 2.267(3), W1-N2 1.845(4), W1-C1 1.961(4), C1-O1 1.158(4), C1-W1-N1 171.12(13), P1-W1-P2 157.68(3), N2-W1-C1 89.55(14).

Attempts to separate the isomers of **1a** and **1b** failed even with column chromatography at low temperature. The isomers showed similar deprotonation behaviour and could therefore be used as a mixture in subsequent deprotonation reactions.

Application of KO*t*Bu in the reaction with **1a** led at room temperature to chloride substitution forming the alkoxide complex Mo(NO)(CO)(PN^{H}P)(O*t*Bu) **2a** (Scheme 3.1). The $^{31}P\{^1H\}$ NMR spectrum of **2a** showed only a single resonance at $\delta = 52$ ppm, which provided evidence for the chemical equivalence of the phosphorus atoms and the absence of isomers. A strong

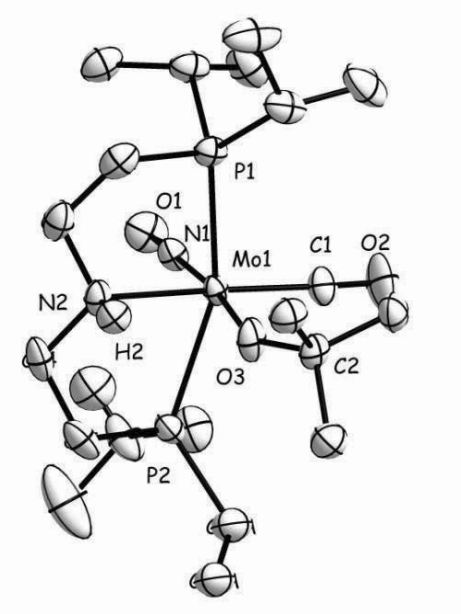

Figure 3.2. Molecular structure of Mo(NO)(CO)(PN^{H}P)(O*t*Bu) **2a**. Thermal ellipsoids are drawn at the 50% probability level. All hydrogen atoms are omitted for clarity. Selected bond distances (Å) and bond angles (°): Selected bond distances (Å) and bond angles (°): Mo1-N2

2.2810(10), Mo1-N1 1.7856(15), Mo1-C1 1.9770(19), C1-O2 1.153(2) N1-O1 1.2298(18) N1-Mo1-O3 172.59(6), P2-Mo1-P1 158.677(17), C1-Mo1-O3 99.16(7).

IR band at 1883 cm^{-1} indicated the presence of a CO group. The X-ray structure analysis of **2a** revealed pseudo octahedral geometry around the metal centre (Figure 3.2).

Attempts to deprotonate the N-H proton of $PN^{H}P$ ligand backbone using exess of KO*t*Bu at elevated temperature however failed.

Reactions of **1a** and **1b** with the comparatively strong and sterically hindered amide base $Na[N(SiMe_3)_2]$ furnished dehydrochlorination with deprotonation of the N-H moieties to form the highly air sensitive and reactive $16e^-$ amido M(NO)(CO)(PNP) {M = Mo, W; PNP = $(^{i}Pr_2PCH_2CH_2)_2N$)} complexes **3a** and **3b** in 57% and 54% yields, respectively (Scheme 3.1). IR bands at 1893 cm^{-1} for **3a** and at 1871 cm^{-1} for **3b** were assigned to the carbonyl ligands. The $^{31}P\{^{1}H\}$ NMR spectra of **3a** and **3b** showed unique signals at δ = 82 and 81 ppm suggesting chemical equivalence of the phosphorus atoms and the absence of isomers. The ^{1}H NMR spectra of **3a** and **3b** showed several distingushable clean multiplet signals in the region δ 3.5- 1.1 owing to the presence of NCH_2, PCH_2, CH, and CH_3 protons. The triplet signals in the $^{13}C\{^{1}H\}$ NMR spectra at δ = 60.5 (t, $^{v}J_{C-P}$ 8.3 Hz) for **3a** and at 63.36 (t, $^{v}J_{C-P}$ = 8.3 Hz) were assigned for the C_{NH2} atoms of **3a** and **3b**, respectively.

These complexes were found to be quite soluble in benzene, toluene and THF. Presumably due to their metal centres with a relatively high degree of unsaturation, they reacted in CH_2Cl_2 gradually to form the chloride complexes **1a** and **1b**. However the formation of the byproduct 1,2-dichloroethene could not be detected in solution ^{1}H NMR. Formation of **1a**,**b** was supported by an exemplary X-ray structure determination of **1a** (obtained from the reaction of **3a** and CH_2Cl_2**)**, ^{1}H and ^{31}P NMR spectroscopy, as well as chemically using the $Na[N(SiMe_3)_2]$ base, the amido complexes **3a**,**b** were regenerated.

Deep red single crystals suitable for X-ray diffraction studies were obtained for **3a** and **3b** from concentrated pentane solutions at -30 °C. It is important to note that the coordinatively unsaturated neutral amides **3a** and **3b** are the first structurally characterized pentacoordinate d^6 Mo and W amido complexes.[23] The perspective views of **3a** and **3b** are shown in Figure 3.3. The N (amido) atoms have shorter separations to the metal centers than NH atoms in **1a** and **1b** indicating $p_\pi(N) - d_\pi(M)$ double bond character. Low ν_{CO} stretching frequencies of **3a** and **3b** provided evidence that the CO groups are located in the trigonal plane of overall pseudo trigonal bipyramidal coordination geometries with significantly "deviating" equatorial

C_{CO}-M-N_{NO} angles close to 90°. It was theoretically rationalized that these CO, NO ligands are expected to have ≈ 90 ° in cases of 16 electron *cis* labilization intermediates.[24]

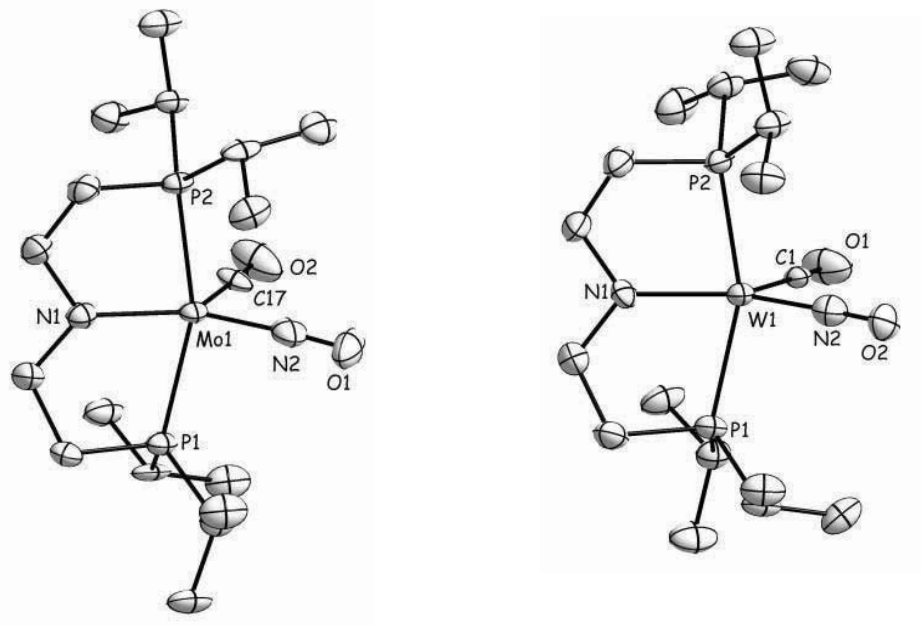

Figure 3.3. Molecular structures of Mo(NO)(CO)(PNP), **3a**, (left) and W(NO)(CO)(PNP), **3b**, (right). Thermal ellipsoids are drawn at the 50% probability level. Selected bond lengths [Å] and angles [°] for **3a**: Mo1-N1 2.055(4), Mo1-N2 1.856(5), Mo1-C17 1.896(5), C17-O2 1.170(6), N1-Mo1-N2 140.34(18), P1-Mo1-P2 158.59(5), N2-Mo1-C17 91.2(2). Selected bond lengths [Å] and angles [°] for **3b**: W1-N1 2.061(5), W1-N2 1.882(5), W1-C1 1.869(6), C1-O1 1.182(6), N1-W1-N2 139.1(2), P1-W1-P2 158.81(6), N2-W1-C1 91.3(2).

3.2.2 Reactivity of M(NO)(CO)(PNP) (M = Mo, 3a; W, 3b) with hydrogen

3a reacts slowly with hydrogen (2 bar) at room temperature to form the pseudo octahedral isomeric complexes **4a(*cis*)** and **4a(*trans*)** {Mo(NO)(CO)H(PN^{H}P)} showing a hydride at the Mo center and a NH group at the PNP ligand indicating H_2 heterolytic splitting across the M=N bond had occurred (Scheme 3.2). $^{31}P\{^1H\}$ NMR pursuit in the first 15 min of the reaction displayed one signal at δ = 78.5 ppm due to the formation of the **4a(*trans*)** isomer for which H_2 had approached to the Mo=N bond from the CO ligand side. After 30 min, an additional resonance was seen at δ = 78.9 ppm indicating build up of the isomeric product **4a(*cis*)** (8% with respect to **4a(*trans*)** according to ^{31}P NMR) with H_2 approaching from the NO side. The ^1H NMR spectra of the **4a(*trans*)** and **4a(*cis*)** mixture revealed two triplets at δ = 0.8 ($^2J_{PH}$ = 26.3 Hz) and at -1.8 ($^2J_{PH}$ = 26.3 Hz) ppm, which were assigned to the hydride

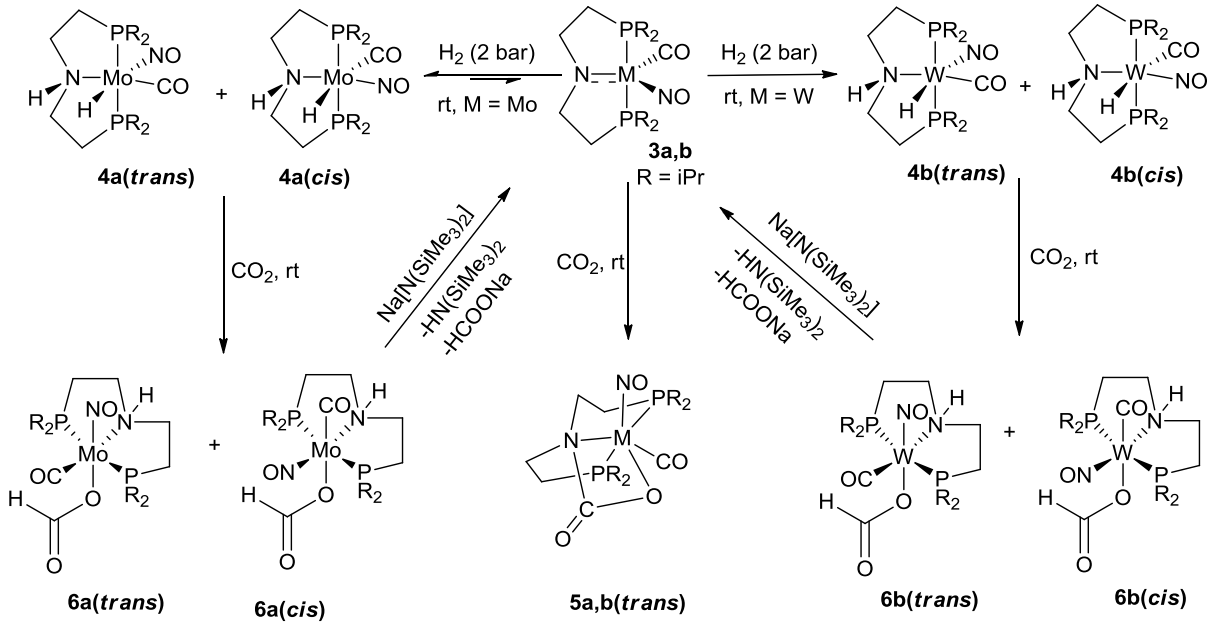

Scheme 3.2. H_2 and CO_2 activation by the amido complexes **3a** and **3b**.

ligands of both complexes. These signals became singlets in the phosphorus decoupled ^{1}H NMR spectra. Further, the ^{1}H and ^{31}P correlation spectra confirmed the two hydride signals to correlate each with two different $^{31}P\{^{1}H\}$ NMR signals, which again spoke for the presence of two isomers. In the initial hour of the reaction the intensities of the $^{31}P\{^{1}H\}$ NMR signals of **4a(*trans*)** and **4a(*cis*)** changed further, which was explained on the basis of **4a(*trans*)** to be the kinetic isomer forming faster which then slowly converts to the thermodynamic 1:1 mixture of both isomers {**4a(*trans*)** and **4a(*cis*)**}. The equilibrium state could be reached for a 0.08 M solution of **3a** under 2 bar H_2 in THF-d_8 only after 30 h. DFT calculations also revealed that there is no significant energy difference between **4a(*trans*)** and **4a(*cis*)** ($\Delta E = 0.01$ kcal mol^{-1}, see Appendix). A plot of the ^{31}P NMR signal intensities of **4a(*trans*)** and **4a(*cis*)** with time is shown in the Figure 3.4. It should be mentioned at this point that when the equilibrium mixture of **4a(*cis*)**, **4a(*trans*)** and **3a** was left under H_2 atmosphere (2 bar), even after 5 days the constituents showed a 7:7:6 equilibrium ratio. However **4a(*cis*)** and **4a(*trans*)** were found stable only in the presence of a H_2 atmosphere, which prevented their isolation. They were characterised in solution by ^{1}H and $^{31}P\{^{1}H\}$ NMR spectroscopy. The isomerization process from **4a(*trans*)** to **4a(*cis*)** is suggested to proceed *via* dissociation of H_2 from **4a(*trans*)** then re-adding from the NO side to form **4a(*cis*)**.

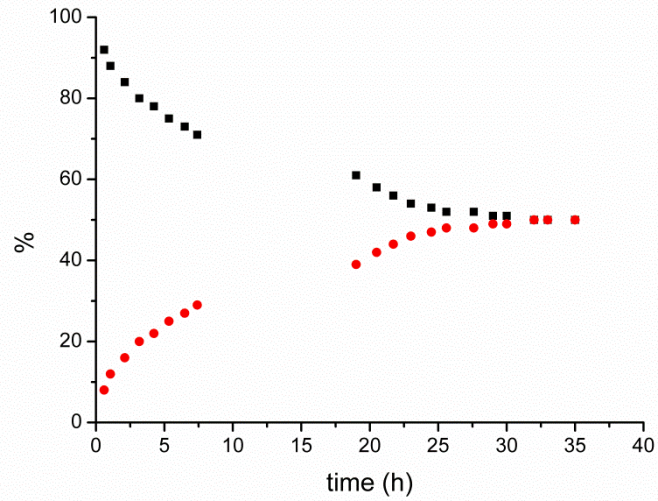

Figure 3.4. Plot of change of ^{31}P NMR signal intensity of **4a(*trans*)**(black square**)** and **4a(*cis*)** **(**red circles**)** over time (0.08 M **3a** was kept under 2 bar H_2 in THF-d_8 at room temperature).

When **3b** was pressurized with H_2 (2 bar) and left for 1h at room temperature, two signals were observed in the $^{31}P\{^1H\}$ NMR spectrum at δ = 64.7 ppm and 65.4 ppm appearing in a 4:1 ratio corresponding to isomers **4b(*trans*)** and **4b(*cis*)** **{**W(NO)(CO)H(PN^{H}P)}. But unlike in the Mo case, complete disappearance of the starting material was observed and no change in the intensities of the $^{31}P\{^1H\}$ NMR signals of **4b(*trans*)** and **4b(*cis*)** occurred even after several weeks suggesting complete formation of products and no equilibrium for the H_2 addition. The ^{1}H NMR spectra exhibited two triplets at δ = 2.85 ($^2J_{PH}$ = 25.5 Hz) and at 2.75 ppm ($^2J_{PH}$ = 22.0 Hz) assignable to the hydride ligands of **4b(*trans*)** and **4b(*cis*)**, respectively. In the IR spectra, one characteristic $\nu_{W\text{-}H}$ band appeared at 1612 cm^{-1} for both isomers **4b(*cis*)** and **4b(*trans*)** mixture along with one sharp signal at 1556 cm^{-1} assigned for the nitrosyl stretching vibrations. These complexes were found to be stable without hydrogen atmosphere and could be isolated in mixtures. Separations however failed. The ratio of the isomers **4b(*cis*)** and **4b(*trans*)** was approximately the same as initially seen for the **4b(*cis*)** and **4b(*trans*)**. We attempted to induce to change the ratio of the **4b(*cis*)** and **4b(*trans*)** mixture by heating **3b** at 140 °C and 60 bar H_2. After 20 min of reaction time and immediate cooling of the mixtures, the ^{31}P NMR spectrum revealed a of **4b(*trans*)**/**4b(*cis*)** ratio of 3:2 (ΔE = 0.4 kcal mol^{-1} from DFT calculations).

3.2.3 Activation of CO_2 by M(NO)(CO)(PNP) (M = Mo, 3a; W, 3b)

Also much to our surprise **3a** and **3b** were found to react quickly with CO_2 (Scheme 3.2).[25] When THF solutions of **3a** and **3b** were charged with CO_2 (2 bar), an immediate color changes were noticed from deep red to purple to orange forming the carbamate complexes Mo(NO)(CO)(PNP)(OCO), **5a**(***trans***) and W(NO)(CO)(PNP)(OCO) **5b(*trans*)**. The purple color indicated a transient species, since it was too short-lived the structure of which could not be established but presumably it constitutes an addition product of C_{CO2} atom to the N_{PNP} atom. The orange species could be isolated in pure form and was found to be the 2+2 addition product of CO_2 across the N=M (M= Mo, W) double bonds. Nevertheless, the transition state of the reaction between **3b** and CO_2 could be optimized and characterized by DFT calculations (see Appendix), which confirmed a low energy barrier of 3.9 kcal mol^{-1} for the CO_2 addition to the thermodynamically favored product **5b(*trans*)** (-19.7 kcal mol^{-1} in comparison with **3b**) The IR spectra of **5a(*trans*)** and **5b(*trans*)** showed besides the ν(NO) and ν(CO) bands at 1593, 1554 cm^{-1} and 1902, 1879 cm^{-1}, respectively, additional strong absorption bands at 1732 and 1741 cm^{-1}, respectively, which were assigned to the ν_{CO2} vibration of the attached CO_2 molecule.

Single crystals suitable for an X-ray diffraction study were obtained for **5b(*trans*)** by layering pentane over a concentrated THF solution of **5b(*trans*)** (Figure 3.5). The molecular structure of **5b(*trans*)** revealed a pseudo octahedral geometry. The W1-N2 bond distance is 2.2603(19) Å, which is significantly longer than that of **3b** by about 0.2 Å. This clearly indicates that the W=N double bond character was reduced further by CO_2 coordination.

Formation of the 2+2 addition stereoisomer of **5a(*cis*)** or **5b(*cis*)** by a CO_2 with approach from the NO side to **3a** or **3b** could not be observed by ^{31}P NMR spectroscopy at room temperature in solution. However, when the reaction of **3a** or **3b** with CO_2 (2 bar) was pursued by ^{31}P NMR spectroscopy at -60 °C, additional weak signals were observed besides those of **5a(*trans*)** or **5b(*trans*)** indicating under these conditions formation of a kinetic mixture of both possible isomers (7:3 ratio), which equilibrated into the thermodynamical stable products **5a(*trans*)** or **5b(*trans*)** at room temperature.

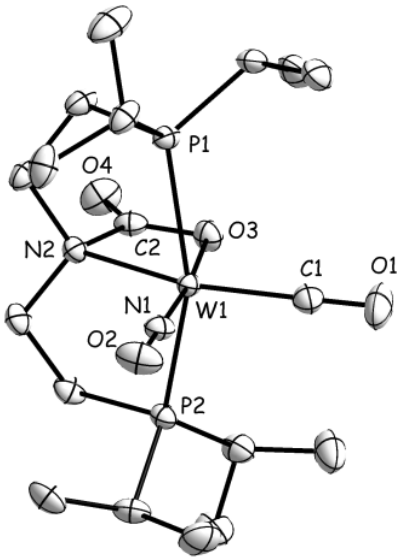

Figure 3.5. Molecular structures of Mo(NO)(CO)(PNP)(OCO), **5b(*trans*)**. Thermal ellipsoids are drawn at the 50% probability level. Selected bond distances [Å] and bond angles [^{o}]: W1-N1 1.789(2), W1-C1 1.969(3), W1-N2 2.2603(19), W1-O3 2.2155(18), C1-O1 1.159(3), C2-O3 1.283(3), C2-O4 1.208(3), N1-W1-C1 88.61(10), N2-W1-O3 172.47(8), N2-C2-O3 108.0 (2) P1-W1-P2 157.60(2).

An attempt to trap the purple color intermediate species in the above mentioned reactions of **3a,b** with CO_2 was carried out in the presence of lewis acid $B(C_6F_5)_3$. When CO_2 was purged (1.5 bar) at room temperature to a red solution of the **3a** and BCF mixture(1:1), the color of the solution changed immediately to purple to pink and $^{31}P\{^{1}H\}$ NMR signal shifted to δ 59.4 ppm. However the color of the obtained species further did not change to orange indicating formation of probably a new species instead of **5a(*trans*)**. Indeed the IR spectra of the obtained species did not show any signal at 1732 cm^{-1} supporting the absence of **5a(*trans*)**. IR band at 1644 cm^{-1} due to the presence of CO_2 moiety could be observed besides those at 1915 and 1606 cm^{-1} for carbonyl and nitrosyl stretching vibrations. A signal at δ 178 ppm in the ^{13}C NMR again supports the presence of CO_2 moiety. The ^{11}B NMR spectrum exhibited a broad signal at δ 2.03 ppm. The ^{19}F NMR revealed signals at -132.8 (d, J_{CF} =19.8 Hz, 6F, ortho-C_6F_5), - 158.8 (t, $^{1}J_{CF}$= 20.6 Hz, 3F, *para*-C_6F_5) and -165.4 ppm (t, $^{1}J_{CF}$= 16.9 Hz 6F, meta -C_6F_5).The structure of the complex remain as yet unidentified. Further investigation needs to be done to establish the real structure of the new species. Nevertheless we also examined the reactivity of **3a,b** with BCF in absence of CO_2.

Treatment of 1 equiv. of $B(C_6F_5)_3$ to a solution of **3a,b** in toluene at room temperature immediately led to formation of new species in quantitative yields which are probably the adduct of $B(C_6F_5)_3$ and **3a,b** since the amido complexes **3a,b** bear highly basic nitrogen centres. The $^{31}P\{^1H\}$ NMR spectra of the $B(C_6F_5)_3$ adduct of **3a,b** revealed single resonances at δ 80.1 and 77.5 ppm respectively. Signals at δ -19.5 and 5.4 ppm in the ^{11}B NMR spectra were attributed to the boron atoms of the coordinated $B(C_6F_5)_3$. In the ^{19}F NMR spectra set of resonances at -133.32 (m, 6F, ortho-C_6F_5), -160.2 (t, $^1J_{CF}$= 19.8 Hz, 3F, *para*-C_6F_5) and -166.38 ppm (t, $^1J_{CF}$= 16.7 Hz 6F, meta -C_6F_5) for [**3a.** $B(C_6F_5)_3$] adduct and at -133.2 (m, 6F, ortho-C_6F_5), -160.6 (t, $^1J_{CF}$= 20.6 Hz, 3F, para-C_6F_5) and -166.6 ppm (t, $^1J_{CF}$= 17.5 Hz 6F, meta -C_6F_5) for [**3b.**$B(C_6F_5)_3$] adduct could be observed.

3.3.4 Reactions of the M(NO)(CO)H(PN^HP) (M = Mo, W) complexes with CO_2

Reaction of the mixtures of **4b(*trans*)** and **4b(*cis*)** with CO_2 at room temperature resulted in rapid formation of the η^1-formate complexes W(NO)(CO)(PNP^H)(OCHO) {**6b(*trans*)** and **6b(*cis*)}**[26] (Scheme 4.2) in a 9:1 ratio. The $^{31}P\{^1H\}$ NMR spectra revealed a strong signal at δ 51.3 ppm for **6b(*trans*)** (with tungsten satellites) along with a weak signal at δ 52.6 ppm for **6b(*cis*)**. The formate protons of **6b(*trans*)** and **6b(*cis*)** in the ^1H NMR spectra were observed at δ 8.5 and 8.0 ppm respectively. In the ^{13}C NMR spectra, only one signals each at δ 244.7 and 164.3 ppm were observed assigned to the carbonyl and formate carbons respectively of the major isomer **6b(*trans*)**. However due to very low concentration of the minor isomer, **6b(*cis*)** the carbonyl and formate carbons could not be observed. The $\nu(as)_{CO2}$ vibration was observed at 1612 cm^{-1} indicating formation of a tungsten bound formato ligand. The additional IR bands at 1863 and 1578 cm^{-1} were attributed to the carbonyl and nitrosyl ligand stretching frequencies respectively.

In a similar way, when an equilibrium mixture of **4a(*trans*)**, **4a(*cis*)** and **3a** (1:1:1) was reacted with CO_2 (2 bar) at room temperature, a mixture of the formate complexes **6a(*trans*)** and **6a(*cis*)** was formed along with **5a(*trans*)** (1:1:1) as indicated by the ^{13}C and $^{31}P\{^1H\}$ NMR spectra. The formate protons appeared in the ^1H NMR spectra for **6a(*trans*)** and **6a(*cis*)**, at δ = 8.1 and 8.5 ppm, respectively in a 1:1 ratio. Signals at δ = 170 and 168 ppm in $^{13}C\{^1H\}$ NMR spectra were assigned to the C (formate) atoms of the isomers **6a(*cis*)** and **6a(*trans*)**, respectively. However **6a(*trans*)** and **6a(*cis*)** could not be separated from the residual **5b(*trans*)**.

Tiny crystals of **6b(*cis*)** were obtained by slow diffusion of pentane into a concentrated THF solution. The X-ray analysis revealed a pseudo octahedral framework, with *trans* carbonyl and formate groups corresponding to the minor isomer **6b(*cis*)** (Figure 3.6). The asymmetric unit of this minor isomer contains two crystallographically independent

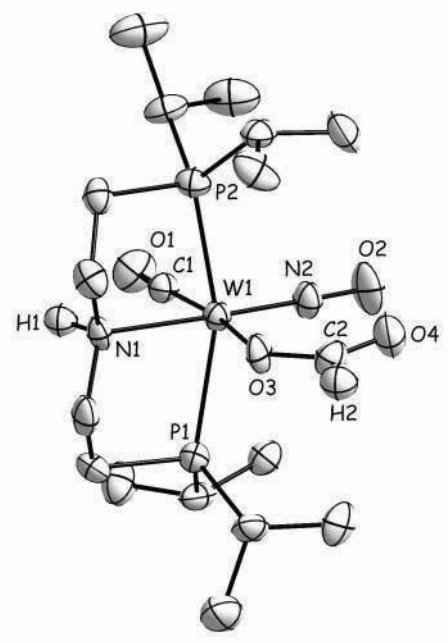

Figure 3.6. Molecular structure of **6b(*cis*)**. Thermal ellipsoids are drawn at the 50% probability level. All hydrogen atoms are omitted for clarity except H1. Selected bond distances [Å] and bond angles [^{o}]: W1-N1 2.287(5), W1-C1 1.930(8), W1-N2 1.792(6), W1-O3 2.185(5), C1-O1 1.172(8), C2-O3 1.271(7), C2-O4 1.213(8), N1-W1-C1 91.6(3), N2-W1-O3 101.9(2), N1-W1-N2 178.3 (3) P1-W1-P2 158.32(7).

molybdenum species showing intermolecular hydrogen bonding between the N-H proton of one molecule and the oxygen atom of the formato ligand of another molecule. This hydrogen bonding establishes linear chains in the three dimensional network, which is indicative of a relatively high acidity of the N-H protons. DFT calculations however support the notion that the *trans* NO/formate isomer **6b(*trans*)** is thermodynamically more stable than the *trans* CO/formate isomer **6b(*cis*)** (ΔE = 3.6 kcal mol^{-1}, see Appendix) viewing **6b(*cis*)** indeed as the kinetic isomer.

3.2.5 Stoichiometric Hydrogenation of Carbon dioxide

In recent years hydrogenation of CO_2 has attracted much attention due to its potential role as a C_1 building block for chemical synthesis.[27] In addition hydrogenation of CO_2 to formic acid is an attractive transformation owing to its industrial applications and application as a reversible H_2 storage material. Though the reaction of H_2 with CO_2 to obtain formic acid is exothermic (ΔH = -8 kcal/mol), it is endergonic due to gaseous starting materials with ΔG = 8 kcal/mol. Therefore addition of base is necessary to drive the reaction towards formic acid formation via salt formation or acid-base hydrogen bonding interactions.

Hence in our case, the obtained mixtures of the formato complexes **6a(*cis*)** and **6a(*trans*)**, and of **6b(*cis*)** and **6b(*trans*)** were deprotonated at room temperature using 1 equiv. of the $Na[N(SiMe_3)_2]$ base with regeneration of **3a** and **3b**. According to Eq. (1) simultaneous formation of sodium formate can close the cycle of stoichiometric consecutive reaction steps of H_2 and CO_2 additions to make it "pseudo-catalytic". Thus the presence of a base seemed to be accomplishable without providing side reactions but the sequence of H_2 before CO_2 addition, which seemed essential to obtain formic acid derivatives (Scheme 3.2) since the CO_2 adducts **5a(*trans*)** and **5b(*trans*)** form faster than the H_2 adducts **4a(*cis*)/4a(*trans*)** or **4b(*cis*)**/**4b(*trans*).**

$$\underset{(10\ bar)}{CO_2} + \underset{(70\ bar)}{H_2} + Na[N(SiMe_3)_2] \xrightarrow[140\ °C,\ THF]{\textbf{cat}\ (5\ mol\%)} [HCOO]Na + HN(SiMe_3)_2 \quad (1)$$

Being aware of this situation we nevertheless tried catalysis and carried out 3 types of hydrogenation experiments of CO_2 applying the simultaneous presence of H_2 (70 bar) and CO_2 (10 bar) and of catalytic amounts of **3a**, **3b** or of the **4b(*cis*)** and **4b(*trans*)** mixture (5 mol% loading) in the presence of $Na[N(SiMe_3)_2]$ at 140 °C. After 15 h all the experiments revealed formation of HCOONa according to Eq. (1), but in low yields of only 4%, 2% and 3%, respectively, as examined by ^{1}H NMR (DMF as internal standard). To improve the yield of the formate salt, we attempted use of the bicyclic DBU, KO*t*Bu or NEt_3 as a base in the presence of **3a** as a catalyst with otherwise the same conditions as above.

Table 3.1. Hydrogenation of CO_2

Entry[a]	Cat	Base	Time (h)	Yield (%)[b]
1	**3a**	$Na[N(SiMe_3)_2]$	15	4
2	**3b**	$Na[N(SiMe_3)_2]$	15	2
3	**4b(cis and trans)**	$Na[N(SiMe_3)_2]$	15	3
4	**3a**	DBU	15	3.5
5	**3a**	KO*t*Bu	15	2.5
6	**3a**	Et_3N	15	0.50
7[c]	**-**	$Na[N(SiMe_3)_2]$	17	0.14
8	**3a**	TMP	15	-
9	**3a**/BCF	$Na[N(SiMe_3)_2]$	15	0.70
10	**3a**/Et_3SiH/BCF	$Na[N(SiMe_3)_2]$	22	0.30

[a]Unless and otherwise stated 10 bar CO_2, 70 bar H_2, THF as solvent, 140 °C temperature and 5 mol% catalyst with respect to base were used as reaction conditions. [b]Yield on the basis of ^1H NMR integration using DMF as internal standard . [c]No catalyst was used.

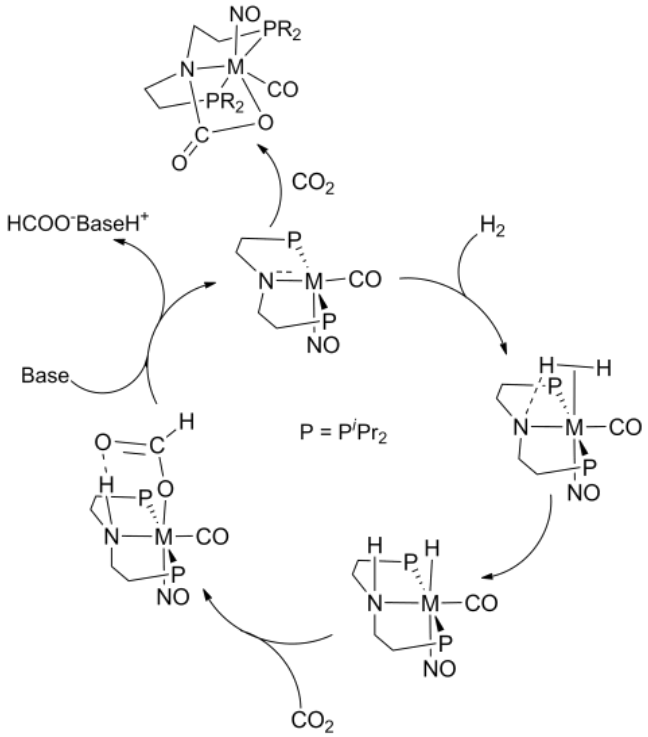

Scheme 3.3 Proposed cycle for the CO_2 hydrogenation

However, the yield of $[HCOO]^-[DBUH]^+$ (3.5%), HCOOK (2.5%) or $HCOOH/NEt_3$ (0.5%) did not increase (Table 3.1). Furthermore, the use of $B(C_6F_5)_3$ or $Et_3SiH/B(C_6F_5)_3$ mixture as cocatalyst in the presence of catalyst**3a** and $Na[N(SiMe_3)_2]$ only led to decrease the yields.

At this stage the principal access to CO_2 hydrogenation was demonstrated but for effective such catalyses further tuning efforts have to be envisaged making the CO_2 adducts of type **5** labile, which is formed prevailingly in the presence of H_2 and CO_2 and blocks the catalyses (Scheme 3.3).

It should be mentioned here that since strong bases can also react with CO_2 at high temperature and pressure, a control experiment was also carried out in the absence of catalysts using $Na[N(SiMe_3)_2]$ as base keeping all the other conditions same. The obtained yield was only 0.14% , which is much lower than the yield obtained from the pseudo-catalytic reactions.

3.2.6 Catalytic Hydrogenations of Imines Using 3a and 3b

We then found out that **3a** and **3b** could be efficiently used for catalytic hydrogenations of imines without addition of a cocatalyst. The catalytic activity of **3a** was tested in initial room temperature experiments probing the hydrogenation of *N*-benzylideneaniline at 60 bar H_2 pressure in toluene with a loading of 2 mol% of **3a**. After 1 h of reaction time, the GC/MS analysis of the reaction mixture revealed formation of phenylbenzylamine as hydrogenated product, but it was obtained in low 30% yield and with a low maximum TOF of 15 h^{-1}. The reaction went to completion within 3.5 h (Table 3.2, entry 1). Under the same conditions as above using **3b** as a catalyst, only 25% phenylbenzylamine was obtained after 12 h of reaction time with a TOF of 1 h^{-1} (Table 3.2, entry 2). To improve the performance of the hydrogenation of imines catalysed by **3a** or **3b** at room temperature, higher catalyst loadings were envisaged and also longer reaction times to achieve full conversions. However, when the temperatures of the catalyses were increased to 140 °C, the catalytic activities of **3a** and **3b** were boosted. Optimization experiments showed that the hydrogenation of *N*-benzylideneaniline could be improved to a great extent applying higher temperature (80-140 °C) and higher pressures of H_2 (20-60 bar). In addition various loadings of the catalyst **3a** (Table 3.2) were tested. It became apparent that these catalytic hydrogenations seemed to work best in aprotic solvents, since no hydrogenation was observed in isopropanol, methanol and ethanol. A temperature of 140 °C and 60 bar H_2 pressure was eventually found to constitute optimum conditions achieving a maximum TOF of 1600 h^{-1} for the hydrogenation of *N*-benzylideneaniline in toluene (Table 3.3, entry 12).

Being aware of the situations of previous work of our group with rhenium complexes where drastic improvement in catalytic hydrogenation of olefins was observed using $B(C_6F_5)_3$[19a] or $R_3SiH/B(C_6F_5)_3$[19d] mixture as cocatalyst, we also attempted to accelerate the activities of imine hydrogenations in these cases. A loading of 0.17 mol% of **3a** in the presence of $B(C_6F_5)_3$ or $Et_3SiH/B(C_6F_5)_3$ mixture as cocatalyst led to TOFs of 528 h^{-1} or 576 h^{-1} respectively (Table 3.2, entries 7 and 8) for the hydrogenation of *N*-benzylideneaniline under 60 bar H_2 at 140°C. Nevertheless, several other imines were tested using **3a** and **3b** as the

Table 3.2. Optimization of the imine hydrogenation conditions using catalyst **3a**.

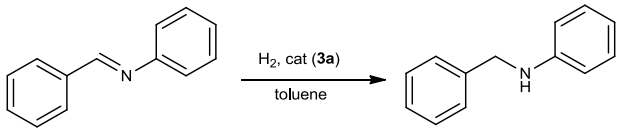

Entry	S/C	Temp [°C]	Press [bar]	TOF[a] [h^{-1}]	Conv[b] [%]
1[c]	50	rt	60	15	100
2[d]	50	rt	60	1	25
3	100	80	60	208	52
4	200	100	60	540	68
5	600	140	20	1272	53
6	600	140	60	1600	68
7[e]	600	140	60	528	22
8[f]	600	140	60	576	24
9[g]	400	140	60	1120	70
10[h]	100	140	60	14	32
11[i]	100	140	60	-	0

[a]TOFs were calculated after initial 15 min. [b]Conversion by GC/MS after 15 min on the basis of the consumption of the starting material. [c]The TOF was determined after 1 h and conversion after 3.5 h by GC/MS. [d]**3b** was used as the catalyst, conversion determined after 12 h and average TOF was calculated from conversion after 12 h. [e]$B(C_6F_5)_3$ was used as cocatalyst. [f]mixture of $Et_3SiH/B(C_6F_5)3$ was used as cocatalyst. [g]THF was used as the solvent. [h]Acetophenone was used as the substrate. TOF calculated after 1 h. [i]Benzaldehyde was used as the substrate.

catalysts and the same physical conditions as in the experiments before, but the catalyst loadings had to be varied for the accomplishment of optimum performance (Table 3.3). **3a** showed the highest catalytic activity for the hydrogenation of *N*-(4-methoxybenzylidene)aniline to reveal a maximum TOF of 2912 h^{-1} (Table 3.3, entry 19), the highest obtained TOF reported for a Mo-based hydrogenation catalyst till date. Various *para*

substituted imines (*p*-ClC_6H_4CH=N-*p*-C_6H_4Cl, PhCH=N-(α-Naph), *p*-$MeOC_6H_4CH$=NPh, PhCH=N-*p*-C_6H_4OMe, *p*-ClC_6H_4CH=NPh, PhCH=N-*p*-C_6H_4Cl, *p*-$MeOC_6H_4CH$=N-*p*-C_6H_4OMe, *p*-$MeOC_6H_4CH$=N-*p*-C_6H_4Cl, *p*-ClC_6H_4CH=N-*p*-C_6H_4OMe, *p*-FC_6H_4CH=NPh and PhCH=N-*p*-C_6H_4F) were found to be fully converted cleanly to their corresponding amines in less than 1h at 140°C and under 60 bar H_2.

The catalytic performance of **3a** in the hydrogenation of carbonyl functionalities was also tested. Acetophenone could be hydrogenated to the corresponding 1-phenylethanol in 32% yield after 3.5 h with a loading of 1 mol% **3a** at 140 °C under 60 bar H_2 in toluene. But the maximum initial TOF was only 14 h^{-1} (Table 3.2, entry 8). No hydrogenation was observed when benzaldehyde was used as a substrate and **3a** as a catalyst at 140°C and 60 bar H_2.

Table 3.3. Hydrogenation of various imines using catalysts **3a** and **3b** under optimized conditions.

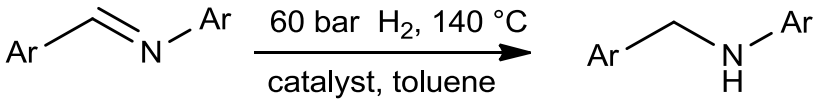

Entry	Substrates	Cat	S/C	TOF[a] [h^{-1}]	Time [h]	Conv [%][b]
12	PhCH=NPh	**3a**	600	1600	<0.5	>97
13	PhCH=NPh	**3b**	200	424	<1	>99
14[c]	PhCH=NPh	**4b**	200	356	1	99
15	*p*-ClC_6H_4CH=N-*p*-C_6H_4Cl	**3a**	400	480	<1	>99
16	*p*-ClC_6H_4CH=N-*p*-C_6H_4Cl	**3b**	400	464	<1	>99
17	PhCH=N-(α-Naph)	**3a**	200	792	0.25	>99
18	PhCH=N-(α-Naph)	**3b**	200	112	1	>98
19	*p*-$MeOC_6H_4CH$=NPh	**3a**	800	2912	0.5	>99
20	*p*-$MeOC_6H_4CH$=NPh	**3b**	400	1120	<1	>99
21[d]	PhCH=N-*p*-C_6H_4OMe	**3a**	600	1440	<1	>99
22	*p*-ClC_6H_4CH=NPh	**3a**	200	496	<1	>98
23	PhCH=N-*p*-C_6H_4Cl	**3a**	800	1979	<1	>97
24	*p*-$MeOC_6H_4CH$=N-*p*-	**3a**	200	546	<1	77

	C_6H_4OMe					
25[d]	*p*-ClC_6H_4CH=N-*p*-C_6H_4OMe	**3a**	100	332	<1	>99
26	*p*-$MeOC_6H_4CH$=N-*p*-C_6H_4Cl	**3a**	200	744	0.25	>93
27	*p*-$NO_2C_6H_4CH$=NPh	**3a**	50	-	14	0
28	*p*-FC_6H_4CH=NPh	**3a**	200	712	<1	99
29	PhCH=N-*p*-C_6H_4F	**3a**	800	1920	<1	>99
30	PhCH=NiBu	**3a**	50	-	1	0

[a] TOFs were calculated after initial 15 min by GC/MS. [b] Conversion by GC/MS on the basis of the consumption of the substrates. [c] **4b** = mixture of **4b(*cis*)** and **4b(*trans*)**. [d] TOF and the conversion were determined from ^{1}H NMR integration.

3.3.7 MECHANISTIC STUDIES OF IMINE HYDROGENATION

Hammett Correlations for the Hydrogenations of Imines

To understand the electronics of the hydrogenation process, we wanted to explore in Hammett[28] correlations, the influence of various *para* substituents of aromatic imines in hydrogenations (Figure 3.7) with the catalyst **3a** and a series of *para*-H, methoxy, fluoro and chloro substituted *N*-benzylideneanilines were applied, the latter substituted on the benzylidene or on the aniline side. The initial rates (s^{-1}) were obtained from the TOF values

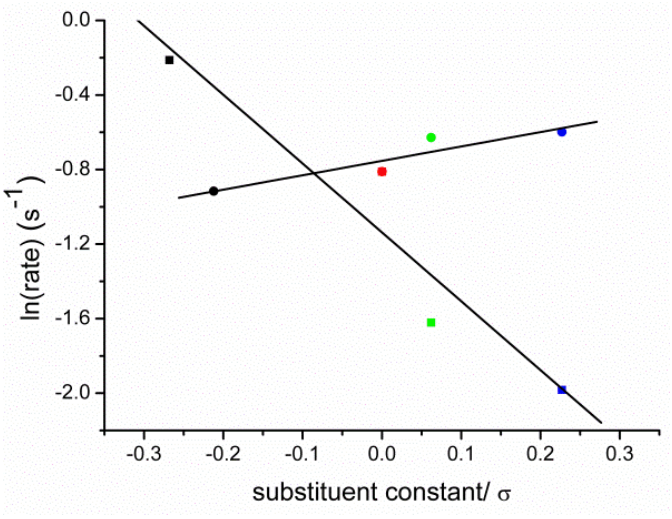

Figure 3.7. Hammett plot for the hydrogenation of various *para* substituted imines catalyzed by **3a** extracted from initial TOF values. Black line, with ρ = -3.69: hydrogenations with *para* substituents at the benzylidene side; Circles, with ρ = 0.68: *para* substitution at the aniline side. Squares: *p*-MeO, red: *p*-H, green: *p*-F, blue: *p*-Cl groups.

(TOF = reaction rate normalized by the catalyst concentration). The Hammett correlations were obtained plotting ln(hydrogenation rate) vs substituent constant (σ) which gave a straight line with a negative slope of -3.69 for the *para* substitution on the benzylidene side.

Para substitution on the aniline side also revealed a straight line, but with a positive slope of 0.68. The Hammett parameter (ρ) indicates the susceptibility of the respective transformation towards the electronic influence of the substituents. A negative ρ value with greater than unity indicates a positive charge build up at the reaction center in the transition state and the rate of the reaction is greatly enhanced by the presence of electron donating groups while a positive ρ value stands for the build up of negative charge at the reaction center, and reaction rates are enhanced by electron withdrawing groups. As expected for the benzylideneaniline hydrogenation, an electron donating group on the benzylidene side and an electron withdrawing group on the aniline side revealed increased activities (Table 3.3, entries 19, 21, 22, 23, 25, 26, 28 and 29). The transition state therefore has a strong polarized C=N bond emphasizing the polar canonical form:

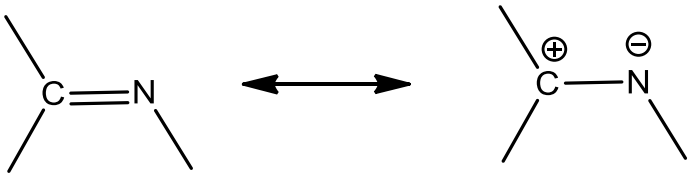

KINETICS:

The rates of hydrogenation in dependence of the concentrations of the amido complex **3a**, the *N*-benzylideneaniline and H_2 in toluene were studied at 140 °C monitoring the conversions of the imines to the amines by ^{1}H NMR and GC/MS analysis. Initially five kinetic experiments were carried out varying the concentrations of the *N*-benzylideneaniline while keeping the catalyst concentration and H_2 pressure fixed at 2 bar (Table 3.4, runs 1-5). Furthermore, the initial rates were determined varying the concentration of the catalyst while keeping the concentration of *N*-benzylideneaniline fixed under 2 bar H_2 (Table 3.4, runs 2, 6-9). The initial rates were derived from ^{1}H NMR after 15 min of reaction time in toluene and are given in Table 3.4. The initial rate data from Table 3.4 revealed that the rate of the reaction is independent of the substrate concentration (Table 3.4, runs 1-5), but varies with the catalyst concentrations (Table 3.4, runs 2, 6-9): Zeroth order in substrate and first order in the catalyst **3a**.

Table 3.4. Zero order rate dependence of the amine production demonstrated by various concentrations of the catalyst **3a** and *N*-benzylideneaniline[a]:

Run	3a (M)	Imine (M)	Initial zero order rate (Ms^{-1})	Amine(M)
1	0.0088	0.22	4.7×10^{-5}	0.0419
2	0.0088	0.44	4.8×10^{-5}	0.0435
3	0.0088	0.662	4.7×10^{-5}	0.0422
4	0.0088	0.882	4.6×10^{-5}	0.0415
5	0.0088	1.104	4.7×10^{-5}	0.042
6	0.0044	0.44	2.5×10^{-5}	0.0231
7	0.0066	0.44	3.7×10^{-5}	0.0331
8	0.011	0.44	6.3×10^{-5}	0.0571
9	0.0130	0.44	7.0×10^{-5}	0.0629

[a]140 °C, 2 bar H_2, product conversions and concentrations were determined from ^{1}H NMR after 15 min of reaction time. Runs 1-5: Variation of [N-benzylideneaniline], Runs 2, 6-9: Variation of [**3a**]

An exemplary kinetic plot of the *N*-benzylideneaniline concentration over time and the initial rate dependency on the variation of catalyst concentration (keeping substrate concentration fixed) are shown in Figure 3.

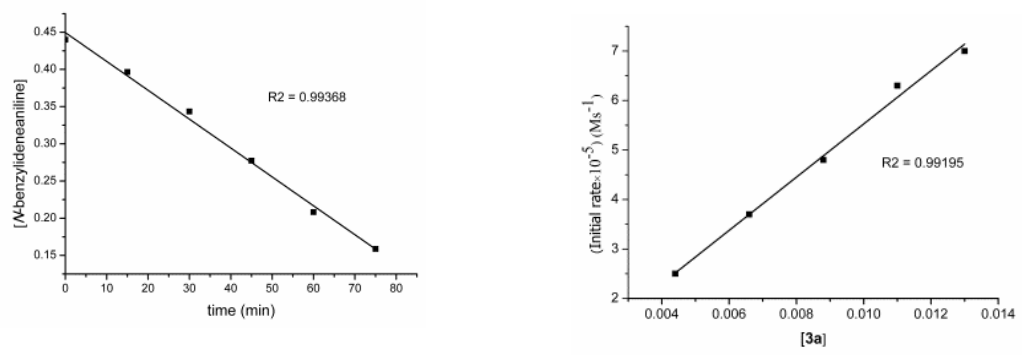

Figure 3.8 Left: Kinetic plot of *N*-benzylideneaniline concentration over time; [*N*-benzylideneaniline] = 0.44 M, [**3a**] = 0.0088 M under 2 bar H_2 and 140 °C. Right: Plot of initial rates at various catalyst concentrations; [*N*-benzylideneaniline] = 0.44 M, 2 bar H_2 and 140 °C temperature.

The H_2 pressure dependence was also investigated determining the initial rates at 20 bar, 40 bar and 60 bar H_2 pressures keeping all other concentrations constant as for runs 10, 11 and 12 (Table 3.5). A plot of the initial rate/[**3a**] vs hydrogen pressure (Figure 3.9) revealed a straight line indicating a linear pressure dependency.

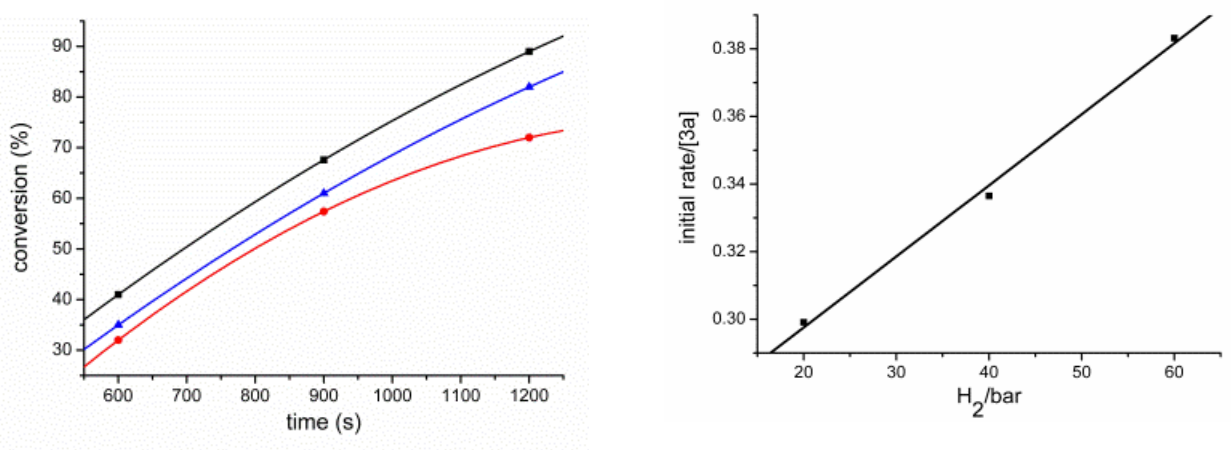

Figure 3.9. Left : Kinetic conversion chart of *N*-benzylidene aniline catalyzed by **3a** at 140 °C. Black: 60 bar H_2; Blue: 40 bar H_2; Red: 20 bar H_2. Right: Plot of initial rate**/[3a]** vs H_2 pressure.

Table 3.5. Zero order rate dependence of the amine production catalyzed by **3a** on H_2 pressure[a]:

Run	3a (M)	Imine (M)	H_2 [bar]	Amine[b] (M)	Zero order rate (Ms^{-1})	Initial rate/[3a]
10	0.0023	1.29	20	0.4127	$6.9 .10^{-4}$	0.299
11	0.0023	1.29	40	0.4644	$7.7.10^{-4}$	0.337
12	0.0023	1.29	60	0.5289	$8.8.10^{-4}$	0.383

[a]140°C, [b]product concentration determined after initial 10 min of reaction from the GC/MS conversions.

Stoichiometric Model Experiments Studies:

To detail the mechanism of the catalytic reaction courses further, stoichiometric experiments were carried out. For instance equal amounts of **3a** and *N*-benzylideneaniline were left for 1 h at room temperature, but no change was observed in the ^1H and ^{31}P NMR

spectra. Even heating of the stoichiometric mixtures to 140 °C for a minimun of 3 h did not reveal any changes in the ^{31}P and ^{1}H NMR spectra, which excluded the possibility of direct binding of the substrate to the catalytic metal center, but also revealed the binding not to be a step of the catalytic reaction course.

Additional mechanistic studies were expected to clarify the H transfer sequence from the NH-MoH moiety, whether it occurs stepwise with hydride before proton transfer or vice versa or simultaneous. But first it had to be examined whether the H transfers to the imine, were rate limiting. For this purpose we chose **4b(*cis*)** and **4b(*trans*)** as a model since the hydride species **4a(*cis*)** and **4a(*trans*)** are only stable under an atmosphere of H_2 which would complicate the measurements. Initially a 0.018 M solution of **3b** in THFd_8 (5 mg of **3b** in 0.5 mL THF-d_8) was filled with 2 bar of H_2 and left for several hours at room temperature. After 90 h of reaction time complete conversion of **3b** to the hydride species **4b(*cis*)** and **4b(*trans*)** was observed. Then the hydrogen pressure was released and 10 equivalents (16. 5 mg) of *N*-benzylideneaniline were added and kept stirring. After 10 min, the ^{31}P NMR spectra of the reaction mixture revealed the complete disappearance of the signals of **4b(*cis*)** and **4b(*trans*)**. The presence of the signal of **3b** at δ 82 ppm indicated complete H transfer from the hydride species to the *N*-benzylideneaniline and regeneration of the amide species. In addition the ^{1}H NMR spectra of the reaction mixture confirmed the presence phenylbenzylamine along with the remaining *N*-benzylideneaniline.

Again, when hydrogenation of *N*-benzylideneaniline (40 equivalents with respect to the catalyst) was carried out using catalyst **3a** or **3b (**5 mg in toluene d_8) under 2 bar H_2 at 140 °C for 15 min, 28% and 15% conversions of *N*-benzylideneaniline to phenylbenzylamine were observed with **3a** or **3b** to be present as the only other detectable species. **3a** or **3b** and *N*-benzylideneaniline and phenylbenzylamine were identified during the course of the catalytic reactions at 140 °C and 60 bar H_2 at an incomplete stage of conversion. Therefore, **3a** and **3b** are presumed to be the active species accumulating before the rate determining step. In contrast the hydride complexes of type **4** are to be considered relatively short-lived intermediates, since the transfer of the hydrogen atoms to the imines is apparantly fast. If the hydride transfer would be rate limiting, one would expect that they would accumulate during the catalytic course[27, 17a] which we did not observe.

In order to compare the kinetics between **3b** and the mixture of the hydride complexes **4b(*cis*)** and **4b(*trans*)** as catalysts, catalytic experiments were carried out in toluene at 140 °C and 60 bar H_2. An initial TOF of 356 h^{-1} was obtained for the hydrogenation of *N*-

benzylideneaniline using the mixture of **4b(*cis*)** and **4b(*trans*)** as catalysts, whereas for **3b** as a catalyst the TOF was found to be 424 h^{-1} (Table 2, entries 13 and 14). There is a slight difference in the catalytic activities but we think this difference is not significant since it might originate from the fact that the mixture of the hydride complexes **4b(*cis*)** and **4b(*trans*)** in toluene have lower solubilities than **3b**.

Deuterium Kinetic Isotope Effect Experiments

For further insights deuterium isotope kinetics were pursued with 20 bar of H_2 or D_2 in the hydrogenation of *N*-benzylideneaniline catalyzed by **3a** at 140 °C. Loading of 0.5 mol% of the catalyst **3a** to a solution of *N*-benzylideneaniline in toluene led to a TOF of 756 h^{-1} under 20 bar D_2 resulting in a DKIE of k_H/k_D = 1.28, which generally is a very small kinetic isotope effect. This might imply that H-H bond splitting is not directly involved in the rate limiting step, since the KIEs of reactions with rate-determining H_2 splitting generally give relatively high positive values or higher negative values in cases of inverse KIEs.

In separate experiments, we also reacted 2 bar of H_2 or D_2 at room temperature with 0.03 M (6.5 mg of **3b** in 0.4 ml THF) solution of **3b** in THF. After 72 h 89% formation of the hydride complexes **4b(*cis*)** and **4b(*trans*)** was observed for the H_2 reaction and in a related experiment with D_2 73% deuterated type **4** compounds were formed as indicated by the ^{31}P NMR spectra to account for a k_H/k_D value of 1.22. This low DKIE value of the H_2 and D_2 reactions to form the type **4** hydride complexes again supported that any type of H_2 splitting is not participating in the rate determining step.

Therefore, it became quite plausible to assume that the addition steps of H_2 to the amido complexes of type **3** are rate determining[28] consisting of initial H_2 uptake to the molybdenum centre. Then heterolytic splitting of the H_2 ligand occurs via proton abstraction by the basic amido nitrogen atom. The H_2 addition step is assumed to be accompanied by extensive structural rearrangements transforming the trigonal bipyramidal geometry of the amido complexes into the octahedral geometry. The concomitant rearrangement energy is naturally independent of the H_2 splitting step but apparantly higher in energy than the H_2 heterolysis.

Based on the given observations of the kinetic studies, specific mechanistic experiments and Hammett correlations, a secondary coordination sphere mechanism analogous to Noyori's bifunctional catalysis is proposed for the H transfers to the imine moieties as depicted in Scheme 3.

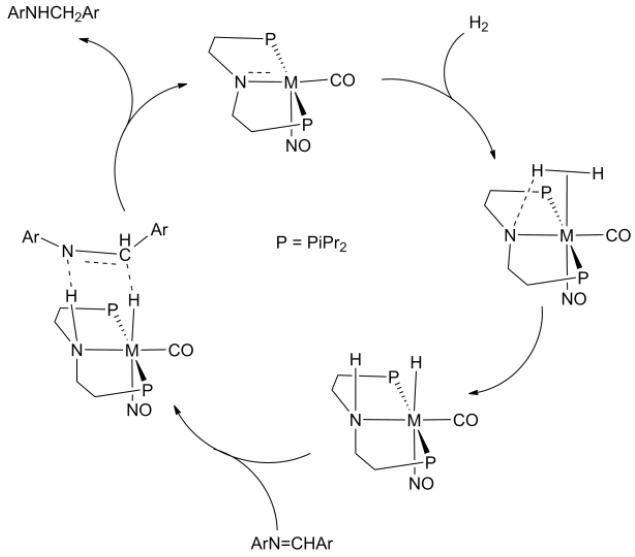

Scheme 3.4. Proposed hydrogenation mechanism

Filtration Experiments as Homogeneity Test of the Imine Hydrogenations:

To exclude any heterogeneous reaction course in the hydrogenation catalyses, filtration experiments[31] were carried out. For this purpose, 1 mol% of the catalyst **3b** was loaded at 140 °C under 60 bar of H_2 in the hydrogenation of *N*-benzylideneaniline. After 7 min of reaction time, the vessel was immediately cooled to room temperature and taken into the glove box. The solution of the reaction mixture was still found to be red and clear without any visible precipitate. A GC/MS analysis of the reaction mixture showed 50% conversion of the imine to corresponding amine. The ^{31}P NMR spectrum and ^{1}H NMR spectrum revealed the presence of only **3b**. After filtration of the solutions, the experiments were repeated, but showed no black precipitate or dark solutions indicating not formation of metal particles.

3.2.8 Preparation of (^{i}Pr$_2$PCH$_2$CH$_2$)$_2$NH ligand based Molybdenum and Tungsten Nitrosyl Complexes in +II and+I oxidation states

Treatment of the (iPr$_2$PCH$_2$CH$_2$)NH ligand with the precursor complexes M(NO)Cl$_3$(NCMe)$_2$ (M = Mo, W) at room temperature in THF led to the precipitation of the isomeric mixtures of Mo(NO)Cl$_3$(PN^{H}P), **7a** and W(NO)Cl$_3$(PN^{H}P), **7b** complexes in moderated yields (**7a**, 55%; **7b**, 62%) (Scheme 3.4). The isomers of **7a** and **7b** correspond to the relative position of the H atom of the internal N-H moiety of PN^{H}P ligand.: N-H adjacent to the Cl atom (*transoid*,

down) and NO ligand (*cisoid*, up). **7a** and **7b** were found to be quite soluble only in CH_2Cl_2. The $^{31}P\{^1H\}$ NMR spectra for **7a** revealed two singlet signals at δ 69.3 {**7a(up)**}and 71{**7a(down)**} ppm in a ratio of 2:1 indicating the presence of isomeric mixture and the equivalence of the phosphorus atoms in each of the isomers of **7a** (Figure 3.10). The $^{31}P\{^1H\}$ NMR spectra for **7b** also exhibited two singlet signals along with tungsten satellites at δ =

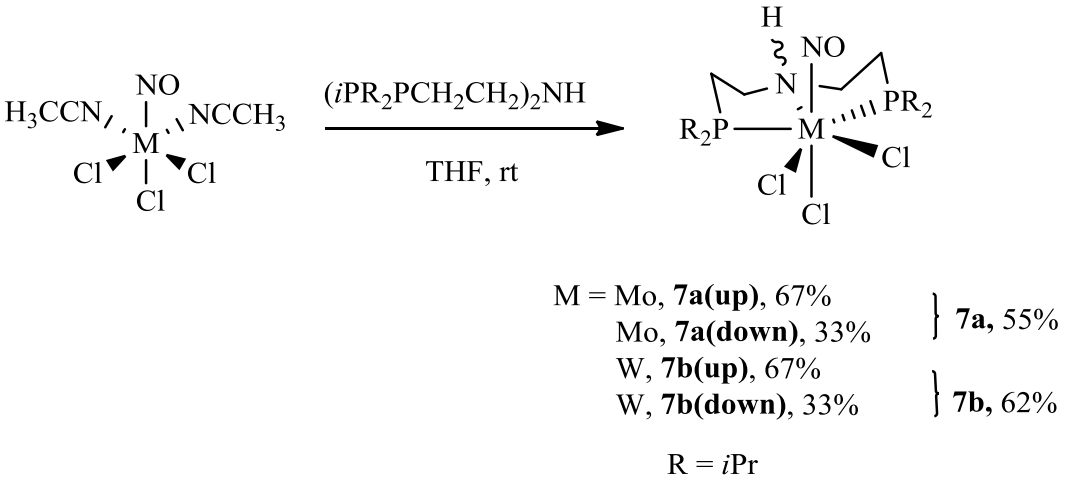

Scheme 3.4. Preparation of the isomeric mixture of $M(NO)Cl_3(PN^HP)$

56.8 [s, $^1J_{P\text{-}W}$ (d, satellite)= 184.8 Hz, **7b**(up)] and 58.3 [s, $^1J_{P\text{-}W}$ (d, satellite)= 189.3 Hz, **7b**(down)] ppm supporting the presence of isomeric mixtures and the equivalence of the phosphorus atoms (Figure 3.10). The IR spectra of **7a** and **7b** showed sharp signals at 1653

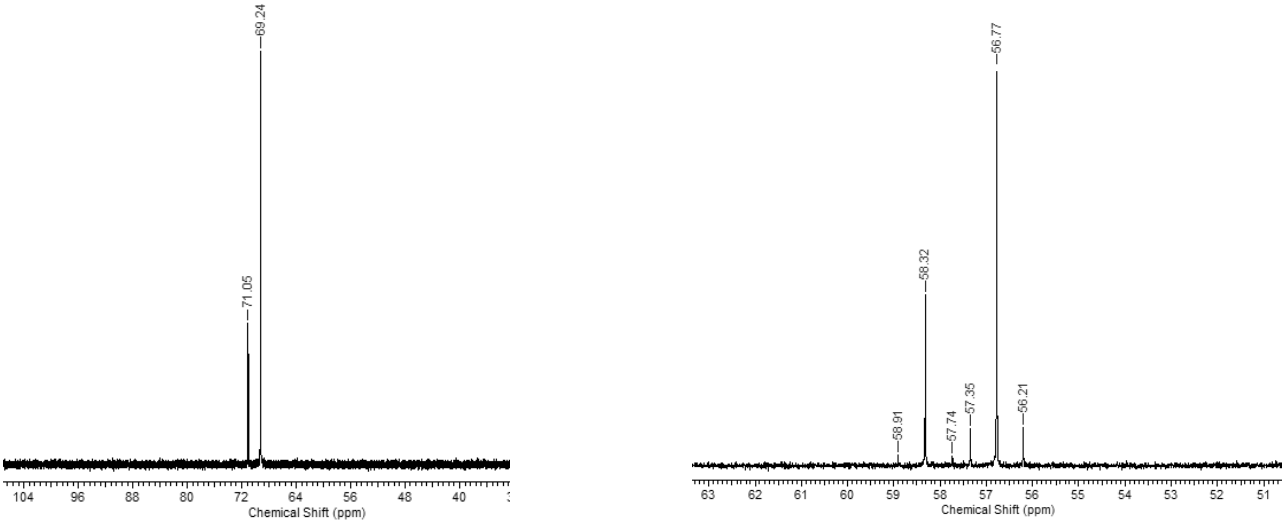

Figure 3.10. $^{31}P\{1H\}$ NMR spectra of the isomers of $Mo(NO)Cl_3(PN^HP)$, **7a** (left) and $W(NO)Cl_3(PN^HP)$, **7b** (right) at room temperature in CD_2Cl_2.

and 1596 cm^{-1} respectively, attributed to the nitrosyl stretching frequencies. The ^{1}H NMR spectra of **7a** and **7b** exhibited several signals for the methyl, methine and methylene protons. The N-H protons of the isomeric mixtures of **7a** was found at δ 4.41 ppm whereas for **7b** it was found at δ 4.47 ppm as broad singlet in the ^{1}H NMR spectra. The triplet signals in the $^{13}C\{^{1}H\}$ NMR at δ = 55.89 (t, $^{v}J_{C\text{-}P}$ = 3.6 Hz, NCH_2) ppm for **7a** and at 55.97 (t, $^{v}J_{C\text{-}P}$ = 5.96 Hz, NCH_2) ppm for **7b** were assigned for the carbon atoms adjacent to the nitrogen atom of the $PN^{H}P$ ligand. Though several attempts to obtain single crystals for X-ray diffraction studies failed, nevertheless the complexes were fully characterised by ^{1}H NMR, ^{31}P NMR, ^{13}C NMR, IR, mass spectrometry, and finally the composition were established by elemental analysis. **7a** and **7b** are heptacoordinated diamagnetic complexes where the metal centres possess the +II oxidation state.

Our initial attempts to deprotonate the N-H moiety of **7a** using $NaN(SiMe_3)_2$ base to obtain 16 e^{-} unsaturated amido complex failed which led to mixture of inseparable decomposed and unidentified products. Therefore we attempted the reduction of these complexes to prepare paramagnetic molybdenum and tungsten complexes (+I).

The reaction of **7a** and **7b** with approximately one equivalent of 1% Na/Hg in THF at room temperature for overnight led to formation of the green 17 e^{-} species $Mo(NO)Cl_2(PN^{H}P)$ (**8a**) and $W(NO)Cl_2(PN^{H}P)$ (**8b**) in 74% and 78% yields, respectively (Scheme 3.5). These complexes are quite soluble in THF and CH_2Cl_2 and sparingly soluble in toluene and benzene.

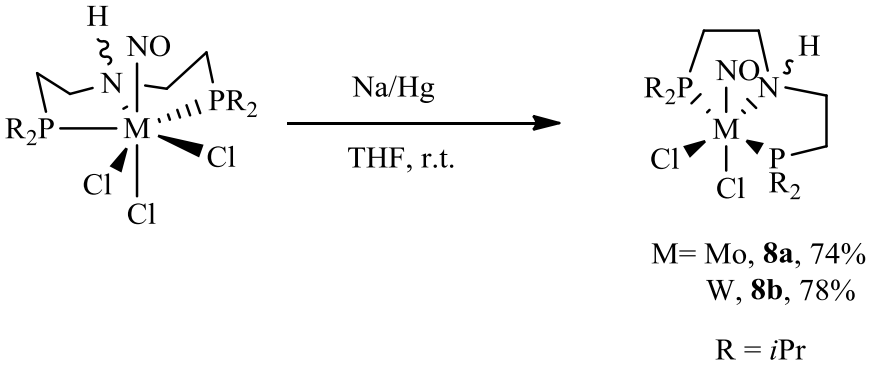

Scheme 3.5. Preparation of $M(NO)Cl_2(PN^{H}P)$ complexes

We could not observe any signals in the $^{31}P\{^{1}H\}$ and ^{1}H NMR spectra of **8a** and **8b** due to the paramagnetic behaviour of these complexes. These compounds were characterized by IR spectroscopy, elemental analysis and X-ray diffraction studies. Sharp bands at 1595 and 1547 cm^{-1} for **8a** and **8b**, respectively, were assigned to the ν_{NO} stretching vibrations. The nitrosyl

stretching frequencies of **8a** and **8b** at lower wave numbers than any for **7a** and **7b** mixtures indicated a higher degree of back-donation from the metal centre to the nitrosyl ligand.

Suitable single crystals for X-ray diffraction studies were grown for **8a** and **8b** from a concentrated toluene/pentane mixtures at -30 °C. The molecular structures of **8a** and of **8b** revealed neutral pseudo octahedral complexes. Perspective views of **8a** and **8b** are shown in Figures 3.11 and Figure 3.12, respectively. Selected bond angles and bond distances for **8a** are given in Table 3.6 and for **8b** are listed in Table 3.7. The two phosphorus atoms and the nitrogen atom of the PN^{H}P ligand and the two chloride ligands attached to the metal centre occupied "equatorial" positions. The nitrosyl and the other chloride ligand were *trans* disposed. No NO/Cl disorder was found in structures of **8a** but despite this the presence of isomeric mixtures in solution with one prevailing component could not be fully ruled out.

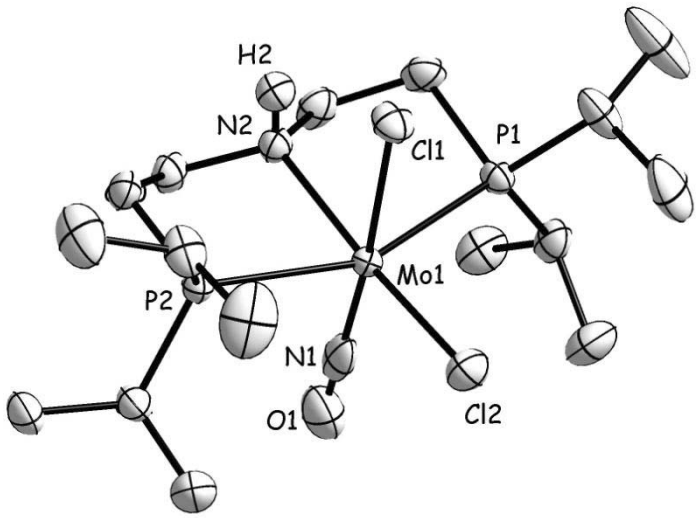

Figure 3.11. Molecular structure of Mo(NO)Cl$_2$(PN^{H}P), **8a**. Thermal ellipsoids are drawn at the 50% probability level.

Table 3.6. Selected bond distances(Å) and bond angles(^{o}) for **8a**:

Bond distances		**Bond angles**	
Mo1-N2	2.255(2)	N1-Mo1-Cl1	174.48(8)
Mo1-N1	1.855(3)	P2-Mo1-P1	156.25(2)
Mo1- Cl1	2.5021(7)	P2-Mo1-Cl2	100.64(2)
Mo1Cl2	2.4258(8)	P2-Mo1-Cl1	87.04(2)

Mo1 P1	2.5372(7)	P2-Mo1-N2	77.86(5)
Mo1 P2	2.5369(6)	Mo1-N1-O1	178.7(3)
N1-O1	1.046(4)		
N2-H2	0.91		

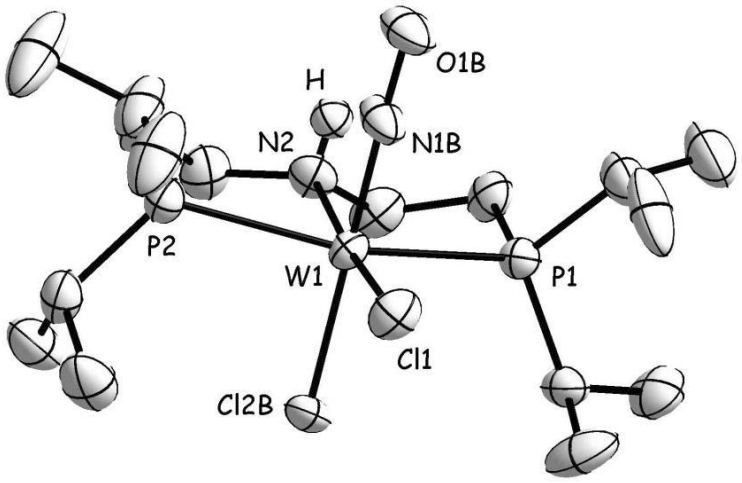

Figure 3.12. Molecular structure of $W(NO)Cl_2(PN^HP)$, **8b**. Thermal ellipsoids are drawn at the 50% probability level.

However the crystal structure analysis of **8a** showed that the *trans* NO/Cl groups are disordered over two positions with site occupancy factors of 0.698(8) and 0.302(8). This NO/Cl disorder supports the presence of isomeric mixtures with respect to the position of N-H moiety with the nitrosyl ligand similar to **7b**.

8a and **8b** are rare paramagnetic complexes with the metal centres in +I oxidation state and of low-spin d^5 configurations. To examine the paramagnetic behavior, solution EPR measurements were carried out on **8a** and **8b** in toluene at room temperature. The spectra are displayed in Figure 3.13 and Figure 3.14. The EPR spectrum of **8a** showed several signals with hyperfine splitting The coupling patterns of the signals are probably due to coupling of

Table 3.7. Selected bond distances (Å) and bond angles (^{o}) for **8b**:

Bond distances		**Bond angles**	
W1-N2	2.232(4)	N1B-W1-Cl2B	172.2(8)
W1-N1B	1.811(19)	P2-W1-P1	157.23(4)
W1- Cl1	2.4211(12)	P2-W1-Cl2B	93.8(2)
W1-Cl2B	2.381(6)	P2-W1-N2	78.82(13)
W1-P1	2.5123(13)	P2-W1-Cl1	101.58(5)
W1-P2	2.5197(14)	W1-N1B-O1B	178(3)
N1B-O1B	1.26(3)		
N2-H	0.79 (4)		

the unpaired electron with the internal nitrogen atom (^{14}N, I =1) of the PN^{H}P ligand. Hyperfine splitting arises from the coupling with the hydrogen atom of the attached nitrogen (^{1}H, I = 1/2). Another very weak signals are observed owing to the coupling of the unpaired electron with the molybdenum centre (^{95,97}Mo I = 5/2, combined 26%). There is no coupling with the terminal phosphorus atoms, which was interpreted in terms of the unpaired electron residing in a d orbital in the (Cl_2, NO, N_{int}) plane.

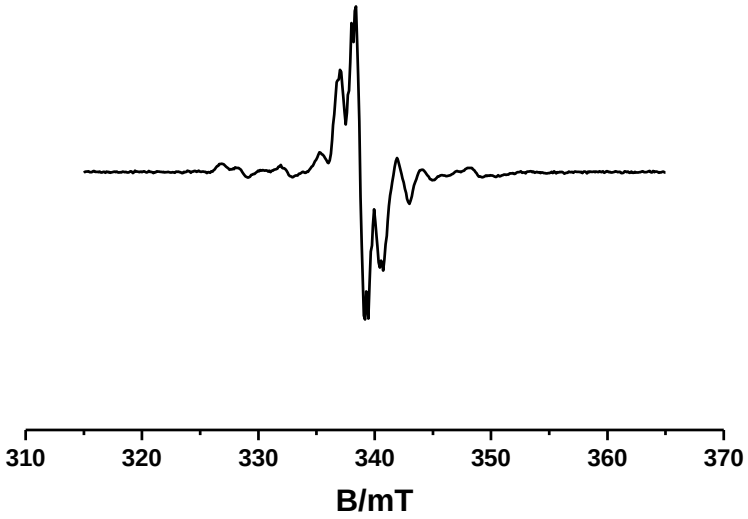

Figure 3.13. Experimental EPR spectra of Mo(NO)Cl_2(PN^{H}P), **8a** at room temperature in toluene.

The EPR spectrum (Figure 3.14) of **8b** in toluene at room temperature showed one signal with doublet splitting along with two weak signals. This could be explained in terms of the coupling of the unpaired electron with the central nitrogen atom attached proton (^{1}H, I = 1/2) along with the coupling with the tungsten nucleus (I = 1/2).

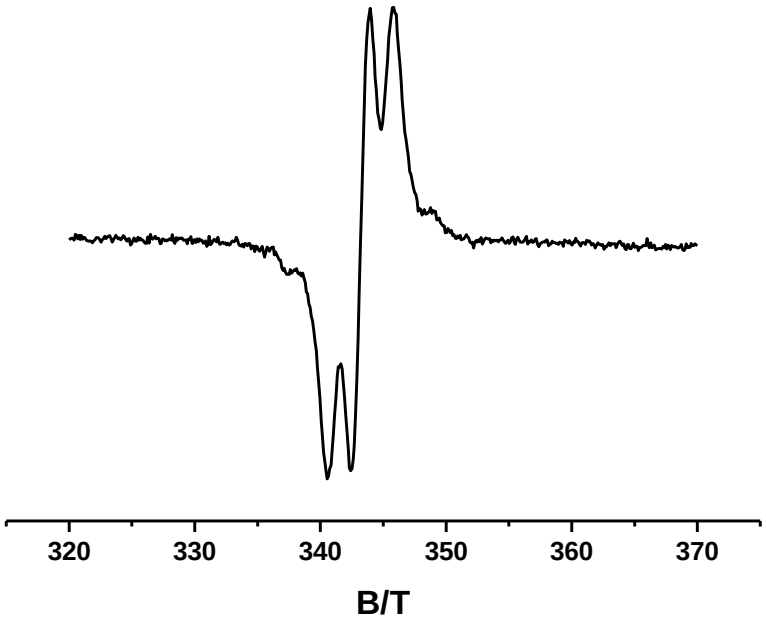

Figure 3.14. Experimental EPR spectra of W(NO)Cl_2(PN^{H}P), **8b** at room temperature in toluene.

However we also attempted to deprotonate the N-H moiety of the PN^{H}P ligand backbone of **8a** and **8b** using $NaN(SiMe_3)_2$ which also led to decomposition and the solution turned black immediately.

Therefore further investigation needs to be done to reduce **8a** and **8b** to low-valent reduced species in presence of weekly coordinating solvents CH_3CN and further deprotonate the species to test them in effective bifunctional catalysis.

3.3 CONCLUSIONS

In conclusion, we have developed highly efficient non-platinum metal catalysts for imine hydrogenations using Mo and W amido centers. The reactive amido complexes of the type M(NO)(CO)(PNP) (M = Mo, **3a**; W, **3b**) were prepared *via* dehydrohalogenation using

$Na[N(SiMe_3)]_2$. The amido complexes **3a** and **3b** cleaved dihydrogen in a heterolytic fashion across the polar M=N double bond to generate the hydride amine complexes with 1,2-addition of the type $M(NO)(CO)H(PNP^H)$ similar to Frustrated Lewis Pairs.[32] Such species were also found to react with carbon dioxide to form unusual 2e+2e addition compounds with four membered strained cycles. The reactions of CO_2 with the amido complexes were found to be much faster when compared to hydrogen reactions. The amine hydride complexes of type **4** reacted with carbon dioxide to produce η^1-formato complexes of the type $M(NO)(CO)(PNP^H)(OCHO)$. Stoichiometric hydrogenations of CO_2 could be accomplished starting from the formato complexes. Catalytic hydrogenations of CO_2 were also attempted at higher temperature and pressures. However, the relatively high stability of the CO_2 addition complexes (**5a,b**) prevented reasonable performance in the CO_2 hydrogenations. Despite this the amido complexes (**3a,b**) could be used as excellently performing imine hydrogenation catalysts. Electron donating groups on the benzylidene side and electron withdrawing groups on the aniline side furnished the highest hydrogenation activities. In Hammett studies a high negative ρ value for various *para* substituted imines on the benzylidene side supported a concerted hydride and proton transfers to the imines. Detailed kinetic studies, mechanistic investigations and the Hammett studies all supported a secondary coordination sphere mechanism similar to Noyori type metal-ligand bifunctional catalysis where the addition of hydrogen to the metal center turned out to be rate determining. Two rare paramagnetic complexes $M(NO)Cl_2(PN^HP)$ (Mo, **8a**; W, **8b**) were also prepared which showed typical paramagnetic signals in the EPR studies. The basis of this work is the ability of the middle transition elements centers of molybdenum and tungsten to add and split H_2 heterolytically and transfer the hydrogen atoms to polar substrates similar to the capabilities of precious metal catalysts.

3.4 EXPERIMENTAL SECTION

General Considerations

All experiments were carried out under an atmosphere of nitrogen using either dry glove box or Schlenk techniques. Reagent grade solvents benzene, tetrahydrofuran, pentane, toluene, diethyl ether were dried with sodium benzophenone and distilled prior to use under N_2 atmosphere. Anhydrous toluene (99.8%, active dry) was bought from Alfa Aesar for catalytic experiments. CH_2Cl_2 and Et_3N were dried over calcium hydride and distilled. Deuterated solvents were dried with sodium benzophenone ketyl (THF-d_8, toluene-d_8 and C_6D_6) and

calcium hydride (CD_2Cl_2) and distilled *via freeze-pump-thaw* cycle prior to use. The $M(NO)(CO)_4(ClAlCl_3)$, (M= Mo, W) complexes and $HN(CH_2CH_2{}^iPr_2)_2$ were prepared according to literature procedures.[33] KO*t*Bu, $Na[N(SiMe_3)_2]$ and DBU were purchased from commercially available sources and used without further purification. The NMR spectra were measured with a Varian Mercury 200 spectrometer (at 200.1 MHz for ^1H, at 81.0 MHz for ^{31}P), with Varian Gemini-300 instrument (^1H at 300.1 MHz, ^{13}C at 75.4 MHz), with Bruker-DRX 500 spectrometer (500.2 MHz for ^1H, 202.5 MHz for ^{31}P, 125.8 MHz for ^{13}C) and Bruker-DRX 400 spectrometer (400.1 MHz for ^1H, 162.0 MHz for ^{31}P, 100.6 MHz for ^{13}C). All chemical shifts for ^1H and $^{13}C\{^1H\}$ are expressed in ppm relative to tetramethylsilane (TMS) and for $^{31}P\{^1H\}$ relative to 85% H_3PO_4 as an external standard reference. Signal patterns are as followed: s, singlet; d, doublet; t, triplet; q, quartet; m, multiplet. IR spectra were obtained either ATR or KBr methods using Bio-rad FTS-45 instrument. Elemental analyses were carried out at Anorganisch-Chemisches Institut of the University of Zurich. The GS-MS spectra were recorded on a Varian Saturn 2000 spectrometer equipped with a Varian 450-GC chromatograph.

General procedure for the preparation of M(NO)(CO)Cl(PN^{H}P) (M = Mo, 1a; W, **1b)**.

To a solution of $M(NO)(CO)_4(ClAlCl_3)$ (1.23 mmol) in 15 mL THF, a solution of $HN(CH_2CH_2P^iPr_2)_2$ (1.23 mmol) in 5 mL THF was added. The resulting mixture was heated at 90 °C for 3 h. After the completion of the reaction, the resulting red solution was filtered off and evaporated to dryness. The solid residue was washed twice with pentane and then dissolved in minimum amount of THF and pentane was added. The solid precipitate was separated and dried in *vacuo.*

1a: Yield: 450 mg (74%). ^1H NMR (400 MHz, THF-d_8): δ = 3.7 (bs, NH, minor isomer), 3.2 (s, NH, major isomer), 3.47-3.36 (m, NCH_2), 2.68-2.53 (m, -NCH_2),), 2.41-2.37 (m, CH), 1.78-1.66 (m, -PCH_2), 1.36-1.23 (m, CH_3). $^{13}C\{^1H\}$ NMR (100.6 MHz, THF-d_8): δ = 246.89 (t, $^2J_{C\text{-}P}$ = 7.2 Hz, CO), 50.95 (t, $^vJ_{C\text{-}P}$ = 4.8 Hz, NCH_2), 25.69 (t, $^vJ_{CP}$ = 7.2 Hz, CH), 21.56 (t, $^vJ_{CP}$ = 8.5 Hz, PCH_2), 18.23 (t, $^vJ_{CP}$ = 3.6 Hz, CH_3), 16.72 (s, CH_3). 14.98 (s, CH_3). $^{31}P\{^1H\}$ NMR (161.9 MHz, THF-d_8): δ = 60.17 (s, major isomer), 59.09 (s, minor isomer). IR (KBr, cm^{-1}): *v* = 1573 (NO), 1912 (CO) Anal. Calcd for $C_{17}H_{37}ClMoN_2O_2P_2$: C, 41.26; H, 7.54; N, 5.66. Found: C, 41.09; H, 7.43; N, 5.37.

1b: Yield: 560 mg (78%). ^1H NMR (500 MHz, THF-d_8): δ = 4.3 (broad singlet, NH, major isomer), 3.7(s, NH, minor isomer), 3.46-3.50 (m, NCH_2), 2.73-2.64 (m, NCH_2), 2.57-2.46 (m,

CH), 1.79-1.78 (m, -PCH_2), 1.24-1.38 (m, CH_3). $^{13}C\{^1H\}$ NMR (100.61MHz ,): δ = 246.46 (t, $^2J_{CP}$ = 3.6 Hz, CO), 52.59 (t, $^vJ_{C-P}$ = 4.8 Hz, NCH_2), 27.03 (t, $^vJ_{C-P}$ = 8.3 Hz, CH), 23.53 (s), 21.77 (t, $^1J_{C-P}$ = 9.5 Hz, CH_2), 19.80 (t, $^1J_{C-P}$ = 9.5 Hz, CH_2). 18.25(t, $^2J_{C-P}$ = 3.6 Hz, CH_3), 16.71 (s, CH_3), 15.38 (s, CH_3) 14.84 (s, CH_3). $^{31}P\{^1H\}$ NMR (161.9MHz, THF-d_8): δ = 52.03 [s, $^1J_{P-W}$ (d, satellite)= 305.9 Hz, major isomer], 51.0 [s, $^1J_{P-W}$ (d, satellite) = 302.9 Hz, minor isomer]. IR (KBr, cm^{-1}): *v* = 1556 (NO), 1894 (CO) Anal. Calcd for $C_{17}H_{37}ClN_2O_2P_2W$: C, 35.04; H, 6.40; N, 4.81. Found: C, 34.98; H, 6.21; N, 5.13.

Mo(NO)(CO)(PN^{H}P)(O^{t}Bu) (2a).

1a (0.1 g, 0.20 mmol) and KO*t*Bu (0.035 g, 0.30 mmol) were mixed in 10 mL of THF in a young Schlenk. The resulting mixture in THF was kept constant stirring for 2 h at room temperature. After completion of the reaction the solution was filtered off and solvent was removed in *vacuo*. The crude product was dissolved in ether and filtered out. Then ether solution of the product was concentrated and kept in the fridge at -30 °C. Suitable yellow single crystals for diffraction were obtained after several days. Yield : 69 mg (65%). ^1H NMR (400 MHz, THF-d_8): δ = 3.40-3.29 (m, NCH_2), 2.69-2.64 (m, 2H, -NCH_2), 2.45-2.33 (m, 4H, CH), 1.62-1.53 (m, 4H, -PCH_2), 1.37-1.19 (m, CH_3), 0.99 (s, CH_3). $^{13}C\{^1H\}$ NMR (100.6 MHz): δ = 246.91 (t, $^2J_{c-p}$ = 7.2 Hz, CO), 26.03 (t, $^vJ_{C-P}$ = 5.9 Hz, CH), 23.57 (t, $^vJ_{C-P}$ = 7.2 Hz, CH_2), 20.94 (t, $^vJ_{C-P}$=7.2 Hz, CH_2), 18.76 (t, $^vJ_{C-P}$ = 4.8 Hz, CH_3). 17.72 (t, $^vJ_{C-P}$ = 2.4 Hz, CH_3), 17.01 (s, CH_3). $^{31}P\{^1H\}$ NMR (161.9 MHz, THF-d_8): δ = 50.98 (s). IR (KBr, cm^{-1}): *v* = 1558 (NO), 1883 (CO). Anal. Calcd for $C_{21}H_{47}MoN_2O_3P_2$: C, 47.28; H, 8.88; N, 5.25. Found: C, 46.90; H, 8.60; N, 5.01.

General procedure for the preparation of M(NO)(CO)(PNP), (**M = Mo, 3a**; **W, 3b**).

To a solution of M (NO)(CO)(PNP^H)Cl (0.81 mmol) in THF, NaHMDS (1.22 mmol, 1.5 eq, 1M in THF) was added. The resulting mixture in THF was kept for stirring for half an hour. After the completion of the reaction monitored by $^{31}P\{^1H\}$ NMR spectroscopy, the product was filtered and dried in *vacuo*. Then the desired product was extracted with pentane. Finally it was concentrated and kept in the fridge at -30 °C. Red crystals were obtained after several days.

3a: Yield: 210 mg (57%).^1H NMR (500 MHz, THF-d_8): δ = 3.50-3.42 (m, 2H, NCH_2), 3.36-3.28 (m, 2H, -NCH_2), 2.36-2.23 (m, 4H, CH), 2.11-2.04 (m, 2H, PCH_2), 1.98-1.92 (m, 2H, -PCH_2), 1.069-1.387 (m, 24H, CH_3). $^{13}C\{^1H\}$ NMR (125.8 MHz, THF-d_8): δ = 60.5 (t, $^vJ_{C-P}$

8.3 Hz, NCH_2), 23.87 (m, CH), 21.29 (t, $^{v}J_{CP}$ = 8.3 Hz, CH_2), 16.2 (m, CH_3). 15.3 (m, CH_3). $^{31}P\{^{1}H\}$ NMR (161.9 MHz, THF-d_8): δ = 82.01 (s). IR (KBr, cm^{-1}): *v* = 1565 (NO), 1893 (CO). Anal. Calcd for $C_{17}H_{36}MoN_2O_2P_2$: C, 44.54; H, 7.92; N,6.11. Found: C, 44.74; H, 8.01; N, 6.23. Assignments in the ^{1}H NMR were confirmed by C-H, long range C-H correlations and ^{13}C DEPT experiments.

3b: Yield: 238 mg (54%). ^{1}H NMR (400 MHz, THF-d_8): δ = 3.52-3.44 (m, 2H, NCH_2), 3.36-3.27 (m, 2H, NCH_2), 2.46-2.32 (m, 4H, CH), 2.11-2.05 (m, 2H, PCH_2), 2.02-1.93 (m, 2H, PCH_2), 1.29-1.13 (m, 24H, CH_3). $^{13}C\{^{1}H\}$ NMR (100.61 MHz, THF-d_8): δ = 253.6 (s, CO), 63.36 (t, $^{v}J_{C-P}$ = 8.3 Hz, NCH_2), 25.06 (t, $^{v}J_{C-P}$ = 11.9 Hz, CH), 24.43 (t, $^{v}J_{C-P}$ = 10.7 Hz, CH), 21.73 (m, CH_2), 16.21 (s, CH_3), 15.36 (s, CH_3) $^{31}P\{^{1}H\}$ NMR (162 MHz, THF-d_8): 81.09 [s, $^{1}J_{pw}$ (d, satellite) = 320.1 Hz]. IR (cm^{-1} , KBr): 1541 (ν_{NO}), 1871 (ν_{CO}). Anal. Calcd for $C_{17}H_{36}N_2O_2P_2W$: C, 37.38; H, 6.64; N, 5.13. Found: C,37.72; H, 6.74; N, 5.01.

Reaction of 3a with hydrogen to form 4a(*cis*) and 4a(*trans*)

A solution of **3a** (18 mg, 0.039 mmol) in 0.5 mL THF-d_8 in a Young NMR tube was frozen with liquid nitrogen. Then the nitrogen atmosphere was removed *via freeze thaw pum*p cycle and the tube was filled with 2 bar of H_2 and sealed. The tube was shaken vigorously and left for few hours. Slow formation of **4a(*cis*)** and **4a(*trans*)** was monitored by $^{31}P\{^{1}H\}$ NMR spectroscopy. After 30 h, an equilibrium mixture of 1:1:1 ratio of **4a(*cis*)**, **4a(*trans*)** and **3a** was observed. Formation of **4a(*cis*)** and **4a(*trans*)** was confirmed by ^{1}H and ^{31}P NMR spectroscopy in solution as well as ^{1}H and ^{31}P correlation spectroscopy.

^{1}H NMR (500 MHz, THF-d_8): δ = 0.8 (t, $^{2}J_{PH}$ = 26.3 Hz, Mo-H, **4a(*trans*)**), -1.8 (t, $^{2}J_{PH}$ = 26.2 Hz, Mo-H, **4a(*cis*)**), $^{31}P\{^{1}H\}$ NMR (202 MHz, THF-d_8): δ = 78.5 (s, **4a(*trans*)**), 78.9 (s, **4a(*cis*)**).

Preparation of W(NO)(CO)H(PN^{H}P) {4b(*cis*) and 4b(*trans*)}:

A solution of **3b** (30 mg, 0.056 mmol) in 0.5 mL THF-d_8 in a Young NMR tube was frozen with liquid nitrogen. The nitrogen atmosphere was removed *via freeze thaw pump* cycle. Then the tube was allowed to warm to room temperature. The tube was filled with 2 bar of H_2 and sealed. Then the tube was shaken vigorously and left for few hours. Formation of **4b(*cis*)** and **4b(*trans*)** was supported by ^{1}H and $^{31}P\{^{1}H\}$ NMR spectroscopy.

Alternative preparation method for the mixture of 4b(*cis*) and **4b(*trans*)**:

To a solution of **3b** (300 mg, 0.51 mmol) in 15 mL THF, the $NaHBEt_3$ solution (0.77 mmol, 1.5 eq, 1M in THF) was added. The resulting mixture in THF was kept for stirring for few hours. After the completion of the reaction (as indicated from ^{31}P NMR), the product was filtered and dried in *vacuo*. Then the dark red product was dissolved in minimum amount of toluene and precipitated out with pentane. The obtained sticky red solid was further washed with pentane twice and dried in *vacuo* to obtain the desired product as powder in 53% (150 mg) yield. ^{1}H NMR (400 MHz, 298K, THF-d_8): δ = 3.5 {br 1H, NH, **4b(*cis*)**}, 3.3 {br, 1H, NH, **4b(*trans*)**}, 3.35 (m, -NCH_2), 3.02 (m, -NCH_2), 2.85 (t, $^{2}J_{PH}$ = 25.5 Hz, W-H, **4b(*trans*)**), 2.75 (t, $^{2}J_{PH}$ = 22 Hz, W-H, **4b(*cis*)**), 2.44-1.99 (m, -CH, -CH_2), 1.29-1.23 (m, CH_3). $^{13}C\{^{1}H\}$ NMR (100.62, THF-d_8): δ = 247.2 (s, CO), 53.89 (t, $^{v}J_{CP}$ = 4.78 Hz, NCH_2), 31.10 (t, $^{v}J_{CP}$ = 11.2 Hz, CH), 31.79 (t, $^{v}J_{CP}$ = 13.1 Hz, CH), 28.52 (-CH_2P), 20.64 (s, CH_3), 19.43 (s, CH_3), 18.56 (s, CH_3), 17.74 (s, CH_3) . $^{31}P\{^{1}H\}$ NMR (161.97 MHz, THF-d_8): δ = 64.7 (s, $^{1}J_{pw}$ = 306.7 Hz, **4b(*trans*)**) 65.4 (s, **4b(*cis*)**). IR (cm^{-1} , KBr): 1556 (ν_{NO}), 1618 (ν_{W-H}), 1864 (ν_{CO}). Anal. Calcd for $C_{17}H_{38}N_2O_2P_2W$: C, 37.24; H, 6.99; N, 5.11. Found: C, 36.89; H, 7.03; N, 5.19.

General procedure for the preparation of M(NO)(CO)(PNP)(OCO), **{M = Mo**, **5a(*trans*)**; **W**, **5b(*trans*)}**:

M(NO)(CO)(PNP) (0.065 mmol) was dissolved in 0.5 mL THF-d_8 in a J Young NMR tube. The tube was taken out from the glove box and frozen with liquid nitrogen. The nitrogen atmosphere was removed *via freeze thaw pump* cycle and the tube was filled with 2 bar of CO_2 and sealed. Formation of **5a(*trans*)** or **5b(*trans*)** took place immediately within five minutes in quantitative yield.

5a(*trans*): ^{1}H NMR (400 MHz, THF-d_8): δ = 3.47-3.35 (m, 2H, -NCH_2), 2.85-2.78 (m, 2H, -NCH_2), 2.42-2.36 (m, 2H, CH), 2.25-2.17(m, 2H, CH), 2.08-2.03 (m, 2H, CH_2), 1.81-1.72 (m, 2H, -PCH_2), 1.35-1.28 (m, 12H, *C*H_3), 1.23-1.15 (m, 12H, CH_3). $^{13}C\{^{1}H\}$ NMR (100.62 MHz THF-d_8): δ = 247.34 (s, CO), 156.43 (s, CO_2), 53.16 (t, $^{v}J_{CP}$ = 3.6 Hz, NCH_2), 23.79 (s, CH), 19.83 (t, $^{v}J_{C-P}$ = 6 Hz, CH_2), 16.59 (s, CH_3), 16.21(s, CH_3), 15.74 (s, CH_3) .$^{31}P\{^{1}H\}$ NMR (161.97 MHz, THF-d_8): δ = 61.96 (s). IR (cm^{-1} , KBr): 1593 (ν_{NO}), 1732 (ν_{CO}), 1902 (ν_{CO}). Anal.Calcd for $C_{18}H_{36}MoN_2O_4P_2$: C, 43.03; H, 7.22; N, 5.58. Found: C, 42.67; H, 7.28; N, 5.34.

5b(*trans*): ^{1}H NMR (400 MHz, THF-d_8): δ = 3.58-3.49 (m, 2H, -NCH_2), 2.92-2.85 (m, 2H, -NCH_2), 2.52-2.46 (m, 2H, CH), 2.28-2.20(m, 2H, CH), 2.11-2.06 (m, 2H, -PCH_2), 1.81-1.76 (m, 2H, -PCH_2), 1.37-1.29 (m, 12H, -CH_3), 1.25-1.11 (m, 12H,-CH_3). ^{13}C{^{1}H} NMR (75.45 MHz, THF-d_8): δ = 250.64 (s, CO), 159.34 (s, CO_2), 57.678 (t, $^{v}J_{C-P}$ = 3.6 Hz, NCH_2), 27.53 (t, $^{v}J_{CP}$ = 10.9 Hz, CH), 26.87 (t, $^{v}J_{CP}$ = 12.23 Hz, CH), 23.62 (t, $^{v}J_{CP}$ = 7.7 Hz, PCH_2), 19.66 (t, $^{v}J_{CP}$= 5.96 Hz, CH_3), 19.05(s, CH_3), 18.61 (s, CH_3) .^{31}P{^{1}H} NMR (161.97 MHz, THF-d_8): 56.36 [s, ^{1}Jpw(d, satellite)= 308.2 Hz]. IR (cm^{-1} , KBr): 1554 (ν_{NO}), 1741 (ν_{CO2}), 1879 (ν_{CO}). Anal. Calcd for $C_{18}H_{36}N_2O_4P_2W$: C, 36.63; H, 6.15; N, 4.75. Found: C, 36.29; H, 6.27; N, 4.72.

R**eaction of 3a and 3b with CO_2 at 213K**:

M(NO)(CO)(PNP) (0.03 mmol) was dissolved in 0.5 mL THF-d_8 in a J Young NMR tube. The tube was taken out of the glove box and frozen with liquid nitrogen. The nitrogen atmosphere was removed *via freeze thaw pump* cycle. The tube was filled with 2 bar of CO_2 under frozen condition and sealed. Then the tube was immediately kept in the 300 MHz NMR spectrometer preset at -60 °C. and ^{31}P NMR spectra was recorded.

^{31}P{^{1}H} NMR data for the reaction of **3a** with CO_2 at 213K: ^{31}P{^{1}H} NMR (121.48 MHz, 213K, THF-d_8): δ = 63.1 (s, **5a(*trans*)**), 62.7 (s, **5a(*cis*)**).

^{31}P{^{1}H} NMR data for the reaction of **3b** with CO_2 at 213K: ^{31}P{^{1}H} NMR (121.48 MHz, 213K, THF-d_8): δ = 58.1 (s, **5b(*trans*)**), 57.9 (s, **5b(*cis*)**).

Reaction of 3a with CO_2 in the presence of $B(C_6F_5)_3$

To a solution of **3a** (10 mg, 0.022 mmol) in 0.5 mL toluene-d_8, 1 equiv. of $B(C_6F_5)_3$ was added in a Young NMR tube. The ^{31}P NMR was measured to ensure complete adduct formation has taken place. The tube was then frozen with liquid nitrogen and nitrogen atmosphere was removed. Then the tube was allowed to warm to room temperature and 1.5 bar of CO_2 s purged. The ^{31}P NMR spectra revealed formation of new species instantaneously in quantitative yield.

^{1}H NMR (300 MHz, 298K, tol d_8): δ = 3.10 (m, -NCH_2), 2.10 (m, CH), 1.72 (m, PCH_2), 0.85-1.23 (m, CH_3). ^{31}P{^{1}H} NMR (161.97 MHz, THF-d_8): δ = 59.4 (s). ^{13}C{^{1}H} NMR (100.62,tol d_8): δ = 178 (CO_2). IR (cm^{-1} , ATR): 1606 (ν_{NO}), 1644 (ν_{CO2}), 1915 (ν_{CO}). ^{11}B NMR (96.28 MHz, tol-d_8): δ 2.03 (br, s). ^{19}F NMR (282.33 MHz, tol-d_8): δ -132.8 (d, 6F, J_{CF} = 19.8 Hz, *ortho*-C_6F_5), - 158.8 (t, $^{1}J_{CF}$= 20.6 Hz, 3F, *para*-C_6F_5) and -165.4 ppm (t, $^{1}J_{CF}$= 16.9 Hz 6F,

meta -C_6F_5). Anal. Calcd for $C_{36}H_{37}BF_{15}MoN_2O_4P_2$(**3a**.$CO_2$.$B(C_6F_5)_3$: C, 42.58; H, 3.67; N, 2.76. Found: C, 42.91; H, 3.94; N, 2.66.

Reaction of 3a and 3b with $B(C_6F_5)_3$

To a solution of M(NO)(CO)(PNP), (M = Mo, **3a**; W, **3b**) (0.022 mmol) in 0.5 mL toluene-d_8, the $B(C_6F_5)_3$ (0.022 mmol) was added. The resulting mixture shaken vigorously and characterized in situ without further purifications. Yield 100% based on ^{31}P NMR.

[3a. $B(C_6F_5)_3$] adduct**:** ^{1}H NMR (300 MHz, 298K, *tol*-d_8): δ = 2.95 (m, -NCH_2), 2.76 (m, -NCH_2), 2.11 (m, CH), 1.58 (m, CH_2), 1.4(m, CH_2), 1.12(m, PCH_2), 0.9-0.55 (m, CH_3). ^{31}P{^{1}H} NMR (161.97 MHz, tol d_8): δ = 80.1 (s). ^{11}B NMR (96.28 MHz, *tol*-d_8): δ -19.5 (s). ^{19}F NMR (282.33 MHz, tol-d_8): -133.32 (m, 6F, *ortho*-C_6F_5), -160.2 (t, $^1J_{CF}$= 19.8 Hz, 3F, *para*-C_6F_5) and -166.38 ppm (t, $^1J_{CF}$= 16.7 Hz, 6F, *meta* -C_6F_5)

[**3b**. $B(C_6F_5)_3$] adduct**:** ^{1}H NMR (300 MHz, 298K, *tol*-d_8): δ = 2.79-2.70 (m, -NCH_2), 2.11-1.03 (m, -CH), 1.66 (m, PCH_2), 1.43 (m, PCH_2), 1.01-0.53 (m, CH_3). ^{31}P{^{1}H} NMR (161.97 MHz, THF-d_8): δ = 77.5 (s). ^{11}B NMR (96.28 MHz, *tol*-d_8): δ 5.4 (s). ^{19}F NMR (282.33 MHz, *tol*- d_8): δ -133.2 (m, 6F, *ortho*-C_6F_5), -160.6 (t, $^1J_{CF}$= 20.6 Hz, 3F, *para*-C_6F_5) and -166.6 ppm (t, $^1J_{CF}$= 17.5 Hz 6F, *meta* -C_6F_5).

Mo(NO)(CO)(PN^{H}P)(OCHO), **{mixture of 6a(*cis*) and 6a(*trans*)}**:

3a (0.015g, 0.033mmol) in 0.5 mL THF was frozen in a young NMR tube. The nitrogen atmosphere was removed *via freeze thaw pump* cycle. Then the tube was filled with 2 bar of H_2 and sealed and kept for three days to allow formation of **4a(*cis*)** and **4a(*trans*)**. After formation of the equilibrium mixture of hydride complexes **4a(*cis*)** and **4a(*trans*)** along with **3a** (1:1:1), the hydrogen pressure was slowly released and CO_2 (2 bar) was purged into that mixture instantaneously. Immediate formation of **6a(*cis*)** and **6a(*trans*)** was observed along with **5a(*trans*)** in a ratio of 1:1:1 as revealed by the ^{31}P{^{1}H} NMR.

^{1}H NMR (400.1 MHz, THF-d_8): δ = 8.5 (s, 1H, OCH, **6a(*cis*)**), 8.1 (s, 1H, OCHO, **6a(*trans*)**). ^{13}C{^{1}H} NMR (100.6 MHz, THF-d_8): δ 248 (s, CO, **6a**(***trans***)), 246.5 (s, CO, **6a(*cis*)**), 170 (s, OCHO, **6a(*cis*)**), 168.8 (s, OCHO, **6a(*trans*)**), 156 (s, CO_2, **5a(*trans*)**). ^{31}P{^{1}H} NMR (161.97 MHz, THF-d_8): 60.9 (s, **6a(*trans*)**), 60.0 (s, **6b(*cis*)**). Since the resulting product contains mixtures of **6a(*cis*)**, **6a(*trans*)** and **5a(*trans*)** and could not be separated.

W(NO)(CO)(PN^{H}P)(OCHO), **{mixture of 6b(*cis*) and 6b(*trans*)}**:

A solution of the mixture of **4b(*cis*)** and **4b(*trans*)** (0.020g, 0.036mmol) in 0.5 mL THF was frozen in a young NMR tube. The nitrogen atmosphere was removed *via freeze thaw pump* cycle. Then the tube was filled with 2 bar of CO_2 and sealed. Formation of (**6b(*cis*)** and **6b(*trans*)**) took place immediately upon shaking the NMR tube in quantitative yield in a 1:9 ratio. Suitable orange crystals were obtained for diffraction upon layering pentane to a concentrated THF solution of the product. Yield (by ^{31}P NMR): 10%, (**6b(*cis*)**; 90%, (**6b(*trans*).**

^{1}H NMR (400.1 MHz, THF-d_8): δ = 8.52 (s, 1H, OCH, **6b(*trans*)**), 8.0 (s, 1H, OCH, **6b(*cis*)**), 2.93 (m, 4H, -NCH_2), 2.41-2.26 (m, 4H, -CH), 1.66-1.62 (m, 4H, CH_2P), 1.35-1.25 (m, 24H, CH_3). ^{13}C{^{1}H} NMR (100.6 MHz, THF-d_8): δ 244.73 (s, CO), 164.26 (s, CO_2H), 57.7 (s, NCH_2), 24.46 (t, $^{v}J_{CP}$= 13.1 Hz, CH), 24.01 (t, $^{v}J_{CP}$ = 9.5 Hz, CH), 19.08 (t, $^{V}J_{CP}$ = 8.3 Hz, CH_2), 17.18(s, CH_3), 14.80 (s, CH_3). ^{31}P{^{1}H} NMR (161.97 MHz, THF-d_8): 51.3 (s, **6b(*trans*)**), 52.6 (s, **6b(*cis*)**). IR (cm^{-1} , KBr): 1578 (ν_{NO}), 1612 (ν_{OCHO}), 1863 (ν_{CO}). Anal. Calcd for $C_{18}H_{38}N_2O_4P_2W$: C, 36.50; H, 6.47; N, 4.73. Found: C, 36.25; H, 6.41; N, 4.53.

Preparation of Mo(NO)Cl$_3$(PN^{H}P), **7a**.

To a solution of $Mo(NO)Cl_3(NCMe)_2$ (0.200 g, 0.636 mmol) in 10 mL of THF, 0.16 g (196 mg, 0.64 mmol) PN^{H}P ligand in 5 mL THF was added. The resulting mixture was kept stirring for overnight to obtain a light green precipitate. Then the solvent was separated from the precipitate and the precipitate was washed with minimum amount of THF and extracted with dichloromethane and dried in *vacuo* to get the powdery product **7a** in 55% yield. ^{1}H NMR (400 MHz, CD_2Cl_2): δ = 4.41 (broad singlet, NH), 3.49 (m, NCH_2), 3.23 (m, NCH_2), 3.00 (m, CH), 2.27 (m, -PCH_2), 2.05 (m, PCH_2), 1.50-1.30 (m, CH_3). ^{13}C{^{1}H} NMR (100.6 MHz, CD_2Cl_2): δ = 55.89 (t, $^{v}J_{C-P}$ = 3.6 Hz, NCH_2), 29 (m, CH), 28(m, PCH_2), 21 (m, CH_3), 20.4 (m, CH_3). ^{31}P{^{1}H} NMR (400 MHz, CD_2Cl_2): 69.3 (s, $^{i}Pr_2P$, **7a(up)**), 71 (s, **7a(down)**). IR (cm^{-1}, ATR): 1653 (ν_{NO}), Expected m/z: 538, Observed m/z: 538.2. Anal.Calcd for $C_{16}H_{37}Cl_3MoN_2OP_2$: C, 35.74; H, 6.94; N, 5.21. Found: C, 36.03; H, 6.39; N, 5.67.

Preparation of W(NO)Cl$_3$(PN^{H}P), **7b**.

$WCl_3(NO)(NCMe)_2$ (200 mg, 0.5 mmol) was dissolved in 10 mL of THF. 0.160 g (0.52 mmol) of aminodiphosphine PN^{H}P ligand was added *via* a syringe. After few minutes stirring red precipitate was observed and it was allowed to stir for overnight. Then the solution was

removed partially under vacuum and the reddish residue is filtered off and washed with THF. The obtained residue was extracted with dichloromethane and the solvent was removed in *vacuo* to obtained **7b** 62% yield. ^{1}H NMR (400 MHz, CD_2Cl_2): δ = 4.47 (broad singlet, NH), 3.71-3.57 (m, NCH_2), 3.19-3.05 (m, CH), 2.30-2.23 (m, -PCH_2), 2.09-2.06 (m, PCH_2), 1.47-1.19 (m, CH_3). ^{13}C{^{1}H} NMR (100.6 MHz, CD_2Cl_2): δ = 55.97 (t, $^{v}J_{C-P}$ = 5.96 Hz, NCH_2), 27.8 (m, CH), 27.3 (m, PCH_2), 20(m, CH_3). ^{31}P{^{1}H} NMR (400 MHz, CD_2Cl_2): 56.8 [s, $^{1}J_{P-W}$ (d, satellite)= 184.8 Hz, **7b(up)**], 58.3 [s, $^{1}J_{P-W}$ (d, satellite)= 189.3 Hz, **7b(down)**]. IR (cm^{-1}, ATR): 1596 (ν_{NO}), Anal.Calcd for $C_{16}H_{37}Cl_3N_2OP_2W$: C, 30.72; H, 5.96; N, 4.48. Found: C, 30.72; H, 5.88; N, 4.55.

Preparation of Mo(NO)Cl$_2$(PN^{H}P), 8a.

$MoCl_3(NO)(PN^{H}P)$ (0.030 g, 0.056 mmol) was added to a stirred suspension of approximately 1% sodium amalgam (0.0013 g, 0.057 mmol) in 15 mL THF. Stirring was continued overnight at room temperature to ensure the completion of the reaction. The final supernatant green solution was filtered off from mercury containing residue and evaporated to dryness. The residue was washed with pentane and extracted with THF. Finally the product was obtained as green powder after removing the THF in *vacuo*. Yield 74%. IR (cm^{-1}, ATR): 1595 (ν_{NO}), Anal.Calcd for $C_{16}H_{37}Cl_2MoN_2OP_2$: C, 38.26; H, 7.42; N, 5.58. Found: C, 37.88; H, 7.12; N, 5.29.

Preparation of W(NO)Cl$_2$(PN^{H}P), 8b.

0.075 g (0.12 mmol) $WCl_3(NO)(PN^{H}P)$ was added to a stirred suspension of 1% sodium amalgam (0.003 g, 0.13 mmol) in 15 mL THF. Stirring was continued overnight at room temperature to ensure the completion of the reaction. The final supernatant solution was filtered off from mercury containing residue and evaporated to dryness. The residue was washed with pentane and extracted with THF and later with toluene. Recrystallisation upon cold toluene/pentane solution afforded green crystals. Yield 78%. IR (cm^{-1}, ATR): 1547 (ν_{NO}). Anal.Calcd for $W(NO)Cl_2(PNP)$: C, 32.56; H, 6.32; N, 4.75. Found: C, 32.71; H, 6.22; N, 4.78.

General procedure for the reaction of formate complexes {mixture of 6a(*cis*) and 6a(*trans*)) and (mixture of 6b(*cis*) and 6b(*trans*)} with the Na[N(SiMe$_3$)$_2$] base:

The mixture of the formate complexes (0.03 mmol) of molybdenum {mixture of **6a(*cis*)** and **6a(*trans*)** along with **5b(*trans*)**} or tungsten {mixture of **6b(*cis*)** and **6b(*trans*)**} were dissolved in THF in a Young NMR tube. Then 1 eq. of the Na[N(SiMe$_3$)$_2$] base was added. The mixture was shaken vigorously. The $^{31}P\{^1H\}$ NMR spectra revealed immediate regeneration of **3a** or **3b** . Then the reaction mixture was dried in *vacuo* and extracted with pentane to remove the **3a** or **3b**. Then the remaining solid insoluble in pentane was dissolved in D_2O. The ^1H NMR spectra in D_2O revealed the formation of HCOONa.

General Procedures for the CO_2 hydrogenations:

A steel autoclave was charged under nitrogen with the catalysts (0.1 mmol, 5 mol% with respect to base) dissolved in 0.5 mL of THF and 20 eq. of the Na[N(SiMe$_3$)$_2$] base (1 M in THF). The tube was pressurized with 40 bar H_2 and allowed to stir at room temperature for half an hour. After this period 10 bar of CO_2 was purged. Then the total pressure was kept at 80 bar filling with H_2 pressure. The reaction mixture was heated to 140°C (Caution!!: pressure rises to 100 bar). After certain reaction times, the autoclave was cooled to room temperature and the pressure was released. The THF solvent was evaporated to dryness and D_2O was added to dissolve the solid residue. Dimethylformamide (2uL) was added to the reaction mixtures as an internal standard for determination of the yield by ^1H NMR spectroscopy. ^1H NMR (300 MHz, D_2O): δ = 8.3 (s, 1H, HCOONa).

General procedure for the catalytic imine hydrogenation experiments:

A stock solution of freshly prepared catalyst (10 mg in 2.5 mL toluene,) was prepared. An aliquot (0.5 mL) of that stock solution was added to a solution of imines (according to substrate catalyst ratio) in 1.5 mL toluene in a steel autoclave. The autoclave was charged with required hydrogen pressure and kept in a preheated (140°C) oil bath. After appropriate reaction times, the autoclave was immediately taken out and cooled to room temperature and the pressure was released. The reaction mixture was taken out of the autoclave and filtered through silica gel. Without further purifications, GC/MS analysis was measured to determine the conversion of the hydrogenation product and to identify the products.

GC/MS data for various imines and amines formed during hydrogenation reaction catalyses by 3a and 3b:

PhCH=NPh: rt = 9.062 min, m/z = 181; $PhCH_2NHPh$: rt = 9.323 min, m/z = 183; PhCH=N(α-naphtyl): rt = 13.260 min, m/z = 231; $PhCH_2NH$(α-naphtyl): rt = 13.673 min, m/z = 233; *p*-ClC_6H_4CH=NPh: rt = 10.284 min, m/z = 215; *p*-$ClC_6H_4CH_2NHPh$: rt = 10.687 min, m/z = 217 ; PhCH=N-*p*-C_6H_4Cl: rt = 10.362 min, m/z = 215; $PhCH_2NH$-*p*-C_6H_4Cl: rt =10.829 min, m/z = 217; *p*-ClC_6H_4CH=N-*p*-C_6H_4Cl: rt = 11.815 min, m/z =248; *p*-$ClC_6H_4CH_2NH$-*p*-C_6H_4Cl: rt = 12.648 min, m/z = 251; *p*-$MeOC_6H_4CH$=NPh: rt = 10.934 min, m/z = 211; *p*-$MeOC_6H_4CH_2NHPh$: rt = 11.012 min, m/z = 213; *p*-$MeOC_6H_4CH$=N-*p*-C_6H_4Cl: rt = 12.554 min, m/z = 245; *p*-$MeOC_6H_4CH_2NH$-*p*-C_6H_4Cl: rt = 12.945 min, m/z = 247; *p*-ClC_6H_4CH=N-*p*-C_6H_4OMe: rt = 12.378 min, m/z = 245; *p*-$ClC_6H_4CH_2NH$-*p*-C_6H_4OMe: rt = 12.521 min, m/z = 247; *p*-$MeOC_6H_4CH$=N-*p*-C_6H_4OMe: rt = 13.299 min, m/z = 241; *p*-$MeOC_6H_4CH_2NH$-*p*-C_6H_4OMe: rt = 12.983 min, m/z = 243. *p*-FC_6H_4CH=NPh: rt = 8.980 min, m/z = 199; *p*-$FC_6H_4CH_2NHPh$: rt = 9.359 min, m/z = 201 ; PhCH=N-*p*-C_6H_4F: rt = 9.061 min, m/z = 199; $PhCH_2NH$-*p*-C_6H_4F: rt =9.292 min, m/z = 201; $Ph(CO)CH_3$: rt = 4.573 min, m/z = 120; $PhCH(OH)CH_3$: rt = 4.486 min, m/z = 122.

Kinetic Experiments Procedures.[30]

For catalytic runs 1-9: In a glove box, a J Young NMR tube was charged with *N*-benzylideneaniline (according to required amount from Table A3.8). A freshly prepared catalyst stock solution of **3a** was prepared in toluene-d_8 and an aliquot amount was added to the *N*-benzylideneaniline. The tube was sealed and taken out from the glove box and pressed with 2 bar H_2. then the tube was kept in an oil bath preheated to 140 °C. The typical CH resonance of the *N*-benzylideneaniline (-CH=N: singlet, δ 8.34 ppm) decreased, and the appearance of CH_2 signal of the hydrogenated amine product (-CH_2-NH: doublet, δ 4.16 ppm) was observed in the ^{1}H NMR spectra. Product concentrations were determined from ^{1}H NMR integration after initial 15 min on the basis of the substrate consumptions and the rates are given in Table 3.4.

For catalytic runs 10-12: In a glove box, a steel autoclave was charged with *N*-benzylideneaniline (according to required amount from Table A3.8). A freshly prepared stock solution of the catalyst **3a** was prepared in toluene and an aliquot amount was added to the *N*-benzylideneaniline. Then again toluene was added to make a total volume of 2 mL. The autoclave was closed and taken out from the glove box and pressed with required amount of

H_2 pressure. Then the autoclave was kept in an oil bath preheated to 140 °C. For each run, three separate experiments were carried out and conversions were determined after 10 min, 15 min and 20 min intervals by GC/MS.

Filtration Experiments

In a 30 mL steel autoclave equipped with a stirring bar, *N*-benzylidene aniline and **3b** (5 mg of the catalyst **3b** and 165 mg *N*-benzylidene aniline) were mixed in 0.8 ml of toluene. The system was charged with 60 bar of H_2 and was heated at 140 °C with constant stirring. After 7 min of reaction time, the reaction was terminated manually by cooling the reaction vessel to room temperature and removing the maximum amount of H_2 pressure. Then the autoclave was transferred to a glove box and the rest of the H_2 was released and the vessel was opened. The solution was found to be still red (same as before the start of the reaction) without any precipitate or colloids formed. The GC/MS analysis revealed a TOF of 428 h^{-1} corresponding to 50% conversions. The solution was examined by ^{31}P NMR spectroscopy, indicating the presence of **3b**. The solution was filtered through Celite into a new vessel with a new stirring bar, to which *N*-benzylideneaniline (165 mg) was readded. No residue was visible on the Celite surface. The catalysis batch was repeated at 140 °C under 60 bar of H_2, and it was found that the activity still remained the same.

X-ray diffraction analyses.

Single-crystal X-ray diffraction data were collected at 183(2) K on a Xcalibur diffractometer (Agilent Technologies, Ruby CCD detector) for all compounds using a single wavelength Enhance X-ray source with MoK_α radiation (λ= 0.71073 Å).[34a] The selected suitable single crystals were mounted using polybutene oil on the top of a glass fiber fixed on a goniometer head and immediately transferred to the diffractometer. Pre-experiment, data collection, data reduction and analytical absorption corrections[34b] were performed with the program suite CrysAlis^{Pro}.[34a] The crystal structures were solved with SHELXS97[34c] using direct methods. The structure refinements were performed by full-matrix least-squares on F^2 with SHELXL97.[34c] All programs used during the crystal structure determination process are included in the WINGX software.[34d] PLATON[34e] was used to check the result of the X-ray analyses and DIAMOND[34f] was used for the molecular graphics.

3.5 Appendix

Table A3.8. Reaction conditions for kinetic measurements for the hydrogenation of *N*-benzylideneaniline catalysed by **3a**:

Runs	**Imine (mmol)**	**3a (mmol)**	**Temp (°C)**	**Toluene(mL)**	**pH_2(bar)**
1	0.110	0.0044	140	0.5	2
2	0.220	0.0044	140	0.5	2
3	0.331	0.0044	140	0.5	2
4	0.441	0.0044	140	0.5	2
5	0.552	0.0044	140	0.5	2
6	0.220	0.0022	140	0.5	2
7	0.220	0.0033	140	0.5	2
8	0.220	0.0054	140	0.5	2
9	0.220	0.0065	140	0.5	2
10	2.59	0.0046	140	2	20
11	2.59	0.0046	140	2	40
12	2.59	0.0046	140	2	60

Table 3.9. Crystallographic data for compounds **1a**, **1b** and **2a**.

	1a	**1b**	**2a**
empirical formula	$C_{17}H_{37}ClMoN_2O_2P_2$	$C_{17}H_{37}ClN_2O_2P_2W$	$8(C_{21}H_{46}MoN_2O_3P_2)$, $C_4H_{10}O$
formula weight ($g \cdot mol^{-1}$)	494.82	582.72	4333.94
temperature (K)	183(2)	183(2)	183(2)
wavelength (Å)	0.71073	0.71073	0.71073
crystal system, space group	monoclinic, *P* 2_1/n	monoclinic, *P* 2_1/n	triclinic, *P* -1
a (Å)	8.4174(1)	8.5072(2)	13.9047(2)
b (Å)	12.8270(1)	12.7509(2)	20.4865(4)
c (Å)	21.5576(2)	21.5572(3)	20.8200(4)

α (deg)	90	90	109.920(2)
β (deg)	97.063(1)	96.583(2)	92.489(1)
γ (deg)	90	90	90.592(2)
volume (Å^3)	2309.91(4)	2322.99(7)	5568.66(19)
Z, density (calcd) (Mg·m^{-3})	4, 1.423	4, 1.666	1, 1.292
abs coefficient (mm^{-1})	0.835	5.238	0.609
F(000)	1032	1160	2298
crystal size (mm^3)	0.36 x 0.21 x 0.15	0.12 x 0.04 x 0.03	0.36 x 0.17 x 0.10
θ range (deg)	2.51 to 30.51	2.48 to 26.37	2.49 to 30.51
reflections collected	48769	30573	103711
reflections unique	7037 / [R_{int} = 0.0261]	4746 / [R_{int} = 0.0430]	33971 / [R_{int} = 0.0429]
completeness to θ (%)	100.0	100.0	99.9
absorption correction	analytical	analytical	analytical
max/min transmission	0.914 and 0.823	0.852 and 0.605	0.908 and 0.756
data / restraints / parameters	6163 / 0 / 234	3717 / 0 / 234	22943 / 6 / 1138
goodness-of-fit on F^2	1.071	0.914	0.895
final R_1 and wR_2 indices [$I > 2\sigma(I)$]	0.0215, 0.0573	0.0241, 0.0452	0.0340, 0.0623
R_1 and wR_2 indices (all data)	0.0264, 0.0585	0.0380, 0.0469	0.0617, 0.0657
largest diff. peak and hole (e·Å^{-3})	0.644 and -0.311	0.758 and -0.963	1.228 and -0.971

The unweighted R-factor is $R_1 = \sum(Fo - Fc)/\sum Fo$; $I > 2\sigma(I)$ and the weighted R-factor is $wR_2 = \{\sum w(Fo^2 - Fc^2)^2/\sum w(Fo^2)^2\}^{1/2}$

Table 3.10. Crystallographic data for compounds **3a** and **3b**.

	3a	**3b**
empirical formula	$C_{17}H_{36}MoN_2O_2P_2$	$C_{17}H_{36}N_2O_2P_2W$
formula weight (g·mol^{-1})	458.36	546.27
temperature (K)	183(2)	183(2)
wavelength (Å)	0.71073	0.71073
crystal system, space group	monoclinic, $P\,2_1/n$	monoclinic, $P\,2_1/n$
a (Å)	13.3760(3)	13.3437(3)
b (Å)	22.7622(5)	22.7022(4)
c (Å)	15.0136(4)	14.9665(3)
α (deg)	90	90

β (deg)	106.336(3)	106.017(2)
γ (deg)	90	90
volume (Å^3)	4386.61(19)	4357.82(15)
Z, density (calcd) (Mg·m^{-3})	8, 1.388	8, 1.665
abs coefficient (mm^{-1})	0.755	5.460
F(000)	1920	2176
crystal size (mm^3)	0.22 x 0.13 x 0.06	0.15 x 0.12 x 0.03
θ range (deg)	2.54 to 28.28	2.55 to 25.68
reflections collected	58319	30726
reflections unique	10877/[R_{int}= 0.0898]	8181 / [R_{int} = 0.0533]
completeness to θ (%)	99.9	98.8
absorption correction	analytical	analytical
max/min transmission	0.980 and 0.953	0.844 and 0.541
data / restraints / parameters	6093 / 0 / 449	6042 / 0 / 449
goodness-of-fit on F^2	0.941	1.028
final R_1 and wR_2 indices [$I > 2\sigma(I)$]	0.0628, 0.1278	0.0408, 0.0819
R_1 and wR_2 indices (all data)	0.1287, 0.1452	0.0639, 0.0924
largest diff. peak and hole (e·Å^{-3})	1.728 and -0.852	3.440 and -1.392

The unweighted R-factor is $R_1 = \sum(Fo - Fc)/\sum Fo$; $I > 2\sigma(I)$ and the weighted R-factor is $wR_2 = \{\sum w(Fo^2 - Fc^2)^2/\sum w(Fo^2)^2\}^{1/2}$

Table 3.11. Crystallographic data for compounds **5b(*trans*)** and **6b(*cis*)**.

	5b(*trans*)	**6b(*cis*)**
empirical formula	$C_{18}H_{36}N_2O_4P_2W$	$8(C_{18}H_{38}N_2O_4P_2W)$, C_4H_8O
formula weight (g·mol^{-1})	590.28	4810.46
temperature (K)	183(2)	183(2)
wavelength (Å)	0.71073	0.71073
crystal system, space group	monoclinic, $P\,2_1/c$	tetragonal, $I\,4_1/a$
a (Å)	7.8847(1)	36.3651(6)
b (Å)	26.3644(4)	36.3651(6)
c (Å)	11.5872(2)	14.8550(3)

α (deg)	90	90
β (deg)	106.979(2)	90
γ (deg)	90	90
volume ($Å^3$)	2303.70(7)	19644.6(8)
Z, density (calcd) ($Mg \cdot m^{-3}$)	4, 1.702	4, 1.626
abs coefficient (mm^{-1})	5.178	4.859
F(000)	1176	9632
crystal size (mm^3)	0.33 x 0.27 x 0.20	0.10 x 0.08 x 0.03
θ range (deg)	2.70 to 28.28	2.44 to 25.68
reflections collected	37089	27807
reflections unique	5720 / [R_{int} = 0.0263]	9319 / [R_{int} = 0.0800]
completeness to θ (%)	99.9	99.9
absorption correction	analytical	analytical
max/min transmission	0.432 and 0.275	0.995 and 0.987
data / restraints / parameters	5574 / 0 / 252	5971 / 0 / 510
goodness-of-fit on F^2	1.294	0.987
final R_1 and wR_2 indices [$I > 2\sigma(I)$]	0.0203, 0.0400	0.0488, 0.0619
R_1 and wR_2 indices (all data)	0.0212, 0.0403	0.0972, 0.0744
largest diff. peak and hole ($e \cdot Å^{-3}$)	0.657 and -1.231	1.241 and -0.845

The unweighted R-factor is $R_1 = \sum(Fo - Fc)/\sum Fo$; $I > 2\sigma(I)$ and the weighted R-factor is $wR_2 = \{\sum w(Fo^2 - Fc^2)^2/\sum w(Fo^2)^2\}^{1/2}$

Table 3.12. Crystallographic data for compounds **8a** and **8b**.

	8a	**8b**
empirical formula	$C_{16}H_{37}Cl_2MoN_2OP_2$	$C_{16}H_{37}Cl_2N_2OP_2W$
formula weight ($g \cdot mol^{-1}$)	502.26	590.16
temperature (K)	183(2)	183(2) K
wavelength (Å)	0.71073	0.71073 A
crystal system, space group	orthorhombic, $P\,2_12_12_1$	Orthorhombic, P 21 21 21
a (Å)	7.3971(1)	7.4129(1
b (Å)	13.2575(2)	13.2003(2
c (Å)	23.8535(4)	23.8800(5)

α (deg)	90	90
β (deg)	90	90
γ (deg)	90	90
volume ($Å^3$)	2339.24(6)	2336.72(7) A^3
Z, density (calcd) ($Mg \cdot m^{-3}$)	4, 1.426	4, 1.678 Mg/m^3
abs coefficient (mm^{-1})	0.933	5.316 mm^-1
F(000)	1044	1172
crystal size (mm^3)	0.30 x 0.11 x 0.06	0.12 x 0.10 x 0.06 mm
θ range (deg)	2.88 to 32.58	2.88 to 28.28
reflections collected	55639	16728
reflections unique	8495 / R_{int} = 0.0485	5804/ R(int) = 0.0372]
completeness to θ (%)	99.9	99.9 %
absorption correction	analytical	Analytical
max/min transmission	0.951 and 0.799	0.765 and 0.644
data / restraints / parameters	7529 / 0 / 225	5804 / 61 / 257
goodness-of-fit on F^2	1.030	0.895
final R_1 and wR_2 indices [$I > 2\sigma(I)$]	0.0351, 0.0852	0.0329, 0.0488
R_1 and wR_2 indices (all data)	0.0420, 0.0872	0.0473, 0.0505
absolute structure parameter	-0.02(3)	-0.007(7)
largest diff. peak and hole ($e \cdot Å^{-3}$)	1.107 and -0.613	2.044 and -1.158 e.A^-3

The unweighted R-factor is $R_1 = \sum(Fo - Fc)/\sum Fo$; $I > 2\sigma(I)$ and the weighted R-factor is $wR_2 = \{\sum w(Fo^2 - Fc^2)^2/\sum w(Fo^2)^2\}^{1/2}$

Computational studies

Geometry optimizations and frequency calculations for all reactants, products and transition states were performed at the density functional level of theory by using the Gaussian 03 program package[35] with the mPW1PW91 hybrid functional, which includes modified Perdew–Wang exchange and Perdew–Wang 91 correlation,[36] in conjunction with the Stuttgart/Dresden ECPs (SDD) basis set for the Mo and W centers,[37] and the polarized 6-31G(d) basis set for the remaining atoms.[38] Pure basis functions (5d, 7f) were used in all calculations. Geometries were fully optimized without symmetry restrictions, and the transition-state structure were obtained by using the QST2 procedure.[39] For each optimized stationary point a frequency analysis was performed to verify its character (minimum or saddle point). For the transition state we carefully checked that the vibrational mode associated to the imaginary frequency corresponds to the correct movement.

Energies and cartesian coordinates of 4a(*cis*)

C	-0.00022000	-1.55672500	1.27502700	H	2.42432200	-0.29609800	-2.75320800
C	-3.67517800	-0.68272900	0.77338100	H	3.37163400	-1.55100500	-1.96497400
H	-4.65592500	-0.48713400	0.32168200	C	3.67574700	-0.68251000	0.77309800
C	-3.49574600	-2.19579900	0.89765100	H	4.65604600	-0.48935400	0.31936700
H	-2.52139500	-2.44707500	1.32362500	C	3.49434300	-2.19501600	0.90103400
H	-3.59918200	-2.71490600	-0.06014400	H	4.26231400	-2.59877800	1.57039500
H	-4.26293700	-2.59987000	1.56772100	H	3.59506800	-2.71628800	-0.05587200
C	-3.61715100	-0.03289600	2.15713800	H	2.52045800	-2.44395900	1.32938600
H	-4.35375800	-0.49872800	2.82145000	C	3.62092200	-0.02939200	2.15542300
H	-3.82777300	1.03864100	2.12792500	H	2.62981600	-0.15727800	2.60178100
H	-2.62570400	-0.16392100	2.60179600	H	3.83392600	1.04160000	2.12344000
C	-3.15812800	1.67311200	-0.98089800	H	4.35739500	-0.49529600	2.81983400
H	-2.53874800	1.85975900	-1.86825000	C	3.15791300	1.67194000	-0.98280200
C	-2.93000700	2.84897200	-0.03224900	H	2.53987200	1.85647700	-1.87153700
H	-3.21743700	3.78423800	-0.52586400	C	2.92713300	2.84937800	-0.03676100
H	-1.87744400	2.91914600	0.25247700	H	3.52435900	2.76731000	0.87618800
H	-3.52969200	2.76515300	0.87893300	H	1.87378800	2.91971000	0.24503100
C	-4.61996700	1.56032700	-1.40987100	H	3.21564000	3.78384600	-0.53127000
H	-5.28498000	1.45126200	-0.54714500	C	4.62050700	1.55950300	-1.40927000
H	-4.79737700	0.71372900	-2.08150500	H	4.92707000	2.46866700	-1.93864400
H	-4.92632400	2.47014700	-1.93824000	H	4.79951800	0.71191900	-2.07925500
C	-2.44337100	-0.97378000	-1.89328100	H	5.28423600	1.45226800	-0.54532600
H	-3.37218100	-1.54765300	-1.96711500	N	0.00031300	1.17393100	1.65031300
H	-2.42289400	-0.29286200	-2.75316000	N	-0.00012000	-1.13590500	-1.76926300
C	-1.23753400	-1.90685200	-1.96065800	H	0.00043800	-0.36410100	-2.43476900
H	-1.28255400	-2.66075400	-1.16904000	O	0.00049600	1.87447500	2.60991900
H	-1.22007000	-2.43509600	-2.92641100	O	-0.00045300	-2.54078300	1.90742900
C	1.23667000	-1.90804700	-1.95988100	P	-2.38742400	0.08637000	-0.34808000
H	1.21906600	-2.43673500	-2.92539000	P	2.38746900	0.08567800	-0.34835200
H	1.28073400	-2.66160700	-1.16787900	Mo	0.00005700	0.11872800	0.19766000
C	2.44336300	-0.97606500	-1.89255000	H	0.00017200	1.41110900	-1.08457700

Zero-point correction=	0.546182 (Hartree/Particle)
Thermal correction to Energy=	0.578091
Thermal correction to Enthalpy=	0.579035
Thermal correction to Gibbs Free Energy=	0.484364
Sum of electronic and zero-point Energies=	-1680.888329
Sum of electronic and thermal Energies=	-1680.856420
Sum of electronic and thermal Enthalpies=	-1680.855476
Sum of electronic and thermal Free Energies=	-1680.950146

Energies and cartesian coordinates of 4a(*trans*)

C	0.00001800	1.44935400	1.59633900	H	-1.26379500	-2.70395200	-1.11517200
C	-3.65449000	-0.70872300	0.77400100	H	-1.20967600	-2.51906600	-2.87809300
H	-4.62170300	-0.64107900	0.25908800	C	1.23281100	-1.96882200	-1.92459500
C	-3.34772800	-2.18454500	1.03422200	H	1.20968000	-2.51908600	-2.87806500
H	-2.38290200	-2.31144000	1.53117800	H	1.26378300	-2.70394200	-1.11514100
H	-3.34585000	-2.78149700	0.11700500	C	2.45251800	-1.05393800	-1.87483700
H	-4.11836500	-2.60552500	1.68999800	H	2.45904200	-0.40810000	-2.76182500
C	-3.73633400	0.05525300	2.09616600	H	3.37196500	-1.64717700	-1.90859500
H	-4.45434600	-0.43342200	2.76443200	C	3.65449100	-0.70868200	0.77402100
H	-4.06145400	1.08993500	1.96259900	H	4.62171400	-0.64096200	0.25913300
H	-2.76342900	0.06965600	2.59628200	C	3.34783100	-2.18453400	1.03418700
C	-3.16548300	1.61763300	-1.04467200	H	4.11845500	-2.60546600	1.69001000
H	-2.57964700	1.76331200	-1.96212200	H	3.34607800	-2.78145900	0.11695200
C	-2.91206700	2.84117800	-0.16626200	H	2.38298000	-2.31153000	1.53106700
H	-3.25040400	3.74469900	-0.68625200	C	3.73626200	0.05525400	2.09621200
H	-1.84707700	2.94650100	0.05069500	H	2.76337200	0.06947900	2.59636200
H	-3.45197400	2.78927900	0.78334800	H	4.06120300	1.08999400	1.96266900
C	-4.63976300	1.47587600	-1.41967300	H	4.45437800	-0.43332600	2.76443500
H	-5.27378000	1.38885100	-0.53149300	C	3.16546700	1.61763000	-1.04468700
H	-4.82913500	0.60482200	-2.05569300	H	2.57961100	1.76331700	-1.96212400
H	-4.97360700	2.36364100	-1.96833000	C	2.91209300	2.84118400	-0.16627800
C	-2.45252700	-1.05393900	-1.87485300	H	3.45203300	2.78929600	0.78331400
H	-3.37196900	-1.64718900	-1.90859400	H	1.84711100	2.94652000	0.05071400
H	-2.45907100	-0.40810000	-2.76183900	H	3.25041900	3.74469400	-0.68629200
C	-1.23281700	-1.96881700	-1.92461500	C	4.63973700	1.47584900	-1.41973400

H	4.97357600	2.36361200	-1.96839800	O	-0.00000700	-2.15146200	2.24395400
H	4.82907300	0.60479900	-2.05577000	O	0.00005700	2.28257700	2.41001500
H	5.27378100	1.38880400	-0.53157500	P	-2.38117700	0.05876300	-0.36161500
N	0.00000600	-1.28945300	1.41588300	P	2.38116400	0.05877100	-0.36160300
N	-0.00000300	-1.18310900	-1.74968400	Mo	-0.00000900	0.05931700	0.19950100
H	0.00000600	-0.43482500	-2.44214200	H	-0.00005300	1.43733900	-1.02733500

Zero-point correction=	0.545635 (Hartree/Particle)
Thermal correction to Energy=	0.577567
Thermal correction to Enthalpy=	0.578511
Thermal correction to Gibbs Free Energy=	0.484756
Sum of electronic and zero-point Energies=	-1680.888339
Sum of electronic and thermal Energies=	-1680.856407
Sum of electronic and thermal Enthalpies=	-1680.855463
Sum of electronic and thermal Free Energies=	-1680.949218

Energies and cartesian coordinates of 4b(cis)

C	-0.00063800	-1.55534100	1.25689100
C	-3.66813700	-0.67752600	0.78301300
H	-4.65435600	-0.48201700	0.34330300
C	-3.49693600	-2.18922500	0.93233600
H	-2.51751300	-2.43881700	1.34728000
H	-3.61964000	-2.72491600	-0.01390100
H	-4.25611500	-2.57479800	1.62201800
C	-3.58023000	-0.00166700	2.15267900
H	-4.31764200	-0.44038900	2.83424700
H	-3.76955900	1.07302200	2.10481200
H	-2.58579200	-0.14322500	2.58711000
C	-3.16986200	1.63177000	-1.04262600
H	-2.54789100	1.80193400	-1.93149700
C	-2.94999800	2.82701100	-0.11643100
H	-3.23257600	3.75175300	-0.63205700
H	-1.90044800	2.90387100	0.17831100
H	-3.55891500	2.76154000	0.79004000
C	-4.62980100	1.50408500	-1.47383200
H	-5.29722300	1.41111500	-0.61116500
H	-4.80230600	0.64284400	-2.12779900
H	-4.93755500	2.40130200	-2.02247000
C	-2.44945700	-1.03682300	-1.89211300
H	-3.37335300	-1.62058500	-1.94624700
H	-2.43979200	-0.37786100	-2.76916300
C	-1.23735900	-1.96266100	-1.94231900
H	-1.27331200	-2.69871900	-1.13386200
H	-1.21752300	-2.51123900	-2.89604000
C	1.23555300	-1.96514900	-1.94080800
H	1.21536600	-2.51441900	-2.89412500
H	1.26948100	-2.70064900	-1.13176000
C	2.44953400	-1.04174600	-1.89043000
H	2.44323700	-0.38496000	-2.76912200
H	3.37215100	-1.62785000	-1.94122200
C	3.66925000	-0.67716300	0.78250600
H	4.65466600	-0.48698400	0.33864300
C	3.49363900	-2.18749900	0.93969300
H	4.25397400	-2.57231000	1.62852500
H	3.61126500	-2.72798900	-0.00445900
H	2.51478400	-2.43188200	1.35892800
C	3.58793200	0.00580900	2.14900200
H	2.59440800	-0.13011300	2.58739500
H	3.78102400	1.07954600	2.09509200
H	4.32591600	-0.43207200	2.83049500
C	3.16952400	1.62905000	-1.04662600
H	2.55056200	1.79449700	-1.93850300
C	2.94381700	2.82778300	-0.12637900
H	3.54792800	2.76679000	0.78360000
H	1.89262900	2.90457600	0.16248600
H	3.22810100	3.75067900	-0.64439300
C	4.63118700	1.50218200	-1.47213800

H	4.93947300	2.39782300	-2.02304600
H	4.80732700	0.63874100	-2.12227200
H	5.29565900	1.41344000	-0.60675300
N	0.00071200	1.19933900	1.62459000
N	-0.00022200	-1.18059800	-1.77345200
H	0.00092400	-0.43685600	-2.47077800
O	0.00110800	1.91778300	2.57722200
O	-0.00130200	-2.54959500	1.88019200
P	-2.39560900	0.06221800	-0.37386400
P	2.39571500	0.06058900	-0.37440900
W	0.00014400	0.11975100	0.16879800
H	0.00040000	1.38743900	-1.16037200

Zero-point correction=	0.546311 (Hartree/Particle)
Thermal correction to Energy=	0.578206
Thermal correction to Enthalpy=	0.579150
Thermal correction to Gibbs Free Energy=	0.484538
Sum of electronic and zero-point Energies=	-1679.790886
Sum of electronic and thermal Energies=	-1679.758991
Sum of electronic and thermal Enthalpies=	-1679.758047
Sum of electronic and thermal Free Energies=	-1679.852658

Energies and cartesian coordinates of 4b(*trans*)

C	-0.00003300	1.47243000	1.57667100
C	-3.64418400	-0.70586000	0.78017000
H	-4.61991500	-0.63675200	0.28180300
C	-3.34081700	-2.18060300	1.05127100
H	-2.36810200	-2.30808200	1.53268400
H	-3.35979000	-2.78807000	0.14109700
H	-4.10239200	-2.58881200	1.72536600
C	-3.69450100	0.07442500	2.09433500
H	-4.40884000	-0.39684300	2.77875600
H	-4.00666600	1.11212900	1.95396100
H	-2.71314500	0.08076600	2.57770500
C	-3.17808200	1.58716300	-1.09496500
H	-2.59499900	1.71864800	-2.01618300
C	-2.92638600	2.82538900	-0.23680100
H	-3.26325100	3.71968300	-0.77336600
H	-1.86212500	2.93461200	-0.01750300
H	-3.46948400	2.78933400	0.71162700
C	-4.65304700	1.43390700	-1.46265800
H	-5.28362300	1.36129000	-0.57078800
H	-4.84221100	0.55099100	-2.08213900
H	-4.99111600	2.31063100	-2.02617600
C	-2.45856400	-1.09980700	-1.87835700
H	-3.37287500	-1.70133700	-1.89762900
H	-2.47260000	-0.47200900	-2.77810600
C	-1.23273500	-2.00759000	-1.91215400
H	-1.25723400	-2.72714000	-1.08870400
H	-1.20532600	-2.57456600	-2.85500000
C	1.23280500	-2.00757500	-1.91209600
H	1.20542600	-2.57457400	-2.85492800
H	1.25729900	-2.72710300	-1.08862600
C	2.45862700	-1.09977800	-1.87829500
H	2.47267700	-0.47199600	-2.77805600
H	3.37294100	-1.70130000	-1.89754100
C	3.64413000	-0.70579300	0.78031500
H	4.61993400	-0.63647600	0.28212200
C	3.34091800	-2.18061300	1.05117600
H	4.10242300	-2.58880000	1.72536200
H	3.36013400	-2.78796900	0.14093400
H	2.36813100	-2.30827700	1.53240100
C	3.69409700	0.07432100	2.09459500
H	2.71268000	0.08034200	2.57784500
H	4.00600500	1.11212500	1.95440500

H	4.40847700	-0.39686100	2.77903200
C	3.17809200	1.58720600	-1.09491900
H	2.59485900	1.71879300	-2.01602900
C	2.92661200	2.82538700	-0.23662800
H	3.46997900	2.78929400	0.71164600
H	1.86241000	2.93459100	-0.01702900
H	3.26331700	3.71971100	-0.77324200
C	4.65298900	1.43389800	-1.46286000
H	4.99102300	2.31066000	-2.02633800
H	4.84200400	0.55103500	-2.08246100
H	5.28370200	1.36115100	-0.57109800
N	0.00002800	-1.29224700	1.38327000
N	0.00002500	-1.21228800	-1.75482000
H	0.00003600	-0.48712500	-2.47195500
O	0.00000900	-2.19392400	2.17666100
O	-0.00006100	2.30641100	2.39374400
P	-2.38975500	0.04250900	-0.38688700
P	2.38977500	0.04254900	-0.38683700
W	0.00000700	0.07705100	0.16886700
H	-0.00005500	1.41347600	-1.12933000

Zero-point correction=	0.545823 (Hartree/Particle)
Thermal correction to Energy=	0.577762
Thermal correction to Enthalpy=	0.578706
Thermal correction to Gibbs Free Energy=	0.484439
Sum of electronic and zero-point Energies=	-1679.790281
Sum of electronic and thermal Energies=	-1679.758342
Sum of electronic and thermal Enthalpies=	-1679.757398
Sum of electronic and thermal Free Energies=	-1679.851664

Energies and cartesian coordinates of 6b(*cis*)

C	0.07015500	-2.14568900	-0.05347900	H	2.54749800	-1.16894600	2.46901800
C	-0.15592400	2.92632400	-0.51268700	H	3.36874200	0.38236900	2.58674100
H	-0.24876900	3.92047900	-0.02641200	C	3.51096000	1.39336200	-0.19463000
C	-3.34112400	1.50684400	0.01248900	H	4.55728700	1.08225600	-0.08188200
H	-2.67611300	2.24020500	0.48468700	C	3.24402500	1.73877800	-1.66312600
C	-4.72504100	1.61541300	0.65149200	H	2.20260100	2.03498400	-1.81820400
H	-5.13349800	2.61516900	0.46672500	H	3.45098000	0.90120800	-2.33364200
H	-4.71216000	1.46834300	1.73522700	H	3.88751100	2.57249700	-1.96637300
H	-5.43136200	0.89769500	0.22152100	C	3.27631000	2.61332400	0.69844600
C	-3.40061800	1.82795600	-1.48350900	H	3.85281700	3.46182300	0.31412300
H	-4.09479800	1.16107100	-2.00573200	H	3.59629300	2.44574100	1.73150300
H	-2.41766000	1.75983400	-1.95596800	H	2.22260200	2.89925700	0.70498900
H	-3.76563100	2.85079000	-1.62563500	C	3.45648000	-1.58856600	-0.12257200
C	-3.57815400	-1.42597600	-0.38151600	H	2.87114000	-2.38089000	0.36164200
H	-4.58792800	-0.99782500	-0.37873400	C	4.87077400	-1.60766600	0.45598000
C	-3.18045600	-1.74381100	-1.82602200	H	5.32381100	-2.59153700	0.29131200
H	-2.19265400	-2.20982600	-1.85855100	H	4.88829000	-1.41472500	1.53306600
H	-3.14008600	-0.85518200	-2.45924700	H	5.51776200	-0.87128100	-0.03048600
H	-3.90510200	-2.43951300	-2.26361500	C	3.45909700	-1.87928300	-1.62345900
C	-3.59470000	-2.70334300	0.45841000	H	4.10732900	-1.18474000	-2.16594000
H	-4.20576400	-3.45937900	-0.04647400	H	2.45511200	-1.81626600	-2.05070100
H	-4.02588800	-2.54731700	1.45146000	H	3.84201500	-2.88967100	-1.80260900
H	-2.58984400	-3.12191000	0.57141900	N	0.02047200	-0.28160900	-1.95152600
C	-2.44954600	-0.28805300	2.15846900	N	0.01473100	-0.14381200	2.19688700
H	-3.36550900	0.09288100	2.61951400	H	0.04898200	-1.12746800	2.46335200
H	-2.39411100	-1.35672800	2.39146600	O	0.11774300	-3.31692800	0.03938000
C	-1.23466900	0.42395600	2.74593400	O	0.03524300	-0.38396000	-3.13216700
H	-1.23625000	1.48399900	2.48202000	O	-0.09568800	1.96371700	0.35085900
H	-1.23741500	0.34263900	3.84238300	O	-0.11909000	2.84272100	-1.73007700
C	1.22019200	0.51370900	2.74400200	P	-2.43940300	-0.10749200	0.30162400
H	1.22141700	0.44651200	3.84159800	P	2.45532400	-0.06916900	0.30407500
H	1.15141700	1.56716300	2.46579700	W	0.00877000	-0.18634600	-0.14325500
C	2.48675600	-0.11405600	2.17153900				

--

```
Zero-point correction=                               0.564212 (Hartree/Particle)
Thermal correction to Energy=                        0.599473
Thermal correction to Enthalpy=                      0.600417
Thermal correction to Gibbs Free Energy=             0.499431
Sum of electronic and zero-point Energies=       -1868.336891
Sum of electronic and thermal Energies=          -1868.301630
Sum of electronic and thermal Enthalpies=        -1868.300686
Sum of electronic and thermal Free Energies=     -1868.401672
---
```

Energies and cartesian coordinates of 6b(*trans*)

C	-0.01366000	0.06443200	-2.12150800	H	2.46792200	-1.40577000	2.35386000
C	-0.10192500	2.96159000	-0.38420200	H	3.38265500	0.07432400	2.61924300
H	-0.21128300	3.92422400	0.15575700	C	3.56979100	1.34305100	-0.03924200
C	-3.40685600	1.46111800	0.05979200	H	4.59611100	0.97788700	0.09632900
H	-2.83234000	2.17401200	0.66515600	C	3.39002300	1.82376200	-1.48167800
C	-4.84974700	1.43982200	0.56479900	H	2.37013000	2.17843800	-1.65406100
H	-5.26998900	2.45055700	0.51811800	H	3.59358500	1.03817900	-2.21241600
H	-4.94247000	1.09672100	1.59946700	H	4.08079100	2.65069700	-1.68186800
H	-5.48255700	0.80133500	-0.05955200	C	3.33927000	2.49545200	0.94059300
C	-3.34714800	1.93527700	-1.39402900	H	3.98149100	3.33978100	0.66731400
H	-3.96220000	1.30520300	-2.04378000	H	3.58044400	2.22568700	1.97304500
H	-2.32747000	1.94674000	-1.78417500	H	2.30330100	2.84043500	0.90754100
H	-3.74438100	2.95389000	-1.46339400	C	3.35869400	-1.63745300	-0.26670000
C	-3.54066900	-1.50966100	-0.31097700	H	2.70517800	-2.43863500	0.10255400
H	-4.57988800	-1.20200200	-0.14298600	C	4.74696000	-1.81590200	0.34832700
C	-3.30901100	-1.69107200	-1.81431700	H	5.14913300	-2.79544800	0.06745900
H	-2.28446400	-2.02021800	-2.00667200	H	4.73706200	-1.76758200	1.44148500
H	-3.47238600	-0.77333300	-2.38275700	H	5.45191200	-1.06251900	-0.01770700
H	-3.99432400	-2.45322700	-2.20158700	C	3.40582200	-1.76583000	-1.78960100
C	-3.30560800	-2.83679400	0.41427300	H	4.12160100	-1.06608300	-2.23151100
H	-3.89912900	-3.61849700	-0.07247100	H	2.42673800	-1.59006900	-2.24035800
H	-3.61608200	-2.80682800	1.46240800	H	3.72765200	-2.77675400	-2.06094400
H	-2.25740500	-3.14475800	0.36021500	N	0.06432700	-1.95041300	-0.32453200
C	-2.46607200	-0.28807200	2.19148000	N	0.00453500	-0.23258300	2.18441800
H	-3.35736900	0.15197000	2.64882500	H	-0.01268400	-1.23466000	2.37500600
H	-2.47288900	-1.35363800	2.44291600	O	-0.01651200	0.10779500	-3.28249000
C	-1.21411700	0.35874300	2.77536500	O	0.13231800	-3.15109700	-0.38900000
H	-1.18214300	1.42646700	2.54678100	O	-0.11300500	1.94317100	0.41762500
H	-1.20153300	0.24125900	3.86875200	O	0.01304600	2.95031200	-1.59877500
C	1.24010200	0.31604700	2.78140800	P	-2.45264700	-0.12897200	0.32658800
H	1.23550600	0.16087600	3.87019900	P	2.44319800	-0.11182700	0.29805400
H	1.22506500	1.39219700	2.59439000	W	-0.00440200	-0.15840900	-0.14099400
C	2.47504200	-0.32569400	2.15709800				

```
--
Zero-point correction=                               0.563885 (Hartree/Particle)
Thermal correction to Energy=                        0.599271
Thermal correction to Enthalpy=                      0.600215
Thermal correction to Gibbs Free Energy=             0.498472
Sum of electronic and zero-point Energies=       -1868.342643
Sum of electronic and thermal Energies=          -1868.307257
Sum of electronic and thermal Enthalpies=        -1868.306313
Sum of electronic and thermal Free Energies=     -1868.408056
--
```

Energies and cartesian coordinates of 3b

C	0.06601100	2.15474500	0.00373100	C	-3.17643700	2.27339400	-1.57779100
C	-3.27430200	-1.15690000	1.05975100	H	-3.86327300	3.12454300	-1.64177300
H	-3.10520400	-0.61746000	1.99985100	H	-3.19268800	1.76994700	-2.54826800
C	-2.56304400	-2.50725000	1.17062600	H	-2.17039800	2.66773400	-1.41489800
H	-2.95199000	-3.06283800	2.03060100	C	-2.53976100	-1.02390500	-1.81763900
H	-1.48425200	-2.38879800	1.30784400	H	-3.41837400	-1.67620800	-1.86599900
H	-2.73186800	-3.12106900	0.27978700	H	-2.64383600	-0.28078400	-2.61349600
C	-4.77746000	-1.34717800	0.86029900	C	-1.25099800	-1.81686700	-2.03886900
H	-5.00228300	-1.80676900	-0.10843300	H	-1.34627900	-2.81658200	-1.58508600
H	-5.33226100	-0.40785500	0.92576700	H	-1.14321900	-1.99308000	-3.12133000
H	-5.17233900	-2.01421900	1.63476400	C	1.11527700	-1.77122600	-2.14134900
C	-3.60459700	1.35812200	-0.43094500	H	0.95086800	-1.87819000	-3.22612700
H	-4.59517500	0.94708500	-0.66404100	H	1.24315600	-2.79752200	-1.76105300
C	-3.68002100	2.14218400	0.88148900	C	2.40272400	-0.97520800	-1.93792400
H	-2.68910700	2.50313600	1.17456100	H	2.43553600	-0.15558600	-2.66509900
H	-4.07629500	1.54317700	1.70649200	H	3.28493800	-1.60176800	-2.10859800
H	-4.33441500	3.01209800	0.76038200	C	3.53865400	1.30073000	-0.55513500

H	2.99575200	1.82717900	-1.35231700	H	3.79408200	0.10152400	2.43267500
C	4.93279500	0.94425200	-1.07122300	H	3.86721300	-1.59145300	2.92279100
H	5.47979400	1.85843700	-1.32762700	C	2.74028500	-2.75223100	0.74729800
H	4.90147300	0.31737700	-1.96729100	H	3.24964900	-3.41748200	1.45324100
H	5.52023800	0.42026100	-0.31021200	H	2.85077000	-3.18398600	-0.25048100
C	3.61263800	2.24674200	0.64454100	H	1.67548300	-2.74699900	1.00441200
H	4.29817400	1.87097900	1.40932700	N	-0.05030000	0.21181300	1.87743000
H	2.63370700	2.40037600	1.10513900	N	-0.05499700	-1.14625200	-1.52753500
H	3.99127100	3.22254000	0.32265300	O	0.12154700	3.31968300	-0.09376100
C	3.33410700	-1.34601100	0.84503700	O	-0.11415000	0.07870900	3.06540100
H	4.36999400	-1.38098100	0.48325700	P	-2.44014800	-0.08605900	-0.22750300
C	3.32164600	-0.87332100	2.30002500	P	2.41238400	-0.16550000	-0.27201900
H	2.30026000	-0.80290600	2.68285700	W	-0.00918700	0.19166300	0.06100900

--

Zero-point correction=	0.525096 (Hartree/Particle)
Thermal correction to Energy=	0.556892
Thermal correction to Enthalpy=	0.557836
Thermal correction to Gibbs Free Energy=	0.463199
Sum of electronic and zero-point Energies=	-1678.620314
Sum of electronic and thermal Energies=	-1678.588518
Sum of electronic and thermal Enthalpies=	-1678.587574
Sum of electronic and thermal Free Energies=	-1678.682211

Energies and cartesian coordinates of 5b(*trans*)

C	0.04350000	-0.82465200	2.15856500	H	2.54516300	2.20025800	-1.32806100
C	0.03454400	2.34603300	-0.66651900	H	3.27023400	0.95831800	-2.33711700
C	-3.48927500	-1.35505800	-0.58238400	C	3.40878400	1.13043300	1.02621000
H	-3.31519000	-2.11484200	0.18903600	H	2.76649900	2.01919100	1.08420900
C	-2.98611900	-1.91857300	-1.91316100	C	4.78634800	1.54546500	0.50852200
H	-3.54134900	-2.83225900	-2.15104400	H	5.23045700	2.28003400	1.18912700
H	-1.92750400	-2.17890000	-1.88211500	H	4.74724200	2.00276600	-0.48430900
H	-3.16025600	-1.21590000	-2.73555300	H	5.47146100	0.69256300	0.46359500
C	-4.98795800	-1.06085100	-0.66873800	C	3.50373900	0.54504000	2.43521800
H	-5.20148500	-0.25742400	-1.38245300	H	4.21025300	-0.28903800	2.48121000
H	-5.42594900	-0.78308200	0.29249800	H	2.53624300	0.19581000	2.80181200
H	-5.51444600	-1.95376900	-1.02304300	H	3.86767200	1.31429400	3.12474500
C	-3.47696100	0.89378600	1.32588900	C	3.48598500	-1.39613900	-0.62476500
H	-4.45552100	1.13407100	0.89074300	H	4.51301700	-1.02038500	-0.72089100
C	-3.66516400	-0.10011000	2.47493300	C	3.44100600	-2.47143300	0.46335100
H	-2.70041900	-0.38238800	2.90622300	H	2.42914600	-2.86968800	0.57094100
H	-4.17500800	-1.01705600	2.16611100	H	3.76273600	-2.10012500	1.43816000
H	-4.26493300	0.36034100	3.26720600	H	4.10256900	-3.29995500	0.18688700
C	-2.83948200	2.18413500	1.84257600	C	3.05426100	-1.98970300	-1.96764800
H	-3.46661200	2.60195800	2.63779200	H	3.70687900	-2.83370900	-2.21680300
H	-2.73623500	2.94964700	1.06944700	H	3.12542400	-1.27222200	-2.79032200
H	-1.84376100	1.99915700	2.25274900	H	2.03102400	-2.37131500	-1.91813700
C	-2.54165000	1.30235600	-1.44493700	N	-0.03453100	-1.97657900	-0.27072200
H	-3.44954500	1.16077200	-2.03998300	N	-0.05929600	1.11777600	-1.56004800
H	-2.59049600	2.31567800	-1.03491900	O	0.06635900	-1.13770500	3.28190600
C	-1.31243300	1.18132500	-2.34602600	O	-0.03601500	-3.10791000	-0.66886600
H	-1.35594400	0.27085300	-2.94971700	O	0.10807700	1.95331000	0.54663700
H	-1.26552400	2.04513800	-3.02101600	O	0.02744100	3.45098600	-1.15976800
C	1.11803700	1.06128200	-2.45737000	P	-2.45616700	0.10112800	-0.01980400
H	1.05871100	1.88252400	-3.18332900	P	2.42867400	0.06741100	-0.16072900
H	1.05858300	0.11288600	-2.99906200	W	-0.00418100	-0.25597200	0.26192800
C	2.42426400	1.16863500	-1.67591200				

--

Zero-point correction=	0.542133 (Hartree/Particle)
Thermal correction to Energy=	0.575846
Thermal correction to Enthalpy=	0.576790
Thermal correction to Gibbs Free Energy=	0.479524
Sum of electronic and zero-point Energies=	-1867.169966
Sum of electronic and thermal Energies=	-1867.136253
Sum of electronic and thermal Enthalpies=	-1867.135308
Sum of electronic and thermal Free Energies=	-1867.232574

--

Energies and cartesian coordinates of TS(3b-5b)

C	-0.03015100	-0.13398300	2.24833400	H	3.16522700	2.17807100	0.47825200
C	-0.09337100	-2.88701700	-0.78887300	C	2.68080400	2.34502000	-1.59466600
C	3.33272000	1.59168500	-0.43331500	H	3.09841700	3.35566800	-1.65349200

H	1.60006800	2.43876600	-1.47075900
H	2.88376700	1.85185800	-2.55069000
C	4.83755300	1.45104400	-0.66647900
H	5.05415600	0.81648700	-1.53288800
H	5.36613200	1.03806800	0.19604400
H	5.26887600	2.43683300	-0.87292400
C	3.58473900	-0.92469500	1.08056700
H	4.55805700	-1.02674100	0.58376600
C	3.75391200	-0.11104300	2.36587200
H	2.78819200	0.04713300	2.85461900
H	4.20565600	0.86891800	2.18913900
H	4.39993200	-0.65124200	3.06616600
C	3.05187200	-2.32047700	1.40456400
H	3.72021900	-2.81248200	2.11962200
H	2.99145600	-2.96470700	0.52257200
H	2.05741100	-2.26737300	1.85738100
C	2.53440400	-0.97409200	-1.68418800
H	3.43426200	-0.73826200	-2.26194200
H	2.59011600	-2.03757900	-1.42966000
C	1.27158800	-0.71361400	-2.50465500
H	1.38253900	0.22498800	-3.07049300
H	1.18006500	-1.51351700	-3.25703500
C	-1.09035400	-0.60653100	-2.58711600
H	-0.99821400	-1.38348500	-3.36370600
H	-1.10036100	0.35657900	-3.12308200
C	-2.41892700	-0.81249500	-1.86430100
H	-2.56290600	-1.88029400	-1.65955400
H	-3.25856100	-0.49499800	-2.49172000
C	-3.56607600	-1.06939800	0.75992200
H	-3.04595800	-2.03266200	0.67077000
C	-4.95995900	-1.21188200	0.14741100
H	-5.51778400	-1.99652600	0.67048900
H	-4.93021700	-1.48057400	-0.91261400
H	-5.53526200	-0.28594800	0.24745500
C	-3.64784700	-0.74019600	2.25021600
H	-4.25174200	0.15213000	2.43612800
H	-2.66178400	-0.58429300	2.69118000
H	-4.12756800	-1.56980000	2.78109500
C	-3.33303300	1.64508800	-0.51271300
H	-4.35399300	1.36230900	-0.80090600
C	-3.38743600	2.51562900	0.74442500
H	-2.38383100	2.80864600	1.06202600
H	-3.87815600	2.01638000	1.58195600
H	-3.95109900	3.43033300	0.52887100
C	-2.70417000	2.42512600	-1.66879400
H	-3.25756800	3.35842700	-1.82117600
H	-2.73027500	1.87142400	-2.61103700
H	-1.66589600	2.68883000	-1.44834200
N	0.08123100	1.93572600	0.57000300
N	0.06053300	-0.66836200	-1.68736400
O	-0.04380200	-0.34365400	3.39652700
O	0.14230500	3.13009300	0.67297600
O	-0.30405200	-2.58929100	0.33765900
O	0.08897500	-3.48813100	-1.77514200
P	2.45149400	-0.02410900	-0.09546600
P	-2.41660900	0.04676200	-0.21427300
W	0.01332400	0.17197500	0.28417100

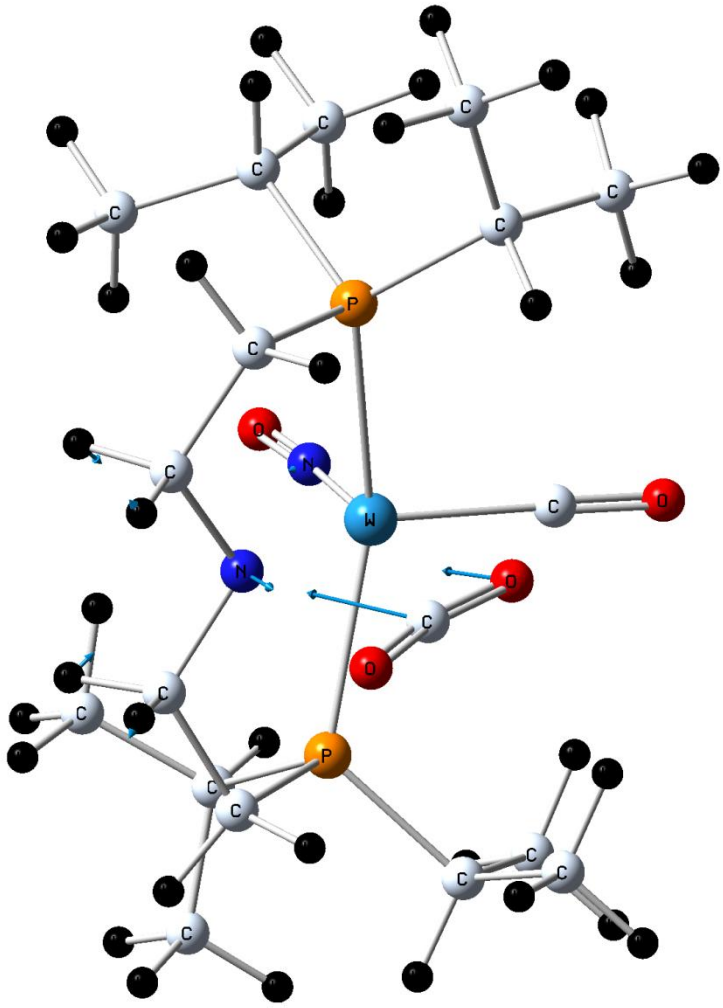


```
--
Zero-point correction=                           0.537860 (Hartree/Particle)
Thermal correction to Energy=                    0.572569
Thermal correction to Enthalpy=                  0.573513
Thermal correction to Gibbs Free Energy=         0.472799
Sum of electronic and zero-point Energies=          -1867.132360
Sum of electronic and thermal Energies=             -1867.097650
Sum of electronic and thermal Enthalpies=           -1867.096706
Sum of electronic and thermal Free Energies=        -1867.197420

                    1                      2                      3
                    A                      A                      A
 Frequencies --  -197.6193               31.7484                34.9797
 Red. masses --    12.6136                4.3752                 3.9005
 Frc consts  --     0.2902                0.0026                 0.0028
 IR Inten    --    74.1468                1.3687                 1.1268
--
```

3.6 REFERENCES

(1) (a) Osborn, J. A.; Jardine, F. H.; Young, J. F.; Wilkinson, G. *J. Chem. Soc*. A **1966**, *12*, 1711-1732. (b) Schrock, R. R.;Osborn, J. A.; *J. Am. Chem. Soc*. **1976**, *98* (8), 2134-2143. (c) Landis, C. R.; J. Halpern, *J. Am. Chem.Soc*. **1987**, *109*, 1746-1754.

(2) (a) Noyori, R.;Yamakawa, M.; Hashiguchi, S. *J. Org. Chem*. **2001**, *66*, 7931-7944. (b) Haack, K. J.; Hashiguchi, S.; Fujii, A.; Ikariya, T.; Noyori, R. *Angew. Chem. Int. Ed.* **1997**, *36*, 285-288. (c) Muniz, K.; *Angew. Chem. Int. Ed*. **2005**, *44*, 6622.

(3) Samec, J. S. M.; Bäckvall, J. E.; Andersson, P. G.; Brandt, P.; *Chem. Soc. Rev*. **2006**, *35*, 237.

(4) (a) Clapham, S. E.; Hadzovic, A.; Morris, R. H. *Coord. Chem. Rev*. **2004**, *248*, 2201. (b) Abdur-Rashid, K.; Faatz, M.; Lough, A. J.; Morris, R. H.; *J. Am. Chem. Soc*. **2001**, *123*, 7473-7474. (c) Abdur-Rashid, K.; Clapham, S. E.; Hadzovic, A.; Harvey, J. N.; Lough, A. J.; Morris, R. H. *J. Am. Chem. Soc*. **2002**, *124*, 15104. (d) Berke, H. *ChemPhysChem* **2010**, *11*, 1837-1849.

(5) (a) Bullock, R. M. *Chem. Eur. J.* **2004**, *10*, 2366–2374. (b) Song, J. S.; Szalda, D. J.; Bullock, R. M.; Lawrie, C. J. C.; Rodkin, M. A.; Norton, J. R. *Angew. Chem. Int. Ed*. **1992**, *31*, 1233.

(6) (a) Noyori, R.; Hashiguchi, S. *Acc. Chem. Res*. **1997**, *30*, 97-102. (b) Noyori, R.; Okhuma, T. *Angew. Chem. Int. Ed*. **2001**, *40*, 40. (c) Noyori, R. *Angew. Chem. Int. Ed.* **2002**, *41*, 2008-2022. (d) Yamakawa, M.; Ito, H.; Noyori, R. *J. Am. Chem. Soc*. **2000**, *122*, 1466-1478.

(7) (a) Ito, M.; Ikariya, T. *Chem. Commun*. **2007**, 5134-5142. (b) Ikariya, T.; Blacker, A. J.; *Acc. Chem. Res*. **2007**, *40*, 1300-1308. (c) Comas-Vives, A.; Ujaque, G.; Lledos, A.; *Organometallics* **2007**, *26*, 4135.

(8) (a) Zhang, J.; Leitus, G.; Ben-David,Y.; Milstein, D. *J. Am. Chem. Soc.* **2005**, *127*, 10840-10841. (b) Zhang, J.; Leitus, G.; Ben-David, Y.; Milstein, D. *Angew. Chem. Int. Ed*. **2006**, *45*, 1113-1115. (c) Gunanathan, C. Ben-David, Y.; Milstein, D. *Science* **2007**, *317*, 790-792. (d) Gnanaprakasam, B.; Zhang, J.; Milstein, D. *Angew. Chem. Int. Ed*. **2010**, *49*, 1468-1471.

(9) (a) Shvo, Y.; Czarkie, D.; Rahamim, Y.; Chodosh, D. F. *J. Am. Chem. Soc.* **1986**, *108*, 7400. (b) Casey, C. P.; Strotman, N. A.; Beetner, S. E.; Johnson, J. B.; Priebe, D. C.; Vos,

T. E.; Khodavandi, B.; Guzei, I. A.; *Organometallics* **2006**, *25*, 1230. (c) Casey, C. P.; Guan, H. R.; *J. Am. Chem. Soc*. **2007**, *129*, 5816. (d) Mum, Y.; Czarkle, D.; Rahamlm, Y .; Shvo, Y. *Organometallics* **1985**, *4*, 1459-1461.

(10) (a) Grützmacher, H. *Angew. Chem. Int. Ed*. **2008**, *47*, 1814-1818. (b) van der Vlugt, J. I.; Reek, J. N. H. *Angew. Chem. Int. Ed*. **2009**, *48*, 8832-8846

(11) (a) Chen, X.; Jia, W.; Guo, R.; Graham, T.W.; Gullons, M. A.; Abdur-Rashid, K. *Dalton Trans* **2009**, 1407-1410. (b) Clarke, Z. E.; Maragh, P. T.; Dasgupta, T. P.; Gusev, D. G.; Lough, A. J.; Abdur-Rashid, K. *Organometallics* **2006**, *25*, 4113-4117.

(12) Askevold, B. Nieto, J. T.; Tussupbayev, S.; Diefenbach, M.; Herdtweck, E.; Holthausen, M. C.; Schneider, S. *Nature Chem*. **2011**, *3*, 532-537.

(13) Käß, M.; Friedrich, A.; Drees, M.; Schneider, S. *Angew.Chem. Int. Ed.* **2009**, *48*, 905-907.

(14) (a)Wu, X. F.; Vinci, D.; Ikariya, T.; Xiao, J. L. *Chem. Commun.* **2005**, 4447. (b) Murata, K.; Ikariya, T. *J. Org. Chem.* **1999**, *64*, 2186. (c) Wu, X.; Liu, J.; Li, X.; Zanotti-Gerosa, A.; Hancock, F.; Vinci, D.; Ruan, J.; Xiao, J. *Angew. Chem. Int. Ed.* **2006**, *45*, 6718. (d) Maire, P.; Büttner, T.; Breher, F.; Le Floch, P.; Grützmacher, H. *Angew. Chem. Int. Ed*. **2005**, *44*, 6318-6323. (e) Schneider, S.; Meiners, J.; Askevold, B.; *Eur. J. Inorg. Chem.* **2012**, 412-429

(15) (a) Bullock, R. M. *Handbook of Homogeneous Hydrogenation*, Wiley-VCH, Weinheim, **2007**. (b) Bullock, M.R. Catalysis without precious metals, Wiley-VCH, Weinheim, **2010**.

(16) (a) Bullock, R. M. *Angew. Chem. Int. Ed.* **2007**, *46*, 7360-7363. (b) Junge, K.; Schröder, K.; Beller, M.; *Chem. Commun.* **2011**, *47*, 4849-4859. (c) Casey, C. P.; Guan. H.; *J. Am. Chem. Soc*. **2007**, *129*, 5816-5817. (d) Langer, R.; Leitus, G.; Ben-David, Y.; Milstein, D. *Angew. Chem. Int. Ed.* **2011**, *50*, 2120 - 2124. (e) Sui-Seng, C.; Freutel, F.; Lough, A. J.; Morris, R. H. *Angew. Chem. Int. Ed.* **2008**, *47*, 940-943. (f) Casey, C. P.; Guan, H. *J. Am. Chem. Soc.* **2009**, *131*, 2499-2507. (g) Lagaditis, P. O.; Alan J. Lough, A. J.; Robert H. Morris, R. H. *J. Am. Chem. Soc.* 2011, 133, 9662–9665.

(17) (a) Bullock, R. M.; Voges. M. H. *J. Am. Chem. Soc.*, **2000**, *122*, 12594-12595.(b) Voges, M. H.; Bullock, R. M. *Dalton Trans*. **2002**, 759-770. (c) Bullock, R. M.; Song J. S. *J. Am. Chem. Soc.* **1994**,*116*, 8602-8612. (d) Kimmich, B. F. M.; Paul J. Fagan, P. J.; Hauptman, E.; William J. Marshall, W. J.; R. Morris Bullock, R. M. *Organometallics* **2005**, *24*, 6220-6229 (e) Song, J. S.; Szalda, D. J.; Bullock, R. M.; Lawrie, C. J. C.; Rodkin, M. A.;

Norton, J. R. *Angew. Chem. Int. Ed.* **1992**, *31*, 1233-1235. (f) Dioumaev, V. K.; Bullock, R. M.; *Nature*, 530-532.

(18) Dybov, A.; Blacque, O.; Berke, H. *Eur. J. Inorg. Chem.* **2011**, 652-659.

(19) (a) Jiang, Y.; Hess, J.; Fox, T.; Berke, H. *J. Am. Chem. Soc*. **2010**, *132*, 18233-18247. (b) Dudle, B.; Rajesh, K.; Blacque, O.; Berke, H. *J. Am. Chem. Soc*. **2011**, *133*, 8168-8178. (c) Choualeb, A.; Maccaroni, E.; Blacque, O.; Schmalle, H. W.; Berke, H. *Organometallics* **2008**, *27*, 3474-3481. (d) Jiang, Y.; Birgitta Schirmer, B.; Blacque, O.; Fox, T.; Grimme, S.; Berke H. *J. Am. Chem. Soc*. **2013**, *135*, 4088-4102.

(20) Dong, H.; Berke, H. *Adv. Synth. Catal*. **2009**, *351*, 1783-1788.

(21) Jiang, Y.; Blacque, O.; Fox, T.; Frech, C., M.; Berke, H. *Chem. Eur. J*. **2009**, *15*, 2121-2128.

(22) Jiang, Y.; Blacque, O.; Fox, T.; Frech, C., M.; Berke, H. *Organometallic*s **2009**, *28*, 5493-5504.

(23) (a) Morales, D.; Pérez, J.; Riera, L.; Riera, V.; Miguel, D.; Mosquera, M. E. G.; Granda, S. G. *Chem. Eur. J.* **2003**, *9*, 4132. (b) Caldarelli, J. L.; White, P. S.; Templeton, J. L. *J. Am. Chem. Soc*. **1992**, *114*, 10097-10103. (c) Legzdins, P.; Rettig, S. J.; Ross, K. J. *Organometallics* **1993**, *12*, 2103-2110. (d) Powell, K. R.; Pérez, P. J.; Luan, L.; Feng, S. G.; White, P. S.; Brookhart, M.; Templeton, J. L. *Organometallics* **1994**, *13*, 1851-1864. (e) Francisco, L. W.; White, P. S.; Templeton, J. L.; *Organometallics* **1996**, *15*, 5127-5136. (f) Darensbourg, D. J.; Draper, J. D.; Frost, B. J.; Reibenspies, J. H.; *Inorg. Chem.* **1999**, *38*, 4705-4714.

(24) (a) Poulton, J. T.; Folting, K.; Streib, W. E.; Caulton K. G. *Inorg. Chem.* **1992**, *31*, 3190-3191. (b) Poulton, J. T.; Sigalas,M. P.; Folting, K.; Streib, W. E.; Eisenstein, O.; Caulton K. G. *Inorg. Chem.* **1994**, *33*, 1476-1485. (c) Kovacs, A.; Frenking, G. *Organometallics* **2001**, *20*, 2510. (d) Flood, T. C.; Lim, J. K.; Deming, M. A.; Keung, W. *Organometallics* **2000**, *19*, 1166. (e) Macgregor, S. A.; MacQueen, D. *Inorg. Chem.* **1999**, *38*, 4868. (f) Atwood, J. D.; Brown, T. L. *J. Am. Chem. Soc.* **1976**, *98*, 3160. (g) Ogasawara, M.; Huang, D.; Streib, W. E.; Huffman, J. C.; Gallego-Panas, N.; Maseras, F.; Eisenstein, O.; Caulton, K. G. *J. Am. Chem. Soc.* **1997**, *119*, 8642-8651.

(25) Vogt, M.; Gargir, M.; Iron, M. A.; Diskin-Posner, Y.; Ben-David, Y.; Milstein, D. *Chem. Eur. J.* **2012**, *18*, 9194-9197.

(26) (a) Chen, Z.; Schmalle, H. W.; Fox, T.; Berke, H. *Dalton Trans.* **2005** , 580 – 587. (b) Höck, J.; Jacobsen, H.; Schmalle, H. W.; Artus, G. R. J.; Fox, T.; Amor, J. I.; Bäth, F.; Berke, H. *Organometallics* **2001**, *20*, 1533-1544. (c) Furno, F.; Fox, T.; Schmalle, H. W.; Berke, H. *Organometallics* **2000**, *19*, 3620-3630. (d) Liang, F.; Jacobsen, H.; Schmalle, H. W.; Fox, T.; Berke, H. *Organometallics* **2000**, *19*, 1950-1962. (e) Zhao, Y. Schmalle, H. W.; Fox, T.; Blacque, O.;. Berke, H. *Dalton Trans.* **2006**, 73-85.

(27) (a) Jessop, P. G.; Ikariya, T.; Noyori R. *Chem Rev*, **1995**, 95, 259-272. (b) Jessop, P. G.; Joó, F.; Tai Chih-C. *Coord. Chem. Rev*. **2004**, *248*, 2425-2442.

(28) (a) Hammett, L. P. *J. Am. Chem. Soc*. **1937**, *59*, 96-103. (b) Hammett, L. P. *Chem. Rev*. **1935**, *17*, 125-136. (c) Yang, X.; Zhao, L.; Fox, T.; Wang, Z. X.; Berke, H. *Angew. Chem. Int. Ed*. **2010**, *49*, 2058.

(29) (a) Guan, H.; M. Iimura, M.; Magee, M. P.; Norton, J. R.; Zhu. G. *J. Am. Chem. Soc.* **2005**, *127*, 7805-7814. (b) Bullock, R. M.; Voges, M. H. *J. Am. Chem. Soc.* **2000**, *122*, 12594-12595.

(30) (a) Abbel, R.; Abdur-Rashid, K.; Faatz, M.; Hadzovic, A.; Lough, A. J.; Morris, R. H. *J. Am. Chem. Soc*. **2005**, *127*, 1870-1882. (b) Abdur-Rashid, K.; Clapham, S. E.; Hadzovic, A.; Harvey, J. N.; Lough, A. J.; Morris, R. H. *J. Am. Chem. Soc.* **2002**, *124*, 15104-15118. (c) Chen, X.; Jia, W.; Guo, R.; Graham, T. W.; Gullons, M. A.; Abdur-Rashid, K. *Dalton Trans.*, **2009**, 1407-1410.

(31) Widegren, J. A.; Finke, R. G. *J. Mol. Catal. A* **2003**, *198*, 317.

(32) Topics Curr. Chem. 2013, in press

(33) (a) Seyferth, K.; Taube, R; *J. Organomet. Chem.* **1982**, *229*, 275-279. (b) Danopoulos, A. A.; Wills, A. R.; Edwards, P. G.; *Polyhedron* **1990**, *9*, 2413-2418.

(34) (a) Agilent Technologies (formerly Oxford Diffraction), Yarnton, England, 2011. (b) Clark, R. C.; Reid, J. S. *Acta Crystallogr. Sect. A* **1995**, *51*, 887 – 897. (c) Sheldrick, G. M.; *Acta Crystallogr. Sect. A* **2008**, ***64***, 112 – 122. (d) Farrugia, L. J.; *J. Appl. Cryst.* **1999**, *32*, 837. (e) Spek, A. L.; *J. Appl. Cryst.* **2003**, ***36***, 7 – 13. (f) Brandenburg, K. *DIAMOND*, Crystal Impact GbR, Bonn, Germany, 2007.

(35) Gaussian 03, Revision D.01. Frisch, M. J.; Trucks, G. W.; Schlegel, H. B.; Scuseria, G. E. Robb, M. A.; Cheeseman, J. R.; Montgomery, J. A.; Jr., Vreven, T.; Kudin, K. N.; Burant, J. C.; Millam, J. M.; Iyengar, S. S.; Tomasi, J.; Barone, V.; Mennucci, B.; Cossi, M.;

Scalmani, G.; Rega, N.; Petersson, G. A.; Nakatsuji, H.; Hada, M.; Ehara, M.; Toyota, K.; Fukuda, R.; Hasegawa, J.; Ishida, M.; Nakajima, T.; Honda, Y.; Kitao, O.; Nakai, H.; Klene, M.; Li, X.; Knox, J. E.; Hratchian, H. P.; Cross, J. B.; Bakken, V.; Adamo, C.; Jaramillo, J.; Gomperts, R.; Stratmann, R. E.; Yazyev, O.; Austin, A. J.; Cammi, R.; Pomelli, C.; Ochterski, J. W.; Ayala, P. Y.; Morokuma, K.; Voth, G. A.; Salvador, P.; Dannenberg, J. J.; Zakrzewski, V. G.; Dapprich, S.; Daniels, A. D.; Strain, M. C.; Farkas, O.; Malick, D. K.; Rabuck, A. D.; Raghavachari, K.; Foresman, J. B.; Ortiz, J. V.; Cui, Q.; Baboul, A. G.; Clifford, S.; Cioslowski, J.; Stefanov, B. B.; Liu, G.; Liashenko, A.; Piskorz, P.; Komaromi, I.; Martin, R. L.; Fox, D. J.; Keith, T.; Al-Laham, M. A.; Peng, C. Y.; Nanayakkara, A.; Challacombe, M.;Gill, P. M. W.; Johnson,B.; Chen, W.; Wong, M. W.; Gonzalez, C.; Pople, J. A. Gaussian, Inc., Wallingford CT, 2004.

(36) (a) Adamo, C.; Barone, V.; *J. Chem. Phys.* **1998**, *108*, 664. (b) Perdew, J. P.; Burke, K.; Wang, Y.; *Phys. Rev. B* **1996**, *54*, 16533. (c) Burke, K.; Perdew, J. P.; Wang, Y.; in *Electronic Density Functional Theory: Recent Progress and New Directions* (Eds.: J. F. Dobson, G. Vignale, M. P. Das), Plenum Press, New York, 1998.

(37) (a) Dunning Jr. T. H.; Hay, P. J. in *Modern Theoretical Chemistry*, Ed. H. F. Schaefer III, Vol. 3 (Plenum, New York, 1976) 1-28. (b) Andrae, D.; Haeussermann, U.; Dolg, M.; Stoll, H.; Preuss, H.; *Theor. Chem. Acc.* **1990**, *77*, 123 – 41.

(38) Ditchfield, R.; Hehre W. J.; Pople, J. A. *J. Chem. Phys.* **1971**, *54*, 724 – 728.

(39) (a) Peng, C.; H. B. Schlegel, H. B. *Israel J. of Chem.* **1993**, *33*, 449. (b) Peng, C.; Ayala, P. Y.; Schlegel, H. B.; Frisch, M. J. *J. Comp. Chem.* **1996**, *17*, 49.

4 A Highly Efficient Large Bite Angle Diphosphine Substituted Molybdenum Catalyst for Hydrosilylation

4.1 INTRODUCTION

The hydrosilylation of unsaturated carbonyl functionalities has received considerable attention as a convenient reduction method both in industry and academia. In addition the alkoxy silane products obtained in these reactions are valuable intermediates for the synthesis of organosilicon polymers owing to its high atom economy and as a one step methodology for the preparation of silyl protected alcohols. Metal mediated hydrosilylation reactions generally operate according to the Chalk-Harrod mechanism for alkenes and alkynes[1] or for carbonyl compounds[2] on the Ojima mechanism *via* following key steps (a) oxidative addition of a Si-H bond to a metal centre (b) coordination of the unsaturated substrate (c) migration of the hydride (or in rare cases of the silyl group) to the unsaturated substrate and finally (d) reductive elimination of a C-O-Si bond to form the hydrosilylated product. Early transition metal systems deviates from this scheme and catalyse hydrosilylation reactions *via* σ bond methathesis.[3] An alternative mechanism[4] was suggested by Chan et al. for the hydrosilylation of unsaturated carbonyls where the carbonyl function undergoes coordination to the silicon atom of the silyl ligand prior to the hydride shift. Toste[5] et al have provided evidence for the catalytic hydrosilylation of carbonyl groups following [2+2] addition of the Si-H bond across a high oxidation state Re=O π bond with heterolytic cleavage of the Si-H bond forming a silyloxo rhenium complex. A pathway with a silylene intermediate was also proposed by Tilley et al.[6] Asymmetric hydrosilylation with high enantioselectivities,[7] ionic hydrosilylations[8] with heterolysis of the Si-H bond, and Lewis acid[9] catalysed hydrosilylation reactions are also well documented by several authors.

Nevertheless, to date the most common and efficient catalysts involved in hydrosilylation reactions are based on platinum group transition metals, which suffer from high cost and recognized toxicities,[10] since in many cases the catalytic metal content cannot be removed from the product. To overcome this problem, the development of iron catalysts[11] and early transition metal catalysts[12] have attracted significant attention. Pursuing catalysis based on molybdenum is also quite appealing on the issue of "Cheap Metals for Noble Tasks" due to its low cost and environmentally benign nature. There are several reports on Mo catalysed hydrosilylation

reactions of carbonyl compounds including indepth mechanistic investigations.[13, 14] Despite the ability of these catalysts to perform hydrosilylation reactions at mild conditions, they lack of high activity and catalyst stability.

Our group has a long-standing interest in rhenium and group VI nitrosyl chemistry. Recently our group had discovered excellent catalytic performance of ligand tuned rhenium nitrosyl complexes in hydrogenations[15] comparable or even superior to precious metal catalysts. Hydrosilylations,[16] dehydrogenative silylations,[17] and dehydrogenative aminoborane coupling[18] reactions and also of molybdenum catalyzed hydrogenation reactions[19] could also be accomplished. We were particularly interested in developing an efficient molybdenum nitrosyl based catalyst for hydrosilylation reactions. We sought to get inspiration particularly from our earlier work with rhenium compounds[20] where large bite angle chelating diphosphine ligands had dramatically influenced the ability of ligand exchanges of the metal centres and directed these towards catalysis of the hydrogenation of alkenes. For this reason, we have initially chosen the simplest of aryl substituted disphosphines the large bite angle 2,2′-bis(diphenylphosphino)diphenylether ligand (DPEphos) and prepared molybdenum nitrosyl derivatives and applied them in efficient hydrosilylation reactions of various substituted aromatic aldehydes and ketones.

4.2 Results and Discussion

4.2.1 Preparation of Molybdenum Nitrosyl Complexes bearing 2,2′-bis(diphenylphosphino)diphenylether (DPEphos) ligand.

The preparation of the large bite angle 2,2′-bis(diphenylphosphino)diphenylether ligand (DPEphos = $(Ph_2PC_6H_4)_2O$, Bite angle = 102.2°)[23a] containing dinuclear species $[Mo(NO)(P\cap P)Cl_2]_2[\mu Cl]_2$ (**1**) was achieved by ligand substitution reactions starting from the $Mo(NO)Cl_3(NCMe)_2$ precursor complex at room temperature in THF (Scheme 4.1). **1** precipitated out from THF solution as a grey material in 86% yield. It is insoluble in organic solvents. Therefore, it could be characterized only by elemental analysis and solid state IR spectroscopy. The IR spectrum showed a sharp signal at 1664 cm^{-1} attributed to the ν_{NO} vibration. An attempt to cleave this chloride dinuclear species **1** by heating it in the coordinating solvent MeCN failed, which resulted in an inseparable mixture of decomposition products including the presence of the free DPEphos ligand as indicated by ^{31}P NMR spectroscopy. It should be

mentioned that an attempt to prepare a similar large bite angle complex using the diphosphine 4,6-bis(diphenylphosphino)-10,l0-dimethylphenoxasilin(Sixanthphos) ligand[23a] from the $Mo(NO)Cl_3(NCMe)_2$ precursor failed completely, even at higher temperatures as revealed by the ^{31}P NMR spectra. Despite its insolubility, the Mo(II) complex **1** could be reduced by Zn or Na/Hg to obtain several low-valent molybdenum nitrosyl complexes.

The reduction of **1** with excess zinc (10 equiv.) in MeCN at room temperature led to formation of the red cationic $[Mo(NO)(P\cap P)(NCMe)_3]^+[Zn_2Cl_6]^{2-}{}_{1/2}$ complex (**2**) in excellent yield (84%) (Scheme 4.1). The $^{31}P\{^1H\}$ NMR spectra revealed a single resonance at δ = 53.5 ppm, which spoke for the equivalence of the phosphorus atoms of the DPEphos ligand. A ν_{NO} band was observed at 1593 cm^{-1}. One broad signal at δ = 2.01 ppm in the ^1H NMR spectra was attributed to the methyl protons of the coordinated MeCN ligands. The signals of the C_{Me} and C_{CN} atom appeared in the $^{13}C\{^1H\}$ NMR spectra at δ = 0.65 and 123 ppm respectively. The complex was further characterized by C,H correlation, long range C,H correlation experiments, elemental analysis, and finally by a single crystal X-ray diffraction study. **2** is soluble in MeCN, THF and sparingly soluble in toluene.

Single crystals for a X-ray diffraction study could be obtained by layering pentane onto a concentrated toluene solution of **2** at -30 °C. The X-ray diffraction study of **2** revealed a pseudo octahedral geometry around the metal centre (Figure 4.1).

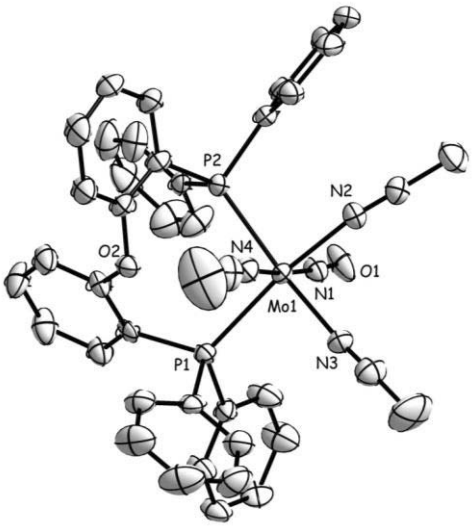

Figure 4.1. Molecular structure of the cationic part of $[Mo(NO)(P\cap P)(NCMe)_3]$ $[Zn_2Cl_6]_{1/2}$ **(2)**. Thermal ellipsoids are drawn at the 50% probability level. All hydrogen atoms, solvent molecule and $[Zn_2Cl_6]_{1/2}$ counter ion are omitted for clarity. Selected bond distances (Å) and bond angles (^{o}): Mo1-N1 1.769(4), Mo1-N2 2.151(5), Mo1-N3 2.149(5), Mo1-N4 2.220(5) Mo1-P1 2.4919(14) Mo1-P2 2.4660(14) N1-O1 1.210(5) N1-Mo1-N4 174.04(18), N2-Mo1-N3 80.60(16), P1-Mo1-P2 96.76(5) P1-Mo1-N2 169.43(12) P1-Mo1-N3 89.72(12)

Two coordinated MeCN ligands occupy the "equatorial" plane along with the phosphorus atoms of the DPEphos ligand. The average Mo-N_{MeCN} bond length is 2.172(5) Å. The asymmetric unit contains one cationic molybdenum molecule, one toluene as solvate and half of the dianionic $[Zn_2Cl_6]^{2-}$ species.

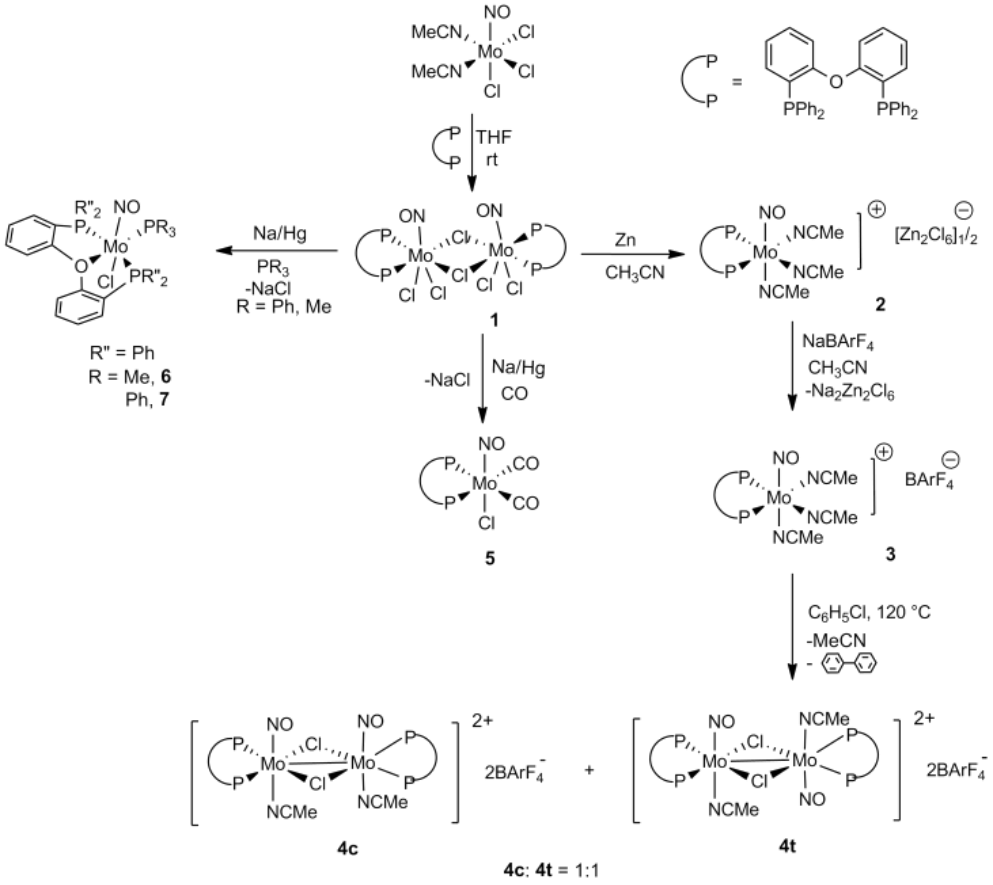

Scheme 4.1. Synthetic access to various molybdenum complexes with the DPEphos ligand.

We opted to choose the bulky non-coordinating $[B\{3,5\text{-}(CF_3)_2C_6H_3\}_4]^-$ anion ($BAr^F{}_4^-$) to replace $[Zn_2Cl_6]^{2-}{}_{1/2}$ species since exchange of the counter-anion could help to increase the solubility of the complex.

The reaction of **2** with $Na^+[B\{3,5\text{-}(CF_3)_2C_6H_3\}_4]^-$ ($NaBAr^F{}_4$) at room temperature in MeCN produced the highly electrophilic cationic complex $[Mo(NO)(P\cap P)(NCMe)_3]^+[BAr^F{}_4]^-$ (**3**) with concomitant formation of $Na_2[Zn_2Cl_6]$ in high yield (90%). Complex **3** is quite soluble in toluene, benzene and chlorobenzene. The $^{31}P\{^1H\}$ NMR spectra exhibited a single resonance at $\delta = 52$ ppm owing to the equivalence of the phosphorus atoms of the DPEphos ligand. The $^{31}P\{^1H\}$ NMR signal of **3** did not display significant shift when compared to **2**. This could presumably be due to a rather loose ion pairing interaction in **2** and **3**. Nevertheless, the exchange of the counterion was confirmed from $^{13}C\{^1H\}$ NMR spectra and X-ray diffraction studies.

Red single crystals suitable for an X-ray diffraction study of **3** were obtained from a toluene/pentane mixture at -30°C. The X-ray structure analysis of **3** exhibited pseudo octahedral coordination (Figure 4.2) around the metal centre similar to **2**. The phosphorus atoms of the DPEphos ligand and the two MeCN ligands were located in the "equatorial" plane.

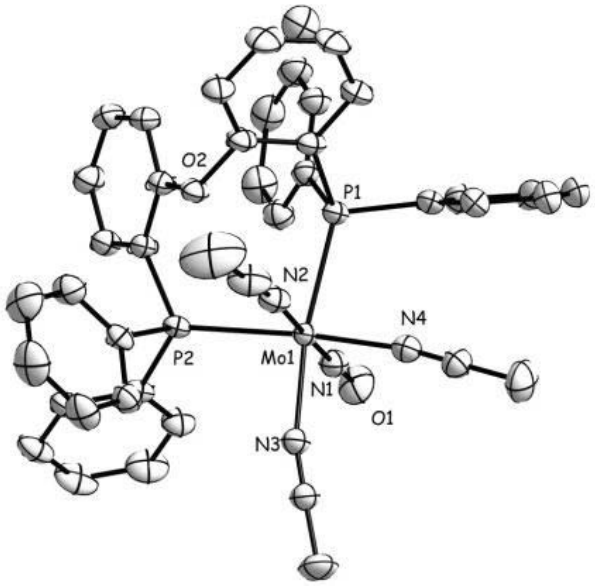

Figure 4.2. Molecular structure of cationic part of **3**. Thermal ellipsoids are drawn at the 50% probability level. All hydrogen atoms, solvent molecule and $BAr^F{}_4$ counteranion are omitted for clarity. Selected bond distances (Å) and bond angles (°): Mo1-N1 1.7691(19), Mo1-N2 2.236(2), Mo1-N3 2.1839(18), Mo1-N4 2.1675(19) Mo1-P1 2.4794(5) Mo1-P2 2.5156(5) N1-O1 1.221(2)

N1-Mo1-N2 177.22(8), N3-Mo1-N4 79.24(7), P1-Mo1-P2 96.857(18) P1-Mo1-N3 170.16(5) P1-Mo1-N2 90.77(5)

The average Mo-N bond length of the acetonitrile ligands were found to be 2.196(2) Å, which is a little longer than the corresponding values of **2**. Similar to **2** the "axially" coordinated MeCN ligand *trans* to NO was found to be at a slightly longer distance than the "equatorially" coordinated one.

When **3** was heated at 120 °C in chlorobenzene, the ^{31}P NMR spectra revealed the formation of two pairs of isomers showing four doublet signals δ 37.6 (**4t**), 33.9 (**4c**), 29.6 (**4c**) and 26.8 (**4t**) ppm which implied that the two phosphorus atoms of chelate ring are chemically inequivalent. When crystallized from chlorobenzene and pentane mixtures, suitable single crystals for X-ray diffraction studies were obtained. The X-ray analysis revealed the formation of the *transoid* dinuclear Mo(I) species **4t** with the hinging DPEphos and the MeCN ligand on the same side and the NO ligands arranged *transoid* (Figure 4.3). The bridging chloride ligands support M-M bonding to attain an 18e$^-$ configuration but are asymmetrically bound due to the asymmetric conformation of the DPEphos ligand. The Mo1-Mo1 bond distance was found to be 3.0162(10) which lies in the range expected for a Mo-Mo contact.[21]

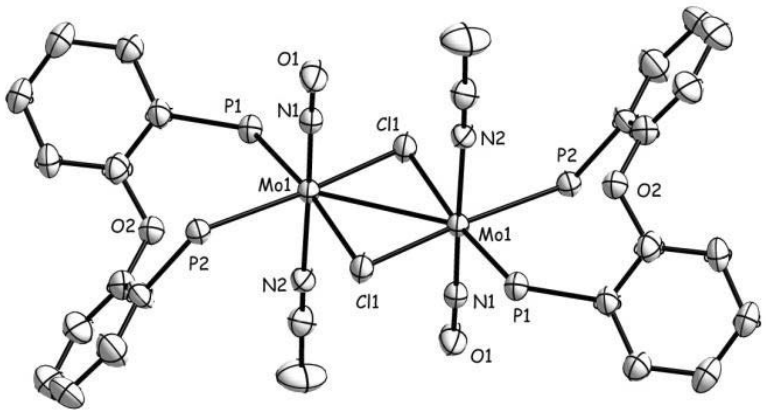

Figure 4.3. Molecular structure of the cation part of **4t**. Thermal ellipsoids are drawn at the 50% probability level. All hydrogen atoms, phenyl rings, pentane and C_6H_5Cl solvates, $[BAr^F{}_4]^-$ counteranions are omitted for clarity. Selected bond distances (Å) and angles (^{o}): Mo1-N1 1.779(6), Mo1-N2 2.188(6), Mo1-Cl1 2.4189(17), Mo1-Cl1^i 2.4106(16), Mo1-P1 2.6270(17),

Mo1-P2 2.6106(17), Mo1-Mo1 3.0162(10), N1-O1 1.178(7), N1-Mo1-N2 177.43(2), P1-Mo1-P2 97.92(5), P1-Mo1-Cl1 167.85(6), Cl1-Mo1-Cl^{i} 102.70(5), Cl1-Mo1-$Mo1^{i}$ 51.23(4), Cl1-$Mo1^{i}$-Mo1 51.47(4). Symmetry operation: i = -*x*, 1-*y*, 1-*z*.

It became apparent from the ^{31}P NMR, ^{31}P COSY and further by ^{1}D-NOE experiments that the *cisoid* isomer **4c** had also formed with the nitrosyls of the dinuclear species on the same side. The four doublet signals in the ^{31}P NMR spectra could be grouped two by two via the coupling constant: **4t** 37.6 and 26.8 ppm ($^{2}J_{PP}$ = 108.7 Hz) and **4c** 33.9 and 29.6 ppm ($^{2}J_{PP}$ = 109.3 Hz), which indicated the inequivalence of the phosphorus atoms in both the isomeric mixtures of the dinuclear complexes **4t** and **4c**. In the ^{1}H NMR spectra the methyl protons appeared at δ 1.9 and 1.8 ppm in an 1:1 intensity ratio for **4t** and **4c**, respectively. The formation of **4t** or **4c** could be explained on the basis of the oxidative addition of chlorobenzene to the highly electrophilic cationic complex **3** *via* preceding replacement of the MeCN ligand. Formation of a dinulcear adduct with chloride bridges, which undergoes two centred reductive elimination of biphenyl (detected by GC/MS) to generate the dinuclear Mo(l) complexes **4c** and **4t**.

1 could be also reduced to various other low oxidation state complexes in the presence of strongly coordinating π accepting or σ donating ligands, such as CO, PPh_3 and PMe_3 using Na/Hg as reducing agent.

Treatment of **1** with excess of Na/Hg (5 equiv.) in the presence of carbon monoxide (1 bar) produced Mo(NO)(P∩P)$(CO)_2$Cl complex (**5**) (Scheme 4.1). However, the yield was quite low (20%) due to the formation of other as yet unidentified products. Nevertheless, **5** could be prepared with good yield (76%) using a modified synthetic procedure starting from Mo(NO)$(CO)_4(ClAlCl_3)$ and the DPEphos ligand at 70 °C in THF. The $^{31}P\{^{1}H\}$ NMR spectra displayed a single resonance at δ = 16.6 ppm. The IR spectra showed strong absorptions at 2028, 1957 and 1630 cm^{-1} assigned to the coordinated carbonyl and nitrosyl ligands, respectively. Single crystals suitable for X-ray diffraction studies were obtained from a toluene/pentane mixture. The X-ray structure analysis displayed the two carbonyl ligands and the two phosphorus atoms of the DPEphos ligand in one plane. The *trans* NO/Cl axis was found to be disordered with a site-occupancy ratio of 0.776:0.224(1) (Figure 4.4).

The monodentate phosphine complexes Mo(NO)(P-O-P)(PR_3)Cl (R = Me, **6**; Ph, **7**) were prepared by the reaction of **1** with 1 equiv. of the PR_3 derivative (R = Me and Ph) in presence of excess of Na/Hg in THF at room temperature and isolated as red (**6**, 50%) and orange (**7**, 55%) solids in moderate yields (Scheme 4.1). The $^{31}P\{^{1}H\}$ NMR spectra of **6** displayed a doublet of doublet signal for the coordinated P-O-P ligand at δ 45 ppm ($^{2}J_{PP}$ = 12 Hz) along with a triplet resonance at lower field (δ 26 ppm, $^{2}J_{PP}$ = 12 Hz) for the trimethyl phosphine ligand. On the other hand, **7** exhibited a triplet signal at δ = 74 ppm (J = 12 Hz) due to the attached triphenyl

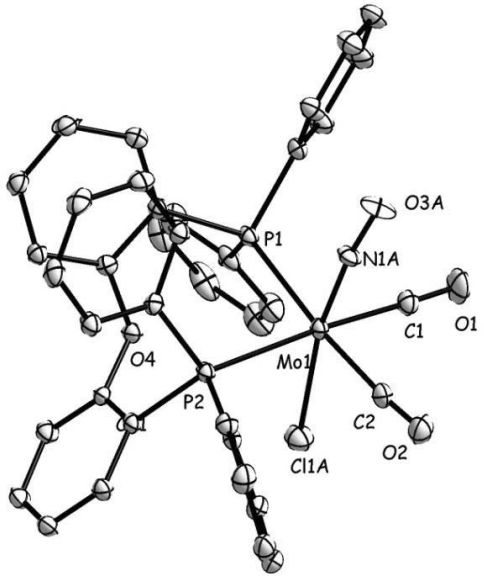

Figure 4.4. Molecular structure of Mo(NO)(P∩P)$(CO)_2$Cl **(5)**. Thermal ellipsoids are drawn at the 30% probability level. All hydrogen atoms, solvent molecule omitted for clarity. *trans* NO/Cl are disordered with site-occupancy ratio of 0.776:0.224. Selected bond distances (Å) and bond angles (°): Mo1-N1A 1.815(2), Mo1-C1 2.0172(16), Mo1-C2 2.0282(18) Mo1-Cl1A 2.4554(8), Mo1-P1 2.6011(4) Mo1-P2 2.6209(4) N1A-O3A 1.283(2), C1-O1 C2-O2 N1A-Mo1-Cl1A 169.91(7), N1A-Mo1-C2 85.34(8), P1-Mo1-P2 96.039(13) P1-Mo1-C2 175.17(5) P1-Mo1-C1 85.96(5).

phosphine ligand and the phosphorus resonance of the DPEphos ligand became transformed into two doublet of doublet signals (ABX spin system) with a strong *trans* $^{2}J_{pp}$ coupling of 165 Hz at

δ = 43 and 37 ppm (J_{pp} = 12 Hz). The inequivalence of the two phosphorus atoms within the chelate arises from a rigid conformation of the complexed ligand typical for large bite angle diphosphines, in which the four P bound phenyl rings adopt pseudo axial and pseudo equatorial positions and inversions not permitted. The molecular structures of **6** and **7** were determined by X-ray diffraction studies and are displayed in Figure 4.5 with selected bond lengths and angles. In both structures, the chelating phosphine behaves tridentate coordinated through all three P, O, P atoms in meridional arrangement with *trans* P-Mo-P angles of 152.23(3)° for **6** and of 151.326(13)° for **7**. Coordination of the oxygen atom is presumably preferred in allowing the

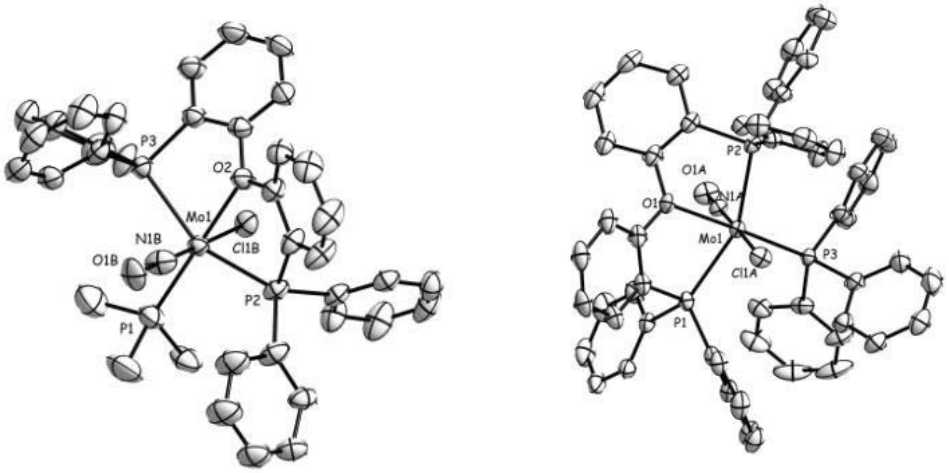

Figure 4.5. Molecular structures of **6** (left) and **7** (right). Thermal ellipsoids are drawn at the 50% probability levels. All hydrogen atoms, solvent molecules are omitted for clarity. Selected bond distances (Å) and bond angles (°) for **6**: Mo1-N1B 1.771(14), Mo1-O2 2.266(2), Mo1-P1 2.3740(11) Mo1-P2 2.4432(10) Mo1-P3 2.4599(9) N1B-O1B 1.27(3) N1B-Mo1-Cl1B 176.4(4), P1-Mo1-N1B 84.4(4) P2-Mo1-P3 152.23(3) P1-Mo1-P3 104.62(4) Selected bond distances (Å) and bond angles (°) for **7**: Mo1-N1A 1.745(4), Mo1-O1 2.2914(10), Mo1-P1 2.4681(3) Mo1-P2 2.4840(3) Mo1-P3 2.4225(4) N1A-O1A 1.198(4) N1A-Mo1-Cl1A 176.89(16), P1-Mo1-N1A 95.41(15) P1-Mo1-P3 101.565(11) P1-Mo1-P2 151.326(13).

complexes to achieve 18-electron configurations.[22] The Mo-$P_{chelate}$ distances (2.44-2.48 Å) are slightly longer than the Mo-PR_3 distances (ca 2.37-2.42 Å), while the Mo-O distances lie within the range of 2.27-2.29Å.

It should be mentioned that attempts to prepare the hydride complexes using the **5**, **6** and **7** precursors and various ionic hydrides and also Et_3SiH as reactants failed. Addition of the borohydrides $NaBHEt_3$ and $LiBH_4$ to **5**, **6** and **7** led to an immediate color change to black. The $^{31}P\{^1H\}$ NMR spectra of the black solutions revealed the resonance of the free DPEphos ligand as the only detectable signal.

4.2.2 Catalytic hydrosilylation reactions of aldehydes and ketones.

Various attempts were made to use **3** as a catalyst in olefin hydrogenations, but all of them were unsuccessful. But **3** was found to catalyze a surprisingly great variety of hydrosilylations. In an optimisation series **3** was tested using benzaldehyde and triethylsilane in a 1:1.2 ratio and a loading of 1 mol% of **3**. The reaction was carried out at 120 °C in C_6D_5Cl over 3 h to obtain the corresponding silylether, triethyl(benzyloxy)silane in 100% yield as revealed from the ^1H NMR spectra (Table 4.1, entry 1). However, the achieved initial TOF was quite low (54 h^{-1}). Acetophenone was found to be even less active and required a longer reaction time for full conversion (Table 4.1, entry 2). To improve the activity we screened various solvents. Toluene, THF and DMSO could not increase the catalytic performance significantly. When MeCN was used as a solvent, no conversion of benzaldehyde to the corresponding silylether was observed as revealed by ^1H NMR spectra (Table 4.1, entry 5). Temperature was suspected to play a crucial role to promote the catalytic transformations. Addition of 1 mol% of catalyst **3** to a solution of PhCHO and Et_3SiH (1:1.2) in C_6D_5Cl at room temperature did not furnish any hydrosilylated products after 20 h of reaction time. When eventually the temperature was raised to 80 °C, 16% conversion was observed after 3 h with an initial TOF of 2 h^{-1} (Table 4.1, entry 7). In addition to these efforts to improve the activity, various silanes were then screened.

The primary aromatic silane $PhSiH_3$ was found to be highly effective in the hydrosilylation of benzaldehyde. A loading of 0.05 mol% of the catalyst **3** led to 100% conversion of benzaldehyde to the corresponding silylether with a maximum TOF of 3520 h^{-1}. However due to the presence of more than one H_{Si} atom, formation of $PhCH_2OSiPhH_2$ (17%) and $(PhCH_2O)_2SiPhH$ (83%) products were observed as revealed by the GC-MS and the ^1H NMR spectra. The secondary silanes, Ph_2SiH_2 and $PhMeSiH_2$, were also found to be quite active in the hydrosilylations of benzaldehyde. Nevertheless, in both cases monosilylated products were predominantly formed (Eq. 1, monosilylated, **a**; disilylated, **b**.).

Among the tertiary silanes, trimethoxysilane appeared to be more active compared to other silanes. A loading of 0.2 mol% of catalyst **3** to a mixture of benzaldehyde and $HSi(OMe)_3$ (1:1.2) in chlorobenzene at 120 °C, revealed full conversion in less than 2 h with an initial TOF of 560 h^{-1} (Table 4.1, entry 15). The sterically hindered aromatic silanes diphenylmethylsilane phenyldimethylsilane turned out to be less active towards hydrosilylation of benzaldehyde (Table 4.1, entries 13 and 14).

Table 4.1. Optimisation reactions for the hydrosilylation of benzaldehyde catalysed by **3**.

Entry[a]	**Cat (mol%)**	**Silane**	**Solvent**	**TOF (h^{-1})**[b]	**Time (h)**	**Conv (%)**[c]	**Yield (%)**[c]
1	1	Et_3SiH	C_6D_5Cl	54	3	100	100
2[d]	1	Et_3SiH	C_6D_5Cl	22	11	100	100
3	1	Et_3SiH	THF	46	12	78	78
4	1	Et_3SiH	toluene	38	3	82	82
5	1	Et_3SiH	MeCN	-	4	0	0
6	1	Et_3SiH	DMSO	10	4	59	59
7[e]	1	Et_3SiH	C_6D_5Cl	2	3	16	16
8	0.05	Ph_2SiH_2	C_6D_5Cl	1860	1	100	83/17[f]
9	0.05	$PhSiH_3$	C_6D_5Cl	3520	1	100	33/67[f]

10	0.05	$PhMeSiH_2$	C_6D_5Cl	2512	1.5	100	67/33[f]
11	0.05	$PhMeSiH_2$	THF	800	0.5	20	20/0[f]
12[g]	0.5	$PhMeSiH_2$	C_6D_5Cl	2.5	16	20	20
13	0.2	$PhMe_2SiH$	C_6D_5Cl	290	3	100	100
14	0.2	Ph_2MeSiH	C_6D_5Cl	30	17	15	15
15	0.2	$HSi(OMe)_3$	C_6D_5Cl	560	<2	100	100
16	1	$^iPr_3SiH$	C_6D_5Cl	-	0.5	0	0
17	0.2	$HSi(SiMe_3)_3$	C_6D_5Cl	-	0.5	0	0
18	0.2	Ph_3SiH	C_6D_5Cl	0	3	0	0
19[h]	0.05	$PhMeSiH_2$	C_6D_5Cl	-	-	0	0

[a]Unless and otherwise stated 3 mg of the catalyst **3**, benzaldehyde as substrate (given ratio with respect to the catalyst according to Table 4.1), 1.2 equiv. of the silane with respect to substrate, 0.4 mL solvent and 120 °C temperature were used as reaction conditions. [b] Initial TOFs were determined from the ^{1}H NMR spectra after 30 min. [c]Conversions and yields were determined from ^{1}H NMR spectra. [d]Acetophenone was used as substrate. [e]80 °C. [f]ratio of monosilylated and disilylated products (**a**/**b**) determined by GC/MS [g]The reaction was carried out at room temperature and average TOF was calculated after 16 h. [h]No catalyst was used.

Catalysis was suppressed with the more sterically encumbered triphenylsilane, triisopropylsilane and tris(trimethylsilyl)silane (Table 4.1, entries 16, 17 and 18) even at higher temperatures. A blank experiment was using $PhMeSiH_2$ and benzaldehyde at 120 °C did not show any hydrosilylated product as indicated by ^{1}H NMR and the GC/MS. The reaction of benzaldehyde with $PhMeSiH_2$ using **3** was then carried out in THF at 120 °C, which resulted in a decrease of the TOF value (800 h^{-1}, Table 4.1, entry 11) in comparision with chlorobenzene as the solvent. However it should be mentioned here that at room temperature a higher catalyst (0.5 mol% **3**) loading led to some activity in the hydrosilylation of benzaldehyde using $PhMeSiH_2$

Table 4.2. Hydrosilylation of various aldehydes catalyzed by **3** using $PhMeSiH_2$.

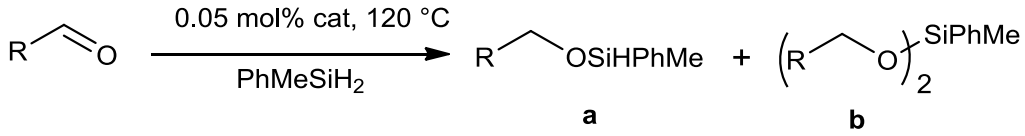

a **b**

Entry[a]	Substrates	Cat (mol%)	TOF (h^{-1})[b]	Time (h)	Conv (%)[c]	Yield (%)[d] (a/b)
1	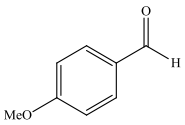	0.05	232	2.5	29	29/0
2	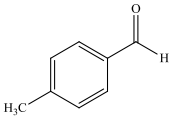	0.05	800	3	89	65/14
3	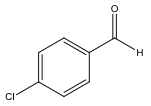	0.05	1760	2.5	100	82/18
4	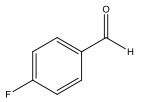	0.05	1680	<3	100	57/43
5	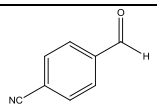	0.05	320	2.5	538	53/0
6	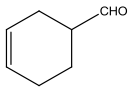	0.05	960	7	90	64/26
7	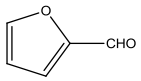	0.05	3600	<2	100	53/47
8	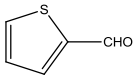	0.05	2720	3	92	67/25
9	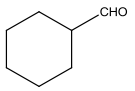	0.05	2400	3	88	61/17
10[e]	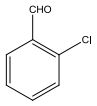	0.05	4864	0.25	60.8	60.8/0

11	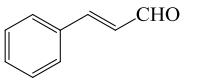	0.05	800	7	100	100/0

[a]Unless and otherwise stated 3 mg of the catalyst **3**, substrate/catalyst ratio according to Table 4.2, 1.2 equiv. of the silane with respect to the substrate, 0.4 mL C_6H_5Cl and 120 °C temperature were used as reaction conditions. [b]Initial TOFs were calculated by GC/MS after 30 min of reaction time. [c]Conversions were determined by GC/MS. [d] Yields on the basis of the substrate consumption determined by GC/MS and **a/b** is the ratio of mono and disilylated products. [e]TOF was determined after initial 15 min.

but after 16 h only 20% conversion was observed with the low TOF value of 2.5 h^{-1} (Table 4.1, entry 12). Nevertheless, at optimized conditions using chlorobenzene as a solvent and phenylmethylsilane at a temperature of 120 °C the catalytic activities of **3** towards various other aldehydes were tested. Several *para* substituted benzaldehydes were converted to their corresponding silyl ethers with excellent rates and yields (Table 4.2). 100% conversions could be achieved running the reactions for longer times. But in the case of 4-methoxy and 4-cyanobenzaldehydes, longer reaction times led to as yet unidentified by-products. The electron donating 4-methoxybenzaldehyde was found to be less active than the electron withdrawing *para* fluoro and *para* chlorobenzaldehydes (Table 4.2, entries 1, 3 and 4). 2-chlorobenzaldehyde showed the highest activity among the various substituted benzaldehydes to obtain a maximum TOF of 4864 h^{-1}. 3-cyclohexenecarboxaldehyde and cinnamaldehyde could be hydrosilylated by **3** without attack on the alkene double bond to obtain a maximum TOF of 960 h^{-1} and 800 h^{-1} respectively (Table 4.2, entries 6 and 11). The catalytic performance of **3** in hydrosilylation of heterocyclic aromatic aldehydes was also tested. The 2-thiophenecarboxaldehyde and 2-furfural were easily converted to their corresponding hydrosilylated products with high turnover frequencies and yields (Table 4.2, entries 7 and 8).

It should be noted that within an initial period of 30 min of the reactions, disilylated products could not be observed by GC/MS nor by ^1H NMR spectroscopy in most cases of the reactions. For entries 7, 8 and 9 15% of disilylation were detected within initial 30 min of reactions. Quite naturally as the reaction progressed the amount of disilylation products increased at a rate slower than monosilylation products. In some cases monosilylated products were obtained exclusively (Table 4.2, entries 1, 5, 10 and 11).

Thus, the performance of **3** in hydrosilylations of various other substrates were additionaly screened. Surprisingly, hydrosilylation of ketones turned out to be much more effective with catalyst **3**. For instance acetophenone was hydrosilylated with $PhMeSiH_2$ with a loading of 0.01 mol% of **3** at 120 °C in 53% conversion within 15 min with an initial TOF of 21232 h^{-1} (Table 4.3, entry 1) as revealed by GC/MS. **3** was also found to catalyze the hydrosilylation of acetophenone at room temperature. When 0.025 mol% of **3** was loaded to a mixture of acetophenone and $PhMeSiH_2$ in chlorobenzene, 38% conversion was observed after 1 h with a TOF of 1520 h^{-1} and within 5 h full conversion of acetophenone to the corresponding

Table 4.3. Hydrosilylation of various other substrates catalysed by **3** using $PhMeSiH_2$.

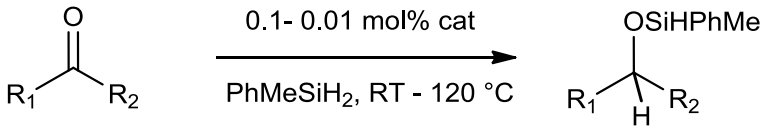

Entry[a]	Substrate	Cat (mol%)	Temp (°C)	Initial TOF (h^{-1})[b]	Time (h)	Yield (%)[c]
1	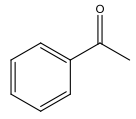	0.025 0.01 0.01	RT 120 120	1520 21230 5400[d]	5 <1 0.25	100 100 13
2	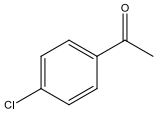	0.025 0.01	RT 120	956 16320	1 0.25	24 40
3	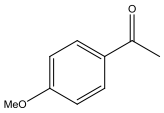	0.02 0.01 0.01	RT 120 120	4420 32000 18400[d]	<2 0.5 0.25	97 100 46
4	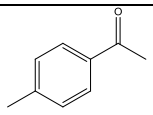	0.025 0.01	RT 120	3200 21800	3 <2	96 100
5	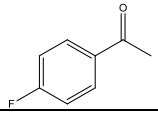	0.025 0.01	RT 120	1480 20200	1 <2	37 100

6	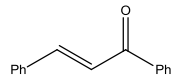	0.05	120	240	7	77
7	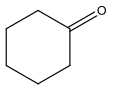	0.1 0.01	RT 120	415 6800	5 0.25	70 17
8	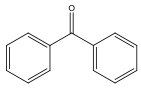	0.025 0.025	RT 120	1200 8288	7 <2	100 100
9	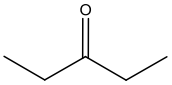	0.1 0.025	RT 120	150 12800	24 <2	98 92[e]
10	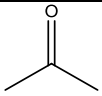	0.1 0.025	RT 120	00 1120	14 <7	00 82[e]
11	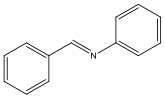	0.2	120	110	7	100
12	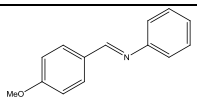	0.2	120	71	7	100
13	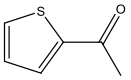	0.1 0.025	RT 120	514 8000	5 1.5	89 96

[a]Unless and otherwise stated 0.3 mL chlorobenzene, 0.5 mg **3** as catalyst, certain amount of substrate/catalyst ratio (according to Table 3), 1.2 equiv. $PhMeSiH_2$ with respect to the substrate were used as reaction conditions and for room temperature reactions, 1 mg catalyst was used, TOFs were calculated from initial 1[st] h. [b] TOFs were determined after initial 15 min of reaction time by GC/MS. [c]Yields by GC/MS on the basis of substrate consumption. [d]THF solvent. [e]Isolated yields.

hydrosilylated products (Table 4.3, entry 1) could be achieved. Thus, we tested various other *para* substituted acetophenones at room temperature and at 120 °C. 4-methoxyacetophenone turned out to be the most active substrate in hydrosilylations catalyzed by **3**. At 120 °C, a maximum TOF of 3.2 x 10^4 h^{-1} was obtained when 0.01 mol% catalyst **3** was loaded to a mixture of 4-methoxyacetophenone and $PhMeSiH_2$ (1:1.2) in chlorobenzene. At room temperature, 4-methoxyacetophenone revealed a maximum TOF of 4420 h^{-1} with a catalyst loading of 0.02 mol%. (Table 4.3, entry 3). Continuing the series of catalyses with *para* substituted acetophenones as substrates, efficient conversions to the corresponding hydrosilylated products were found to also reach excellent yields within a few hours. Electron withdrawing groups on the

para position of the acetophenone were slightly less active than *para* electron donating groups (Table 4.3, entries 2, 3, 4 and 5). However, unlike in the cases of aldehyde hydrosilylation, ketone hydrosilylation brought about exclusively monosilylated products as revealed by GC/MS.

In further studies extension of the scope of hydrosilylation reactions catalyzed by **3** was explored. Benzophenone, cyclohexanone, 2-acetylthiophene could indeed be converted to their corresponding silylether with high activities and yields (Table 4.3, entries 7, 8 and 13). However, the hydrosilylation of α, β unsaturated aromatic ketones turned out to be sluggish with a maximum TOF of 240 h^{-1}.

It turned out that imines could be hydrosilylated as well. *N*-benzylideneaniline, *N*-(4-methoxybenzylidene)aniline were fully converted to their corresponding silylamines within 7 h with a loading of 0.2 mol% of **3** (Table 4.3, entries 11 and 12).

Hydrosilylation could not be observed when styrene and benzonitrile were used as substrates. Applying hydrosilylation reactions with **3** to aliphatic ketones showed that acetone and 3-pentanone could be converted to the corresponding hydrosilylated products at 120 °C within 7 h in 100% yields as revealed by ^{1}H NMR and ^{13}C NMR spectroscopy (Table 4.3, entries 9 and 10). With a loading of 0.1 mol% catalyst **3**, 3-pentanone was found to be hydrosilylated at room temperature sluggishly showing an initial TOF of 150 h^{-1} and the reaction went to completion in just 24 h. On the other hand, acetone did not show any activity towards hydrosilylation with **3** at room temperature even after 14 h of reaction time and a loading of 0.1 mol% catalyst (Table 4.3, entries 9 and 10).

4.2.3 Kinetic studies for the hydrosilylation of ketones

We carried out four initial kinetic experiments to determine the rate of the hydrosilylation reactions of acetophenone catalysed by **3** at room temperature with varying concentrations of acetophenone, the silane and the catalyst. The Kinetic plots of [Product] over times are given in Figure 4.6. The initial 1st hour rates were determined from conversion of substrate to product by ^{1}H NMR integration. The initial rates are listed in Table 4.4 at various concentrations of substrate, silane , catalyst **3.** The initial reaction rates were found to be first order with respect to the concentration of the catalyst and the silane. However the rate was zeroth order with respect to the substrate concentration indicating that catalyst saturation already takes place at low concentration of the substrates. The first order dependency with respect to silane and zero oreder

dependency with respect to substrate was further supported by the obtained straight line when ln[$PhMeSiH_2$] over time and [$PhCOCH_3$] over time were plotted (Figure 4.7).

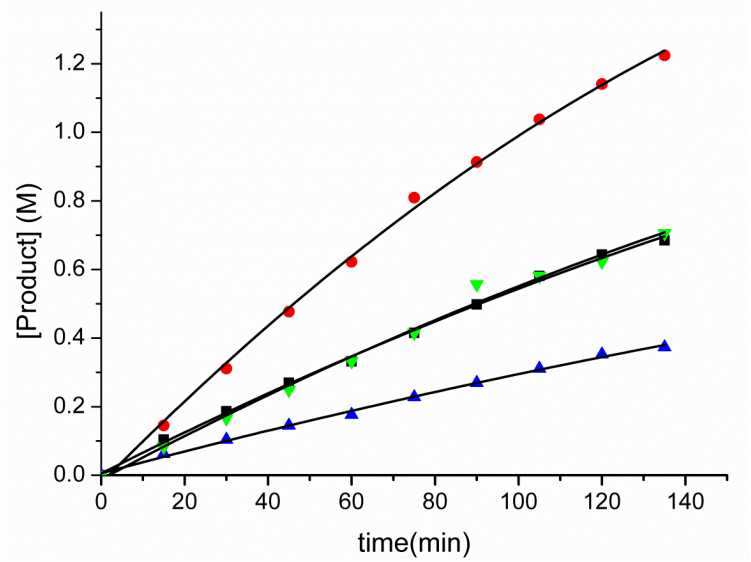

Figure 4.6. Kinetic plots of product concentrations over time. Red circles: [$PhC(O)CH_3$], = 2.075 M, [cat] = 0.002 M, [$PhMeSiH_2$] = 4.86 M; Black squares: [$PhC(O)CH_3$] = 2.075 M, [cat] = 0.002 M, [$PhMeSiH_2$] = 2.43 M; Green triangles: [$PhC(O)CH_3$]= 4.023 M, [cat] = 0.002 M, [$PhMeSiH_2$] = 2.43 M. Blue triangles: [$PhC(O)CH_3$]= 2.075 M, [cat] = 0.001 M, [$PhMeSiH_2$] = 2.43 M.

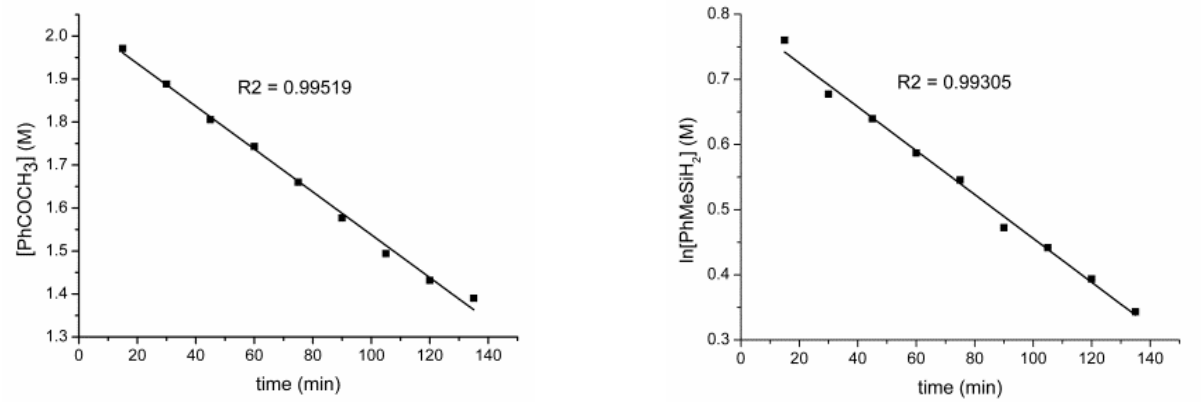

Figure 4.7. Left: Kinetic plot of [$PhCOCH_3$] vs time. Right: Kinetic plot of ln[$PhMeSiH_2$] vs time. [$PhCOCH_3$] = 2.075 M, [cat] = 0.002 M, [$PhMeSiH_2$] = 2.43 M. C_6D_5Cl solvent.

Table 4.4. Dependence of the initial rate of hydrosilylations products on the concentrations of substrate, catalyst and silane[a]

Runs	Cat (3)	$PhMeSiH_2$ (M)	$PhC(O)CH_3$ (M)	Initial rate (M min^{-1})
1	0.002	2.43	2.075	$5.5x10^{-3}$
2	0.002	4.86	2.075	$1.04x10^{-2}$
3	0.002	2.43	4.14	$5.5x10^{-3}$
4	0.001	2.43	2.075	$2.9x10^{-3}$

[a]Reactions were carried out at room temperature. Initial rates were determined after 1h from ^1H NMR integration. Runs 1 and 2 - Variation of [$PhMeSiH_2$], Runs 1 and 3 - Variation of [$PhC(O)CH_3$], Runs 1 and 4 - Variation of [Catalyst].

Based on these kinetic experiments (Table 4.4) the initial rate equation was established as:

$$\text{rate} = 1.131\ (M^{-1}min^{-1})[\text{catalyst}][\text{silane}]$$

4.2.4 Hammett correlation study for the hydrosilylation of various para substituted acetophenones.

To understand the influence of various *para* substituted acetophenones, Hammett[23] correlations were established applying catalyst **3** in hydrosilylations of *para*-methoxy, -methyl, -H, -fluoro and -chloro substituted acetophenones at room temperature and at 120 °C (Figure 4.8). The initial rates (s^{-1}) were determined from the initial TOF values (s^{-1}). A Hammett plot of ln(rate) vs substituent constant (σ) showed linear correlations with a negative slope (ρ) of -1.14 at 120 °C and -3.18 at room temperature. The Hammett parameters (ρ) reflect indeed substituent susceptibility of the reaction. A negative ρ value greater than unity indicates a positive charge build up in the transition states and vice versa. The rate limiting step of the hydrosilylation reactions is apparently greatly affected at room temperature by the presence of the electron donating groups in the *para* position of the acetophenone. Normally, at higher temperature the rate was less sensitive to *para* substitution of the acetophenones (Table 4.3, entries 1, 2, 3, 4 and 5).

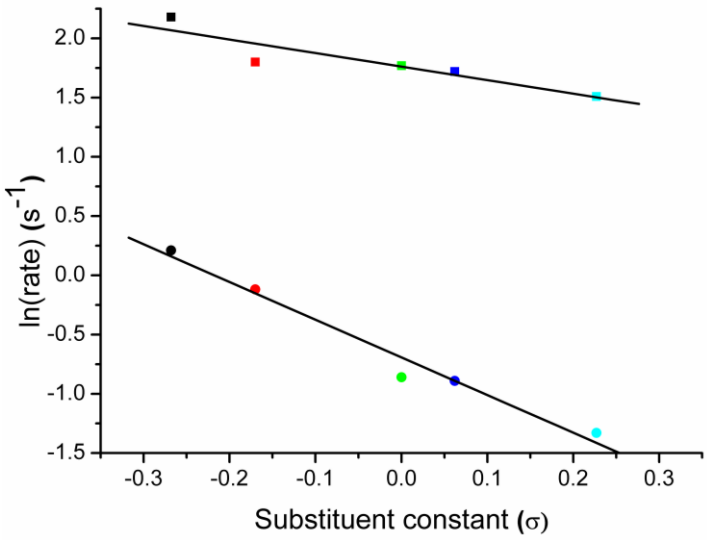

Figure 4.8. Hammett plot for the hydrosilylation of various *para* substituted acetophenones catalyzed by **3** extracted from initial TOF values. Squares, with ρ = -1.14, hydrosilylations at 120 °C. Circles with ρ = -3.18, at room temperature. Black: *p*-MeO, red: *p*-CH_3, green: *p*-H, blue: *p*-F, cyan: *p*-Cl groups. $PhMeSiH_2$ was used as silane.

4.2.5 Deuterium Labeling Study

A ^2H NMR experiment was performed to confirm that hydride was transferred selectively from the silane moiety. For this purpose, benzaldehyde and Et_3SiD were mixed and heated to 120 °C for 1 h in the presence of catalyst **3** (1 mol%). ^2H NMR in chlorobenzene revealed the appearance of a doublet signal at δ 4.8 ppm {$^2J(^1H, ^2H)$ = 1.8 Hz} corresponding to 27% conversion, which became a singlet in the proton decoupled ^2H NMR spectra. This clearly spoke for the transfer of deuterium from the Et_3SiD moiety and formation of $PhCHDOSiEt_3$.

4.2.6 Search for Catalytic Intermediates and Mechanistic Proposal

Additional mechanistic investigations were directed towards detection of catalytic intermediates. When a solution of catalyst **3** (6 mg) in chlorobenzene (or THF) was mixed with 25 equiv.. of acetophenone at room temperature, the ^{31}P NMR spectra showed appearance of a new doublet signal at δ 52.9 ppm (J_{PP} = 15.9 Hz) (15%) along with the signal of **3** (δ 50.8 ppm, 85%). However after addition of excess of acetophenone another signal at appeared δ 52 ppm and the signal of **3** in the ^{31}P NMR spectra decreased. In a similar way, addition of 25 equiv. of benzalde

hyde with **3** (6 mg) in chlorobenzene (or THF) led to two new doublet signals in the ^{31}P NMR spectra at δ 37 (J_{PP} = 97.9 Hz) and 30 ppm (J_{PP} = 98.4 Hz) and the complete disappearance of the ^{31}P NMR signal of **3**. These observations were interpreted in terms of formation of new species with coordination of the aldehyde or the ketones *via* exchange of one of the labile acetonitrile ligands. When excess of $PhMeSiH_2$ was added to a solution of **3** in absence of the ketone or the aldehyde at room temperature, no change was observed in the ^{31}P NMR. But when **3** and excess of $PhMeSiH_2$ were heated at 120 °C, the ^{31}P NMR spectra showed new signals at δ 44 ppm along with signals at δ -9 and δ -17 ppm due to the formation of as yet unidentified species.

The room temperature hydrosilylation of acetophenone catalyzed by **3** (4 mol%) using $PhMeSiH_2$ revealed in the ^{31}P NMR spectra the presence of the signals mentioned above (δ 52.9 and 50.8 ppm) throughout the hydrosilylation process and after completion of the hydrosilylation reaction only **3** was observed. However, when **3**, acetophenone (25 equiv. with respect to the catalyst) and $PhMeSiH_2$ were heated at 120 °C for two minutes, the ^{1}H NMR showed completion of the hydrosilylation reaction and ^{31}P NMR instaneously revealed the presence of only **3** along with a weak unidentified signal at δ 49 ppm (10%) which presumably indicates a resting state of the catalyst and the intensity of which increases with heating for longer period of times with concomitant decrease of the ^{31}P NMR signal of **3**.

Taking into account that **4t** and **4c** only appears in the absence of silane and substrate at 120°C, these species seemed less plausible to be involved in the catalytic cycle. Based on this observation and those described just before a Ojima type mechanism for the hydrosilylation of ketones and aldehydes catalysed by **3** is proposed in Scheme 4.2.[16a] **3** takes the role of a pre-catalyst. Then initial exchange of one MeCN ligand by the substrate takes place and a second labile acetonitrile coordination site is taken by rate limiting oxidative addition of silane molecule forming species **5**. A consecutive silyl transfer and H-shift with subsequent reductive elimination generates the silyl ethers.

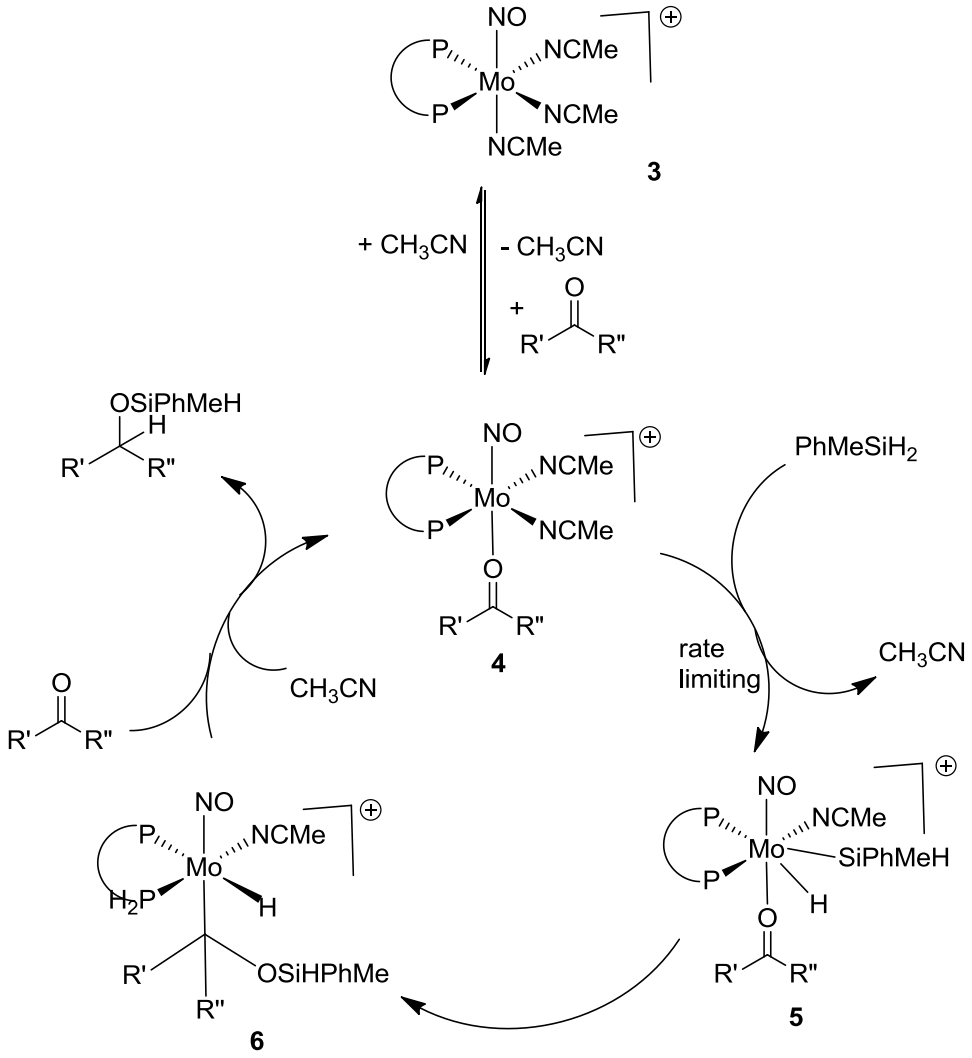

Scheme 4.2. Proposed Ojima Type Mechanism for the Hydrosilylation Reactions Catalyzed by **3**

4.3 Conclusion

In conclusion, we have demonstrated that low a valent cationic molybdenum nitrosyl complex bearing a large bite angle diphosphine and labile MeCN ligands is highly efficient catalyst for the hydrosilylation of ketones and aldehyde particularly in the presence of the secondary silane $PhMeSiH_2$. A great variety of silyl ethers derived from ketones and aryl aldehydes were accessed

with good activities and in excellent yields using catalyst 3 at 120 °C. Ketones were found to show excellent catalytic performance even at room temperature. Kinetic studies revealed that the rates of the reactions depend 1st order on the concentration of the catalyst and silane (1st order) and are independent of the substrate concentration which is in agreement with a Ojima type hydrosilylation mechanism.

4.4 Experimental Section

General Considerations

All manipulations were carried out under an atmosphere of nitrogen using either standard Schlenk techniques or in glove box. All reagent grade solvents were dried according to standard laboratory procedure and distilled prior to use under N_2 atmosphere. Deuterated solvents were dried with sodium benzophenone ketyl (THF-d_8, toluene-d_8, C_6D_6) and calcium hydride (C_6D_5Cl and CD_2Cl_2) and distilled *via freeze-pump-thaw* cycle prior to use. The DPEphos ligand and $Mo(NO)Cl_3(NCMe)_2$ were prepared according to literature procedures.[24] All other chemicals were purchased from commercially available sources and used without further purifications. NMR spectra were measured with a Varian Mercury 200 spectrometer (200.1 MHz for ^{1}H, 81.0 MHz for ^{31}P), with Varian Gemini-300 instrument (^{1}H at 300.1 MHz, ^{13}C at 75.4 MHz), with Bruker-DRX 500 spectrometer (500.2 MHz for ^{1}H, 202.5 MHz for ^{31}P, 125.8 MHz for ^{13}C) and Bruker-DRX 400 spectrometer (400.1MHz for ^{1}H, 162.0 MHz for ^{31}P, 100.6 MHz for ^{13}C). All chemical shifts for ^{1}H and $^{13}C\{^1H\}$ are expressed in ppm relative to tetramethylsilane (TMS) and for $^{31}P\{^1H\}$ relative to 85% H_3PO_4 as an external standard reference. Signal patterns are as followed: s, singlet; d, doublet; t, triplet; q, quartet; m, multiplet. IR spectra were obtained either ATR or KBr methods using Bio-rad FTS-45 instrument. Elemental analyses were carried out at Anorganisch-Chemisches Institut of the University of Zürich. The GC/MS spectra were recorded on a Varian Saturn 2000 spectrometer equipped with Varian 450-GC chromatograph.

$[Mo(NO)(P\cap P)Cl_2]_2[\mu Cl]_2$ (P∩P = DPEphos) (1)

$Mo(NO)Cl_3(NCMe)_2$ (0.200 g, 0.636 mmol) was dissolved in 10 ml THF. A solution of DPEphos (0.342 g, 0.635 mmol) in 5 ml THF was added into that solution. The resulting mixture was kept

stirring for 3 h at room temperature. The formed precipitate was filtered off and was washed first with minimum amount of THF and then with pentane. Finally the solid was dried in *vacuo* to obtain **1** in 86 % yield (0.420 g). IR (cm^{-1}, ATR): 1664 (ν_{NO}). Anal.Calcd for $[C_{36}H_{28}Cl_3MoNO_2P_2]_2$: C, 56.09; H, 3.66; N, 1.82. Found: C, 56.21; H, 3.75 ; N, 1.68.

$[Mo(NO)(P\cap P)(NCMe)_3]$ $[Zn_2Cl_6]_{1/2}$ (P∩P = DPEphos) (**2**)

To a suspension of **1** (0.20 g, 0.129 mmol) in 10 mL MeCN, zinc granules (10 equiv.) were added. The resulting mixture was kept overnight in acetonitrile with constant stirring at room temperature. After completion of the reaction the solution was filtered off, the solvent was removed in *vacuo* and washed with pentane. The solid residue was dissolved in THF and filtered off. The pure product was obtained as an orange powder after removal of the THF in *vacuo* in 84% yield (0.209 g). IR (cm^{-1}): 1593 (s, ν(NO)). ^{1}H NMR (500 MHz, THF-d_8, 293K): δ 7.52-(broad singlet, Ph), 7.42-7.39 (m, Ph), 7.34-7.30 (m, Ph), 7.26-7.22 (m, Ph), 7.21-7.17 (m, Ph), 7.1 (m, Ph), 7.04-7.02 (m, Ph), 6.95- 6.92 (m, DPEphos H), 6.58 (broad singlet, DPEphos H), 2.01 (broad singlet, 9H, CH_3) ppm. ^{31}P{^{1}H} NMR (125 MHz, THF-d_8, 20 °C): δ 53.5 (s). ^{13}C{^{1}H} NMR (125.8 MHz, THF-d_8, 293K): δ = 159.3 (m, Ph), 135 (m, Ph), 134 (m, Ph), 132(m, Ph), 130 (m, Ph), 129 (m, Ph), 128.8 (m, Ph), 124 (m, DPEphos), 123 (m, CN), 120 (m, DPEphos), 0.75 (m, CH_3) ppm. Anal. Calcd for $C_{42}H_{37}Cl_3MoN_4O_2P_2Zn$ (959.41): C, 52.58; H, 3.89; N, 5.84. Found: C, 52.53; H, 3.97; N, 5.64.

$[Mo(NO)(P\cap P)(NCMe)_3][BAr^F{}_4]$ (P∩P = DPEphos) (**3**)

$Mo(NO)(DPEphos)(NCMe)_3]$ $[Zn_2Cl_6]_{1/2}$ (0.070 g, 0.072 mmol) was dissolved in 10 mL of acetonitrile. $NaBAr^F{}_4$ (0.080 g, 0.09 mmol) dissolved in 10 mL acetonitrile was added to that solution with constant stirring and kept stirring overnight. Then the solution was filtered off, the solvent was removed in *vacuo* and washed with pentane. The obtained product was extracted with toluene, concentrated and kept in the fridge (layering with pentane) to reveal pure red colored crystals of **3** in 90% yield. IR (cm^{-1}): 1595 (NO). ^{1}H NMR (500 MHz, THF-d_8, 293K): δ 7.79 (s, $BArF_4$), 7.58 (s, $BArF_4$), 7.38 (m, Ph), 7.28 (m, Ph), 7.22 (m, Ph), 7.12 (m, Ph), 7.0 (m, Ph), 6.7(m, DPEphos H), 2.16 (s, 3H, CH_3), 1.41 (s, 6H, CH_3), ppm.^{31}P{^{1}H} NMR (162 MHz, THF-d_8, 20 °C): δ 52 (s). ^{13}C{^{1}H} NMR (100.8 MHz, THF-d_8, 293K): δ = 163 (q, *i*-$BAr^F{}_4$, $^1J_{BC}$ =

50.0 Hz,), Ph 159 (m, Ph), 135 (m, Ph), 133 (m, Ph), 132 (m, Ph), 130 (m, Ph), 129 (m, Ph), 128.8 (m, Ph), 127 (m, BAr^F_4), 125 (m, DPEphos), 123 (s, CN), 121 (s, BAr^F_4),), 120 (m, CN), 118 (m, DPEphos), 3.06 (s, CH_3), 0.62 (s, CH_3) ppm. Anal. Calcd for $C_{74}H_{49}BF_{24}MoN_4O_2P_2$(1650.89): C, 53.84; H, 2.99; N, 3.39. Found: C, 53.75; H, 2.92; N, 3.20.

$[\{Mo(NO)(P\cap P)(NCMe)\}_2\{\mu Cl\}_2]^{2+}$ $2[BAr^F_4]^-$ (4t and 4c) (P∩P = DPEphos)

A solution of **3** (50 mg, 0.03 mmol) in chlorobenzene was heated at 120 °C for 30 min. The resulting solution was monitored by ^{31}P NMR to ensure completion of the reaction. The resulting mixture was filtered and evaporated to dryness. The obtained red oily residue was washed twice with pentane to remove the biphenyl side product and finally the pure dinuclear isomeric mixture of **7t** and **7c** were obtained as a red solid in 92% yield after drying in *vacuo*.

^{1}H NMR (500 MHz, C_6D_5Cl, 293 K): δ 8.2 (s, BAr^F_4), 8.0 (m, Ph), 7.9 (m, Ph), 7.7 (m, Ph), 7.6 (s, BAr^F_4), 7.5 (m, Ph), 7.4-7.3 (m), 7.2-7.1 (m), 6.9 (m), 1.9 (s, CH_3, **7t**), 1.8 (s, CH_3, **7c**). ^{31}P{^{1}H} NMR (202 MHz, C_6D_5Cl, 293 K): δ 37.5 (d, $^2J_{PP}$ = 108.7 Hz, **7t**), 26.8 (d, $^2J_{PP}$ = 108.5 Hz, **7t**), 33.9 (d, $^2J_{PP}$ = 109.3 Hz, **7c**), 29.6 (d, $^2J_{PP}$ = 109.1 Hz, **7c**). Anal.Calcd for $C_{140}H_{86}B_2Cl_2F_{48}Mo_2N_4O_4P_4$(3208): C, 52.41; H, 2.70; N, 1.75. Found: C, 52.85; H, 2.80; N, 1.75. Further the presence of isomer mixtures was confirmed by 1D NOE and ^{31}P COSY experiments.

$Mo(NO)(P\cap P)(CO)_2Cl$ (P∩P = DPEphos) (5)

To a solution of $Mo(NO)(CO)_4(ClAlCl_3)$ (0.20 g, 0.49 mmol) in 15 mL THF, a solution of DPEphos (0.265 g, 0.49 mmol) in 5 mL THF was added. The resulting mixture was heated at 70 °C for 3 h. After completion of the reaction, as indicated by ^{31}P NMR, the resulting red solution was filtered off and evaporated to dryness. The solid residue was washed with pentane and then extracted with toluene. Layering the concentrated toluene solution with pentane afforded tiny yellow crystals of **4** after several days. Yield (76%, 280 mg). IR (cm^{-1}): 1630 (NO), 2028(CO)). 1957 (CO). ^{1}H NMR (500 MHz, CD_2Cl_2, 300K): δ 7.58 (Ph), 7.40 (m, Ph), 7.18 (m, Ph), 7.08 (m, Ph), 6.64 (m, DPEphos H) ppm. ^{31}P{^{1}H} NMR (125 MHz, CD_2Cl_2, 300K): δ 16.63 (s). Anal. Calcd for $C_{38}H_{28}ClMoNO_4P_2$(755.97): C, 60.37; H, 3.73; N, 1.85. Found: C, 60.42; H, 3.92; N, 1.68.

[Mo(NO)(κ^3-P,P,O-DPEphos)Cl(PMe_3)](6)

0.13 g (0.084 mmol) of $[Mo(NO)(P\cap P)Cl_2]_2[\mu Cl]_2$ was added to a stirred suspension of 1% Na/Hg in 5 mL THF in a Young Schlenk tube and 0.03 ml (9 µL) of PMe_3 was introduced via a syringe. This was kept 6 h with constant stirring at room temperature. The resulting red colored solution was filtered and the solvent was removed in *vacuo* and washed with pentane. Then it was extracted with benzene. The benzene solution was concentrated and kept in the fridge layering with pentane to obtain the pure red crystals of **5**. Yield 50% . IR (cm^{-1}): 1546 (NO). ^1H NMR (400 MHz, C_6D_6, 300K): δ 7.5-7.44 (m, Ph), 7.35 (m, Ph), 7.22 (m, Ph), 7.01 (m, Ph), 6.8 (m, Ph). $^{31}P\{^1H\}$ NMR (162 MHz, C_6D_6, 300K): δ 45 (dd, $^2J_{PP}$ = 11.97 Hz), 26 (t, $^2J_{PP}$ = 11.97 Hz) $^{13}C\{^1H\}$ NMR (100.6 MHz, C_6D_6, 300K): δ = 159.7 (d, J = 17.88 Hz, C_6H_4OP), 134 (m, Ph), 130 (s, Ph), 128 (m, Ph), 124 (s, C_6H_4OP), 118 (s, C_6H_4OP),21 (m, CH_3) ppm. Anal. Calcd for $C_{39}H_{37}ClMoNO_2P_3$(776.05): C, 60.36; H, 4.81; N, 1.80. Found: C, 60.45; H, 5.04; N, 1.62.

[Mo(NO)(κ^3-P,P,O-DPEphos)Cl(PPh_3)](7)

$[Mo(NO)(P\cap P)Cl_2]_2[\mu Cl]_2$ (0.30 g, 0.195 mmol) and PPh_3 (0.102 g, 0.39 mmol) were added to a suspension of 1% Na/Hg in 10 ml THF. The resulting mixture in THF was kept overnight with constant stirring at room temperature. After completion of the reaction, the red colored solution was filtered and the solvent was removed in *vacuo* and the residue washed with pentane. Then the crude product was extracted with toluene first and then with benzene. The concentrated benzene solution was layered with pentane and kept at room temperature for several days to obtain the pure orange product of **6** in crystalline form in 55% yield. IR (cm^{-1}): 1561 (NO). ^1H NMR (400 MHz, C_6D_6, 300K): δ 8.2 (m, Ph), 7.86-7.76 (m, Ph), 7.73-7.68 (m, Ph), 7.40 (bs, Ph), 7.06-7.03 (m, Ph), 7.0-6.96 (m, Ph), 6.83-6.79 (m, DPEphos), 6.76- 6.72 (m, DPEphos H), 6.68-6.64 (m, DPEphos H). $^{31}P\{^1H\}$ NMR (162 MHz, C_6D_6, 300K): δ 75 (t, $^2J_{PP}$ = 11.22 Hz, PPh_3), 45 (dd, $^2J_{PP}$ = 165.3 Hz, $^2J_{PP}$ = 11.22 Hz, DPEphos), 39 (dd, $^2J_{PP}$ = 165.3 Hz, $^2J_{PP}$ = 11.22 Hz, DPEphos). $^{13}C\{^1H\}$ NMR (100.6 MHz, C_6D_6, 300K): δ = 157 (m, Ph), 139 (d, J_{CP} = 35.75 Hz, Ph), 136 (s, Ph), 135 (d, J_{CP} = 34.57 Ph), 133 (s, Ph), 129 (m, Ph), 124 (m, DPEphos), 118 (m, DPEphos), 115 (m, DPEphos). Anal.Calcd for $C_{54}H_{43}ClMoNO_2P_3$(962.24): C, 67.40; H, 4.50; N, 1.46. Found: C, 66.96; H, 5.09 ; N, 1.15.

X-ray diffraction analyses

Single-crystal X-ray diffraction data were collected at 183(2) K on an Agilent Technologies Xcalibur Ruby area-detector diffractometer using a single wavelength Enhance X-ray source with MoKα radiation (λ= 0.71073 Å).[25] The selected suitable single crystals were mounted using polybutene oil on a flexible loop fixed on a goniometer head and immediately transferred to the diffractometer. Pre-experiment, data collection, data reduction and analytical absorption correction[26] were performed with the program suite *CrysAlisPro*.[27] The structures were solved by direct methods using *SHELXS97*.[28] The structure refinements were performed by full-matrix least- squares on F^2 with *SHELXL97*.[28] *PLATON*[29] was used to check the result of the X-ray analysis. All programs used during the crystal structure determination process are included in the *WINGX* software.[30]

General procedures for the catalytic hydrosilylation reactions.

Table 1: Appropriate amounts of the catalyst **3** (3 mg) and substrate at a given ratio with the catalyst **3**, 1.2 equiv. of the silane with respect to the substrate in deuterated solvents (0.4 mL) were placed in a Young tap NMR tube. The reaction mixture was heated to 120 °C. The TOF was determined after initial 30 min of reaction times by ^{1}H NMR spectroscopy. After the reaction (reaction times according to Table 1), the resulting solution was analyzed by ^{1}H NMR spectroscopy. The resonances were in accord with those of the literature. The yields were determined by integration of the ^{1}H NMR spectra.

Table 2: The reactions were carried out in C_6H_5Cl in a Young Schlenk tube. The TOF values (after initial 30 min.) and the final yields were determined by GC/MS on the basis of substrate consumption.

Table 3: A fresh stock solution of catalyst **3** (6.5 mg in 650 μL C_6H_5Cl) was prepared. An aliquot (50 μL) of that stock solution was added to a mixture of the ketone and the silane (amount of ketone with respect to catalyst **3** according to Table 3, ketone: silane = 1:1.2) in 250 μL C_6H_5Cl in a Young tap Schlenk tube. Then the Schlenk tube was kept in a preheated oil bath (120 °C). After 15 min of reaction time the Schlenk tube was immediately taken out and cooled to room temperature and taken into the glove box. Without further purification a GC/MS analysis was carried out to determine the yield of the product (on the basis of the substrate consumption). The same reaction mixture was taken out from the glove box and heated for longer period of reaction times (Table 3) to achieve complete conversions. For room temperature reactions: A fresh stock

solution of catalyst **3** (10 mg in 1 mL C_6H_5Cl) was prepared. An aliquot (100 µL) of that stock solution was added to a mixture of ketone and silane (amount of ketone with respect to catalyst **3** according to Table 3, ratio of ketone: silane = 1:1.2) in 300 µL C_6H_5Cl in a Young Schlenk tube. The TOFs were determined after initial 1h by GC/MS.

General procedures for the kinetic experiments

For kinetic experiments of Figure 4: In a glove box, catalyst stock solution was freshly prepared in C_6D_5Cl (5 mg in 1.5 mL C_6D_5Cl) and an aliquot (0.3 mL) amount was added to a mixture of acetophenone and phenylmethylsilane in a Young NMR tube (see Supporting Information). Then the tube was sealed and kept in a oil bath preheated to 120 °C. The reaction was monitored by ^{1}H NMR after each 15 min time intervals. Yields and product concentrations were determined from the integration of the ^{1}H NMR spectra.

GC/MS data for the hydrosilylated products of various substituted benzaldehydes and acetophenones (other products see Table 4.6).

PhCHO: rt = 3.727 min, m/z = 106; $PhCH_2OSiPhH_2$: rt = 8.519 min, m/z = 213; $(PhCH_2O)_2SiPhH$: rt = 13.924 min, m/z = 320; $PhCH_2OSiPh_2H$: rt = 12.534 min, m/z = 289; ; $(PhCH_2O)_2SiPh_2$: rt = 24.231 min, m/z = 395; $PhCH_2OSiPhMeH$: rt = 8.808 min, m/z = 227; $(PhCH_2O)_2SiPhMe$: rt = 14.109 min, m/z = 333; *p*-$MeOC_6H_4CHO$: rt = 6.127 min, m/z = 135 ; *p*-$MeOPhCH_2OSiPhMeH$: rt = 10.346 min, m/z = 257; *p*-MeC_6H_4CHO: rt = 4.718 min, m/z = 119; *p*-$MePhCH_2OSiPhMeH$: rt = 9.420 min, m/z = 241; (*p*-$MePhCH_2O)_2SiPhMe$: rt =16.757 min, m/z = 361; *p*-ClC_6H_4CHO: rt = 5.128 min, m/z = 139; *p*-$ClPhCH_2OSiPhMeH$: rt = 10.039 min, m/z = 261; (*p*-$ClPhCH_2O)_2SiPhMe$: rt =22.023 min, m/z = 402; *p*-FC_6H_4CHO: rt = 3.652 min, m/z = 124 ; *p*-$FPhCH_2OSiPhMeH$: rt = 8.746 min, m/z = 245; (*p*-$FPhCH_2O)_2SiPhMe$: rt =13.741 min, m/z = 369; *p*-CNC_6H_4CHO: rt = 6.019 min, m/z = 131; *p*-$CNPhCH_2OSiPhMeH$: rt = 10.933 min, m/z = 252; *o*-ClC_6H_4CHO: rt = 5.033 min, m/z = 139; *o*-$ClPhCH_2OSiPhMeH$: rt = 9.863 min, m/z = 261; $PhC(O)CH_3$: rt = 4.560 min, m/z = 120; $PhCH(CH_3)OSiPhMeH$: rt = 8.634 min, 8.725 min m/z = 241; *p*-$MeOC_6H_4C(O)CH_3$: rt = 6.863 min, m/z = 150; *p*-$MeOC_6H_4CH(CH_3)OSiPhMeH$: rt = 10.115 min, 10.233 m/z = 272; *p*-$CH_3C_6H_4C(O)CH_3$: rt = 5.556 min, m/z = 134; *p*-$CH_3C_6H_4CH(CH_3)OSiPhMeH$: rt = 9.209 min, 9.320 min, m/z = 255; *p*-

$FC_6H_4C(O)CH_3$: rt = 4.461 min, m/z = 138; *p*-$FC_6H_4CH(CH_3)OSiPhMeH$: rt = 8.581 min, 8.864 min m/z = 259; *p*-$ClC_6H_4C(O)CH_3$: rt = 5.967 min, m/z = 154 ; *p*-$ClC_6H_4CH(CH_3)OSiPhMeH$: rt = 9.808 min, 9.930 min, m/z = 275; *p*-$CNC_6H_4C(O)CH_3$: rt = 6.830 min, m/z = 145 *p*-$CNC_6H_4CH(CH_3)OSiPhMeH$: rt = 10.696 min, 10.836 min, m/z = 266.

4.6 APPENDIX

Table 4.5. Reaction conditions for kinetic measurements for the hydrosilylations of acetophenone catalysed by **3** at room temperature.

Runs	1	2	3	4
$PhCOCH_3$(mmol)	0.62	0.62	1.24	0.62
3 (mmol)	0.0006	0.0006	0.0006	0.0003
C_6D_5Cl (mL)	0.3	0.3	0.3	0.3
$PhMeSiH_2$(mmol)	0.73	1.46	0.73	0.73

Table 4.6. GC/MS data for various hydrosilylated products of aldehydes and ketones:

Entry[a]	**substrates**	**Product a**	**Product b**
1	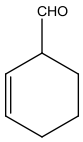 rt = 3.624 min m/z = 110	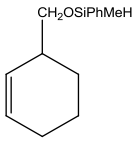 rt = 8.692 min m/z = 231	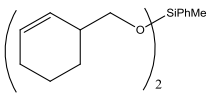 rt =13.662 min m/z = 342
2	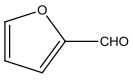 rt = 2.759 min	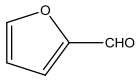 rt = 7.581 min	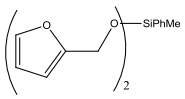 rt = 10.901min

	m/z 96	m/z 217	m/z 315
3	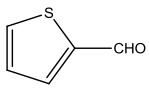 rt = 4.035 min m/z 112	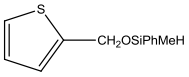 rt = 8.847 min m/z 234	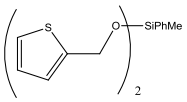 rt = 14.486 min m/z 346
4	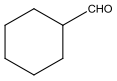 rt = 3.562 min m/z = 113	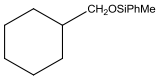 rt = 8.598 min m/z = 233	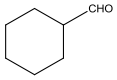 rt = 13.281 min m/z = 346
5	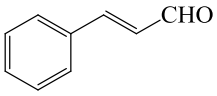 rt = 6.266 min m/z 131	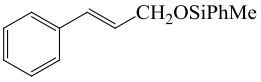 rt = 10.584 min m/z 254	-
6	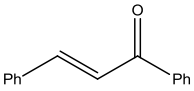 rt = 11.230 min m/z 15.234	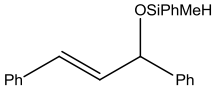 rt =15.234 min m/z 331	-
7	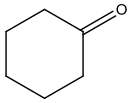 rt = 3.101 min m/z = 99	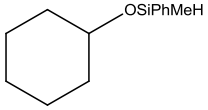 rt = 7.738 min m/z = 219	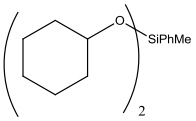 rt = 11.266 min m/z = 318
8	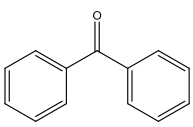	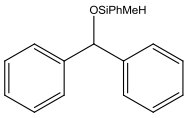	-

	rt = 8.884 min m/z = 182	rt = 12.095 min m/z = 8.884	
9	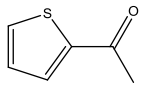 rt = 4.660 min m/z = 126	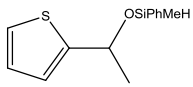 rt = 8.666, 8.741 min m/z = 248	-
10	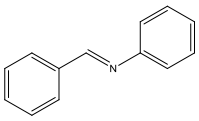 rt = 9.173 min m/z = 181	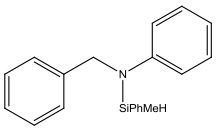 rt = 13.070 min m/z = 303	-
11	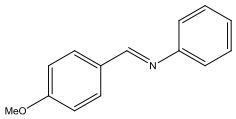 rt = 11.131min m/z 211	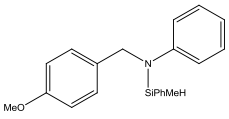 rt = 16.173 min m/z 333	-

[a]rt = retention time, a = monosilylated products, b = disilylated products.

^{1}H and ^{13}C NMR data for the hydrosilylation reactions between acetone and phenylmethylsilane catalysed by 3.

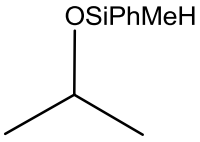

^{1}H NMR (300 MHz, $CDCl_3$, 300K): δ 7.64 (m, Ph), 7.44- 7.42 (m, Ph), 5.1 (q, 1H, -OSiPhMeH), 4.1 (CH), 1.25 - 1.12(6H, CH_3), 0.49 (d, 3H, -OSiPhMeH)

^{13}C NMR data: $^{13}C\{^{1}H\}$ NMR (75.45 MHz, $CDCl_3$, 300K): δ = 137 (s, Ph), 133.8 (s, Ph), 129.9 (s, Ph), 127.9 (s, Ph), 66.8 (s, CH), 25.3 (d, Ph), -2 (s, OSiPhMeH)

^{1}H and ^{13}C NMR data for the hydrosilylation reactions between 3-pentanone and phenylmethylsilane catalysed by 3.

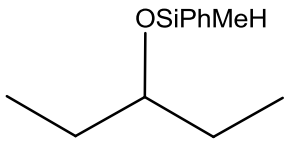

^{1}H NMR (300 MHz, $CDCl_3$, 300K): δ 7.64 (m, Ph), 7.5-7.45 (m, Ph), 5.2 (q, 1H, -OSiPhMeH), 3.6 (pent, 1H, CH), 1.65- 1.55 (m, 4H, CH_2), 1.1- 0.94, (m, CH_3), 0.57 (d, 3H, -OSiPhMeH).

^{13}C NMR data: $^{13}C\{^{1}H\}$ NMR (75.5 MHz, $CDCl_3$, 300K): δ = 136 (s, Ph), 134 (s, Ph), 130 (s, Ph), 128 (s, Ph), 77 (s, CH), 29.4(d, CH_3), 10.03(d, CH_2), -1.92(s, OSiPhMeH).

Table 4.7. Summary of crystallographic data for **2** and **3**

	2	**3**
empirical formula	$C_{42}H_{37}MoN_4O_2P_2$, $0.5(Cl_6Zn_2)$, C_7H_8	$2(C_{42}H_{37}MoN_4O_2P_2)$, $2(C_{32}H_{12}BF_{24})$, C_5H_{12}
formula weight ($g\cdot mol^{-1}$)	1051.51	3373.87
temperature (K)	183(2)	183(2)
wavelength (Å)	0.71073	0.71073
crystal system, space group	monoclinic, $P\ 2_1/c$	triclinic, P -1
a (Å)	20.0576(4)	12.4979(2)
b (Å)	14.3652(3)	15.4233(3)
c (Å)	17.2290(4)	19.7740(4)
α (deg)	90	88.382(2)
β(deg)	95.415(2)	81.163(2)
γ(deg)	90	87.527(1)
volume ($Å^3$)	4942.06(18)	3761.96(12)
Z, density (calcd) ($Mg\cdot m^{-3}$)	4, 1.413	1, 1.489
abs coefficient (mm^{-1})	1.008	0.325
F(000)	2144	1702
crystal size (mm^3)	0.26 x 0.21 x 0.03	0.38 x 0.32 x 0.23
θ range (deg)	2.48 to 25.68	2.64 to 30.51
reflections collected	36864	66387

reflections unique	9379 / R_{int} = 0.0898	22919 / R_{int} = 0.0268
completeness to θ (%)	99.9	99.9
absorption correction	analytical	analytical
max/min transmission	0.974 and 0.812	0.941 and 0.908
data / restraints / parameters	5081 / 85 / 602	17440 / 184 / 1025
goodness-of-fit on F^2	0.916	1.115
final R_1 and wR_2 indices [$I > 2\sigma(I)$]	0.0620, 0.0893	0.0480, 0.1423
R_1 and wR_2 indices (all data)	0.1531, 0.1070	0.0637, 0.1478
largest diff. peak and hole (e·Å^{-3})	1.101 and -0.624	1.143 and -0.855

The unweighted R-factor is $R_1 = \Sigma(Fo - Fc)/\Sigma Fo$ and the weighted R-factor is $wR_2 = \{\Sigma w(Fo^2 - Fc^2)^2/\Sigma w(Fo^2)^2\}^{1/2}$

Table 4.8. Crystallographic data for **4t**, and **5.**

	4t	**5**
empirical formula	$C_{76}H_{62}Cl_2Mo_2N_4O_4P_4$, $2(C_{32}H_{12}BF_{24})$, C_5H_{12}, C_6H_5Cl	$C_{38}H_{28}ClMoNO_4P_2$, C_7H_8
formula weight (g·mol^{-1})	3393.10	848.08
temperature (K)	183(2)	183(2)
wavelength (Å)	0.71073	0.71073
crystal system, space group	triclinic, $P\bar{1}$	monoclinic, $P\,2_1/c$
a (Å)	16.0776(9)	11.5883(1)
b (Å)	17.0716(13)	13.8586(1)
c (Å)	18.0135(14)	24.9475(2)
α (deg)	105.257(7)	90
B (deg)	115.011(7)	101.155(1)
γ (deg)	98.938(5)	90
volume (Å^3)	4116.7(6)	3930.82(5)
Z, density (calcd) (Mg·m^{-3})	1, 1.369	4, 1.433

abs coefficient (mm^{-1})	0.344	0.528
F(000)	1706	1736
crystal size (mm^3)	0.38 x 0.28 x 0.06	0.28 x 0.12 x 0.12
θ range (deg)	2.82 to 25.03	2.58 to 30.51
reflections collected	43069	67377
reflections unique	14519 / R_{int} = 0.0745	12004 / R_{int} = 0.0321
completeness to θ (%)	99.8	99.9
absorption correction	analytical	analytical
max/min transmission	0.978 and 0.914	0.944 and 0.891
data / restraints / parameters	10291 / 238 / 1064	9437 / 3 / 498
goodness-of-fit on F^2	1.179	1.081
final R_1 and wR_2 indices [$I > 2\sigma(I)$]	0.1156, 0.2968	0.0323, 0.0809
R_1 and wR_2 indices (all data)	0.1467, 0.3276	0.0450, 0.0834
largest diff. peak and hole ($e \cdot Å^{-3}$)	6.031 and -1.128	0.602 and -0.688

The unweighted R-factor is $R_1 = \sum(Fo - Fc)/\sum Fo$ and the weighted R-factor is $wR_2 = \{\sum w(Fo^2 - Fc^2)^2/\sum w(Fo^2)^2\}^{1/2}$

Table 4.9. Crystallographic data for **6**, and **7**

	6	**7**
empirical formula	$2(C_{39}H_{37}ClMoNO_2P_3)$, $C_4H_{10}O$	$C_{54}H_{43}ClMoNO_2P_3$
formula weight ($g \cdot mol^{-1}$)	1626.11	962.19
temperature (K)	183(2)	183(2)
wavelength (Å)	0.71073	0.71073
crystal system, space group	monoclinic, $P\,2_1/n$	monoclinic, $P\,2_1/n$
a (Å)	10.2639(1)	19.3956(3)
b (Å)	21.2569(3)	12.6738(2)
c (Å)	18.3320(3)	20.4746(3)
α(deg)	90	90

β(deg)	105.192(2)	114.639(2)
γ (deg)	90	90
volume (Å^3)	3859.88(10)	4574.74(14)
Z, density (calcd) (Mg·m^{-3})	2, 1.399	4, 1.397
abs coefficient (mm^{-1})	0.571	0.493
F(000)	1676	1976
crystal size (mm^3)	0.26 x 0.16 x 0.07	0.44 x 0.34 x 0.20
θ range (deg)	2.49 to 26.37	2.57 to 30.51
reflections collected	47560	96389
reflections unique	7882 / R_{int} = 0.0490	13957 / R_{int} = 0.0307
completeness to θ (%)	99.9	99.9
absorption correction	analytical	analytical
max/min transmission	0.964 and 0.899	0.935 and 0.870
data / restraints / parameters	5943 / 166 / 547	11579 / 4 / 569
goodness-of-fit on F^2	1.052	1.080
final R_1 and wR_2 indices [$I > 2\sigma(I)$]	0.0472, 0.1100	0.0270, 0.0714
R_1 and wR_2 indices (all data)	0.0696, 0.1160	0.0361, 0.0733
largest diff. peak and hole (e·Å^{-3})	1.528 and -0.725	0.393 and -0.610

The unweighted R-factor is $R_1 = \Sigma(Fo - Fc)/\Sigma Fo$ and the weighted R-factor is $wR_2 = \{\Sigma w(Fo^2 - Fc^2)^2/\Sigma w(Fo^2)^2\}^{1/2}$

4.6 REFERENCES

(1) Chalk, A. J.; Harrod, J. F. *J. Am. Chem. Soc.* **1965**, *87*, 16.

(2) (a)Ojima, I.; Nihonyanagi, M.; Nagai, Y. *J. Chem. Soc., Chem. Commun*. **1972**, *938*. (b) Ojima, I.; Nihonyanagi, M.; Kogure, T.; Kumagai, M.; Horiushi, S.; Nakatsugawa, K. *J. Organomet. Chem*. **1975**, *94*, 449. (c) Ojima, I.; Kogure, T. *Organometallics* **1982**, *1*, 1390. d) Ojima, I.; Kogure, T.; Kumagai, M.; Horiuchi, S.; Sato, Y. *J. Organomet. Chem.* **1976**, *122*, 83.

(3) Berc, S. C.; Kreutzer, K. A.; Buchwald, S. L. *J. Am. Chem. Soc*. **1991**, *113*, 5093.

(4) Zheng, G. Z.; Chan, T. H. *Organometallics* **1995**, *14*, 70.

(5) (a) Kennedy-Smith, J. J.; Nolin, K. A.; Gunterman, H. P.; Toste, F. D. *J. Am. Chem. Soc*., **2003**, *125*, 4056. (b) Nolin, K. A.; Krumper, J. R.; Pluth, M. D.;. Bergman, R. G; Toste, F. D. *J. Am. Chem. Soc.* **2007**, *129*, 14684. (c) Nolin, K. A. Ahn, R. W.; Kobayashi, Y. Kennedy-Smith, J. J.; Toste, F. D.; *Chem. Eur. J*. **2010**, *16*, 9555.

(6) (a) Glaser, P. B.; Tilley, T. D. *J. Am. Chem. Soc*. **2003**, *125*, 13640-13641. (b) Elisa Calimano, E.; Tilley, T. D. *Organometallics* **2010**, *29*, 1680-1692.

(7) (a) Corma, A.; Gonzalez-Arellano, C.; Iglesias, M.; Sanchez, F. *Angew. Chem. Int. Ed*. **2007**, *46*, 7820 – 7822. (b) Shaikh, N. S.; Enthaler, S.; Junge, K.; Beller, M. *Angew. Chem. Int. Ed*. **2008**, *47*, 2497 – 2501. (c) Han, J. W.; Tokunaga, N.; Hayashi, T. *J. Am. Chem. Soc*. **2001**, *123*, 12915 – 12916. (d) Jensen, J. F.; Svendsen, B. Y.; Cour, T. V.; Pedersen, H. L.; Johannsen, M. *J. Am. Chem. Soc*. **2002**, *124*, 4558-4559. (e) Flückiger, M. ; Antonio Togni, A. *Eur. J. Org. Chem.* **2011**, 4353 – 4360. (f) Junge, K.; Wendt, B.; Addis, D.; Zhou, S.; Das, S.; Beller, M. *Chem. Eur. J*. **2010**, *16*, 68-73.

(8) (a) Ison, E. A.; Trivedi, E. R.; Corbin, R. A.; Abu-Omar, M. M. *J. Am. Chem. Soc*. **2005**, 127, 15374. (b) Du, G.; Fanwick, P. E.; Abu-Omar, M. M. *J. Am. Chem. Soc*. **2007**, *129*, 5180.

(9) (a) Roesler, R.; Har, B. J. N.; Piers, W. E. *Organometallics,* **2002**, *21*, 4300. (b) Song, Young-S.; Yoo, B. R.; Lee, Gyu-H.; Jung, N. *Organometallics* **1999**, *18*, 3109-3115. (c) D. J. Parks, J. M. Blackwell, W. E. Piers, *J. Org. Chem.* **2000**, *65*, 3090 - 3098; (d) M. Rubin, T. Schwier, V. Gevorgyan, *J. Org. Chem.* **2002**, *67*, 1936-1940; (e) N. Asao, T. Sudo, Y. Yamamoto, *J. Org. Chem.* **1996**, *61*, 7654-7655.

(10) (a) Gigler, P.; Bechlars, B.; Herrmann, W. A.; Kühn, F. E. *J. Am. Chem. Soc*. **2011**, *133*, 1589-1596. (b) Do, Y.; Han, J.; Rhee, Y. H.; Park, J. *Adv. Synth. Catal*. **2011**, *353*, 3363 – 3366; c) Hashimoto, H.; Atani, I.; Kabuto, C.; Mitsuo Kira,M. *Organometallics* **2003**, *22*, 2199-2201. (d) Park, S.; Brookhart, M. *Organometallics* **2010**, *29*, 6057-6064. (e) Gutsulyak, D. V.; Sergei, F.; Vyboishchikov, S. F.; Nikonov, G. I. *J. Am. Chem. Soc*. **2010**, *132*, 5950–5951. (f) Nishibayashi, Y.; Takei, I.; Uemura, A.; M. Hidai, M. *Organometallics* **1998**, *17*, 3420-3422. (g) Riener, K.; Högerl, M. P.; Gigler, P.; Kühn, F. E.; *ACS Catal*. **2012**, *2*, 613 −

621. (h) Gibson, S. E.; Rudd, M.; *Adv. Synth. Catal*. **2007**, *349*, 781. (i) Marciniec, B. *Comprehensive Handbook on Hydrosilylation*, Pergamon, Oxford, **1992**.

(11) (a) Yang, J.; Tilley, T. D.; *Angew. Chem. Int. Ed*. **2010**, *49*, 10186; (b) Shaikh, N. S.; Enthaler, S.; Junge, K.; Beller, M.; *Angew*. *Chem. Int. Ed*. **2008**, *47*, 5429. (c) Bhattacharya, P.; Krause, J. A.; Guan, H.; *Organometallics* **2011**, 30, 4720–4729. (d) Buitrago, E.; Tinnis, F.; Adolfsson, H.; *Adv. Synth. Catal*. **2012**, *354*, 217 – 222. (e) Jessica Y. Wu, J. Y.; Stanzl, B. N.; Ritter, T.; *J. Am. Chem. Soc*. **2010**, *132*, 13214 – 13216. (f) Dieskau, A. P.; Begouin, J. M.; Plietker, B.; *Eur. J. Org. Chem.* **2011**, 5291 – 5296. (g) Kamata, K.; Suzuki, A.; Nakai, Y.; Nakazawa, H.; *Organometallics* **2012**, 31, 3825−3828. (h) Hashimoto, T.; Urban, S.; Hoshino, R.; Ohki, Y.; K. Kazuyuki Tatsumi, K.; Glorius, F.; *Organometallics* dx.doi.org/10.1021/om300298q; i) A. M. Tondreau, E. Lobkovsky, P. J. Chirik, *Org.lett*. **2008**, *19*, 2789-2792.

(12) (a) Carter, M. B.; Schiøtt, B.; Gutiérrez, A.; Buchwald, S. L.; *J. Am. Chem. Soc*., **1994**, 116, 11667. (b) Yun, J.; Buchwald, S. L.; *J. Am. Chem. Soc.*, **1999**, *121*, 5640. (c) Halterman, R. L.; Ramsey, T. M.; Chen, Z.; *J. Org. Chem.* **1994**, *59*, 2642–2644. (d) Kesti, M. R.; Waymouth, R. H. *Organometallics* **1992**, *11*, 1095-1103.

(13) (a) Dioumaev, V. K.; Bullock, R. M.; *Nature,* **2000**, *424* 530-532. (b) Fernandes, A. C.; Fernandes, R.; Romão, C. C.; Royo, B.; *Chem. Commun.*, **2005**, 213-214. (b) Reis, P. M.; Romão, C. C.; Royo, B.; *Dalton Trans.* **2006**, 1842 –1846. (c) Ziegler, J. E.; Du, G.; Fanwick, P. E.; Abu-Omar, M. M.; *Inorg. Chem*. **2009**, *48*, 11290;. (d) Costa, P. J.; Romão, C. C.; Fernandens, A. C.; Royo, B.; Reis, P.; Calhorda, M. J.; *Chem.-Eur. J.* **2007**, *13*, 3934. (g) Shirobokov, O. G.; Kuzmina, L. G.; Nikonov, G. I.; *J. Am.Chem. Soc*. **2011**, 133. (h) Khalimon, A. Y.; Ignatov, S. K.; Simionescu, R.; Kuzmina, L. G.; Howard, J. A. K.; Nikonov, G. I. *Inorg. Chem*. **2012**, 51, 754−756. (i) Khalimon, A. Y.; Shirobokov, O. G.; Peterson, E.; R. Simionescu, R.; Kuzmina, L. G.; Howard, J. A. K.; Nikonov, G. I.; .dx.doi.org/10.1021/ic300010c *Inorg. Chem.*

(14) (a) Peterson, E.; Khalimon, A. Y.; Simionescu, R.; Kuzmina, L. G.; Howard, J. A. K.; Nikonov, G. I. *J. Am. Chem. Soc*. **2009**, *131*, 908. (b) Shirobokov, O. G.; Simionescu, R.; Kuzmina, L. G. Nikonov, G. I. *Chem. Commun*. **2010**, *6*, 7831.

(15) (a) Jiang, Y.; Hess, J.; Fox, T.; Berke, H.; *J. Am. Chem. Soc*. **2010**, *132*, 18233–18247. (b) Choualeb, A.; Maccaroni, E.; Blacque, O.; Schmalle, H. W.; Berke, H.; *Organometallic*s **2008**, *27*, 3474–3481.

(16) (a) Dong, H.; Berke, H.; *Adv. Synth. Catal*. **2009**, *351*, 1783 – 1788. (b) Jiang, Y.; Berke, H.; *Chem. Commun*. **2007**, 3571 – 3573. (b) W. J. Huang, H. Berke, Chimia **2005**, 59, 113 – 115.

(17) Jiang, Y.; Blacque, O., Fox, T.; Frech, C. M.; H. Berke, H.; Chem.-Eur. J. **2009**, *15*, 2121 – 2128.

(18) Jiang, Y.; Blacque, O.; Fox, T.; Frech, C. M.; Berke, H.; *Organometallic*s **2009**, 28, 5493 – 5504.

(19) Dybov, A.; Blacque, O.; Berke, H.; *Eur. J. Inorg. Chem.* **2011**, 652-659.

(20) Dudle, B.; Rajesh, K.; Blacque, O.; Berke, H.;*J. Am. Chem. Soc*. **2011**, *133*, 8168–8178.

(21) (a) Adams, R. D.; Collins, D. M. Cotton, F. A.; *Inorg. Chem.*, **1974,** *13*, 1086. (b) Adams, R. D.; Brice, M.; Cotton, F. A.; *J . Amer. Chem. Soc*., **1973**, *95*, 6594. (b) Mathew M.; Palenik, G. J.; *J . Organometallic Chem.*, **1973,** *61***,** 301**.** (c) Bowerbank, R.; Green, M.; Kirsch, H. P.; André, M.; Smart, L. E.; Stone, F. G. A. *J.C.S. Chem Comm.* **1977,** 245.

(22) (a) Ledger, A. E. W.; Moreno, A.; Ellul, C. E.; Mahon, M. F.; Pregosin, P. S.; Whittlesey, M. K.; Williams, J. M. J.; *Inorg. Chem*. **2010**, *49*, 7244–7256. (b) Dallanegra, R.; Chaplin, A. B.; Weller, A. S.; *Organometallics* **2012**, *31*, 2720−2728.

(23) (a) Hammett, L. P. *J. Am. Chem. Soc*. **1937**, *59*, 96 – 103. (b) Hammett, L. P. *Chem. Rev*. **1935**, *17*, 125 – 136. (c) Hansch, C. Leo, A.; Taft, R. W. *Chem. Rev.* **1991**, *91*, 165-195. (d) Yang, X.; Zhao, L.;. Fox, T.; Wang, Z.-X.; Berke, H. *Angew. Chem. Int. Ed*. **2010**, *49*, 2058.

(24) (a) Kranenburg, M.; Burgt, Y. E. M. van der; Kamer, P. C. J.;. van Leeuwen, P. W. N. M. *Organometallics* **1995**, *14*, 3081-3089. (b) L. Bencze, J. Kohan, Inorg. *Chim. Acta*, **1982,** 65, L17-L19.

(25) Agilent Technologies (formerly Oxford Diffraction), Yarnton, Oxfordshire, England, **2012**.

(26) Clark, R. C.; Reid, J. S. Acta Crystallographica Section A **1995**, **51**, 887.

(27) *CrysAlisPro*, Version 1.171.36.20, Agilent Technologies, Yarnton, Oxfordshire, England, **2012**.

(28) Sheldrick, G. Acta Crystallographica Section A **2008**, *6*4, 112.

(29) Spek, A. L. J Appl Crystallogr **2003**, *36*, 7.

(30) Farrugia, L. J Appl Crystallogr **1999**, *3*2, 837.

5.1 SUMMARY

The search for alternatives to platinum group metal catalyses became in recent years more and more intense and expected to experience increased growth in the future. The most obvious reason for replacing these platinum group metals is that they are very expensive. The high cost is obviously connected to the low abundance of these metals. Substantial costs are involved in industrial processes when recovery and recycle of the metal is required. In this perspective, the "middle transition elements" which are the "rising stars" in modern homogeneous catalysis field are apt for replacing the platinum group metals. The research presented in this thesis shows the potential of new catalysts that do not require precious metals may ultimately supplant the use of precious metals in Wilkinson and Osborn type hydrogenations, Bullock type ionic hydrogenations, Noyori type bifunctional hydrogenation and Ojima type hydrosilylation reactions.

Preparation of a new class of molybdenum and tungsten nitrosyl complexes were realised bearing a tridentate ($^{i}Pr_2PCH_2CH_2)_2PPh$, (etp^{i}p) ligand. Pentagonal bipyramidal complexes M(NO)Cl_3(etp^{i}p) (M = Mo, **3a**; W, **3b**) were isolated as isomeric mixtures starting from the precursors M(NO)$Cl_3(NCMe)_2$ (M = Mo, W)**. 3a** and **3b** were reduced to 17 e^- rare paramagnetic complexes Mo(NO)Cl_2(etp^{i}p), **4a** and W(NO)Cl_2(etp^{i}p), **4b** showing characteristic paramagnetic behavior determined by EPR spectroscopy, as well as by SQUID measurements. Treatment of 1% Na/Hg to the THF solutions of **3a** and **3b** in the presence of 1 bar carbon monoxide at room temperature led to the formation of low-valent Mo(NO)(CO)Cl(etp^{i}p), **6a** and W(NO)(CO)Cl(etp^{i}p), **6b** complexes. Reduction of **3a,b** with 1% Na/Hg under 1 bar ethylene furnished the ethylene coordinated complexes Mo(NO)Cl(η^2-ethylene)(etp^{i}p), **7a** and W(NO)Cl(η^2-ethylene)(etp^{i}p), **7b**. The reaction of the **7a** with $NaHBEt_3$ at 75°C revealed formation of the hydride complex Mo(NO)H(η^2-ethylene)(etp^{i}p), **8a**. On the other hand $LiBH_4/Et_3N$ combination was found to be suitable to prepare W(NO)H(η^2-ethylene)(etp^{i}p), **8b** complex from **7b**. **8a** and **8b** were found to be highly efficient for the hydrogenation of several olefins. A maximum TOF of 5253 h^{-1} was achieved for the hydrogenation of 1-hexene using **8a** and $Et_3SiH/B(C_6F_5)_3$ mixture as cocatalyst under 60 bar H_2 and 140 °C and for 8b a maximum TOF of 8000 h^{-1} could be achieved for the hydrogenation of 1-hexene under the similar condition. Two hydride complexes Mo(NO)(CO)H(etp^{i}p), **11a** and W(NO)(CO)H(etp^{i}p), **11b** were also prepared from **6a** and **6b** using $LiBH_4$ in Et_3N at elevated temperature. **11a** and **11b**

were tested for the catalytic hydrogenation of imines in the presence of $[H(Et_2O)_2][B(C_6F_5)_4]$ as a cocatalyst. A maximum TOF of 1960 h^{-1} was reached for the hydrogenation of *N*-(4-methoxybenzylidene)aniline using a mixture of **11a** and a stoichiometric amount of $[H(Et_2O)_2][B(C_6F_5)_4]$. Contrary to this, the tungsten catalyst **11b** showed generally lower activities than **11a** with a maximum TOF of 740 h^{-1} for the hydrogenation of *N*-(4-methoxybenzylidene)aniline. An "ionic" mechanism with heterolytic splitting of H_2 and "proton before hydride" transfer has been proposed.

Furthermore, synthetic access to several amino and amido complexes of molybdenum and tungsten bearing $(i\text{Pr}_2\text{PCH}_2\text{CH}_2)_2\text{NH}$, ($\text{PN}^H\text{P}$) ligand and their catalytic application in bifunctional hydrogenation of imines were demonstrated in this dissertation. $\text{M(NO)(CO)(PN}^H\text{P)Cl}$ (M = Mo, **1a**; W, **1b**) complexes were accessed via reaction of the precursors $\text{M(NO)(CO)}_4(\text{ClAlCl}_3)$ (M = Mo, W) with $(i\text{Pr}_2\text{PCH}_2\text{CH}_2)_2\text{NH}$, ($\text{PN}^H\text{P}$). Attempts to deprotonate the N-H ligand backbone of **1a** using KO*t*Bu base failed which yielded the alkoxide complex $\text{Mo(NO)(CO)(PN}^H\text{P)(O}t\text{Bu)}$ **2a**. The acidic H_N protons of the PN^HP ligand moieties of **1a** and **1b** were deprotonated at room temperature using the comparatively strong and sterically amide base $\text{Na[N(SiMe}_3)_2]$ inducing dehydrochlorination to the highly reactive unsaturated 16 e^- amido complexes M(NO)(CO)(PNP) (M = Mo, **3a**; W, **3b**; PNP = $[i\text{Pr}_2\text{PCH}_2\text{CH}_2)_2\text{N}]$). At room temperature **3a** and **3b** are capable of adding dihydrogen with heterolytic splitting forming pairs of isomeric amine hydride complexes $\text{Mo(NO)(CO)H(PN}^H\text{P)}$ {**4a(*cis*)** and **4a(*trans*)**} and $\text{W(NO)(CO)H(PN}^H\text{P)}$ {**4b(*cis*)** and **4b(*trans*)**}. **3a** and **3b** also reacted with carbon dioxide at room temperature forming M(NO)(CO)(PNP)(OCO) carbamate complexes (M = Mo, **5a(*cis*)**; M = W, **5b(*cis*)**) which possess stable four-membered cycles. The amine hydride complexes {**4a,b**(*cis* and *trans*)**}** were reacted with CO_2 (2 bar) to form the η^1-formato complexes $\text{M(NO)(CO)(PN}^H\text{P)(OCHO)}$, (M = Mo, **6a(*cis*)** and **6a(*trans*)**; M = W, **6b(*cis*)** and **6b(*trans*)**). The reaction of the formato complexes {**6a(*cis*)** and **6a(*trans*)**; M = W, **6b(*cis*)** and **6b(*trans*)**} with 1 equiv. of the $\text{Na[N(SiMe}_3)_2]$ base regenerates the amido complexes **3a** and **3b** with concomitant formation of sodium formate salt. **3a** and **3b** were found to be efficient catalysts in imime hydrogenations. At 140 °C and a pressure of 60 bar showed a maximum TOF value of 2912 h^{-1} in the hydrogenation of *N*-(4-methoxybenzylidene)aniline using **3a** as the catalyst. **3b** furnished a maximum TOF value of 1120 h^{-1} in the hydrogenation of *N*-(4-methoxybenzylidene)aniline under the same conditions. A Hammett plot for various *para*

substituted imines revealed linear correlations with a negative slope of -3.69 for *para* substitution on the benzylidene side and a positive slope of 0.68 for *para* substitution on the aniline side. Kinetics revealed the initial rate of the hydrogenations to be 1st order in c(cat) and c(H_2) and zeroth order in c(imine). Deuterium kinetic isotope effect experiments (DKIE) furnished a low k_H/k_D value (1.28) which among other facts made a Noyori type metal-ligand bifunctional mechanism plausible, where H_2 addition to **3a** or **3b** is supposed to be rate limiting.

Finally in the last part of our research we reported a large bite angle 2,2′-bis(diphenylphosphino)diphenylether (DPEphos) ligand based highly efficient molybdenum based catalyst for hydrosilylation reactions. A dinuclear species $[Mo(NO)(P\cap P)Cl_2]_2[\mu Cl]_2$ (P∩P = DPEphos = $(Ph_2PC_6H_4)_2O$) (**1**) was isolated when $Mo(NO)Cl_3(NCMe)_2$ was reacted with the diphosphine, 2,2′-bis(diphenylphosphino)diphenylether (DPEphos) ligand. **1** was reduced in the presence of Zn and MeCN to the cationic complex $[Mo(NO)(P\cap P)(NCMe)_3]^+[Zn_2Cl_6]^{2-}{}_{1/2}$ (**2**). In a metathetical reaction the $[Zn_2Cl_6]^{2-}{}_{1/2}$ counteranion was replaced with $NaBAr^F{}_4$ ($BAr^F{}_4$ = $[B\{3,5\text{-}(CF_3)_2C_6H_3\}_4]$) to obtain the $[BAr^F{}_4]^-$ salt $[Mo(NO)(P\cap P)(NCMe)_3]^+[BAr^F{}_4]^-$ (**3**). Reaction of **3** with chlorobenzene led at 120 °C to formation of the cationic dinuclear species $[Mo(NO)(P\cap P)(NCMe)]_2[\mu Cl]_2{}^{2+}$ $2[BAr^F{}_4]^-$ showing *transoid* (**4t**) and *cisoid* (**4c**) regio isomeres with respect to the position of the NO ligand. **3** was found to catalyse hydrosilylations of various *para* substituted benzaldehydes, cyclohexanecarboxaldehyde, 2-thiophenecarboxaldehyde, and 2-furfural at 120 °C. Also ketones could be hydrosilylated even at room temperature using **3** and $PhMeSiH_2$. A maximum TOF of 3.2×10^4 h^{-1} at 120 °C and of 4400 h^{-1} was obtained at room temperature for the hydrosilylation of 4-methoxyacetophenone using $PhMeSiH_2$ in the presence of **3**. Kinetic studies revealed the reaction rate to be first order each with respect to the catalyst and silane concentrations and zero order with respect to the substrate concentrations. A Hammett study for various *para* substituted acetophenones was also carried out which showed linear correlations with negative ρ values of -1.14 at 120 °C and -3.18 at room temperature.

This thesis explored the versatility of the earth abundant middle transition elements molybdenum and tungsten as catalysts in hydrogenations of olefins, "Noyori type" bifunctional hydrogenations of imines, stepwise ionic hydrogenation of imines and hydrosilylation of aldehydes and ketones. We believe that this thesis work will contribute significantly to new and beneficial developments regarding the issue of "Cheap Metals for Noble Tasks".

5.2 Zusammenfassung

Die Suche nach Alternativen zur Platingruppen-basierten Katalyse nahm in den letzten Jahren mehr und mehr zu und es lässt sich erwarten, dass dieser Trend auch in Zukunft zunimmt. Der augenscheinlichste Grund Platingruppenmetalle zu ersetzen, liegt in ihren hohen Kosten begründet. Die hohen Kosten stehen in Verbindung mit ihrem geringen natürlichem Verkommen. Substantielle Kosten entstehen ebenfalls, wenn das Metall in industriellen Prozessen wiedergewonnen und "recycled" werden muss. Aus dieser Perspektive sind die mittleren Übergangsmetalle, welche die "aufsteigenden Sterne" in der modernen homogenen Katalyse sind, in der Lage die Platinmetalle zu ersetzen. Die in dieser Arbeit vorgestellten neuen Katalysatoren, welche keine Edelmetalle enthalten, zeigen das Potential, wertvolle Metalle in Wilkinson- und Osborn-artigen Hydrierungen, Bullock-artiken ionische Hydrierung, Noyori-artigen bifunktionelle Hydrierung und Ojima-artigen Hydrosilylierung letztendlich zu ersetzen.

Die Darstellung einer neuen Klasse von Molybdän- und Wolframnitrosylkomplexe mit dreizähnigen ($^{i}Pr_2PCH_2CH_2)_2PPh$ (etp^{i}p) Ligand wurde erfolgreich durchgeführt. Pentagonale bipyramidale Komplexe $M(NO)Cl_3$(etp^{i}p) (M = Mo, **3a**; W, **3b**) werden ausgehend von den Startmaterialien $M(NO)Cl_3(NCMe)_2$ (M = Mo, W) wurden als isomere Mischung isoliert**. 3a** und **3b** wurden zu seltenen, paramagnetischen 17 Elektronenkomplexen $Mo(NO)Cl_2$(etp^{i}p) **4a** and $W(NO)Cl_2$(etp^{i}p) **4b** reduziert. Diese zeigen charakteristisches paramagnetisches Verhalten, welches durch ESR- und SQUID-Untersuchungen gezeigt werden konnte. Behandlung der THF-Lösung von **3a** und **3b** mit 1% Na/Hg in Gegenwart von 1 bar Kohlenmonoxid bei Raumtemperatur führte zur Bildung niedrigvalenter Komplexe Mo(NO)(CO)Cl(etp^{i}p) **6a** und W(NO)(CO)Cl(etp^{i}p) **6b**. Reduktion von **3a,b** mit 1% Na/Hg unter 1 bar Ethen ergab die Ethenylkomplexe, Mo(NO)Cl(η^2-ethylene)(etp^{i}p) **7a** und W(NO)Cl(η^2-ethylene)(etp^{i}p) **7b**. Die Reaktion von **7a** mit $NaHBEt_3$ bei 75 °C ergab den Hydridkomplex Mo(NO)H(η^2-ethylene)(etp^{i}p) **8a**. Anderseits war die Kombination $LiBH_4/Et_3N$ geeignet zur Darsteleung des Komplexes W(NO)H(η^2-ethylene)(etp^{i}p) **8b** aus **7b**. **8a** und **8b** zeigten eine hohe Effizienz bei der Hydrierung vieler Olefine. Ein maximaler TOF-Wert von 5253 h^{-1} wurde bei der Hydrierung von 1-Hexen durch **8a** und $Et_3SiH/B(C_6F_5)_3$ als Co-Katalysator unter 60 bar H_2 bei 140 °C und für **8b** eine maximale TOF von 8200 h^{-1} bei der Hydrierung von 1-Hexene unter gleichen Bedingungen erreicht. Die zwei Hydridkomplexe Mo(NO)(CO)H(etp^{i}p) **11a** und W(NO)(CO)H(etp^{i}p) **11b** wurden aus **6a** und **6b** mit $LiBH_4$ in Et_3N bei erhöhten Temperaturen

dargestellt. **11a** und **11b** wurden bezüglich der katalytischen Hydrierung von Iminen in Gegenwart von $[H(Et_2O)_2][B(C_6F_5)_4]$ als Co-Katalysator untersucht. Eine maximale TOF von 1960 h^{-1} wurde bei der Hydrierung von *N*-(4-methoxybenzyliden)anilin mit einer Mischung von **11a** und stoichiometrischen Mengen $[H(Et_2O)_2][B(C_6F_5)_4]$ erzielt. Im Gegesatz dazu zeigte der Wolfamkomplex **11b** generell geringere Aktivitäten als **11a** mit einer maximalen TOF von 740 h^{-1} bei der Hydrierung von *N*-(4-methoxybenzyliden)anilin. Ein "ionischer" Mechanismus mit heterolytischer H_2-Spaltung und "Proton vor Hydrid"-Übertragung wurde hier vorgeschlagen.

Desweiteren wurden verschieden Amino- und Amidokomplexe mit Molybdän und Wolfram als Metallzentren und dem $(i\text{Pr}_2\text{PCH}_2\text{CH}_2)_2\text{NH}$ (PN^HP) Liganden synthetisch zugänglich und ihre katalytische Verwendung in bifunktioneller Hydrierung von Iminen konnte in dieser Arbeit demonstriert werden. M(NO)(CO)(PN^HP)Cl (M = Mo, **1a**; W, **1b**) Komplexe wurden durch die Reaktion der Startmaterialien $M(NO)(CO)_4(ClAlCl_3)$ (M = Mo, W) mit dem $(i\text{Pr}_2\text{PCH}_2\text{CH}_2)_2\text{NH}$ Liganden, (PN^HP) dargestellt. Versuche die N-H Gruppe des Liganden von **1a** mit KO*t*Bu zu deprotonieren schlugen fehl und führten zum Alkoxidkomplex Mo(NO)(CO)(PN^HP)(O*t*Bu) **2a**. Die aciden H_N-Protonen des PN^HP-Liganden von **1a** und **1b** konnten bei Raumtemperatur mit der vergleichsweise starken, sterisch anspruchsvollen Amidbase $Na[N(SiMe_3)_2]$ unter Dehydrochlorierung zu hochreaktiven, ungesättigten 16-Elektronen Amidokomplexen M(NO)(CO)(PNP) (M = Mo, **3a**; W, **3b**; PNP = $[i\text{Pr}_2\text{PCH}_2\text{CH}_2)_2\text{N}]$) deprotoniert werden. Bei Raumtemperatur sind **3a** und **3b** fähig, Wasserstoff unter heterolytischer Spaltung zu übertragen und so Paare von isomeren Mo(NO)(CO)H(PN^HP) {**4a(*cis*)** und **4a(*trans*)**} und W(NO)(CO)H(PN^HP) {**4b(*cis*)** und **4b(*trans*)**} auszubilden. **3a** und **3b** reagierten ebenfalls mit Kohlendioxid bei Raumtemperatur unter Bildung der cyclischen M(NO)(CO)(PNP)(OCO)-Carbamatkomplexe (M = Mo, **5a(*trans*)**; M = W, **5b(*trans*)**) welche stabile Vierringe besitzen. Die Aminhydridkomplexe {**4a,b**(*cis* und *trans*)**}** wurden mit CO_2 (2 bar) zu η^1-Formatokomplexen M(NO)(CO)(PN^HP)(OCHO), (M = Mo, **6a(*cis*)** und **6a(*trans*)**; M = W, **6b(*cis*)** und **6b(*trans*)**) umgesetzt. Die Reaktion der Formatokomplexe {**6a(*cis*)** und **6a(*trans*)**; M = W, **6b(*cis*)** und **6b(*trans*)**} mit 1 equiv. $Na[N(SiMe_3)_2]$ führte zur Regeneration der Amidokomplexe **3a** und **3b** unter gleichzeitiger Bildung von Natriumformat. **3a** und **3b** zeigten effiziente Iminhydrierungskatalyse. Bei 140 °C und einem Druck von 60 bar wurde ein maximaler TOF-Wert von 2912 h^{-1} bei der Hydrierung von *N*-(4-methoxybenzyliden)anilin für **3a** als Katalysator erhalten. **3b** erzielte einen maximalen TOF-Wert von 1120 h^{-1} bei der

Hydrierung von *N*-(4-methoxybenzyliden)anilin unter gleichen Bedingungen. Ein Hammett-Plot für verschiedene *para*-substituierte Imine ergab einen linearen Zusammenhang mit negativer Steigung von -3.69 für die *para*-Substitution auf der Benzyliden Seite und eine positive Steigung von 0.68 für die *para*-Substitution auf der Anilin Seite. Kinetische Untersuchungen ergaben, dass die Anfangsgeschwindigkeit der Hydrierungen erster Ordnung in c(Kat) und c(H_2) und nullter Ordnung in c(Imin) waren. Kinetische Deuterium-Isotopeffekt-Experimente (DKIE) ergaben einen niedrigen k_H/k_D-Wert (1.28), welche unter anderem einen Noyori-artigen Metall-Liganden bifunktionellen Mechanismus wahrscheinlich machen, bei der die H_2-Addition an **3a** oder **3b** wahrscheinlich geschwindigkeitsbestimmend ist.

Schliesslich wird im letzten Teil dieser Arbeit über einen Molybdän-basierten Komplex mit einem grossen Bisswinkel-Liganden 2,2′-Bis(diphenylphosphino)diphenylether (DPEphos) berichtet, der eine hohe katalytische Effizienz für Hydrosilylierungen zeigte. Eine dinukleare Spezies $[Mo(NO)(P\cap P)Cl_2]_2[\mu Cl]_2$ (P∩P = DPEphos = $(Ph_2PC_6H_4)_2O$) (**1**) wurde durch die Reaktion von $Mo(NO)Cl_3(NCMe)_2$ mit dem Diphosphin-Liganden 2,2′-bis(diphenylphosphino)diphenylether (DPEphos) dargestellt. **1** wurde in Gegenwart von Zink und MeCN zum kationischen Komplex $[Mo(NO)(P\cap P)(NCMe)_3]^+[Zn_2Cl_6]^{2-}{}_{1/2}$ (**2**) reduziert. Durch Ionenaustauschreaktion konnte das $[Zn_2Cl_6]^{2-}{}_{1/2}$-Gegenion durch $NaBAr^F{}_4$ ($BAr^F{}_4$ = $[B\{3,5\text{-}(CF_3)_2C_6H_3\}_4]$) ausgetauscht werden und so das $[BAr^F{}_4]^-$-Salz $[Mo(NO)(P\cap P)(NCMe)_3]^+[BAr^F{}_4]^-$ (**3**) isoliert werden. Die Reaktion von **3** mit Chlorbenzol bei 120 °C führte zur Bildung der kationischen, dinuklearen Spezies $[Mo(NO)(P\cap P)(NCMe)]_2[\mu Cl]_2{}^{2+}$ $2[BAr^F{}_4]^-$, welche ein *transoides* (**4t**) und ein *cisoides* (**4c**) Regioisomer in Bezug auf die Position des NO-Liganden besitzt. **3** katalysierte Hydrosilylierungen verschiedener *para*-substituierter Benzaldehyde, Cyclohexancarboxaldehyden, 2-thiophencarboxaldehyden und 2-Furfural bei 120 °C. Ketone konnten sogar bei Raumtemperatur unter Verwendung von **3** und $PhMeSiH_2$ hydrosilyliert werden. Eine maximaler TOF Wert von $3.2\cdot10^4$ h^{-1} bei 120 °C und von 4400 h^{-1} bei Raumtemperatur wurde für 4-Methoxyacetophenon mit $PhMeSiH_2$ in Gegenwart von **3** ermittelt. Kinetische Untersuchungen zeigten, dass die Reaktionsgeschwindigkeit erster Ordnung in Bezug auf Katalysator und der Silankonzentration war und nullter Ordnung bezüglich der Substratkonzentration. Eine Hammett-Experimente unit für verschiedenen *para*-substituierten Acetophenonen, ergaben einen linearen Zusammenhang mit negativen ρ-Werten von -1.14 bei 120°C und -3.18 bei Raumtemperatur.

Die vorliegende Arbeit untersucht die Vielseitigkeit als Katalysatoren der reichlich vorkommenden mittleren Übergangsmetalle Molybdän und Wolfram in Hydrierungen von Olefinen, "Noyori-artigen" bifunktionellen Hydrierung von Iminen, stufenweisen ionischen Hydrierung von Iminen und Hydrosilylierung von Aldehyden und Ketonen. Wir glauben, dass diese grundlegende Arbeit erheblich zur Entwicklung von neuen und vorteilhaften Katalysatoren unter dem motto "Billige Metalle für edle Augaben" beitragen wird.

ACKNOWLEDGEMENTS

I would like to thank several people who were involved in various ways during the accomplishment of my research work.

First of all, I would like thank a lot to my supervisor Prof. Heinz Berke for giving me the opportunity to work in his group and introducing me an interesting and challenging field of scientific research. I will remain indebted to him for ever for lot of scientific discussions, ideas, guidance towards proper directions, encouragement and support.

Appreciation is also gratefully expressed to Prof. Dr. Greta Patzke for her kind acceptance to co-referee this dissertation.

I thank to Dr. Olivier Blacque for solving lot of valuable crystal structures and also for the DFT calculations that he performed during my research work.

My thanks also goes to Dr. Thomas Fox for measuring plenty of NMR samples and for useful discussions regarding NMR spectra explanations.

I would like to extend my thanks to Heinz Spring and Barbara Spring for measuring all the elemental analyses.

Many thanks to Dr. Koushik Venkatesan for his enormous help in various ways and providing encouragement throughout my research works.

Thanks to Hanspeter Stadler for extending helping hand anytime for technical problems regarding glove box or the hydrogenation gas room. I would really appreciate his innovative set up in the gas room.

Thanks to Dr. Sergey Semenov for EPR and magnetic measurements, and Dr. Alexander Dybov for lot of initial scientific discussions.

I would like to express my gratitude to the administrative staff:

Beatrice Spichtig, Susanna Sprokkereef, Nathalie Fichter, Dr. Jae Kuoung Pak, Manfred Jöhri, Dr. Ferdinand Wild.

My thanks also goes to Gabriele for the help regarding GC/MS.

I would like to thank my colleagues and friends for making nice working ambiences and extending helping hands in various ways during these years: Samir, Jai, Rajesh, Rajkumar, Carolina, Michael, Anne, Balz, Yanfeng, Franziska, Alex, Pascal, Yan Li, and Partha. Thanks a lot to all of you for making my stay in Zürich memorable.

I thank the Swiss National Science Foundation for financial support.

Finally my special thanks to my parents and brother for their endurance and support.

Surname: **CHAKRABORTY**
First Name: **SUBRATA**
Date of Birth: 10th January, 1986
Place of Birth: Bankura, West Bengal, India
Nationality: Indian

ACADEMIC QUALIFICATIONS:

Oct 2008 - present:	Institute of Inorganic Chemistry, University of Zurich, Switzerland.
	Ph.D. thesis work
	Title of Ph.D. Thesis: "Cheap Metals for Noble Tasks: Low-Valent Molybdenum and Tungsten Nitrosyl Complexes in Homogeneous Hydrogenations and Hydrosilylations"
2006 - 2008:	Master of Science (Chemistry)
	Indian Institute of Technology Kanpur, India
2003 - 2006:	Bachelor of Science (Chemistry Major)
	University of Burdwan, West Bengal, India
2001-2003:	Higher Secondary Education
	West Bengal Council of Higher Secondary Education, India
2001	Secondary Education
	West Bengal Board of Secondary Education, India

PUBLICATIONS:

1. "Cheap Metals for Noble Tasks: Low-Valent Molybdenum and Tungsten Amides for Bifunctional Splitting of Hydrogen and Efficient Imine Hydrogenations" **S. Chakraborty**, O. Blacque, T. Fox and H. Berke (submitted).

2. "A Highly Efficient Large Bite Angle Diphosphine Substituted Molybdenum Catalyst for Hydrosilylation" **S. Chakraborty**, O. Blacque, T. Fox and H. Berke *ACS Catalysis* **DOI:** 10.1021/cs4004276.

3. "Cheap Metals for Noble Tasks: Effective Olefin Hydrogenations Using Trisphosphine Chelate Substituted Molybdenum and Tungsten Nitrosyl Hydride Complexes" S. Chakraborty, O.Blacque, T. Fox and H. Berke (in preparation).

4. "Ionic Hydrogenation of Imines Catalysed by Molybdenum and Tungsten Nitrosyl Hydride Complexes Bearing Trisphosphine Ligand", **S. Chakraborty**, O.Blacque, T. Fox and H. Berke (in preparation).

5. "Molybdenum and Tungsten Nitrosyl Complexes Bearing Cooperative $PN^{H}P$ Ligand, Carbon dioxide Activation and Stoichiometric CO_2 Hydrogenations" **S. Chakraborty**, O. Blacque and H. Berke (in preparation)

6. "Coexistence of Lewis Acid and Base Functions: A Generalized View of the Frustrated Lewis Pair Concept with Novel Implications for Reactivity". H. Berke, Y. Jiang, X. Yang, C. Jiang, **S. Chakraborty**, and A. Landwehr. *Top Curr Chem* (**2013**) 334: 27–58.

7. "Manganese and Rhenium Formyl Complexes of Diphosphinoborane Ligands: Stabilization of the Formyl Unit from Intramolecular B-O Bond Formation", R. Jana, **S. Chakraborty**, O. Blacque, and H. Berke, *Eur. J. Inorg. Chem*. DOI:10.1002/ejic.201300482.

CONFERENCES:

- **"**Heidelberg Forum of Molecular Catalysis (HFMC)", Heidelberg, Germany (22nd July, 2011).

  Title of Poster: "Synthesis of Molybdenum and Tungsten Nitrosyl Complexes with New Tridentate Phosphine Ligand and Their Application in Homogeneous Hydrogenation of imines".

- Swiss Chemical Society -2011 Fall Meeting, EPFL Lausanne (9th Sept, 2011).

  Title of Poster: **"**Molybdenum and Tungsten Nitrosyl Complexes with New Tridentate Phosphine Ligand and Their Application in Homogeneous Hydrogenation of Imines".

- "International symposium on Homogeneous Catalysis", Toulouse, France (June 9-13, 2012).

  Title of Poster: "Ligand Assisted Heterolytic Splitting of Hydrogen with Molybdenum and Tungsten Amides and Their Application in Efficient Imine Hydrogenations".

RESEARCH INTEREST:

Organometallic Chemistry, Homogeneous Catalysis, Hydrosilylation, Bifunctional and Ionic hydrogenations, CO_2 hydrogenation, Asymmetric Hydrogenation, Frustrated Lewis Pair Chemistry.

ACHIEVEMENTS:

- Qualified in the all India based joint CSIR-UGC test for Junior Research Fellowship (JRF) and Lecturer ship (LS) held in June, 2008.
- Selected for the prestigious MCM (Merit- cum-Means) and SBF (Students Benefit Fund) scholarship in IIT Kanpur, India during Masters programme (2006-2008).
- Qualified in the JAM examination in 2006 (an all India based entrance test for M.Sc.).